

Sheffield Hallam University

Assessing human morphology using statistical shape analysis.

THELWELL, Michael

Available from the Sheffield Hallam University Research Archive (SHURA) at:

<https://shura.shu.ac.uk/28734/>

A Sheffield Hallam University thesis

This thesis is protected by copyright which belongs to the author.

The content must not be changed in any way or sold commercially in any format or medium without the formal permission of the author.

When referring to this work, full bibliographic details including the author, title, awarding institution and date of the thesis must be given.

Please visit <https://shura.shu.ac.uk/28734/> and <http://shura.shu.ac.uk/information.html> for further details about copyright and re-use permissions.

Assessing human morphology using statistical shape analysis.

Michael John Thelwell

A thesis submitted in partial fulfilment of the requirements of
Sheffield Hallam University for the degree of Doctor of Philosophy

December 2020

Candidate Declaration

I hereby declare that:

1. I have not been enrolled for another award of the University, or other academic or professional organisation, whilst undertaking my research degree.
2. None of the material contained in the thesis has been used in any other submission for an academic award.
3. I am aware of and understand the University's policy on plagiarism and certify that this thesis is my own work. The use of all published or other sources of material consulted have been properly and fully acknowledged.
4. The work undertaken towards the thesis has been conducted in accordance with the SHU Principles of Integrity in Research and the SHU Research Ethics Policy.
5. The word count of the thesis is 40,000.

Name	Michael John Thelwell
Date	December 2020
Award	PhD
College	Health, Wellbeing and Life Sciences
Director(s) of Studies	Dr Simon Choppin

Abstract

Measurements of human body size and shape are an important source of information for a range of scientific fields and applications; however, practitioners still rely on traditional tools and methods which limit the kinds of measurements that can be taken. Recent literature has suggested that 3D imaging technology is a more sophisticated tool that could enable the comprehensive characterisation of human body shape. The aim of this programme of doctoral study was to determine whether shape anthropometrics can complement existing techniques in the assessment of human morphology.

A novel analytical procedure was developed using geometric morphometrics and statistical shape analysis methods to extract numeric parameters from 3D imaging data, which describe scale-invariant characteristics of human torso shape. Though errors in anatomical landmark identification and participant scanning posture can affect the acquisition of shape anthropometrics, the developed methods were found to have high test-retest reliability, suitable for use within subsequent investigations.

A series of investigations were conducted to determine whether shape measures provide additional information which is not captured by existing anthropometric techniques. The findings of these investigations suggest that body shape measures show a complex dependence on body size. Though certain shape features demonstrate a degree of allometric scaling and change with increases in body size, there are significant proportions of shape variation which cannot be explained by existing anthropometrics. These non-allometric variations in body shape have been shown to improve the estimation of subcutaneous abdominal adiposity in a small cohort of participants, and have demonstrated the potential for misclassification of individuals using existing indices, such as BMI and WHR. This programme of research provides a more detailed understanding of human morphological variation, which could inform the development of improved tools for characterising how body shape relates to its underlying mass distribution.

Acknowledgements

I would like to express my deepest thanks to my supervisors: Dr Simon Choppin, Professor Jon Wheat, Dr John Hart and Dr Alice Bullas for your encouragement, support and guidance throughout this project. I would like to extend these thanks to all researchers and staff within the Sports Engineering Research Group at Sheffield Hallam University, in particular Dr Chuang-Yuan Chiu, Carole Harris and Amanda Brothwell.

I would also like to thank collaborating researchers at Leipzig University, Dr Peter Ahnert, Dr Andreas Kuehnappel and Professor Markus Scholz, for their invaluable assistance in conducting my final study with the LIFE-Adult dataset. These thanks are extended to all researchers and staff at the Institute for Medical Informatics, Statistics, and Epidemiology, for welcoming me during my stay in Leipzig.

Thank you all those individuals who kindly volunteered to participate in the studies conducted throughout this programme of research, providing me with high level data that was vital to the success of this project and will always be greatly appreciated.

Thank you to my fellow PhD students in Chestnut Court, past and present, who have always been there to provide inspiration, laughter and support whenever it was needed.

Finally I would like to thank my family and friends for their continued encouragement and support. Special thanks to Alison for spending countless hours reviewing this thesis and to Rosa for your eternal patience and love.

Personal bibliography

Journal articles:

- Choppin, S., Clarkson, S., Bullas, A., Thelwell, M., Heller, B., Wheat, J. (2020). Anatomical and principal axes are not aligned in the torso: considerations for users of geometric modelling methods. *Journal of Biomechanics*.
- Thelwell, M., Chiu, C-Y., Bullas, A., Hart, J., Wheat, J., & Choppin, S. (2020). How shape-based anthropometry can complement traditional anthropometric techniques: a cross-sectional study. *Scientific Reports*, 10, 12125.
- Chiu, C-Y., Thelwell, M., Goodwill, S., Dunn, M. (2020). Accuracy of anthropometric measurements by a video-based 3D modelling technique. In: Ateshian G., Myers K., Tavares J. (eds) *Computer Methods, Imaging and Visualization in Biomechanics and Biomedical Engineering. CMBBE 2019. Lecture Notes in Computational Vision and Biomechanics*, vol 36. Springer, Cham.
- Chiu, C-Y., Thelwell, M., Senior, T., Choppin S., Hart J., Wheat J. (2019). Comparison of depth cameras for three-dimensional reconstruction in medicine. *Proceedings of the Institution of Mechanical Engineers, Part H: Journal of Engineering in Medicine*. 2019; 233(9):938-947.

Conference proceedings:

- Thelwell, M., Kuehnappel, A., Bullas, A., Hart, J., Ahnert, P., Wheat, J., Loeffler, M., Scholz, M., Choppin, S. (2020). Allometry between measures of body size and shape in a large population-based cohort. In: *Proc. of 3DBODY.TECH 2020 - 11th Int. Conference and Exhibition on 3D Body Scanning and Processing Technologies*.
- Chiu, C.-Y., Thelwell, M., Goodwill, S., Dunn, M. (2019). Accuracy of anthropometric measurements by a video-based 3D modelling technique. In: *CMBBE 2019 Conference Proceedings E-06.3 (pg. 246)*, New York, USA.
- Thelwell, M., Chiu, C.-Y., Bullas, A., Hart, J., Wheat, J., Choppin, S. (2018). The application of 3D shape-based anthropometry. In: *Sheffield Hallam University Creating Knowledge Conference*, Sheffield, UK.

Contents

Abstract	I
Acknowledgements	II
Personal bibliography	III
Contents	IV
List of tables	X
List of figures	XII
Nomenclature	XVII
Abbreviations	XVII
Symbols	XVIII
Chapter 1 - Introduction	1
1.1 Introduction	1
1.2 Motivation for the research	1
1.3 Aims and objectives	3
1.4 Thesis structure	4
Chapter 2 - Literature review	5
2.1 Introduction	5
2.2 Review of anthropometric techniques	5
2.2.1 Traditional anthropometry	6
Basic measures.....	7
Girths.....	9
Lengths	12
Breadths	12
Skinfolds	13
Somatotype	15
ISAK accreditation and guidelines.....	16
2.2.2 Digital anthropometry.....	17
Types of imaging techniques.....	19
Anthropometric standards.....	21
Anatomical landmark identification.....	23
Scanning posture.....	25
Complex anthropometrics	27
Area and volume	28

Curvature.....	29
Statistical approaches to assessing body shape	30
2.2.3 Summary	31
2.3 Review of quantitative methods for analysing shape.....	32
2.3.1 Morphometrics	32
2.3.2 Geometric Morphometrics	34
Semi-landmarks.....	36
2.3.3 Outline-based analysis	37
2.3.4 Allometry.....	39
2.3.5 Summary	40
2.4 Chapter summary	41
Chapter 3 - Methodology for 3D imaging data collection and post-processing	42
3.1 Introduction	42
3.2 Data acquisition.....	43
3.2.1 Participants	43
3.2.2 Define body segment region of interest	43
Rationale	43
Anatomical landmarking	45
3.2.3 Acquire 3D imaging data.....	45
3dMDbody5 imaging system	45
System calibration.....	46
3D imaging protocol.....	47
3.3 3D imaging data post-processing.....	48
3.3.1 Digitise anatomical landmarks	48
3.3.2 Align 3D imaging data	49
3.3.3 Segment 3D imaging data	51
3.3.4 Scale 3D imaging data to uniform size.....	52
3.3.5 Dimensionality reduction.....	55
3.3.6 Shape feature detection	59
3.4 Chapter summary.....	62
Chapter 4 - Test-retest reliability and observer error for shape anthropometrics	64
4.1 Introduction	64
4.2 Methods	65

4.2.1 Assessment of observer error	65
4.2.2 Participants	67
4.2.3 Research protocol	67
4.2.4 3D imaging data post-processing.....	68
4.2.5 Statistical analysis	68
Test-retest reliability of torso shape measurement	68
Assessing principal components of postural variation	71
4.3 Results	71
4.3.1 Test-retest reliability of shape measures - ICC	71
4.3.2 Assessing components of postural variation - MANOVA.....	73
4.4 Discussion.....	76
4.4.1 Limitations.....	78
4.5 Conclusion	79
Chapter 5 - Complementing traditional anthropometrics with shape anthropometrics	80
5.1 Introduction	80
5.2 Methods	81
5.2.1 Participants	81
5.2.2 Experimental protocol	81
Bony landmark palpation	81
Manual measurement.....	82
3D imaging.....	83
5.2.3 3D imaging data post-processing.....	83
5.2.4 Statistical analysis	83
5.3 Results	84
5.3.1 Torso shape features within cohort.....	84
5.3.2 Correlations between size and shape measures	84
5.3.3 Regression analysis	85
5.4 Discussion.....	93
5.4.1 Limitations.....	96
5.5 Conclusion	97
Chapter 6 - Allometry of human morphology within a large population-based cohort	98
6.1 Introduction	98

6.2 Methods	99
6.2.1 Participants	99
6.2.2 Data acquisition	100
6.2.3 Pre-processing of extracted size measures.....	100
Removal of participants with missing measurements.....	101
Normalisation of body size measures	101
6.2.4 3D imaging data post-processing.....	103
Identification of inferior and superior boundaries of the torso segment	103
Creating local anatomical coordinate system.....	105
Torso shape feature detection.....	107
6.2.5 Statistical analysis	108
6.3 Results	110
6.3.1 Torso shape features within LIFE-Adult cohort	110
6.3.2 Relationships between size and shape measures.....	112
6.3.3 Regression analysis	113
Predicting shape from size - Partial Least Squares Regression (PLSR).....	113
Predicting size from shape - Multiple Linear Regression (MLR)	114
6.3.4 Allometric model between torso size and shape measures in LIFE-Adult cohort.....	115
Shape variations explained by changes in size	115
Shape variations unexplained by changes in size	117
6.4 Discussion.....	120
6.4.1 Limitations.....	123
6.5 Conclusion	124
Chapter 7 - Application of shape anthropometrics for obesity categorisation.	125
7.1 Introduction	125
7.2 Methods	126
7.2.1 Participants	126
7.2.2 Data processing.....	126
7.2.3 Data analysis	127
7.3 Results	128
Associations between existing classifications and body shape clusters.....	129
Age-associated torso shape variations within BMI categories	134

Observed torso shape variations within combined risk classifications	135
7.4 Discussion	138
7.4.1 Limitations	141
7.5 Conclusion	141
Chapter 8 - Overall discussion	142
8.1 Introduction	142
8.2 Summary of work	142
8.2.1 Objective One	142
8.2.2 Objective Two	143
8.2.3 Objective Three	144
8.2.4 Objective Four	144
8.2.5 Objective Five	145
8.3 Contribution to knowledge	145
8.4 Practical applications	147
8.4.1 Healthcare	147
8.4.2 Apparel	148
8.4.3 Kinanthropometry	149
8.5 Limitations	150
8.6 Future research	152
8.7 Conclusions	153
Chapter 9 - References	154
Chapter 10 - Appendices	175
Appendix 1	175
A.1.1 Anthropometrics included in the restricted and full ISAK profiles	175
Appendix 2	176
A.2.1 Research ethics approval	176
A.2.2 Participant consent form	177
A.2.3 Participant information sheet	179
Appendix 3	182
A.3.1 Research ethics approval	182
A.3.2 Participant information sheet	183
A.3.3 Participant consent form	187
Appendix 4	189

A.4.1 Data sharing agreement with LIFE Consortium and Leipzig University.....	189
A.4.2 Research ethics approval.....	190
A.4.3 Sex differences in size and shape measures.....	191
A.4.4 Pearson correlation and effect size - size measures male and female.	192
A.4.5 Pearson correlation and effect size - size and shape male participants.	199
A.4.6 Pearson correlation and effect size - size and shape female participants. .	200
A.4.7 Allometric Model - Residual vs Fitted Male Shape Variation Plots PC's 1-9.	202
A.4.8 Allometric Model - Residual vs Fitted Female Shape Variation Plots PC's 1-9.	203
Appendix 5	204
A.5.1 Pearson correlation coefficients and effect sizes male participants.....	204
A.5.2 Pearson correlation coefficients and effect sizes female participants.....	204
A.5.3 Shape PC1 by age and BMI category in a) males and b) females.....	205
A.5.4 Shape PC2 by age and BMI category in a) males and b) females.....	205
A.5.5 Shape PC3 by age and BMI category in a) males and b) females.....	205
A.5.6 Shape PC4 by age and BMI category in a) males and b) females.....	206
A.5.7 Shape PC5 by age and BMI category in a) males and b) females.....	206
A.5.8 Shape PC6 by age and BMI category in a) males and b) females.....	206
A.5.9 Shape PC7 by age and BMI category in a) males and b) females.....	207
A.5.10 Shape PC8 by age and BMI category in a) males and b) females.....	207
A.5.11 Shape PC9 by age and BMI category in a) males and b) females.....	207

List of tables

Table 2.1. WHO recommended BMI cut-off points for overweight and obesity (61).	8
Table 2.2. WHO cut-off points for WC and WHR and associated risk of metabolic complications (61).	10
Table 2.3. Overview of different techniques and commercially available 3D imaging systems used for body measurement.	20
Table 2.4. Maximum allowable error between manual and 3D scan-derived body measurements (140).....	22
Table 2.5. Different methods to obtain landmark coordinates in digital anthropometry (145).....	24
Table 4.1. RMSE of shape measures for the torso mannequin in different conditions.	67
Table 4.2. Summary characteristics of participants.....	67
Table 4.3. ICCs for torso shape measurements within each data collection session, assessing the torso as a whole and for individual slices along the length of the torso segment.....	72
Table 4.4. ICCs for torso shape measurements between repeat data collection sessions, assessing the torso as a whole and for individual slices along the length of the torso segment.....	73
Table 4.5. Results of one-way repeated measures MANOVA, for repeated shape measures within each data collection session and between the averages of both sessions.....	74
Table 5.1. Summary characteristics of participant manual measurements.....	82
Table 5.2. Pearson correlation coefficients between skinfolds, size measures, anthropometric indices and shape PCs.	87
Table 5.3. Linear regression models showing associations between derived indices and sum-of-skinfold thickness.....	87
Table 5.4. Multiple linear models showing associations between sum-of-skinfold thickness and 1) size measures; 2) shape PCs; 3) derived indices and shape PCs.	88
Table 5.5. Linear models showing associations between derived indices and individual skinfold thickness measures.....	89
Table 5.6. Multiple linear models showing associations between individual skinfold thickness and 1) size measures; 2) shape PCs; 3) derived indices & shape PCs. ..	89
Table 6.1. Basic characteristics of participants in LIFE-Adult cohort.....	100

Table 6.2. Estimated coefficients of linear models for allometric height normalisation for participants in LIFE-Adult cohort.	102
Table 6.3. Variable importance in projection statistic scores and predicted variance in male PLSR models.	113
Table 6.4. Variable importance in projection statistic scores and predicted variance in female PLSR models.	114
Table 7.1. Sample characteristics (mean \pm standard deviation).	126
Table 7.2. Chi-square (χ^2) results showing percentage of participants within each BMI classification at each risk level according to WC and WHR.	130
Table 7.3. Chi-square (χ^2) results showing percentage of participants within each BMI, WC and WHR classification within each shape cluster.	131
Table 7.4. Chi-square (χ^2) results showing the percentage of participants within combined classifications (BMI & WC, and BMI & WHR) that are within each shape cluster.	132

List of figures

Figure 2.1. Stretched stature measurement method (53).....	7
Figure 2.2. Commonly used body girth measures and locations (35,88).	12
Figure 2.3. Skinfold thickness measurement locations according to ISAK guidelines, anterior view (left) and posterior view (right) (53).	14
Figure 2.4. XYZ coordinate system for measuring the human body using a 3D imaging system, in both a standing and sitting position (140).	22
Figure 2.5. a) Manual palpation and landmarking (53); b) Manually placed raised landmarks that can be manually digitised or identified automatically by scanning software (18).	24
Figure 2.6. Anthroscan ScanWorX software (151) a) Automatic anatomical landmark identification and b) body measurement extraction.	25
Figure 2.7. Standing imaging postures recommended in ISO 20685 (140). a) Posture for taking height and manual measurements; b) Posture for acquiring scan-derived body measures (e.g. girths).	26
Figure 2.8. Comparisons of two individuals with the same BMI but different weight distribution, measured by body volume (27).	29
Figure 2.9. Body surface curvature. a) Gaussian curvature calculated across a human torso surface (24); b) 2D intensity image of surface curvature extracted from 3D body scan data (169).	30
Figure 2.10. First eight principal components of torso shape variation identified from a cohort of 650 female participants (170).....	31
Figure 2.11. Example of traditional morphometric analysis limitations when comparing length and width measures taken from two fish of different shape. adapted from (180).....	33
Figure 2.12. Procrustes superimposition procedure. a) Identify anatomical landmark coordinates; b) Calculate centroid; c) Translation of configuration centroids to origin; d) Scaling landmark configurations to unit centroid size; e) Minimise rotational differences between landmark configurations (185).....	35
Figure 2.13. Kendall's shape space, showing all possible variations in triangle shape from the mean (181).	36
Figure 2.14. Landmarks and semi-landmarks positioned on the surface of 3D computed tomography (CT) scans of a) a human skull and b) a human tooth (189).....	37

Figure 2.15. Fourier descriptor analysis and reconstruction of the boundary outline curve of a binary image. a) binary image of a printed numeral of the number 4, b) polygonal boundary description of binary image, c) first ten pairs of harmonic amplitude and phase angle of boundary, d) reconstructed boundary from the first ten Fourier descriptors (195).	38
Figure 2.16. Allometric analysis in geometric morphometrics. a) Allometric regression of shape on size; b) Size-correction (181).	39
Figure 3.1. Modification of trunk segment boundaries defined by Wicke (205); red crosses show the location of the xiphoid process and ASIS landmarks used to define the superior and inferior boundaries of the torso segment, respectively, dashed lines show the planes created by these landmarks.	44
Figure 3.2. Marked anatomical landmarks on a human participant; anterior torso aspect (left) and posterior torso aspect (right).	45
Figure 3.3. a) 3dMDbody5 system; b) 3dMD calibration board; c) plan view of 3dMDbody5 imaging system layout and calibrated volume.	47
Figure 3.4. Scanning pose for torso segment scanning adapted from ISO 20685 (140).	48
Figure 3.5. Digitised torso scan image in KinAnthroScan; anterior aspect (left) and posterior aspect (right).	49
Figure 3.6. The location of landmarks used to create a local coordinate system within the torso segment.	50
Figure 3.7. Segmentation of a captured scan to include only the coordinate points relating to the torso region of interest (shown in red) between the superior and inferior segment boundaries.	51
Figure 3.8. Extraction of 2 mm thick slices of coordinate data points at 5% intervals along the torso segment between the inferior and superior segment boundaries.	52
Figure 3.9. Extracted data point slice with a fitted cubic smoothing spline.	53
Figure 3.10. Resampled point slice with calculated distances from each coordinate to the centroid.	53
Figure 3.11. Torso shapes of two individuals with the effects of non-shape variation - location, rotation and scale - removed.	54
Figure 3.12. Extraction of Fourier descriptors from torso outlines. a) Polar coordinates of a typical torso shape outline; b) Polar coordinates of the torso shape outline	

plotted as a signal waveform, red dots showing the corresponding start and end points on the polar diagram; c) Representation of the torso shape outline in the frequency domain.....	57
Figure 3.13. Average root mean square error (RMSE) between the original and reconstructed torso outlines for all extracted shape profiles along the length of the torso segment for all participants. Vertical dotted line shows the initial cut-off point for the number of Fourier coefficients used to reconstruct the original curve, though has been shown to depend on the complexity of the input curve.	58
Figure 3.14. Visual comparison between an original torso outline curve (black markers) and reconstructed torso outline curves using 7 Fourier coefficients (blue) and 10 Fourier coefficients (red).	59
Figure 3.15. Extracted torso shape features; (a) Average torso shape; (b) Maximum and minimum deviations from the sample mean along the first 5 principal components and their explained variance. Blue and red regions represent areas that protrude less, or more than the average torso, respectively.	61
Figure 3.16. Analytical procedure for extracting shape features from torso 3D imaging data; a) Acquire and digitise 3D geometry of an individual; b) Segment, scale and rotate torso segment; c) Extract transverse data slice profiles; d) Obtain signal waveform from profiles; e) Extract frequency content from signals; f) Detect shape principal components from Fourier coefficients.	63
Figure 4.1. a) Non-deformable torso mannequin; b) Simulated errors in landmark locations on the surface of the torso mannequin and the subsequent effects on the vectors used to create the local coordinate system, shown as dashed lines .	66
Figure 4.2. Examples of measured differences in polar coordinates between two corresponding torso outline curves, obtained from repeated measures of a single participant.....	70
Figure 4.3. Within-participant standard deviation (s_w) values for all identified torso shape principal components, both within each data collection session and between sessions.....	74
Figure 4.4. Comparison of torso shape PC's from two repeat measures of participant #25 within data collection session 1. a) front profile i) measure 1, ii) measure 2,	

b) side profile, i) measure 1, ii) measure 2, c) Radar diagram comparing shape principal components from measure 1 (blue) and measure 2 (red).....	75
Figure 6.1. Typical 3D body scan provided by the Vitus XXL Smart Laser Scanner and selected anatomical landmarks identified within the software.....	104
Figure 6.2. Determining the superior and inferior boundaries of the torso segment of interest.....	105
Figure 6.3. Vitus scanner coordinate system. a) Correct positioning of participant; b) Incorrect positioning of participant.....	106
Figure 6.4. Creating local coordinate system torso segment. a) Extract cross-sectional slice from 3D image; b) Identification of anterior, posterior and midpoint landmarks in slice; c) Creation of coordinate system within torso segment.	107
Figure 6.5. First 9 principal components capturing 90.6 % of variation in torso shape in the LIFE-Adult cohort, shown as the maximum positive (left) and negative (right) deviations from the sample mean. Blue and red regions represent areas that protrude less, or more than the average torso, respectively.	111
Figure 6.6. Average torso shape of male (left) and female (right) participants in the LIFE-Adult cohort.	112
Figure 6.7. Allometric scaling between size and shape measures for male participants. a) Predicted changes in shape features using PLSR models; b) Reconstructed allometric torso shapes for males with waist girths of 68, 110 and 152 cm.	115
Figure 6.8. Allometric scaling between size and shape measures for female participants. a) Predicted changes in shape features using PLSR models; b) Reconstructed allometric torso shapes for females with waist girths of 59, 102 and 143 cm.	116
Figure 6.9. Non-allometric male torso shape variation. a) Predicted torso shape for males with waist girth 100 cm; b) Examples of observed torso shapes of males with waist girth 100 cm; c) Boxplots showing the amount of residual variation for each shape principal component in PLSR model, with deviations from the predicted torso shape displayed by the participants in b).....	118
Figure 6.10. Non-allometric female torso shape variation. a) Predicted torso shape for females with waist girth 91 cm; b) Examples of observed torso shapes of females with waist girth 91 cm; c) Boxplots showing the amount of residual variation for	

each shape principal component in PLSR model, with deviations from the predicted torso shape displayed by the participants in b).....	119
Figure 7.1. Hierarchical clustering of male participants in LIFE cohort according to shape. a) Dendrogram showing cluster 1 (blue), cluster 2 (red) and cluster 3 (green); b) Reconstructed torsos of cluster centroids and their deviations from the average male torso.....	128
Figure 7.2. Hierarchical clustering of female participants in LIFE cohort according to shape. a) Dendrogram showing cluster 1 (blue), cluster 2 (red) and cluster 3 (green); b) Reconstructed torsos of cluster centroids and their deviations from the average female torso.	129
Figure 7.3. Associations between current indices and shape. BMI vs WC vs Shape: a) male, b) female; BMI vs WHR vs Shape: c) male, d) female.....	133
Figure 7.4. Shape PC1 by BMI category and age group in a) males and b) females.....	134
Figure 7.5. Shape PC5 by BMI category and age group in a) males and b) females.....	135
Figure 7.6. Shape PC6 by BMI category and age group in a) males and b) females.....	135
Figure 7.7. Male torso shape variations within combined BMI and WHR obesity/risk classifications, with representative torsos of shape cluster 1 (blue), cluster 2 (red) and cluster 3 (green).....	136
Figure 7.8. Female torso shape variations within combined BMI and WHR obesity/risk classifications, with representative torsos of shape cluster 1 (blue), cluster 2 (red) and cluster 3 (green).....	137

Nomenclature

Abbreviations

1D	One dimensional
2D	Two dimensional
3D	Three dimensional
ANOVA	Analysis of variance
ASIS	Anterior superior iliac spine
BIA	Bioelectrical impedance
BMI	Body mass index
BVI	Body volume index
BW	Body weight
CSA	Cross sectional area
CT	Computed tomography
DFT	Discrete Fourier transform
FFT	Fast-Fourier transform
GM	Geometric morphometrics
ICC	Intra-class correlation coefficient
ICP	Iterative closest point
ISAK	International Society for the Advancement of Kinanthropometry
ISO	International Standards Office
IWGK	International Working Group on Kinanthropometry
kg	Kilogram
LIFE	Leipzig Research Center for Civilisation Diseases
MANOVA	Multivariate analysis of variance
MDC	Minimum detectable change
MRI	Magnetic resonance imaging
PC	Principal component
PCA	Principal component analysis
PLSR	Partial least squares regression
RMSE	Root mean squared error
SA	Surface area

SEM	Standard error of the measurement method
TEM	Technical error of measurement
TOF	Time of flight
VIP	Variable importance in projection
WC	Waist girth/circumference
WHO	World Health Organisation
WHR	Waist-to-hip ratio
WHTR	Waist-to-height ratio
WHT.5R	Waist divided by stature ^{0.5}

Symbols

χ^2	Chi-square statistic
μ	Mean
σ	Standard deviation
D	Difference between measurements
k	Number of observations
m	Value of the measurement
n	Number of individuals measured
r	Pearson correlation coefficient
R^2	Coefficient of determination
X Y Z	3D real world components, comprising horizontal, vertical, and depth components

Chapter 1 - Introduction

1.1 Introduction

This thesis documents a three-year programme of doctoral study investigating the use of statistical shape analysis for assessing human morphology, improving current understanding regarding differences between measures of size and shape of the human body. This chapter outlines the motivation for this research by reviewing the history of human measurement, existing anthropometric techniques and geometric morphometrics. The aims, objectives and thesis structure are given at the end of this chapter.

1.2 Motivation for the research

For centuries, civilisations have been fascinated with the human body and measurement of its dimensions, believing that an individual's physical health can be determined through subjective descriptions of their body shape (1–3). Hippocrates (460-370 B.C.) suggested that an individual's general constitution and susceptibility to certain diseases, could be categorised based on their physical build: "*habitus phthisicus*" - wasting of the lungs (pulmonary tuberculosis), and *habitus apoplecticus* - apoplexy (stroke) (3,4). This practice of describing body shape and its relation to physical health is still in use today with the use of somatotyping, which suggests that human body shape can vary along 3 dimensions: endomorphy (relative fatness), mesomorphy (relative musculo-skeletal fatness) and ectomorphy (relative linearity) (5–7). The short technical manual *Anthropometria*, published in the 17th century by naturalist Johann Sigismund Elsholtz, was the earliest recorded investigation of the human body for scientific and medical purposes (1,4). Elsholtz's work established a quantitative approach for acquiring body measurements, describing variations and changes in human form and their relationships with certain diseases (4,8). Anthropometry, derived from the Greek: *anthropos* (human) and *metron/metrein* (measure/to measure), was then the formal term given to the technique of collecting human measurements and is defined as: "*The scientific study of the measurements and proportions of the human body*" (9). During the 18th century the "season of measurers" began, with the development of new measurement instruments, as well as the application of mathematics and statistics to advance the field of anthropometry (1). It was at this time that there was a distinct move away from subjective

descriptions of human form towards the development of specialist equipment and techniques to quantitatively measure the body. Today, anthropometric techniques are used in several applications, including: health monitoring (10), epidemiological studies (11,12), apparel sizing (13,14) and predicting sporting performance (15–17). However, though the field of anthropometry has seen major developments since its origins, the tools which are predominantly used in practice to measure the human body are the same as those used by Richter in 1890 (14,18). Traditional anthropometric techniques rely on the use of tape measures and callipers to acquire body lengths, breadths and girths, with combinations of these used to create proxies of weight status and body shape, such as the body-mass-index (BMI) and the waist-hip ratio (WHR). These approaches for assessing the human body are prone to error and limited by their relative simplicity, as they do not capture the complex variations in shape and mass distribution (4,19–21). It is increasingly recognised that existing anthropometrics, such as body lengths, girths and diameters, are one-dimensional, and can only express shape information when adjusted for other measures such as body height (21). More sophisticated, scale-invariant measures are required to identify the subtle curvatures and contours which are present on the three-dimensional (3D) topographical landscape of human body shape that existing measures fail to capture (2,22,23).

Recently there have been significant advances in the development and manufacture of 3D imaging systems capable of capturing detailed and accurate external dimensions of the human body, in a more timely and non-invasive manner than manual measures (20,24,25). Studies have investigated the use of more complex anthropometrics using data captured by these devices, such as volume and surface area, which have been shown to distinguish differences in body size and shape unattainable using simple anthropometrics (17,26,27). However, the majority of anthropometric studies use a specific definition of shape, based on the ratios and relative proportions of one-dimensional anthropometrics, such as waist girth and stature, to create proxies of shape. This approach to assessing body shape based on combinations of size measures discards the geometric information captured by 3D imaging systems and is a common misconception within the literature (28). Whilst 3D imaging technology is well established, the methods and metrics used to analyse human shape information is not. Therefore, there is a need to investigate more sophisticated methods of analysis to enable comprehensive characterisation of human body shape (2,19).

Morphology is a branch of biology which studies the form of living organisms and the relationships between their external and internal structures (9). Geometric morphometrics (GM) is an established method within the fields of anthropology and evolutionary biology to analyse variations in shape and its covariation with other variables (29). These methods have emerged from established shape theory (30) and a conceptual understanding of mathematical shape, defined by Kendall as: "*the geometrical information that is left when the differences which can be attributed to translations, rotations, and dilations have been quotiented out from an object*" (31)(p82). GM provides a framework for the statistical analysis of shape information, which quantifies the variation of anatomical landmark coordinates, curves and surfaces present between biological structures, whilst retaining the geometric form of organisms throughout the analysis (29). These methods have been used to analyse shape in a wide range of biological and anthropological studies (32,33) and has recently been applied to assess variations in human hip and lumbar spine shape (34). However, few investigations have explored how geometric methods of shape analysis can complement existing anthropometric techniques in the assessment of external human form.

1.3 Aims and objectives

The aim of this programme of research was to determine whether shape anthropometrics can complement existing anthropometric techniques in the assessment of human morphology. The objectives were to:

- Review published literature regarding existing anthropometric techniques and quantitative methods for analysing the shape of biological organisms.
- Develop analytical procedures for extracting scale-invariant features of human body shape from 3D imaging data.
- Determine the test-retest reliability of developed methods for acquiring measures of body shape and the effect of identified sources of measurement error.
- Critically evaluate the degree of allometric scaling between measures of body size and shape, as well as identifying non-allometric variations in torso shape which cannot be explained by existing anthropometric techniques.
- Determine if body shape measurement can complement anthropometric techniques currently used in population-based studies and obesity assessment.

1.4 Thesis structure

This programme of doctoral study will be presented as a traditional thesis, comprising seven further chapters. These chapters are structured as follows:

- Chapter Two provides a critical review of the literature relevant to the programme of doctoral study. The literature review examines the applications of human body measurement, traditional and digital anthropometric techniques, and quantitative methods of statistical shape analysis.
- Chapter Three details the development of analytical procedures, enabling the implementation of geometric morphometric methods for analysing human torso shape to be used throughout this programme of research.
- Chapter Four evaluates the test-retest reliability of developed analytical procedures and the effects of potential sources of measurement error when assessing verification artefacts and human participants.
- Chapter Five details a preliminary investigation with a small cohort of participants, examining whether shape measures can complement traditional anthropometric techniques in the estimation of subcutaneous abdominal adiposity.
- Chapter Six characterises a large population-based cohort to establish a database of body shape information and determine the degree of allometric scaling between measures of torso size and shape.
- Chapter Seven demonstrates the application of body shape measurement within obesity classification and how it can complement existing anthropometric techniques.
- Chapter Eight discusses the main findings of this programme of doctoral study, followed by practical applications, limitations, potential areas for further research and an overall conclusion of the research programme.

Chapter 2 - Literature review

2.1 Introduction

This chapter reviews the relevant literature in two main sections:

- Review of existing anthropometric techniques.
- Review of quantitative methods for analysing shape.

2.2 Review of anthropometric techniques

Throughout history an individual's body size and shape has been used as a direct indicator of their physical health characteristics (1). Since the 19th century, systematic body measurements and records have gained importance and have been employed extensively in several fields, principally healthcare and apparel sizing. For example, military organizations previously used height measurement as the basic procedure to determine whether young men were suitable for military service (1,2). In addition, large-scale anthropometric surveys have been conducted to facilitate mass production of clothing and equipment for military personnel as early as the American Civil War (35,36). Throughout the 19th and 20th centuries measures of height and weight, followed later by girths and skinfolds, have gained importance as tools within clinical practice as measures of public health, due largely to the work of Adolphe Quetelet (37) in the 1830's (38) and 1870's (39). Since then, medical practitioners have measured the outside of the human body to assess various aspects of an individual's health, guide their treatment and evaluate the prevalence of disease within the population (10). Large-scale anthropometric surveys have been fundamental to epidemiological studies of the distribution and determinants of health-related states or events in specified populations during the last century (10,12). More recently, the application of anthropometric techniques within sport, known as kinanthropometry, has become vital to understanding how body dimensions can enable athletes to meet the demands of their sport (40–45).

Before proceeding further, it is essential that differences in terminology are clarified. First, anthropometry - as mentioned in Section 1.2 - refers to the scientific procedures and processes of acquiring surface anatomical measurements of the human body (height, weight, lengths and girths) by means of specialist equipment (callipers and tape measures) (41). Nutritional status is an individual's health condition as it is

influenced by the intake and utilisation of nutrients, with optimal nutritional status in theory being attained by consuming sufficient, but not excessive sources of energy, nutrients and other food components (46). Poor nutritional status can refer to both undernutrition (low intake) and excessive intake (inadequate expenditure) of food energy. Body composition, refers to the composition of different molecular-level components within the human body, primarily: water, fat, proteins and minerals. However, body composition is most commonly assessed at the tissue-level in terms of the amounts and distributions of adipose, skeletal and muscle tissues, or more broadly into fat mass (FM) and fat-free mass (FFM), according to the two-component model (47–49). Though anthropometrics are commonly utilised as proxies of nutritional status (e.g. BMI), and as indirect methods of assessing body composition, they can only directly provide information relating to the external dimensions of the human body. Body composition can vary along several axes, including the ratios of fat to lean tissue, and organs to muscle tissue, as well as the distribution of adiposity between central and peripheral depots. However, though these traits manifest themselves outwardly as variations in body build and shape, the relationship between external body measures and body composition are considered controversial (47). With these definitions in mind, this literature review and programme of work focuses primarily on anthropometric methods for measuring the external dimensions of the human body and their use in different applications. Currently, there are two types of anthropometric techniques used to obtain human body measures: traditional anthropometry, using manual measurement tools; and digital anthropometry, using 3D imaging devices.

2.2.1 Traditional anthropometry

Manual anthropometrics are currently the dominant method used by practitioners to assess variations in human size and shape within the population, as well as performing initial health screening of individuals and population-level diagnostics of disease risk and obesity prevalence (49–51). Since Richter first used callipers in 1890, a standard set of instruments, including tape measures, callipers and weight scales, have been used to obtain manual anthropometrics (14,18). The continued popularity of manual anthropometrics is due primarily to the ease of use of these low-cost, portable tools and remain the standard which new anthropometric devices are evaluated against

(52). During the last century, approximately 2,000 different anthropometric variables have been used by different professional groups to define the size and shape of the human body within various applications (35). As a result, a degree of confusion and lack of standardisation has emerged within the field of anthropometry (53). This has further complicated the choice of measurements practitioners and researchers should take during anthropometric assessments, and made the comparison of measurements over time more difficult. In general, traditional anthropometrics can be divided into five broad categories: basic measures, girths, lengths, breadths and skinfolds, which are then commonly combined to calculate derived indices and somatotypes (51,53).

Basic measures

Basic measures include stature and body mass, collected using a stadiometer and a standard set of weighing scales, respectively. Stature measurement enables tracking of overall growth and calculation of height normalised indices. Measures of stature should be taken in the morning, since the human body tends to decrease in height during the day, typically with losses of approximately 1% over the course of the day (54). An additional technique used to account for these losses, the stretched stature method, is the preferred technique for acquiring measures of stature (53) (Figure 2.1).



Figure 2.1. Stretched stature measurement method (53).

Changes in an adult's body mass correspond primarily to changes in their levels of body water, fat and/or lean tissue, whilst in children changes in body mass mostly relate to their overall growth. Body mass is an important tool for understanding the development of children and adolescents, and is recognised as an important indicator of proper development (55,56). Obesity in children has become a widespread problem, and there have been calls for improved measures that are able to differentiate

between normal physiological and pathological development in children (56). However, simply measuring body mass without other measures of body size can be misleading, since body mass is highly correlated with stature (49). To overcome this, medical practitioners typically combine measures of stature and body mass to calculate an individual's body-mass-index (BMI), providing a proxy of nutritional status (2,49,50). BMI has been found to be a reasonable measure of general adiposity and is calculated as body mass divided by stature squared (kg/m^2) (57). In addition to its simplicity, another benefit of BMI is considerable amounts of reference data and literature regarding its relationships with levels of body fatness, risk of cardiovascular disease (CVD), morbidity, and mortality in adults (58). Thus, the primary use of BMI is to classify individuals within the population into groups based on their risk of suffering from obesity related diseases (59). Obesity is defined according to BMI and is stratified into categories according to the World Health Organization (WHO) (60,61). The current WHO recommended guidelines for obesity classification according to BMI are given in Table 2.1.

Table 2.1. WHO recommended BMI cut-off points for overweight and obesity (61).

Category	Body Mass Index (BMI)
Underweight	< 18.5
Normal Weight	18.5 - 24.9
Overweight	25.0 - 29.9
Obesity: Class I	30.0 - 34.9
Obesity: Class II	35.0 - 39.9
Obesity: Class III	> 40.0

However, the use of BMI in isolation, especially in atypical populations, should be performed with caution since it is now widely acknowledged that BMI is unable to distinguish between fat and lean tissue, or provide information regarding the distribution of mass around the body (2). It has been shown that obesity, when defined using only BMI, is a heterogeneous condition whereby people with the same BMI can have distinct cardiovascular and metabolic risk profiles (12,62). In fact, susceptibility to adverse metabolic and cardiovascular diseases has been shown to not be purely determined by total fat mass, but rather depends on factors including the ratio of fat-lean tissue (63), and the distribution of adipose tissue between central and peripheral deposits (12,64). The limitations of BMI are highlighted when assessing certain populations, for example: relatively muscular individuals such as athletes are often categorised as being overweight or obese; individuals with high body fat and low

lean mass are classed within the normal weight range; while individuals with certain medical conditions, such as sarcopenia or edema, where distributions of mass may be altered significantly, are hard to distinguish (49).

In addition to these between-individual differences in fat and lean mass distribution that are unidentified by BMI, body shape and its underlying composition are further influenced by sex, ethnicity and age-associated factors. First, previous studies have shown that there are underlying sexual dimorphisms in adipose tissue biology and deposition, related to reproductive function, as well as genetic and hormonal factors, which cause differences in external body size and shape between males and females (65,66). These differences between male and female body shape are further complicated by the effect of age. A previous study (67) observed that though male body shape remains consistent within different BMI classifications between early adulthood and old age, females change from more of an hourglass shape (low waist girth relative to hip and bust girths) in early adulthood, to having greater abdominal fat deposition and central obesity as they become older regardless of their BMI, causing sexual dimorphisms in body shape to largely disappear in older adults. The lack of such age-associated shape changes in men implies that hormonal correlates of female reproductive biology, such as concentrations of androgens and estrogen, changes how fat mass is deposited with increased age in females (68).

Finally, several components of body composition that are expressed as body shape, such as fat-lean mass ratio and fat distribution, as well as associated cardio-metabolic risk have been found to vary significantly across ethnic groups at a given BMI value (63,69). For example, African Americans exhibit low levels of visceral fat compared to Europeans, while South Asians have higher total body fat content for a given BMI and greater amounts of visceral fat. In addition, differences in birth weight between ethnic groups has been shown to lead to reduced amounts of muscle mass and organ size in later life, causing individuals from certain ethnic groups to have a reduced metabolic capacity to maintain metabolic homeostasis at a given body mass (63,69).

Girths

Body girths (circumferences) are the distance measured around the outside of a body segment and should be obtained using steel tape measures to eliminate stretching (53). The tape should be aligned perpendicular to the length of the measured body

segment and held tight enough to prevent gaps between the tape and the skin, but not so tight as to cause skin indentation (51). Body girths, particularly waist girth, have been found to be more closely related to increased morbidity risk than BMI, with the Endocrine Society suggesting that waist girth is the key anthropometric variable for establishing metabolic risk in the general population (2,70,71). Waist girth is most commonly used in clinical assessments, due to its ease of capture and relationship with visceral adiposity volume (50). In addition, practitioners often calculate ratios of different body girths and size measures to create proxies of central adiposity and abdominal shape, such as the waist-hip (WHR), waist-chest (WCR), waist-height (WHT) or waist-by-height^{0.5} (WHT.5R) ratios (2,50,72–75). Recent studies by Nevill et al. have suggested that scaling waist girth for differences in body size provide improved measures of central adiposity and cardio-metabolic risk assessment at the population level (72,76). In addition to its relationship with adiposity, waist girth also has been shown to be significantly correlated with absolute measures of lean mass (77), with variations in lean mass often overlooked. For example, birth weight has been shown to be lower in neonates in Asian, African and Central/South American populations due to substantially reduced organ and muscle mass, indicative of reduced metabolic capacity. These disparities in lean mass and organ size remain in later life, with individuals of different ethnicity displaying differences in metabolic capacity and health risk (69). The WHO has stated that combining BMI with a measure of abdominal obesity can provide improved anthropometric tools to establish prevalence of metabolic risk in the general population and treat patients with obesity-associated metabolic conditions (12,61). The current WHO recommended guidelines for establishing metabolic risk according to WC and WHR are given in Table 2.2.

Table 2.2. WHO cut-off points for WC and WHR and associated risk of metabolic complications (61).

Anthropometric Index	Cut-off Points		Risk of Metabolic Complications
	Male	Female	
Waist Circumference (WC)	> 94 cm	> 80 cm	Increased
	> 102 cm	> 88 cm	Substantially Increased
Waist-Hip Ratio (WHR)	≥ 0.90	≥ 0.85	Substantially Increased

Though the majority of previous research focuses on measures of the torso, girth measures of other parts of the body also provide important information about disease risk. For example, previous studies have shown that larger thigh and hip girths are associated with improved glucose tolerance (78). Increased WHR can result from

increased waist girth, decreased hip circumference or both, with smaller hip circumference reflecting either decreased lower body fat or muscle mass. Using computed tomography (CT) measurements of human thigh segments has shown that after adjustment for abdominal subcutaneous and visceral fat, as well as inter-muscular thigh fat, larger subcutaneous fat area was significantly associated with more favourable glucose and lipid levels. Changes in thigh girth were found to be equally dependent on quantities of fat and muscle in men, whereas in women the fat component was the main contributor to changes in thigh girth (78,79). Girth measures are often used to classify individuals as exhibiting characteristics of either one of two body shapes, associated with their level of disease risk (50,80):

- Android - apple shape or upper-body obesity, increased risk of metabolic dysfunction and obesity-related conditions.
- Gynoid - pear shape or lower-body obesity, regarded as protective, with both hip and thigh circumferences inversely related to type 2 diabetes risks.

Though anthropometric indices of central obesity are easy to implement clinically, they remain relatively crude indices of body shape and adipose tissue distribution (2,49,81). It has been suggested that waist circumference is only a valid measure of abdominal fat mass and disease risk for individuals with BMI < 35, while for individuals with BMI > 35 this measure adds little to the determination of risk (82). Other potential issues with classifying an individual's central obesity level and abdominal shape using waist girth or WHR are that of inter-rater reliability and differences in protocol for where to take girth measurements (50). The reliability of girth and other manual measures can vary significantly depending on the amount of training undertaken by a practitioner, their level of certification and level of obesity of the participant (15). Also, even with a highly certified practitioner, there are 14 varying descriptions of how to take a waist girth measurement, in 3 separate reference manuals (83). Therefore, assessment of central obesity and abdominal shape using girth measurements and their ratios should be performed with caution.

Large numbers of defined body girths are commonly acquired from participants to aid in the design of well-fitting apparel (Figure 2.2). International standards have since been established for the designation of clothing sizing and standard methods of garment measurement, such as ISO 8559:1-3 (84–86) and ISO 18890:2018 (87).

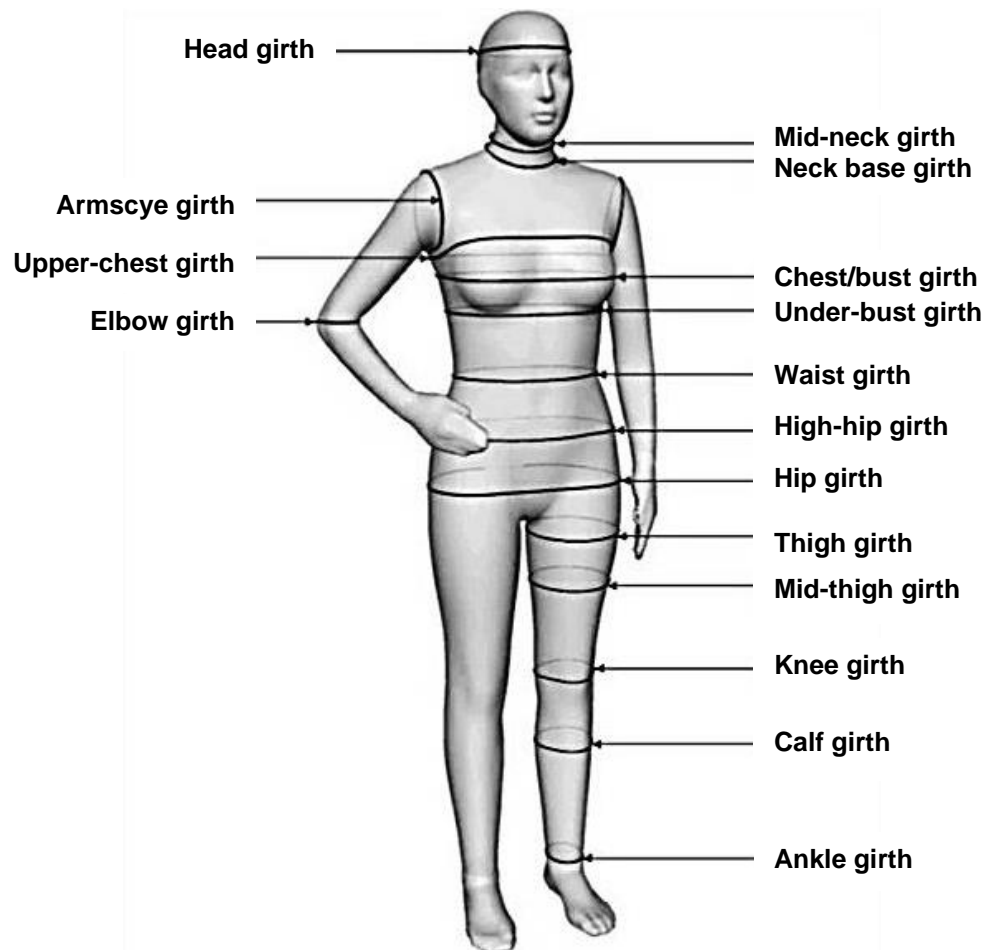


Figure 2.2. Commonly used body girth measures and locations (35,88).

Lengths

Lengths are the distance measured between two ends of a line segment along the longest dimension of an object. Body segment lengths provide measures of body proportionality and are obtained using tape measures, large sliding callipers, segmometers or anthropometers with a foot plate and can be acquired using both derived and direct measures (53). Derived lengths are acquired by first measuring projected heights - vertical distances from the floor to marked anatomical landmarks - and then subtracting the lengths of individual segments. Direct lengths of body segments are measured between manually palpated and marked landmarks using a sliding calliper or a segmometer. Previous studies have found that errors are more common when using projected lengths, so direct measures are recommended (89).

Breadths

Bone breadths are used to estimate body frame size, with distributions or summations of bone breadth values used to categorise individuals as having small, medium, or large frames, or to calculate indexes of frame size (90). Classifying a person as having a

small, medium, or large frame is intended to adjust for supposed skeletal mass and size in describing body composition, or adjusting for ideal body weight (90). The most commonly used breadth measures are the biepicondylar humerus (elbow) and biepicondylar femur (knee) breadths, measured using a small sliding calliper (53). The underlying soft tissue must be compressed so that the correct bone breadth is measured (51).

Skinfolds

Skinfold thickness measurement is a manual anthropometric technique for assessing subcutaneous adiposity at a given location on the body and for estimating body composition from the sum of several skinfold sites (Figure 2.3) (53,91). Skinfold thickness describes the amount of subcutaneous adipose tissue present within a lifted fold of skin measured using specialised callipers. Subcutaneous adiposity is a metabolically active tissue, which stores fat and releases it in response to a variety of nervous and hormonal stimuli, as well as acting as an insulator to maintain body temperature and provide padding (4). Studies often use the sum-of-skinfold thickness taken from around the waist (supraspinale, abdominal and iliac crest) as a measure of central subcutaneous adiposity to assess the efficacy of new anthropometric indices to be used in clinical practice (76). Though the primary compartment for fat storage in the body is the subcutaneous adipose tissue depot, with prolonged weight gain over time, excess fat is then distributed to other compartments of the body, including intra-abdominal depots which include visceral adipose tissue (12). Subcutaneous skinfold thickness have previously been found to be significantly correlated with total amounts of adipose tissue ($r = \sim 0.7$ (92)), with certain parts of the body storing greater amounts of subcutaneous fat than others, depending on sex, age and overall fatness level (4). Relationships between the different fat compartments has since been used to derive between 150-200 different regression equations for predicting total percentage body fat from skinfold values. However, due to errors in measurement, it is recommended that raw skinfold measures, or sums of skinfolds, are used to assess and monitor changes in adiposity levels (93). The ease of access to subcutaneous fat makes skinfold thickness a reasonable indirect measure of assessing subcutaneous fat across the body and providing estimates of total body fat. However, though subcutaneous fat accounts for over 80% of total body fat mass (4,12), there are complex inter-individual

differences in body fat distribution resulting from variations in the expandability of subcutaneous adipose tissue to store surplus energy when required (12,94). This failure of subcutaneous fat in some individuals to expand sufficiently is thought to lead to higher lipid and ectopic fat deposition in other organs (skeletal muscle, the liver and visceral adipose tissue), which have been found to be a critical factor in the development of insulin resistance. Abdominal visceral adiposity in association with excess ectopic fat deposition has been shown to be significantly associated with cardiac and metabolic abnormalities, independently of the amount of total or subcutaneous fat accumulation. However, variations in these internal adiposity depots cannot be identified by skinfold measurement techniques. Although adverse effects of excessive abdominal adiposity have often been linked to visceral adipose tissue, the role of abdominal subcutaneous adiposity in the regulation of metabolic health has been overlooked until recently. Adverse metabolic effects, like insulin resistance or dyslipidemia dependent on abdominal adiposity, are likely to result from both dysfunctional abdominal subcutaneous and visceral adipose tissue accumulation (12,95).

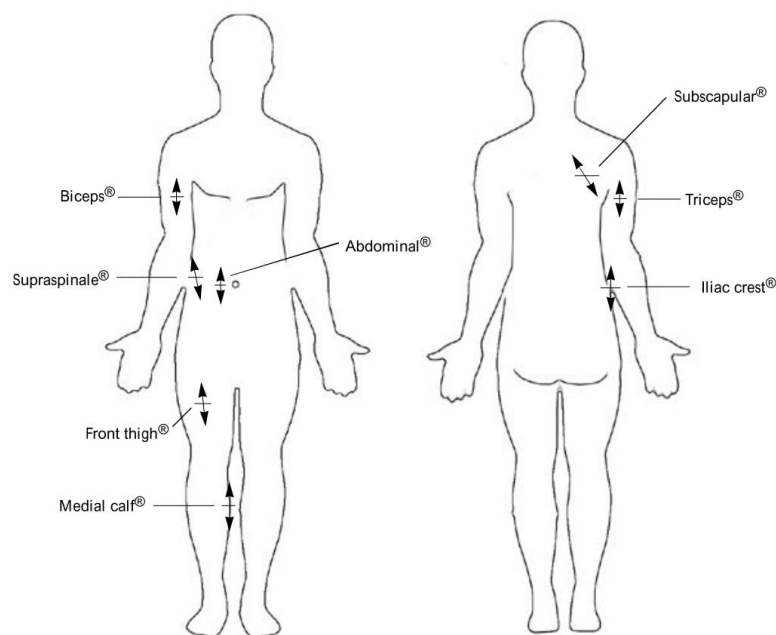


Figure 2.3. Skinfold thickness measurement locations according to ISAK guidelines, anterior view (left) and posterior view (right) (53).

There are several potential sources of error when taking skinfold thickness measures. These include questionable accuracy due to skin and adipose tissue being measured together in a compressed state without considering their individual compressibility (96). Most skinfold calipers have an upper measurement limit of 45 - 55 mm,

restricting their use to individuals who are moderately overweight or less (49). Also, there are considerable variations in protocol for taking skinfolds, both in the duration of compression during measurement and the location of skinfolds sites around the body, depending on the guidelines being followed. This issue is exacerbated as skin has varying levels of thickness and compressibility at different locations around the body, which again are dependent on age, sex and levels of tissue hydration (4).

Somatotype

The somatotype approach, originally proposed by Sheldon, was based on subjective descriptions of college students photographs and theorised to be linked to personality traits (97,98). Though Sheldon's physical taxonomy is still in use, the idea that body type is an indicator of temperament or potential has subsequently been disputed, in addition to strong criticism of using thousands of photographs of naked undergraduate students, obtained without their explicit consent (99). Methods of somatotyping were later modified by anthropologists Heath and Carter to provide a quantification of the shape and composition of the human body (6,51,100). The purpose of somatotype is to reduce a large number of body measures or visual observations to a simple three number rating based on components of characteristics (Endomorphy-Mesomorphy-Ectomorphy) providing a general description of body shape and physique, which is independent of size, age, and sex (5). The Heath-Carter method of somatotyping remains the most commonly used (6) and can be obtained in one of three ways:

- Anthropometric method - 10 manual measurements are used to calculate the anthropometric somatotype and estimate the criterion somatotype.
- Photoscopic method - ratings are made from a standardised photograph of an individual.
- Anthropometric plus photoscopic method - combines anthropometry and ratings from a photograph and is considered the criterion method.

The photoscopic somatotype can only be rated objectively by those who have had their validity and reliability established against those of an experienced practitioner. However, it is generally accepted that the anthropometric method provides a reasonable estimate of the photoscopic procedure, with equations using anthropometric inputs validated against subjective visual ratings (101). The procedure of somatotyping has attracted criticism because it oversimplifies the complex nature of

human body shape, losing details of physique within the tri-axial physique rating (6,102). In addition, somatotype categories are determined by a qualitative description of the individual somatotype in terms of the dominant component or components, which relies on a subjective rating and is open to interpretation (101). Finally, somatotyping lacks discriminatory power since large changes in manual skinfold and girth measurements are required to cause a change in an individual's somatotype rating, meaning it is not sensitive to small changes in physique (40).

ISAK accreditation and guidelines

Body measures acquired using manual methods are only ever as accurate or reliable as the practitioner who obtains them (18). Differences are typically observed between repeated measures taken independently by one observer (intra-observer) and between measures performed by multiple anthropometrists (inter-observer) (18,103). Previous studies have identified intra-observer error of over 30 mm in thigh girth taken from the same participants (104). Observer error of anthropometrists tasked with collecting body measures is the most troublesome source of error within anthropometry, leading to imprecision in locating anatomical landmarks (105,106), as well as subject positioning and instrument application (14). These issues are exacerbated when measuring atypical body types (107). These issues with accuracy and reliability have led to the establishment of industry standards, guidelines and accreditation for performing manual body measurement.

Kinanthropometry is the scientific discipline investigating relationships between anthropometrics and performance parameters, such as movement, biomechanics and physiology (16,108). The International Working Group in Kinanthropometry (IWGK) was founded in 1978, with their focus being the promotion and development of kinanthropometry research (53), later becoming the International Society for the Advancement of Kinanthropometry (ISAK). ISAK accreditation provides protocols for field assessments of body size and shape, as well as the types of equipment and techniques to be used when acquiring traditional anthropometrics (51,53). ISAK also administers training courses for practitioners to meet a minimum degree of accuracy and repeatability in their measurements, according to the technical error of measurement (TEM) (109). According to ISAK guidelines, manual anthropometrics are recorded while participants adopt fixed, standardized postures (35), based on the work

of authors, such as Kroemer and Kroemer to standardise anthropometric methods (110). The primary measuring posture is referred to as the “anatomical position”, in which the participant’s body is placed in a defined, straight, upright posture, with the body segments at 180°, 0°, or 90° to each other (111). Anatomical landmarks are sites on the body that serve as endpoints for the defined anthropometric variables, specifically located on a bony prominence or other physically definable point on the human body (35,53). These bony landmarks are manually palpated and marked on the skin by a trained anthropometrist to identify anchor points for measuring tools and to ensure that measures are taken as consistently and accurately as possible (14,35). ISAK accreditation is based around two general anthropometric profiles, the restricted and full. Measures collected in both the restricted and full ISAK manual anthropometric profiles are detailed in Appendix 1.

2.2.2 Digital anthropometry

Recent developments in digital devices, capable of acquiring external 3D geometries, have resulted in an emergent field known as digital anthropometry - utilising 3D imaging technology to acquire anthropometrics. Methods to evaluate the human body as a 3D object were first proposed by Lovesey, using a light sectioning technique (112). In 1989 these methods were developed into the first automated, non-contact 3D imaging device, known as the Loughborough Anthropometric Shadow Scanner (LASS) (113). Since the end of the 20th century, there have been significant advances in the development of 3D imaging systems beyond these early shadow-based techniques (18,114,115). Modern 3D imaging systems, acquire point cloud data that explicitly captures surface topography. These can provide detailed and accurate external dimensions and shape characteristics of the human body, such as curvature and partial volumes (24,27). Surface features can be used to characterise individuals according to their shape as well as their size, to a higher degree of precision and complexity than existing manual methods (19,116).

The recent technological development of 3D imaging systems used for anthropometric applications has largely been driven by the apparel industry, to enable surveys and improved personalised fitting of garments for all body types (117–119). However, this has placed a growing demand on product development teams to reconsider their approach to prototyping and sizing apparel (118). Significant, related changes are also

being made in the fashion retail environment, including innovations in virtual fitting to enable consumers to optimise the fit of their clothing when shopping online. Recent growths in ecommerce, combined with the inclusion of depth sensing 3D imaging technology within modern smartphones has facilitated the development of phone-based 3D scanning apps that provide virtual try-on and garment sizing recommendations (120). One of the major areas of discussion at the recent 3DBODY.TECH conference and expo (121) was to enable the mapping of simple 2D images - such as front and side body profiles that online customers take of themselves using their smartphone - to large 3D scan databases using machine learning techniques to enable the estimation of an individual's 3D body shape information and prediction of optimal fit characteristics for their clothing. As a result, it is expected that in future, more and more organizations will be moving towards establishing 3D digital human databases of their target population and using them directly to solve design problems (35). However, such advances also need to relate to existing manufacturing practices and the entrenched methods of practitioners used in clothing product development and garment fitting, otherwise these exciting new techniques for developing products might not be fully exploited. New methods of categorising the body in terms of its shape should allow recognition of the restrictions of proportional theories in pattern construction, affording promising opportunities for advancing the practices of sizing and fitting in clothing product development.

3D imaging has also been used in a wide range of other anthropometric applications, due to the detailed body shape information these devices produce, including: kinanthropometry (15,25,43), epidemiology (19,122) and clinical practice (10,123). 3D imaging has been used to assess large cohorts of participants in population-based epidemiological and anthropometric surveys, due to its ability to rapidly acquire large numbers of body measures (11,13). In addition, 3D imaging creates a digital image of an individual's external geometry, which can be stored and reanalysed enabling longitudinal changes in their shape to be monitored over time, in response to changes in diet or exercise interventions (10). It has also been suggested that 3D imaging of the external surface of the body for anthropometric applications can have a major impact on medical research and clinical practice; since a 3D image contains all aspects of an individual's shape, not just their size, which could surpass existing indices, such as the BMI or WHR (2,21).

Types of imaging techniques

Several imaging techniques can be used to create full body geometries, with a range of commercial 3D imaging systems currently available (18,115), each varying in underlying technologies, cost, functionality and accuracy - as presented in Table 2.3. Most imaging techniques utilise some form of projected light to acquire body shape data (laser line, infrared), with the exception of millimetre wave systems which analyse patterns of reflected non-ionising electromagnetic radiation, as well as radiation emitted naturally by human skin to assess body shape. Millimetre waves pass through most clothing, but not human skin, meaning the shape of an individual's body can be evaluated without needing to remove their clothes. This provides an ideal alternative to x-ray scanners for airport security, though the risks of thermal effects associated with millimetre waves are unknown (124).

It is apparent from Table 2.3 that different forms of 3D imaging systems currently utilised for body measurement have advantages and disadvantages, which must be accounted for when performing digital anthropometric assessments. For the purposes of this programme of research it is posited that more sophisticated body shape measures could be used to identify subtle variations in human morphology which existing manual anthropometrics cannot detect. However, to ensure that these features are not masked by a system's variability, it is essential that the amount of measurement method error is minimal. Whilst it is acknowledged that the high cost of imaging systems with increased levels of accuracy may not be accessible to all researchers and clinical practitioners, potentially limiting the uptake of any findings using these systems, the accuracy of findings must remain of paramount importance.

Table 2.3. Overview of different techniques and commercially available 3D imaging systems used for body measurement.

Imaging technique	Brands/Models	System type	Cost (USD\$)	Accuracy	Scan duration	Remarks
Laser line	Cyberware WBX Vitronics Vitus Smart	-	~37,000 - 240,000	< 2 mm 27 points/cm ³	~10 - 15 secs	High accuracy and often used in large-scale anthropometric surveys, but high cost and long scan duration (125,126).
Millimetre wave	Intellifit	Active Passive	~100,000 - 200,000	± 6 mm	~2 - 5 secs	Scan without needing to remove clothing, but high cost and currently unknown physical health risks (124,127).
Stereo photogrammetry	Cranfield Vectra 3dMDbody e.g. Flex8	Passive Hybrid	~190,000	0.2 mm < 0.2 mm	~2 - 8 msecs ~1.5 msecs	High accuracy and short scan duration, but high cost and small capture volume (128,129).
Structured light	Artec Eva/Spider TC2 KX-16 SizeStream	Blue light Infrared Infrared	~10,000 - 20,000	0.1/0.05 mm 1 mm 1 mm	161/8 fps 3 secs 6 secs	High accuracy and frame rate, and relatively lower cost, but long overall scan duration increasing the potential risk of movement artifacts in data, such as breathing cycle, as well as blinking of the eyes, caused by flashing of Artec scanners (130–132).
Depth sensor	Microsoft Kinect V2 Intel Realsense D435	Time of flight (ToF) Stereoscopic	~200/per device (~1000/system)	< 6.5 mm > 6.5 mm	< 10 secs (single camera)/ ~0.8 secs (multi camera)	Low cost and potentially short scan duration, but relatively low accuracy (133–136).

Anthropometric standards

Typically in applications that use 3D imaging, such as ergonomic design and healthcare, the point cloud data acquired by 3D imaging systems has been used to extract 1D body measurements, comparable to those obtained using traditional anthropometric methods (21). As discussed, there are an increasing number of different technologies that underlie commercially available 3D imaging systems, as well as a wide range of proprietary and bespoke software applications to process and extract body dimensions from the acquired data. In addition, though 3D imaging presents several advantages over manual methods, such as time to acquire measures and the information provided, there are a greater number of complex processing steps required to produce usable anthropometric data, which can contribute to measurement errors (18). As a result, there can be considerable differences in body measures acquired from different imaging systems, caused by variations in the locations of anatomical landmarks and scanning postures (137). These considerations have led to the establishment of international standards to ensure the reliability and validity of anthropometric data.

ISO 7250-1:2017

Based on the work of authors to standardise methods of measuring human participants, such as Kroemer and Kroemer (110), international standards of human measurement for technological design have also been established (138). ISO 7250-1:2017 provides a description of manual measurements and standardised measurement postures, which can be used as a basis for comparing population groups and for the creation of anthropometric databases in accordance with ISO 15535 (139). The ISO 7250-1:2017 document is intended to serve as a guide for ergonomists on how to define population groups, take anthropometric measurements and apply this knowledge to the geometric design of the places where people work and live (138).

ISO 20685-1:2018

ISO 20685-1:2018 (140) defines standardised data collection protocols and acceptable reliability standards for 3D imaging systems used to perform human body measurement. These standards are intended to ensure comparability of body measurements obtained using manual and digital methods, specified in ISO 7250 (138) and enables the data collected in digital anthropometric studies to be included in international anthropometric databases, as described in ISO 15535 (139). ISO 20685-

ISO 20685-1:2018 defines the coordinate axis system which should be adopted when conducting anthropometric assessment using 3D imaging with respect to a standing or sitting human (Figure 2.4). According to ISO 20685-1:2018 (140), X refers to the anterior-posterior direction (sagittal axis), Y refers to the side-to-side direction (transverse axis) and Z refers to the superior-inferior direction (longitudinal axis). ISO 20685-1:2018 suggests that researchers should establish their own origin for this axis system, convenient to their research, while keeping the direction of the axes as indicated and reporting the origin in any publications. ISO 20685-1:2018 also details the maximum acceptable error between scan-derived and manual body measures (Table 2.4).

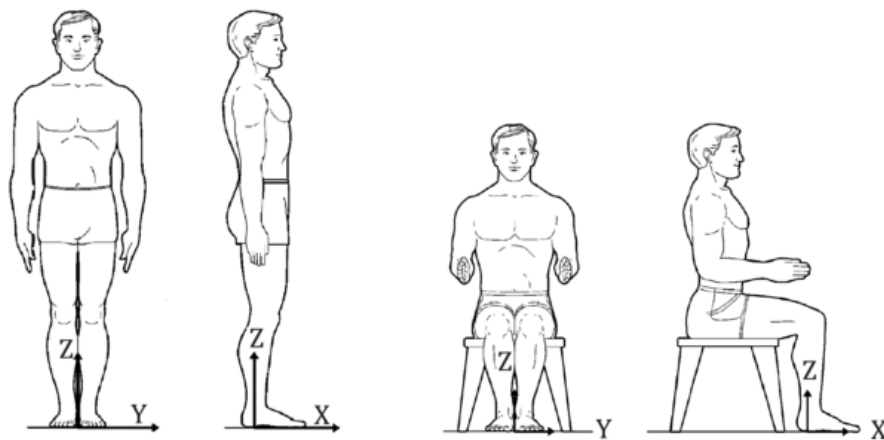


Figure 2.4. XYZ coordinate system for measuring the human body using a 3D imaging system, in both a standing and sitting position (140).

Table 2.4. Maximum allowable error between manual and 3D scan-derived body measurements (140).

Measurement type	Max. error (mm)
Segment lengths (e.g. buttock-popliteal length)	5
Body heights (e.g. shoulder height)	4
Large circumferences (e.g. chest circumference)	9
Small circumferences (e.g. neck circumference)	4
Body breadths (e.g. biacromial breadth)	4
Body depths (e.g. chest depth)	5
Head dimensions without hair	1
Head dimensions with hair	2
Hand dimensions	1
Foot dimensions	2

Several previous studies have investigated whether human body measures acquired using 3D imaging are comparable to those obtained using traditional manual techniques, to assess the validity and reliability of measures obtained using digital anthropometry (15,55,70,141–143). Body length and height measures have been found to be comparable between manual and 3D scan-based techniques, with high levels of repeatability (15,55). Bullas et al. (15) demonstrated that scan-derived

measures of thigh length were within 2 % of manual measures and had TEM < 1.5 %, suggesting that they were comparable to manual measures and repeatable. Similarly, Kuehnappel et al. (55) demonstrated good concordance between manual and scan measures of arm and thigh lengths, as well as good to excellent reliability for scan-derived length measures. However, it was observed that length measures of obese individuals had lower concordance with manual measures and reduced reliability, which was suggested to have been caused by errors in the automatic landmark identification algorithms caused by higher levels of body fat (55). Previous studies have demonstrated that 3D imaging systems systematically overestimate girth measures of body segments, but have higher levels of reliability compared to manual measures (15,70,125,144). It has been suggested that these differences in girth measures between manual and digital anthropometry are attributable to soft tissue compression and the tape measure not following all the external contours of the segment during manual measurement procedures, which would be captured during 3D imaging (15,141). Also, the agreement and reliability of upper arm and upper thigh girths measures were reduced for obese participants, due to postural variations and increased amounts of body fat in these regions preventing automatic landmarking algorithms correctly identifying the armpit and crotch landmark points (143).

Anatomical landmark identification

The ability of a body measurement system to produce consistent measurements is dependent on its ability to accurately and reliably identify the locations of anatomical landmarks and is one of the most important procedures within digital anthropometry (18,105). Landmarks are used to define body dimensions and ensure anatomical correspondence between 3D imaging data of different participants and repeated scans of an individual. Also, measurements derived from reliable landmarks can be used for statistical analysis, reconstructing variation in human body shape and creating homologous models (105,145). Consequently, wrongly identifying landmarks can have significant effects on the derived data used to define body dimensions and perform body shape analysis. Several methods have been used to locate anatomical landmarks in previous investigations. The key stages involved in obtaining 3D coordinates of anatomical landmarks are: 1) determining landmark locations on the surface of the body; 2) obtaining 3D coordinates of landmarks from the 3D imaging data; 3) labelling

of landmarks to extract body measures and align individual scans. According to Kouchi et al. (145) these stages in landmark identification can be performed either: entirely manually by an operator; entirely automatically by body measurement software; or by using a combination of manual and automatic techniques (Table 2.5).

Table 2.5. Different methods to obtain landmark coordinates in digital anthropometry (145).

Decision of landmark location	Detection of marker location	Labelling
Manual	Manual	Manual
	Automatic	Automatic
Automatic	Automatic	Automatic

Manual landmark identification

Several anatomical landmarks used in traditional anthropometrics to define body dimensions, as defined in ISO 7250 (138), cannot easily be determined from the surface shape of the body and must be determined manually by an anthropometrist. Manual palpation and marking of anatomical landmarks prior to scanning is a time-consuming, invasive process that requires training to enable landmarks to be identified accurately and reliably (51,53) (Figure 2.5a). Manual identification of landmark locations can be further complicated when assessing individuals with higher levels of body fat that obscure bony landmarks (146) and individuals who are in wheelchairs preventing access to required landmarks (147). In addition, even with training it has been shown that there can be significant intra-observer and inter-observer errors in manual landmarking, which can contribute to errors in derived body measurements and 3D scan processing (105). These manually palpated landmarks, marked either as coloured points or as raised objects stuck to the skin, can then be identified and labelled from the acquired 3D scan data, either through manual digitisation by an operator, or automatically by the imaging system's software (Figure 2.5b).

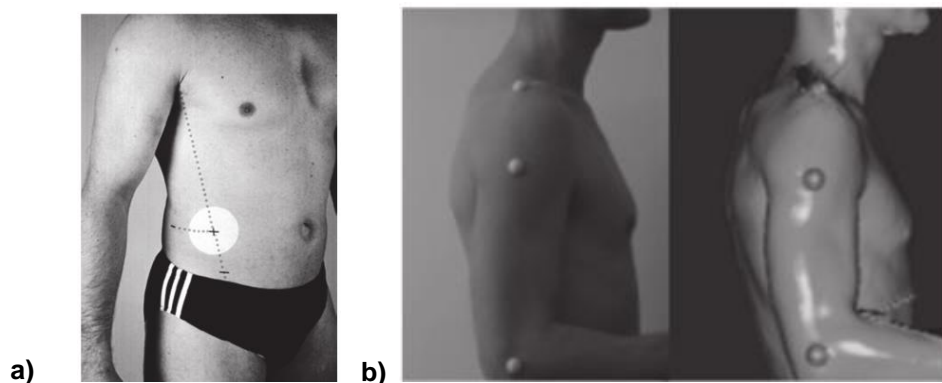


Figure 2.5. a) Manual palpation and landmarking (53); b) Manually placed raised landmarks that can be manually digitised or identified automatically by scanning software (18).

Automatic landmark identification

Alternatively, anatomical landmark locations can be identified automatically within 3D scan images based on either geometrical features present on the surface of the human body, such as: umbilic points - where two principal curvatures coincide, minimal saddle points and ridges (24,148,149). Alternatively, a template mapping approach can be employed, which uses information from existing 3D anthropometric databases (150). Different 3D imaging systems use accompanying proprietary body measurement software, which automatically locates landmarks and calculates large numbers of linear body dimensions, such as lengths and girths, from the acquired 3D imaging data. For example, Human Solutions provides dedicated Anthroscan ScanWorX software (151) for scan processing, automatic anatomical landmark identification and body measure extraction (Figure 2.6). However, though automatic landmarking saves time compared to manual palpation, the landmark locations identified using software may not always match those identified by an anthropometrist. This has been shown to significantly affect comparability between manual and scan-derived body measures, with overall concordance correlation coefficient (OCCC) values as low as 0.1 observed for upper arm and thigh length measures (55).

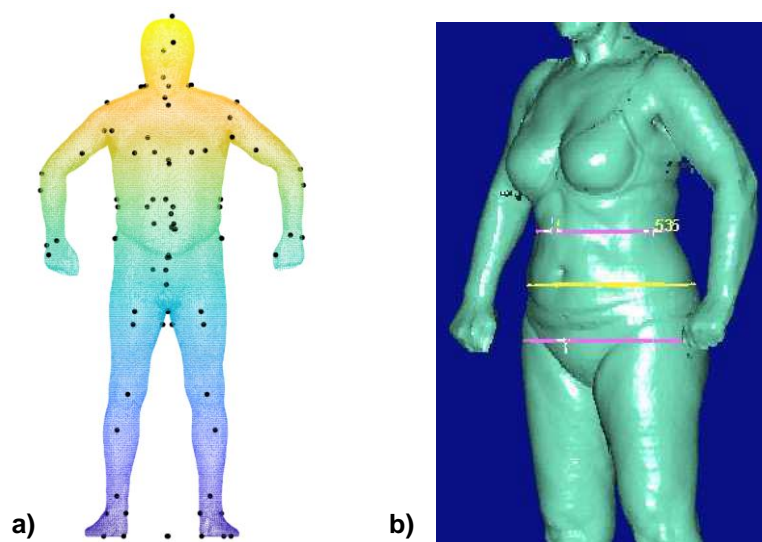


Figure 2.6. Anthroscan ScanWorX software (151) a) Automatic anatomical landmark identification and b) body measurement extraction.

Scanning posture

Posture adopted by participants during 3D imaging can have significant effects on the reliability and accuracy of extracted body dimensions and can also emerge from principal components analysis of body shape (18,145,152). The postures used for

measurements in traditional anthropometry are not suitable for 3D body scanning, due to the occlusion of large areas of the body, particularly in the armpit and crotch regions. Instead, it is recommended that participants stand with their arms abducted and legs 30 cm apart, enabling the 3D imaging device to view all surfaces of the limbs and torso (140). ISO 20685 recommends two standing postures for 3D scanning: 1) basic standing posture - same as posture for taking manual measures (Figure 2.7a); 2) posture with arms and legs abducted for extracting scan-derived body measures, such as breadths and girths (Figure 2.7b). Kouchi et al. (145) observed that even this relatively small change in posture can alter some body measurements when compared to those acquired using standard anthropometric tools. However, as discussed previously, there are several 3D imaging systems currently available, which employ different technologies and methods for acquiring scan data. As a result, the optimal scanning posture for participants may vary between different systems and should be adapted for each study being conducted (18). Once the optimal position for a particular scanning system has been determined it should be strictly adhered to by all participants in the study to minimise measurement error and ensure reliability (153). In response, studies have investigated the use of positioning aids to reduce the effect of postural variability during scanning and increase the precision of measures (154).

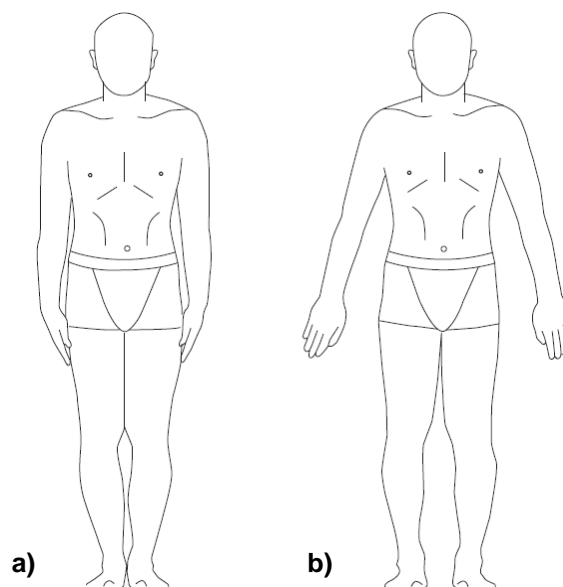


Figure 2.7. Standing imaging postures recommended in ISO 20685 (140). a) Posture for taking height and manual measurements; b) Posture for acquiring scan-derived body measures (e.g. girths).

Complex anthropometrics

Due to the rapid and repeatable quantification of human body dimensions possible when using digital anthropometry, previous studies have been able to collect imaging data from large cohorts of participants. For example, certain studies have collected full body imaging data from over 10,000 participants from specific populations (2,19,70), while a study by Jurca et al. (119) collected 3D images of feet from over one million individuals. These large-scale anthropometric surveys are vital as they allow researchers to consider measurements of individuals with a wide range of body characteristics. In particular, the significance of anthropometrics is recognised within the global apparel industry, with researchers continually tracking changes in consumers' dimensions through population-based anthropometric surveys, such as SizeUSA, SizeUK (13), and recently ShapeGB (155). 3D imaging data collected in these surveys have contributed to the ergonomic design of cars, aircraft, workplaces and military equipment (13,14,36), as well as enabling garment manufacturers to revise their sizing systems for mass produced, ready-to-wear (RTW) clothing for consumers (156–158).

The measures typically derived from 3D scan images to describe body shape have been combinations of simple lengths and girths, adopted from the context of clothes sizing (118) and commonly used indices, such as the WHR (2,70). Recent studies by Loffler-Wirth et al. (19) and Pluess et al. (122) are the most sophisticated of these, demonstrating the use of machine learning techniques to evaluate large numbers of 1D human body measurements and establish clusters of individuals exhibiting similar traits. These studies demonstrate that large cohorts of participants can be stratified into distinct body-types based on a higher number of independent parameters. Similarly, a study by Olds et al. (100) attempted to progress the somatotyping approach by using scan-derived body measures, combined with k-means cluster analysis to determine different body shapes. Though this technique was able to find distinct body shape clusters for both men and women, the scan-derived measures were still combinations of size measurements obtainable with manual methods, meaning that these clusters would have been similar to those found using traditional methods of somatotyping. These studies all use a specific definition of body shape, which is based on the ratios and relative proportions of 1D anthropometrics, such as

waist girth and stature. It has been suggested that this approach does not utilise the full potential of 3D imaging and discards the shape information captured by these systems (152). As a result, a number of studies have investigated the use of complex anthropometrics captured using digital anthropometry - area, volume and curvature.

Area and volume

Body surface area is related to several physiological processes, including water turnover and metabolic rate (10), and is commonly measured in healthcare to improve skin transplants for burn injuries, calculating drug dosages and the treatment of obesity (159,160). 3D imaging enables the surface area of the entire body, or of individual limbs and body parts to be captured from a single scan (161). Previous studies have also investigated combining measures of surface area captured using 3D imaging with existing measures such as BMI to create novel body shape indices, such as the health index (HI) (162) and the surface-based body shape index (SBSI) (163). In addition, measures of cross-sectional area have been used in kinanthropometric assessments of cyclists (164) and rowers (17) to capture variations in the dimensions of body segments that would not be identified using traditional size measures alone.

Calculation of whole body and segmental volume has been used within kinanthropometry (42,108,165) and health (166,167) applications. It has been suggested that volume, measured using 3D imaging, can provide improved predictions of sporting performance than traditional size measures (26,168) and could complement body composition assessment modalities, such as ultrasound and DEXA (93). The body volume index (BVI) has been proposed as a novel 3D scan-based measure within healthcare and the estimation of body composition (27). It has been suggested that comparisons of part-volumes of human body segments, in particular the abdominal volume, can be an effective method of assessing body fat distribution, providing an indicator for obesity-related diseases that could replace BMI (Figure 2.8). However, though the measurement of body volume has been shown to have relatively good precision and high correlation with MRI-based measurements of whole-body adiposity, whether by using 3D imaging or air displacement plethysmography (ADP), does demonstrate a significant volume-dependent bias (48). Since these methods only measure the volume or density of the body, they cannot be used for regional body

composition measurements of fat or lean mass, limiting them to gross body composition estimation.

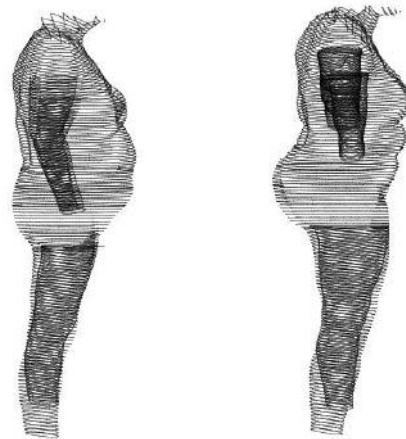


Figure 2.8. Comparisons of two individuals with the same BMI but different weight distribution, measured by body volume (27).

Though measures of area, both cross-sectional and surface area, and volume have been shown to provide additional information compared to traditional anthropometrics (25,26), they still represent measures of absolute scale rather than shape. Area is a general term that expresses the size of a 2D surface, while surface area measures the amount of exposed surface present on any given 3D solid object (9). Volume is the quantity of 3D space enclosed by a closed surface, comprising measures of length, width and height (9). In contrast, shape is defined as the external form, contours, or outline of an object (9) and is invariant to the effects of scale. This means that two individuals could have the same surface area or volume, but exhibit differences in their external shape features, meaning these measures would miss subtle variations in curvatures and contours present on the external human surface.

Curvature

Humans intuitively perceive differences in body shape between individuals by identifying scale-invariant external features, such as surface curvature, body proportions and lateral contours (169). Recent studies by Douros (24) and Lu et al. (169) have analysed external human body shape using measures of surface curvature derived from 3D scan data to identify differences between individuals and predict body fat percentage, respectively. Douros' PhD thesis developed methods of extracting the differential geometry properties of the human body surface from 3D point cloud data in order to calculate its surface curvature features (Figure 2.9a). It was suggested that these features could then be used to interpret the topology of human body, enabling

classification of individuals according to their shape, rather than their size, as seen in current anthropometric practice (24). Similarly, Lu et al. (169) proposed using measures of curvature, described as a second-order shape descriptor, as a way of modelling different body shapes and predicting body fat percentage (Figure 2.9b). These studies stated that further research was needed to associate configurations of these external features with distinct phenotypes, at various body sizes in order to establish reliable associations between human shape and body composition.

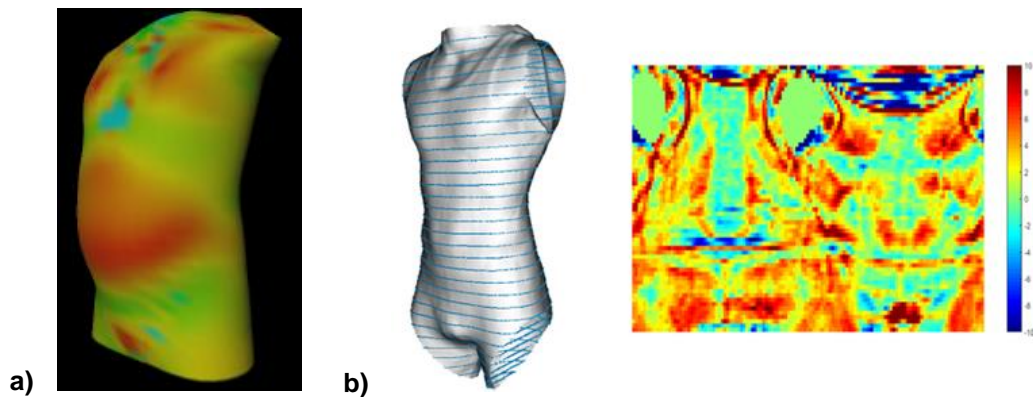


Figure 2.9. Body surface curvature. a) Gaussian curvature calculated across a human torso surface (24); b) 2D intensity image of surface curvature extracted from 3D body scan data (169).

Statistical approaches to assessing body shape

It has been shown that directly processing 3D imaging data, rather than deriving traditional anthropometrics, can provide more detailed information about the human body. Further developments within digital anthropometrics has seen the application of novel statistical approaches to analyse large databases of 3D body scan data and identify significant features of human shape variation (21,152). The most popular method has been principal components analysis (PCA) (170). PCA is a mathematical procedure for dimensionality reduction, which transforms a large number of possibly correlated variables into a smaller number of uncorrelated variables called principal components (171). This technique is ideal for capturing complex variations in body shape from highly detailed 3D meshes, which can then be used to describe subtle nuances in human form (Figure 2.10). PCA has been used in a number of applications, including: human body modelling (170,172) body composition assessment (23), categorisation of female lower body shapes for clothing sizing (173), development of improved bra shape and sizing systems (174) and statistical shape modelling of craniofacial shape (175). However, the use of PCA has been criticised, due to its assumption of Gaussian distribution of the underlying data and the resulting features

not being visually intuitive, with independent components analysis (ICA) proposed as a potential alternative (21,170). Also, though previous studies have often standardised the scan data into a common format, using template mesh registration or voxel representation (21,23), they have not removed elements of body size from the underlying data, causing the resulting PCs to be dominated by variations in body size, not shape. Other proposed alternatives to PCA include Gaussian Process Morphable Models (GPMs) (176) and self-organising map (SOM) machine learning (19). Both of these methods have been suggested as outperforming PCA-based statistical shape models, but may be beyond the scope of this current programme of research.

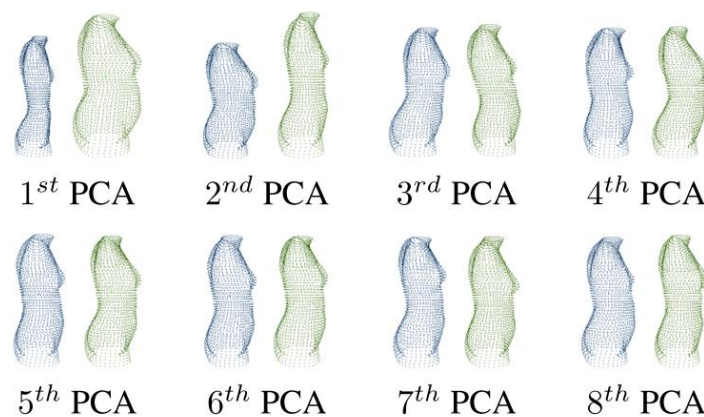


Figure 2.10. First eight principal components of torso shape variation identified from a cohort of 650 female participants (170).

2.2.3 Summary

Manual anthropometrics remain the most common method of acquiring body dimensions for practitioners in several fields, due to the use of low cost, accessible equipment and established industry standards and guidelines. However, researchers and practitioners are critical of manual anthropometrics due to their time-consuming procedures and susceptibility to human error, limiting its suitability for assessing large populations. Manual techniques are also limited to extracting one-dimensional measures of body size, such as lengths, breadths and girths. Though these measures are easy to capture they suffer from the limitation that neither the reference points nor the path of the measures strictly follow the curvatures and contours present on the surface of the human body, which has implications for apparel design and identifying mass distributions in healthcare. Though individual size measures can be combined to create proxies of weight status, relative measures of abdominal shape or descriptions of overall body shape, they do not capture the complex 3D variations in human form. There have been rapid technological developments in 3D imaging

systems which capture external dimensions of the human body with varying cost and accuracy. 3D imaging can rapidly and reliably acquire traditional anthropometrics with minimal physical contact between the researcher and the participant. The data provided by 3D imaging can also be used to extract more complex anthropometrics, such as volume and surface area, as well as directly evaluate the differential geometric properties of the body surface and identify features of body shape variation through statistical analysis. However, there are several potential sources of measurement error, such as scan accuracy, anatomical landmark identification, as well as postural and movement artefacts that must be considered when acquiring body measures using digital anthropometric methods. It has been suggested that current approaches used to assess body shape in practice do not capture all of the available geometric information that comprise the complex landscape of human body shape. More sophisticated, scale-invariant measures of shape, which have greater associations with accumulations and distributions of mass, could surpass existing anthropometrics.

2.3 Review of quantitative methods for analysing shape

Biologists and naturalists have been fascinated with the diversity of life on earth for centuries, leading to several attempts to explain how and why these differences have occurred (177). The analysis of shape is the process of understanding and describing the diverse morphological variability of a population of geometric objects and individuals, as well as its causes and is fundamental within biological research (32). However, until recently the study of external form has been mostly descriptive, using simple common terms to classify the shape of objects or organisms (28,178). Only since the mid-20th century has the study of form become a quantitative discipline, most commonly known as morphometrics (33). This was made possible when the quantitative description of shape was combined with newly developed statistical techniques, such as the correlation coefficient and PCA, which enabled the description of patterns of shape variation within and among groups of biological organisms (32).

2.3.1 Morphometrics

Morphometrics is the study of shape variation and its covariation with other variables (29). The field of study is concerned with methods for the description and statistical analysis of shape variation within and among samples of organisms, as well as the

analysis of shape change as a result of growth, experimental treatment or evolution (179). Though morphometric methods can be used to describe the form of any object, it is primarily used in fields such as biology and anthropology to describe the form of organisms (180). Similarly to anthropometry, the field of morphometrics has seen a recent shift from traditional to more modern methods. For much of the 20th century morphometric analyses were performed using either univariate or multivariate statistics with sets of measured variables, such as lengths, widths and distances between bony landmarks to describe patterns of shape variation within and among groups (32,33,179,180). The applications of these traditional methods were typically concerned with allometry, the study of size-related changes of morphological traits (179,181). The results of these analyses could then be expressed either numerically or graphically as linear combinations of the measured variables. However, while these methods were useful their primary disadvantage was that the geometric relationships among variables were not preserved in the measurements taken of organisms. As a result, measures taken from two individuals of different shape could produce identical results, since the data did not account for where measures were taken relative to each other. Figure 2.11 shows an example where size variables cannot sufficiently describe the shape of two specimens.

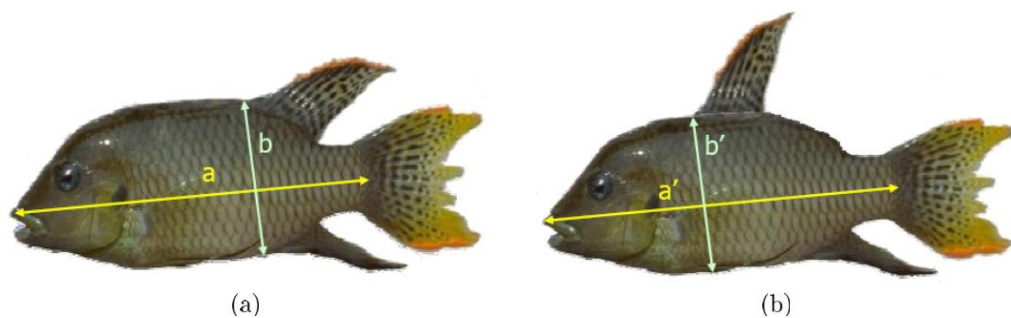


Figure 2.11. Example of traditional morphometric analysis limitations when comparing length and width measures taken from two fish of different shape. adapted from (180).

Also, no single method could be decided upon to scale organisms to a common size (32). This was significant, since different methods of scaling would lead to different results in the subsequent shape analysis. Finally, since geometric information was not preserved among the measured variables it was not possible to create graphical representations depicting differences or changes in shape following the analysis (179,182).

2.3.2 Geometric Morphometrics

The inherent issues in the data being collected and the methods being used previously led to the development of an established framework for the statistical analysis of shape, known as geometric morphometrics (GM) (32,33). These methods quantify biological shape variation using the coordinates of anatomical landmarks after the effects of non-shape variation - location, rotation and scale - have been mathematically held constant, otherwise known as the Procrustes paradigm (33). These methods have emerged as a result of developments in statistical shape theory (30), as well as a conceptual understanding of mathematical shape, defined by Kendall as: "*Geometric information that is left when differences attributed to translations, rotations, and dilations have been quotiented out from an object*" (31) (p82). This development represented a significant shift within the field of morphometrics, involving changes in both the types of data that were collected to quantify shape - landmarks, curves and surfaces - and the methods used to analyse biological shape variation (33). The process of superimposing landmark configurations and obtaining shape variables is achieved using a Generalised Procrustes Analysis (GPA), consisting of a series of procedures (183,184). Figure 2.12 provides a simplified demonstration of the Procrustes superimposition procedure between two skulls, by Baab et al. (185). First, configurations of landmark coordinates are obtained to describe each specimen, recording the relative positions of meaningful anatomical landmarks (Figure 2.12a), which must be equal for all specimens within a sample. The geometric centres (centroids) of these configurations are calculated (Figure 2.12b) and then translated to the origin (Figure 2.12c), superimposing the configurations of landmarks into a common coordinate system. Both landmark configurations are then scaled to unit centroid size, defined as the square root of the sum of squared distances of landmark points from the centroid (Figure 2.12d). Finally, both configurations are optimally rotated to minimize the squared differences between corresponding landmarks (Figure 2.12e).

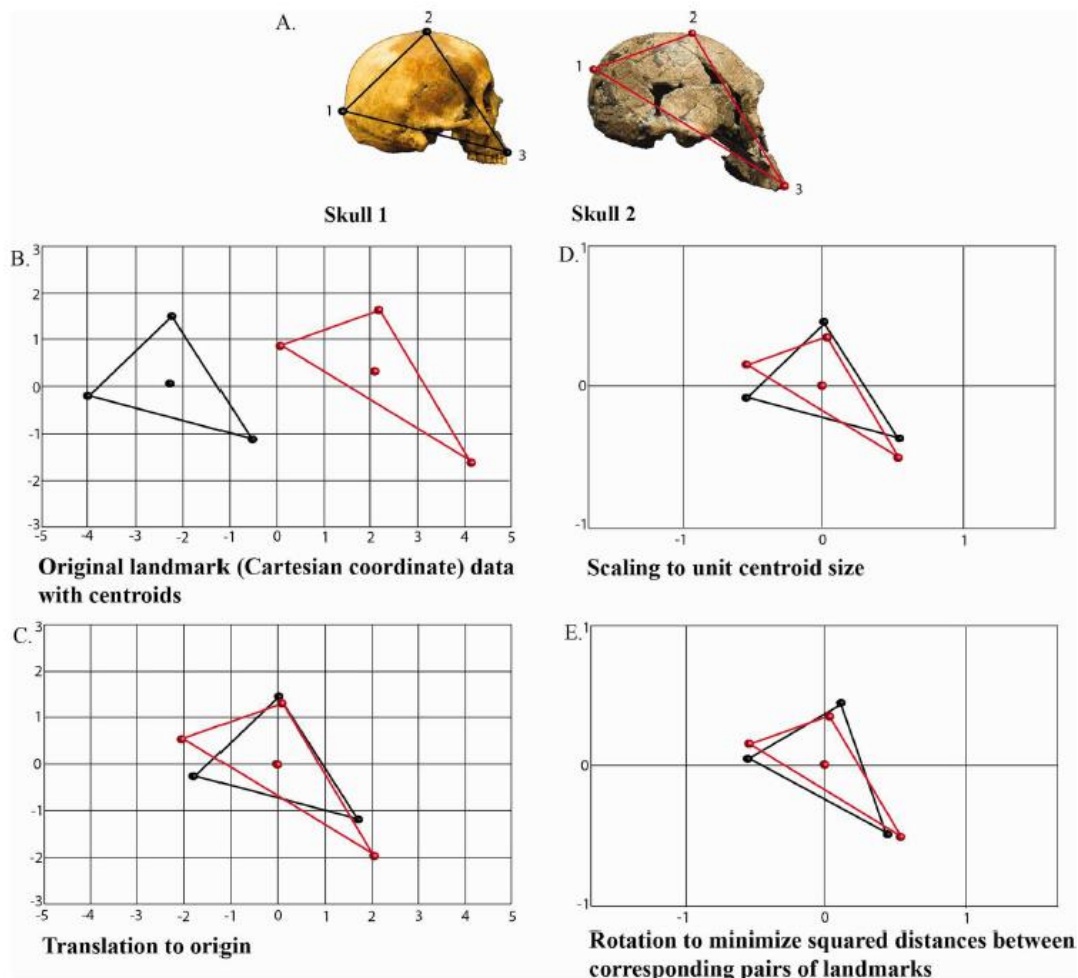


Figure 2.12. Procrustes superimposition procedure. a) Identify anatomical landmark coordinates; b) Calculate centroid; c) Translation of configuration centroids to origin; d) Scaling landmark configurations to unit centroid size; e) Minimise rotational differences between landmark configurations (185).

Following superimposition, these "*Procrustes shape coordinates*" describe the location of each specimen within a high-dimensional space - Kendall's shape space - which represents all possible variations of organisms described by a given number of landmarks points (30,31,186). This constructed shape space is a complex, multi-dimensional analogue of curved surfaces, the dimensionality of which is calculated as $2k - 4$ (for 2D configurations), or $3k - 7$ (for 3D configurations), where k is the number of landmarks, and are therefore difficult to visualize for all but the simplest landmark configurations. For example, variations of 2D triangle landmark configurations can be viewed as points on the surface of a sphere (Figure 2.13). The distances between individual specimens within this shape space represent their differences in shape, with most analyses quantifying the multi-dimensional deviations from the sample mean at the pole (187). Multi-dimensional ordination methods, such as PCA, or canonical

variates analysis (CVA) are most commonly used to analyse the identified shape variations within the sample (180,185).

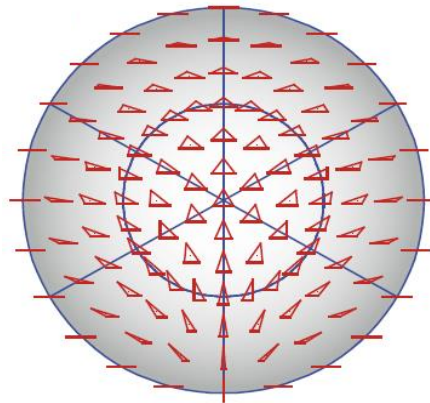


Figure 2.13. Kendall's shape space, showing all possible variations in triangle shape from the mean (181).

Semi-landmarks

A typical GM analysis uses biologically homologous landmark points between all specimens. However, a limitation of landmark-based GM methods is that the external shape of many biological structures cannot be sufficiently captured using traditional landmarks, such as smooth outlines or surfaces. Important shape variations may also be located in the regions between biologically meaningful landmarks. Therefore, the sliding semi-landmark method was developed, which is an extension of standard Procrustes superimposition, whereby a number of points are digitised along an outline and optimally positioned to enable the analysis of 2D or 3D outline curves and surfaces (188,189). Semi-landmarks are used to represent homologous curves and surfaces by sets of points, establishing a geometric homology between corresponding semi-landmarks across the sample (Figure 2.14a). The requirement for homology must guide any landmark and semi-landmark measurement protocol. Points that are well defined by the local anatomy in all directions should be treated as traditional landmarks, such as the red points shown in Figure 2.14b. Semi-landmark points can then be positioned between these more traditional landmarks along clearly observable curves, such as ridges (Figure 2.14b). The number of semi-landmarks required depends on the complexity of the curve or surface and the spatial scale of shape variation that is of interest (189). This new form of GM analysis has been used to analyse shape in several studies where the forms under investigation cannot be sufficiently quantified using

only traditional landmarks, including: orthodontics (190,191), human hip and lumbar spine morphology Pavlova (34) and recently analyses of human body shape (192).

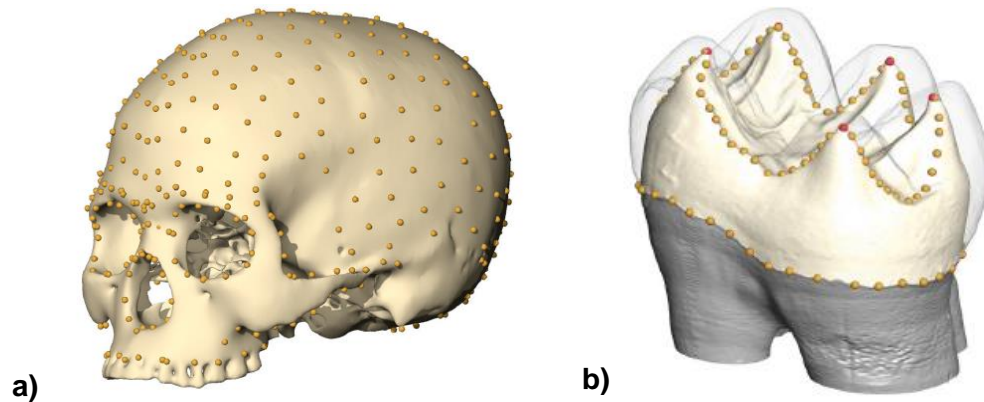


Figure 2.14. Landmarks and semi-landmarks positioned on the surface of 3D computed tomography (CT) scans of a) a human skull and b) a human tooth (189).

2.3.3 Outline-based analysis

The biggest disadvantage of landmark-based GM methods is that certain organisms have an insufficient number of anatomical landmarks available to capture their morphology, such as bird feathers (193) and taxonomic analysis of fish (194). An alternative to GM landmark-based analyses is to use outline-based methods, which extracts a finite set of numerical features from the outline boundary of an object (180,195). There is substantial psychological evidence to suggest that humans intuitively perceive shape differences between objects and individuals by identifying scale-invariant features, such as curves and lateral contours, present on the outside of a body (169,196). Several studies have investigated different methods to characterise the shape of boundary curves (195,197–199), the most common relying on the use of Fourier descriptors, first described by Cosgriff (200). This approach consists of a series of analytical steps (Figure 2.15). First, points are digitised along an outline boundary and a mathematical function $\theta(l)$ is defined, which measures the angular direction of the curve as a function of arc length (195) (Figure 2.15a and 2.15b). After normalisation this periodic function is expanded in a Fourier series, with the coefficients calculated from a fast-Fourier transform used to describe the shape features of the original curve as a sequence of complex numbers representing amplitude and phase angle (Figure 2.15c and 2.15d). Though these Fourier descriptors obtained using outline-based methods differ from landmark-based analyses, they are also scale-invariant and can therefore be used to evaluate shape according to Kendall's mathematical definition. Higher order Fourier coefficients have been shown to

represent direction changes of the curve over very small arc lengths and can be removed whilst preserving the overall shape of the original curve and reducing the noise present within the signal (195).

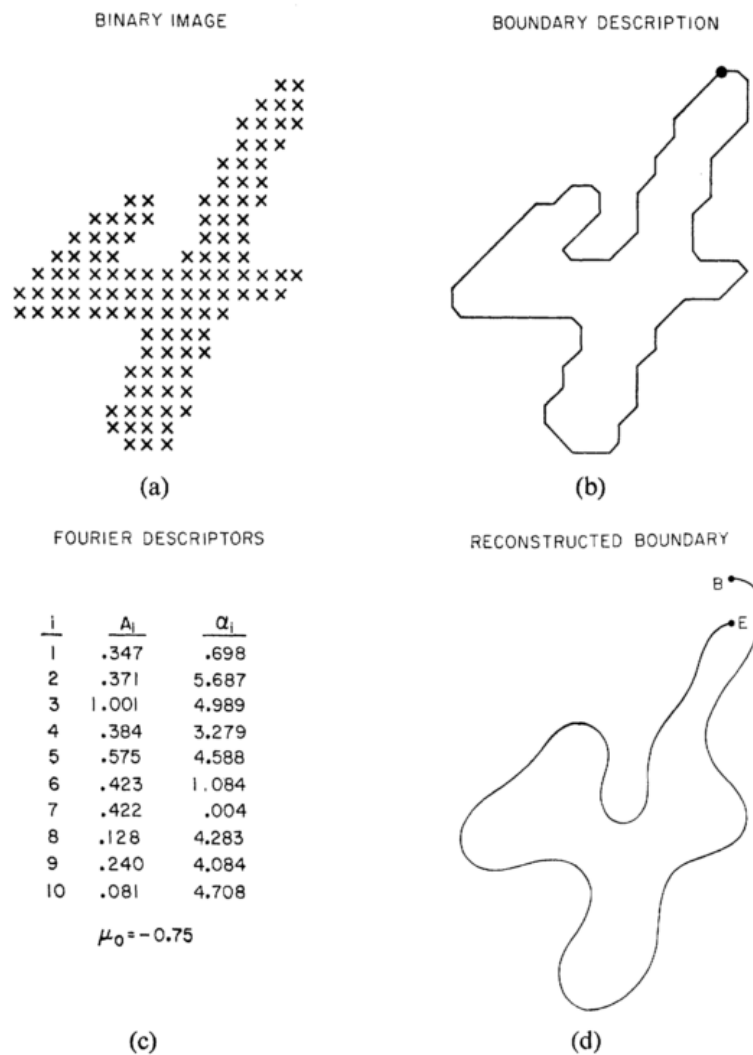


Figure 2.15. Fourier descriptor analysis and reconstruction of the boundary outline curve of a binary image. a) binary image of a printed numeral of the number 4, b) polygonal boundary description of binary image, c) first ten pairs of harmonic amplitude and phase angle of boundary, d) reconstructed boundary from the first ten Fourier descriptors (195).

A limitation of outline-based approaches is that they are unable to capture shape changes in locations which aren't along the boundary of an object when analysing 2D image data, and are difficult to implement when analysing 3D objects without the use of 3D imaging devices (180). However, recent developments in 3D imaging devices and their increased availability has provided new types of data which can be used to perform in-depth 3D shape analyses of organisms (33). In addition, a recent development within GM has been the combination of landmark-based and outline-based analyses into a single method, which uses the advantages and addresses the

limitations of both methods (180). This method proposes the use of sliding semi-landmarks positioned between meaningful anatomical landmarks along the outline boundaries of objects, as well as using the coordinates of traditional landmarks on the object surface. However, currently there is no established methodology when using these proposed combined methods, requiring further study.

2.3.4 Allometry

The term allometry is defined as the dependence of shape on size and tends to be one of the dominant factors of morphological variation and can be studied effectively using GM (181). The most common method for studying allometry in GM is the multivariate regression of shape on a measure of size, such as centroid size or log-transformed centroid size (181,201). According to statistical shape theory, measures of size and shape are logically separate, so multivariate regression analysis is therefore able to test whether there is a statistical association between them and characterise the expected change in shape per unit of increase in the measured size variable. The calculated regression model partitions the total variation of each dependent variable into a component of variation that is predicted by the independent variable(s) and a residual component of variation for which the regression cannot account (Figure 2.16). In the context of allometric analyses, the dependent variables are measures of shape, which can be represented as Procrustes coordinates, Fourier descriptors of outline curves, or features of shape variation resulting from multivariate analysis, such as principal components analysis.

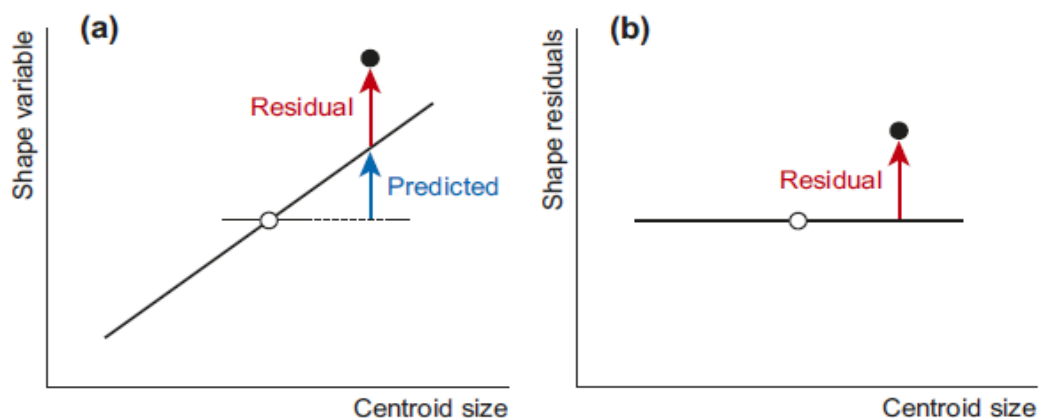


Figure 2.16. Allometric analysis in geometric morphometrics. a) Allometric regression of shape on size; b) Size-correction (181).

The predicted and residual components of shape variation can be expressed as a percentage of the total variation, which is a useful and intuitive way to quantify the

relative importance of allometry for the shape variation within a dataset. Several studies of allometry have used this approach in different contexts and often found that allometry accounts for small to moderate proportions of the total shape variation (201,202). This procedure of partitioning predicted and residual shape variation is also referred to as size correction and is an important application of allometry (181,203). Though the Procrustes superimposition procedures conducted at the start of any GM analysis extracts shape information from the raw data, the shape data may still contain a component of size-related shape variation due to the effects of allometry. The multivariate regression offers a logical and straightforward approach to identify and possibly remove this allometric component of shape variation (Figure 2.16). The residual component encompasses the non-allometric shape variation and is uncorrelated with the size measure used as the independent variable in the regression. In addition, if a linear relationship between the size and shape variables can be assumed, the expected value of the residual (non-allometric) variation will be the same for individuals of any size within the sample. However, when performing allometric analysis using multivariate regressions of shape on size, estimates of allometry can be unstable if the sample only includes a limited range of sizes. If only a small range of body sizes are considered only a short section of the allometric trend is being evaluated by the data, which could result in the proportion of shape variation that allometry does account for being underestimated (181). Therefore, when performing allometric analyses of a particular population researchers should always try to include the extremes of the body size distribution, the smallest and largest specimens, to enable stable estimates of allometry.

2.3.5 Summary

Geometric morphometrics is an established framework for the statistical analysis of biological shape based on the coordinates of biologically homologous landmarks, which has emerged as a result of developments in statistical shape theory and a conceptual understanding of mathematical shape. Alternative methods also exist, based on the quantification of boundary outline curves of organisms through Fourier analysis, with variations in shape then able to be compared using multivariate analyses. Relationships between the size and shape of organisms can also be evaluated through allometry and size correction, to isolate the variations in shape which cannot

be explained by traditional measures of size. However, few investigations have explored how of shape analysis methods can complement existing anthropometric techniques in the assessment of external human morphology.

2.4 Chapter summary

This literature review suggests that measures of human body size and shape are an important source of information for several applications. Traditionally, practitioners and researchers acquire body measures using low cost, manual measurement tools, such as tape measures and callipers, which provide measures of body size, including lengths and girths, as well as derived indices, such as the BMI and WHR. However, though manual measures are easy to acquire, they are prone to human error and are unable to capture complex 3D variations in human body shape.

Since the end of the 20th century, there have been significant advances in 3D imaging devices which capture detailed and accurate external dimensions of the human body and have the potential for use within health applications. However, previous studies which have employed 3D imaging systems to capture external human geometries have only assessed body shape based on the ratios and relative proportions of simple anthropometrics. This reduces the rich, complex data acquired by 3D imaging devices to simple 1D measures, which do not fully utilise the capabilities of this technology. As such it would appear that further research into more sophisticated shape anthropometrics which capture additional information that cannot be explained by existing anthropometrics is warranted. However, there are several potential sources of measurement error, such as scan accuracy, anatomical landmark identification, as well as postural and movement artefacts caused by the participant that must be considered when performing digital anthropometry.

Geometric morphometrics is an established set of methods within the fields of anthropology and evolutionary biology to analyse morphological variation and allometry between the size and shape of organisms. Though these methods have been used extensively to analyse biological shape, few studies have investigated how geometric morphometrics can be used to analyse the external form of the human body from an anthropometric perspective.

Chapter 3 - Methodology for 3D imaging data collection and post-processing

3.1 Introduction

More sophisticated measures of body shape, obtained using 3D imaging technology, could provide additional information regarding variations in human morphology, which cannot be captured by existing anthropometric techniques (2,114,152). The literature review highlighted an established set of methods, known as geometric morphometrics (33,182), which have the potential to be used for analysing variations in human body shape. These methods typically use Procrustes superimposition methods to align configurations of anatomical landmarks on the surface of skeletal structures to quantify shape variations of biological organisms. However, due to the lack of homologous landmarks present on the external human form few studies have utilised geometric morphometric methods to analyse human body shape (34,192). Alternative outline-based methods have been proposed in order to identify scale-invariant shape features (195,197–199). These methods often rely on the use of Fourier descriptors to describe curves and contours present on the surface of smooth bodies (200). Though 3D imaging and geometric morphometrics present several advantages over traditional anthropometric techniques, both require several complex processing steps to obtain shape measures, which can also contribute to measurement error (18). This chapter details the development of data acquisition and post-processing procedures, based on modifications of geometric morphometrics, to enable the measurement of human body shape for use throughout this programme of research. This procedure will consist of the following stages:

1. Define body segment region of interest.
2. Acquire 3D imaging data.
3. Digitise anatomical landmarks.
4. Align 3D imaging data.
5. Segment 3D imaging data.
6. Scale 3D imaging data to uniform size.
7. Dimensionality reduction
8. Shape feature detection.

3.2 Data acquisition

3.2.1 Participants

Through convenience sampling, 43 male participants (age 33 ± 12 years, stature 179.8 ± 7.2 cm, mass 82.9 ± 16.2 kg), volunteered to participate in this investigation. Before testing all participants completed an initial screening form and provided written informed consent. Participants were required to be over the age of 18 years and able to stand unaided during manual and 3D scan measurement procedures. All procedures and documents were approved by the Sheffield Hallam University Research Ethics Committee, reference number ER5855905 (Appendix 2). 3D imaging data acquired from this sample of participants was used to develop methods used throughout this programme of research. Further analysis of this participant sample is conducted in Chapter Five.

3.2.2 Define body segment region of interest

Rationale

The analytical procedure developed for this programme of research is only concerned with the torso segment. It has been suggested that the torso is the region of the body that has the greatest potential for differences in size and shape between participants, due to considerable variations in the types and amounts of tissue present within the abdomen (204,205), and therefore a new technique for assessing human morphology would be more sensitive to changes in this segment. However, as discussed in Chapter Two, variations in body composition and subsequent external body shape in other parts of the body provide information about different disease risks; such as larger amounts of subcutaneous thigh fat being independently associated with more favourable glucose and lipid levels after accounting for abdominal fat depots (79). Though it is accepted that only assessing the torso segment is a limitation of the developed procedure, this programme of research represents an initial exploration of geometric morphometric techniques for assessing human morphology and future work will aim to extend these techniques to enable assessment of the rest of the body.

Previous studies evaluating the human torso have used different configurations of anatomical landmarks to define the boundaries of the torso segment (144,205,206). A modified version of the lower trunk segment proposed by Wicke (205) was used to

define the limits of the torso for this investigation, as the area encompassed between the xiphoid process and the anterior superior iliac spine (ASIS) landmarks (Figure 3.1). The xiphoid process was chosen as the superior boundary of the torso as it has high palpation repeatability compared to other upper body bony landmarks, even among newly accredited anthropometrists (106). In addition, the xiphoid process represents a homologous landmark that is consistent between different participants, as opposed to the nipples which can vary greatly in their location due the sex and total body fat mass of participants. Finally, using the xiphoid process as the superior boundary of the torso reduces potential complications in scan segmentation caused by occlusion at the axilla (armpit), discussed further in Section 3.3.3. Similarly, the ASIS landmarks were used as the inferior boundary of the torso segment due to their relative ease of palpation and to reduce issues with scan segmentation due to occlusion at the perineum (crotch), which can be caused by variations in participant posture and adiposity.

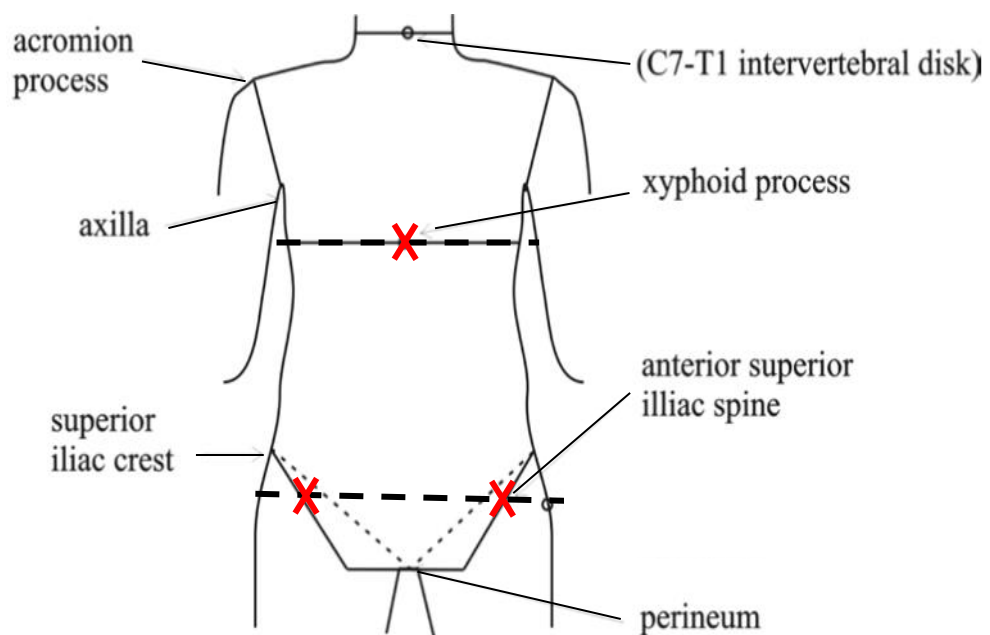


Figure 3.1. Modification of trunk segment boundaries defined by Wicke (205); red crosses show the location of the xiphoid process and ASIS landmarks used to define the superior and inferior boundaries of the torso segment, respectively, dashed lines show the planes created by these landmarks.

Anatomical landmarking

To define the torso segment as outlined above and to facilitate the creation of a local coordinate system during post-processing, four anatomical landmarks were marked on the surface of each participant:

- Xiphoid process - the most inferior aspect of the sternum (207) (p.104).
- Iliospinale (left and right) - the tip of the anterior superior iliac spine (53) (p.36).
- 9th Thoracic vertebra - the spinous process of the vertebra level with the xiphoid process on the posterior torso aspect.

These anatomical locations were manually palpated and identified by a level one ISAK kinanthropometrist (the author) and marked with a cross on the skin using a fine-tipped surgical marker (e.g. Viscot 1451) (Figure 3.2). These marks assisted in the identification and digitisation of the anatomical landmarks in the acquired 3D images. All manual palpation was conducted by the same level one ISAK anthropometrist to ensure a consistent approach.



Figure 3.2. Marked anatomical landmarks on a human participant; anterior torso aspect (left) and posterior torso aspect (right).

3.2.3 Acquire 3D imaging data

3dMDbody5 imaging system

3D imaging data of the torso segment was captured using a 3dMDbody5 (3Q Technologies Inc., Atlanta, GA) surface imaging system. Previous studies have demonstrated that the 3dMDbody5 imaging system is capable of providing reliable and valid measures of human torso morphology, which can be used to assess clinical outcomes in studies of bony and soft tissue pathologies, such as scoliosis, obesity and

edema (208). The 3dMDbody5 system produces 3D geometries using stereo photogrammetry, with multiple synchronized cameras acquiring images of an individual taken from different viewpoints. 3dMDbody5 is a hybrid stereo photogrammetry system, which uses natural landmarks on the surface of the target object, as well as deformation of a projected light pattern to enable triangulation and image processing to create 3D representations of a bodies external geometry (115,131). The additional landmark points provided by hybrid systems makes the procedure of matching and alignment both quicker and easier, resulting in higher accuracy (point-point distance < 0.2 mm) and very short scan duration (~1.5 ms) (128). The 3dMDbody5 system used in this programme of research consisted of five synchronised modular units, each containing three machine vision cameras, which were arranged around a square 258 × 258 cm aluminium Bosch (Bosch Rexroth AG) strut frame (Figure 3.3a).

System calibration

The 3dMDbody5 system uses a single computer (64 Bit Windows 7 Professional 4 Core CPU @ 3.6GHz 8GB RAM) to drive the imaging system, with calibration and data collection procedures performed by proprietary 3dMD acquisition software. The calibration procedure followed 3dMD guidelines using a calibration plate and was conducted at the start of each testing session. Each camera unit was manually aligned to the centre point of a calibration plate (Figure 3.3b) positioned in the centre of the imaging system. Once aligned, a series of images were captured of the calibration board in five rotated positions using the 3dMDbody5 acquisition software, with each individual camera unit obtaining two images of the calibration board. The 3dMDbody5 acquisition software then automatically calibrated the system. This process took ~3-5 minutes and created a calibrated cylindrical capture volume of 0.089 m³; 0.56 m in height, with a radius of 0.23 m (Figure 3.3c).

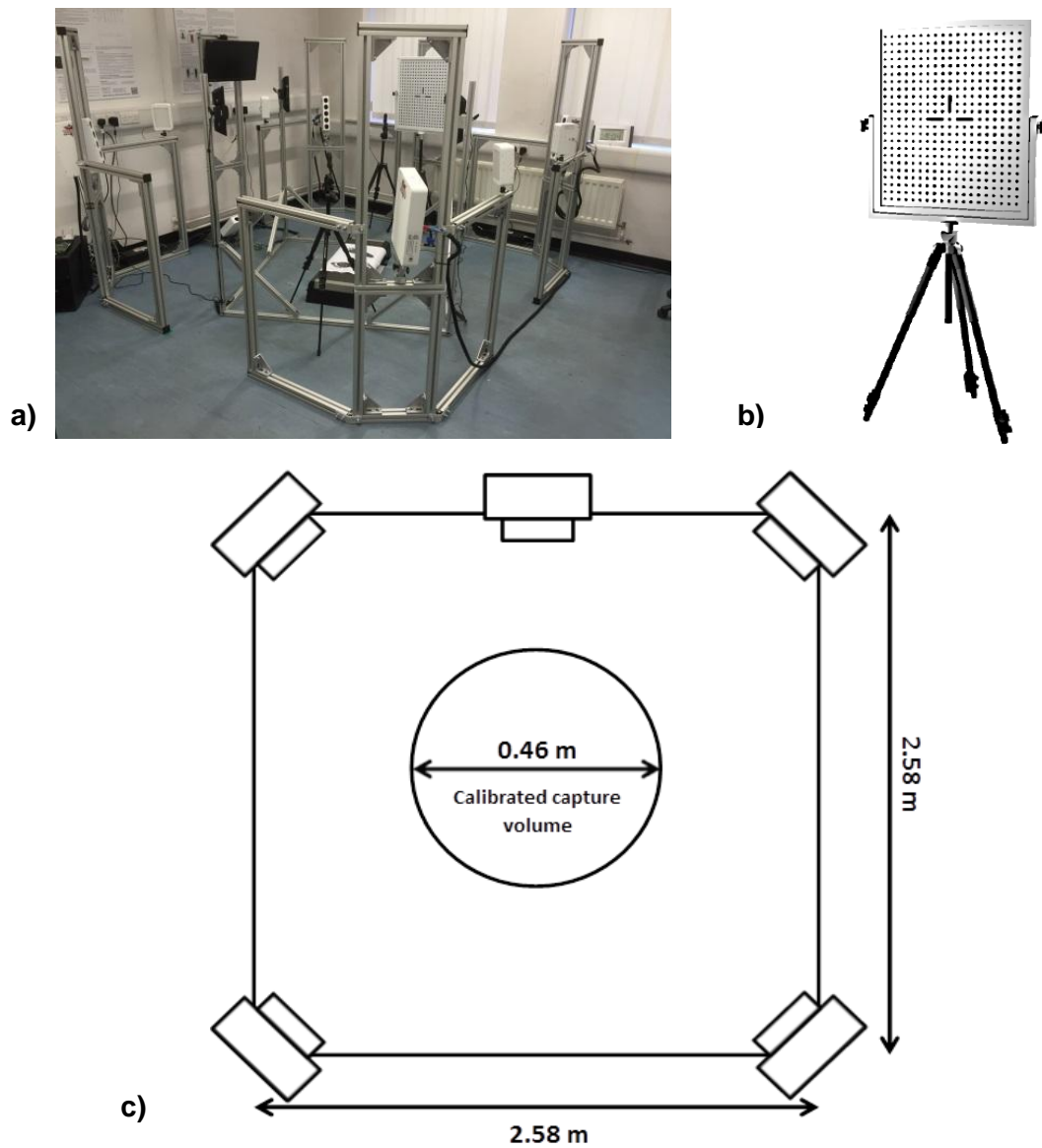


Figure 3.3. a) 3dMbody5 system; b) 3dMD calibration board; c) plan view of 3dMbody5 imaging system layout and calibrated volume.

3D imaging protocol

For torso scanning, participants were asked to adopt a modified version of the standing anatomical pose defined by ISO 20685-1:2018 (140), with their arms abducted from the torso by approximately 35° and their legs apart (Figure 3.4). Correct adoption of this posture was verified by visual inspection. This posture ensured that participants' arms were well separated from their torso segment, reducing the risk of occlusion within the acquired 3D image, whilst enabling participants to maintain a relaxed position during the imaging process. Variations in posture could affect the test-retest reliability of the analytical procedures presented in this chapter and will be considered further in Chapter 4.

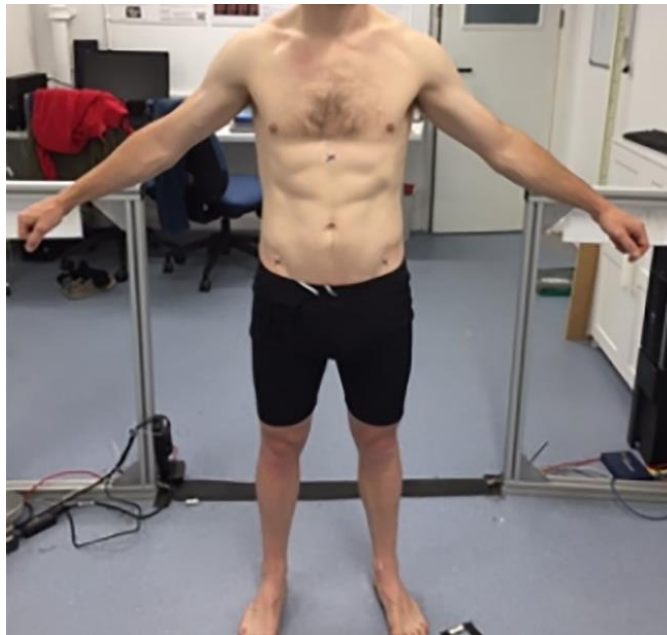


Figure 3.4. Scanning pose for torso segment scanning adapted from ISO 20685 (140).

To minimise postural sway all participants were asked to visually focus on markers mounted on the wall of the scanning area, since it has been shown that focusing gaze on a stationary target during standing reduces postural sway (209). The typical human breathing cycle has been shown to cause significant changes to the shape and size of the lower torso, due to movements of the diaphragm (126). For this reason it was important to control breathing during the scanning process, ensuring that scans were always taken during the same part of the breathing cycle to improve repeatability of torso shape measures. Participants were asked to hold their breath at end-tidal expiration throughout the short duration of the 3D scan process (~1.5 ms); ensuring participants were in a repeatable and relaxed state.

3.3 3D imaging data post-processing

Following data acquisition, several key post-processing steps were required to remove the effects of non-shape variation - location, rotation and scale - from the acquired imaging data using modified Procrustes superimposition procedures. This enabled variations in human body shape to be analysed, according to mathematical shape (31).

3.3.1 Digitise anatomical landmarks

Initially, a manual digitisation procedure was used to identify the locations of the marked anatomical landmarks within the acquired 3D imaging data. Manual digitisation was implemented, rather than automatic landmark identification or 3D feature identification algorithms, since although the xiphoid process and ASIS

landmarks can be identified reliably when palpated, they cannot be determined from the surface shape of the body alone. Also, since initial investigations would only be analysing relatively small cohorts of participants ($n < 100$) a manual process was deemed acceptable, with the digitisation of landmarks taking approximately 1 minute per participant. A single researcher digitised the xiphoid process, ASIS and 9th thoracic vertebra bony landmarks within each 3D scan image using KinAnthroScan - custom software created in-house - by clicking directly on each manually marked landmark location. Figure 3.5 shows a typical digitised human torso segment, with blue circular markers generated during digitisation to confirm their registration on the surface of the 3D geometry. Once completed, KinAnthroScan returned a set of 3D coordinates for these marked anatomical landmarks, to be used in subsequent post-processing stages.

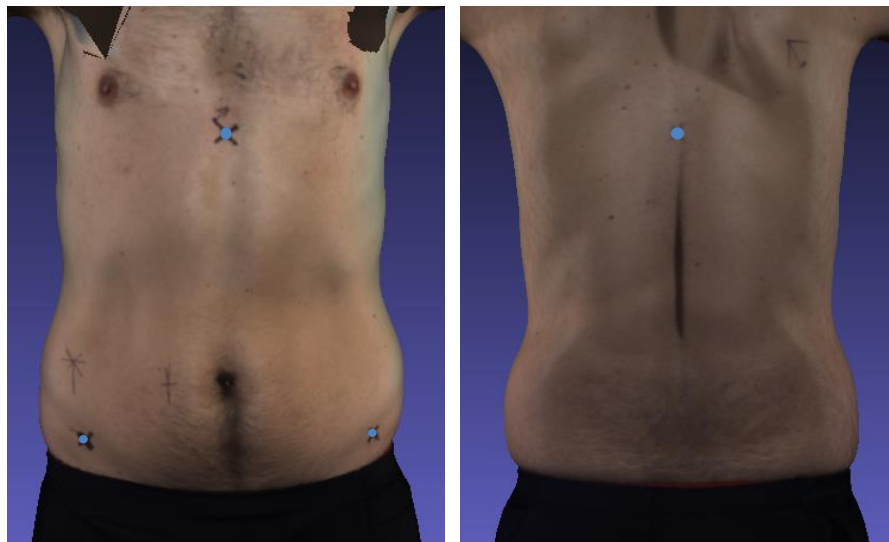


Figure 3.5. Digitised torso scan image in KinAnthroScan; anterior aspect (left) and posterior aspect (right).

3.3.2 Align 3D imaging data

Typically, geometric morphometric analyses use the centroid of landmark configurations to remove variations in location between individual organisms (210). However, since differences in human morphology are caused by variations in the types and amounts of tissue present within the torso region, the centroid of the acquired surface 3D imaging data points would not represent a homologous skeletal landmark between individuals. As a result, centering torso 3D geometries based on the location of the centroid would in fact reduce the morphological variations caused by tissue distributions within the torso segment, which are the features of interest in this programme of study. Therefore, a local co-ordinate system, based on the location of

the digitised homologous bony anatomical landmarks, was created to remove non-essential differences in location and orientation between participants.

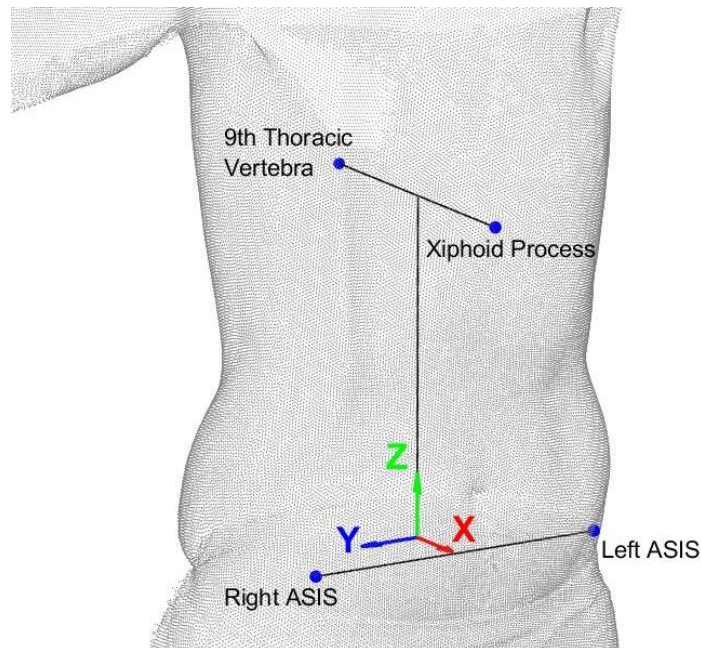


Figure 3.6. The location of landmarks used to create a local coordinate system within the torso segment.

Figure 3.6 demonstrates how the locations of the digitised landmarks were used to create a local coordinate system located at the anatomical centre of each torso scan, according to the convention defined in ISO 20685-1:2018 (140). The centre of the torso was defined as the midpoint between the xiphoid process and the 9th thoracic vertebra. The vector from the xiphoid process to the 9th thoracic vertebra was defined as the sagittal (x) axis. The vector from the left to right anterior superior iliac spine (ASIS) was defined as the transverse (y) axis. The cross product of these two vectors defined the longitudinal (z) axis. Finally, the transverse axis was redefined as the cross product of the longitudinal and sagittal axis to ensure that all axes in the coordinate system were orthogonal. This local anatomical axis system is in accordance with the coordinate axis system recommended in ISO 20685-1:2018 and enabled the 3D geometry of each participant to be aligned to the global coordinate system. This was the first stage in the Procrustes superimposition procedure, minimising differences in location and orientation between participants within the sample.

3.3.3 Segment 3D imaging data

Each acquired 3D image was segmented to include only the coordinate data points relating to the region of interest. This procedure required two segmentation planes to be defined at the inferior and superior torso segment boundaries (Figure 3.7). The inferior segmentation plane was required to pass through the digitised ASIS landmarks while being planar to the x-y plane. Similarly, the superior segmentation plane was required to pass through the digitised xiphoid process and thoracic vertebra landmarks while being planar to the x-y plane. Following alignment, the longitudinal axis of each 3D image was assumed to be at the origin of the global coordinate system and orientated parallel to the vertical axis. As a result, the coordinate points between the two defined segmentation planes could be assumed to contain the coordinate points relating to the torso segment (Figure 3.7).

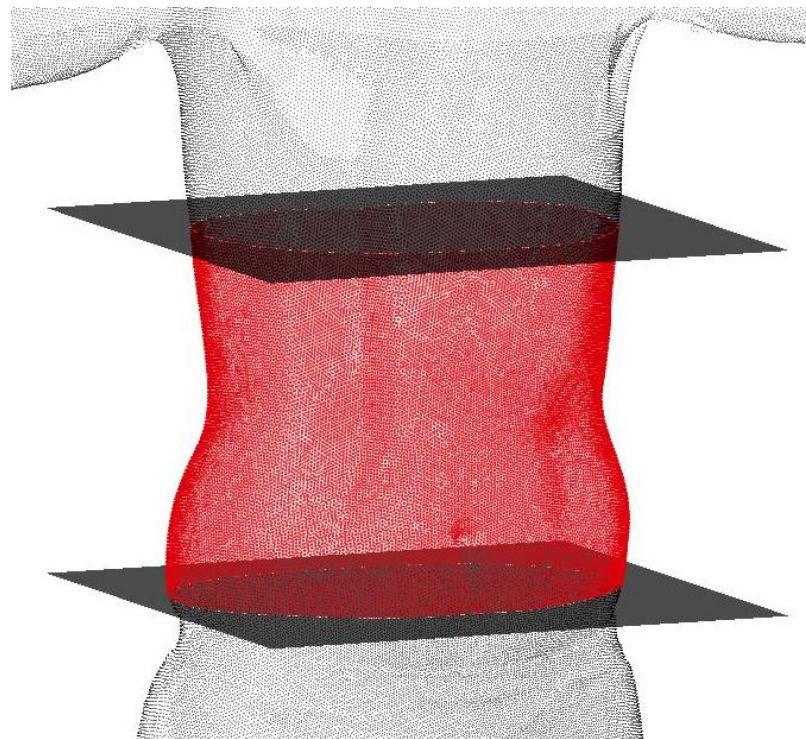


Figure 3.7. Segmentation of a captured scan to include only the coordinate points relating to the torso region of interest (shown in red) between the superior and inferior segment boundaries.

3.3.4 Scale 3D imaging data to uniform size

The final stage in the Procrustes superimposition procedure was to remove the effects of scale. The most commonly used size measure in geometric morphometrics is centroid size, defined as the square root of the sum of squared distances of landmark points to their centroid (33). To ensure that all individuals within a sample are scaled to uniform centroid size, they must all have the same number of landmark points. However, since each torso point cloud will consist of a different number of raw coordinate points, all torso segments needed to be resampled. For this, 21 separate 2 mm thick bands of 3D coordinate points were extracted from each torso segment point cloud, at 5% intervals along their length. Figure 3.8 illustrates this process for a typical torso segment point cloud, with all of the extracted 2 mm thick bands of 3D data points shown. The height of each data slice was set at 2 mm to ensure that the external shape features of the torso segments were preserved, while allowing for any potential gaps in the 3D point cloud. This was based on a previous study by Clarkson et al. (144), which determined that data point slices of 2 mm thickness extracted from low accuracy Kinect depth sensor data sufficiently captured the external features of a torso segment. The increased accuracy of the 3dMDBody5 system imaging data should therefore ensure all torso shape features were suitably captured using this same method.

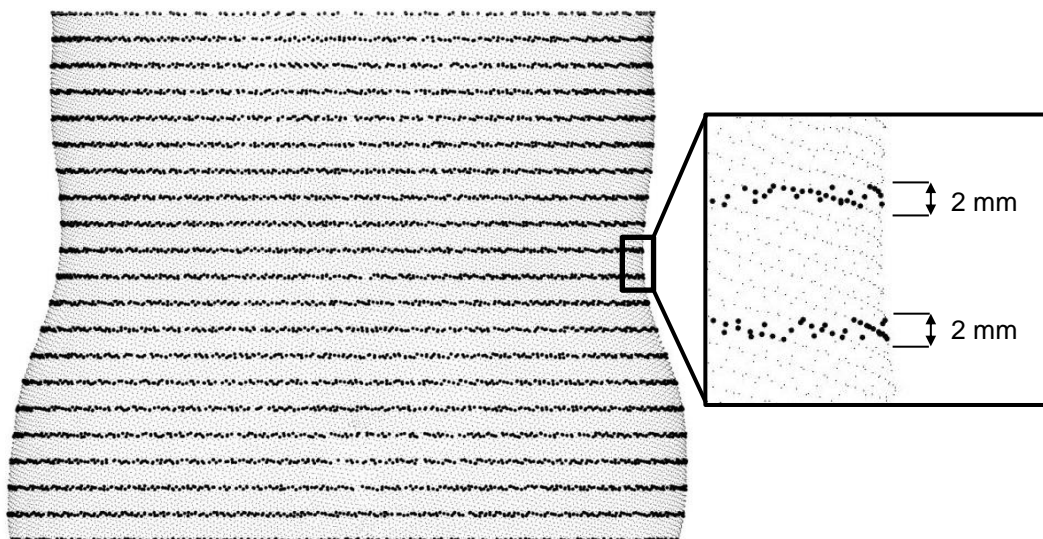


Figure 3.8. Extraction of 2 mm thick slices of coordinate data points at 5% intervals along the torso segment between the inferior and superior segment boundaries.

The inferior-superior z component of all raw data points within each extracted slice were then disregarded, considering the planar dimensions of all data points only in the

x-y plane. Cubic smoothing splines were then calculated for each data slice extracted from the torso segment (211), to represent the underlying curvature present on the external surface of each 3D image and smooth random variations in the raw data (Figure 3.9).

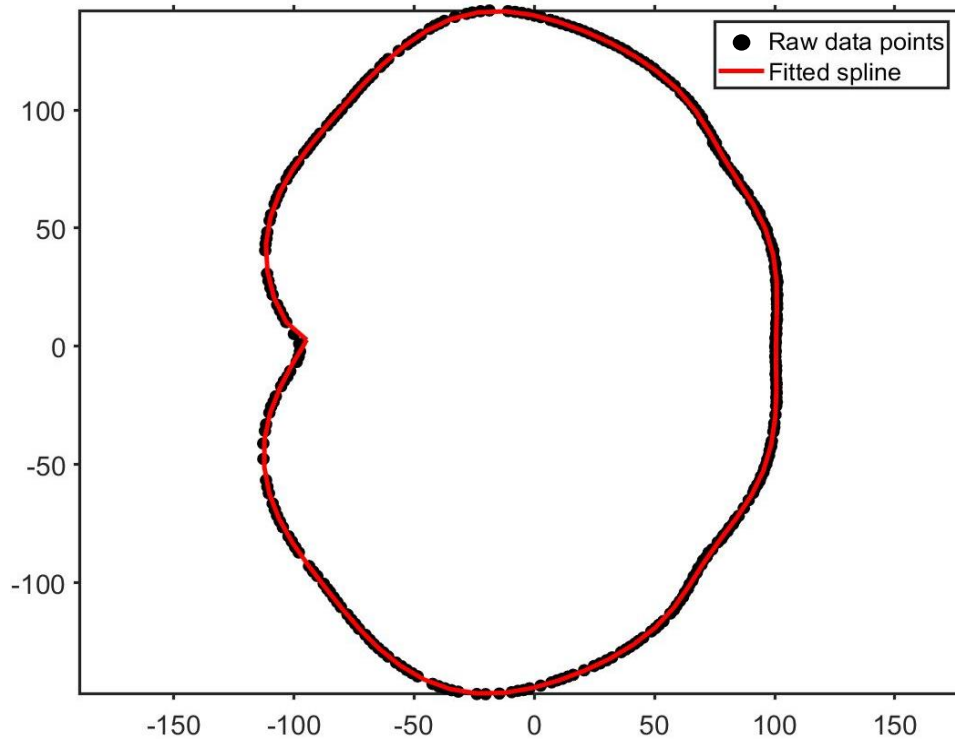


Figure 3.9. Extracted data point slice with a fitted cubic smoothing spline.

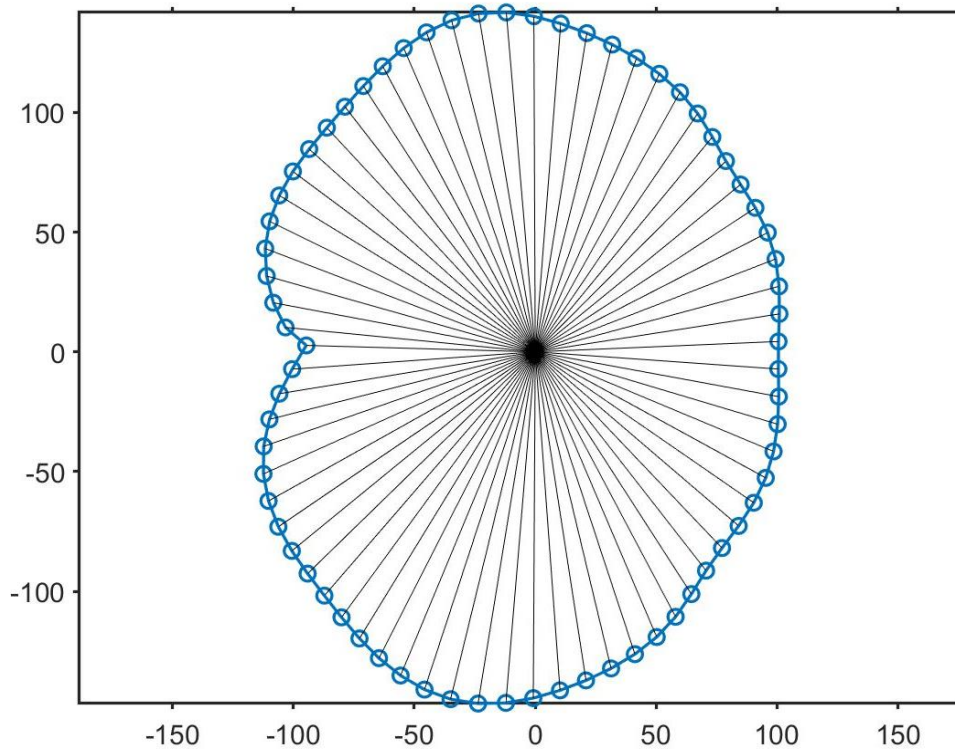


Figure 3.10. Resampled point slice with calculated distances from each coordinate to the centroid.

The calculated smoothing splines of each data slice were then resampled, with a uniform number of equally spaced coordinate points positioned along the length of the outline curve (Figure 3.10). It was determined through experimentation that 70 uniformly spaced coordinate points were required to adequately describe the features present around the torso shape outline and perform subsequent Fourier decomposition procedures. The centroid size of all extracted data point slices along the length of the torso was calculated and summed to give the total centroid size for the entire torso (Figure 3.10). All extracted torso shape profiles were then scaled by a single scale factor, so that the sum of distances from each point to its centroid for all profiles along the torso segment was equal for all participants within the sample.

Finally, the torso segment of each participant within the sample was scaled to uniform height, removing the effect of torso length from the analysis. For this, a uniform distance along the inferior-superior z axis was fixed between each extracted shape profile along the length of the torso segment for all participants (Figure 3.11). Since shape profiles were extracted at proportional distances along each torso segment, they could be assumed to represent the same aspect of the torso for all participants regardless of their torso length. Figure 3.11 shows the meshed torso segments of two individuals, which initially differed in both size and shape, but have been scaled to the same size using the above procedure. According to the mathematical definition of shape and the Procrustes paradigm, any measured differences between these individuals can now be considered differences purely in shape.

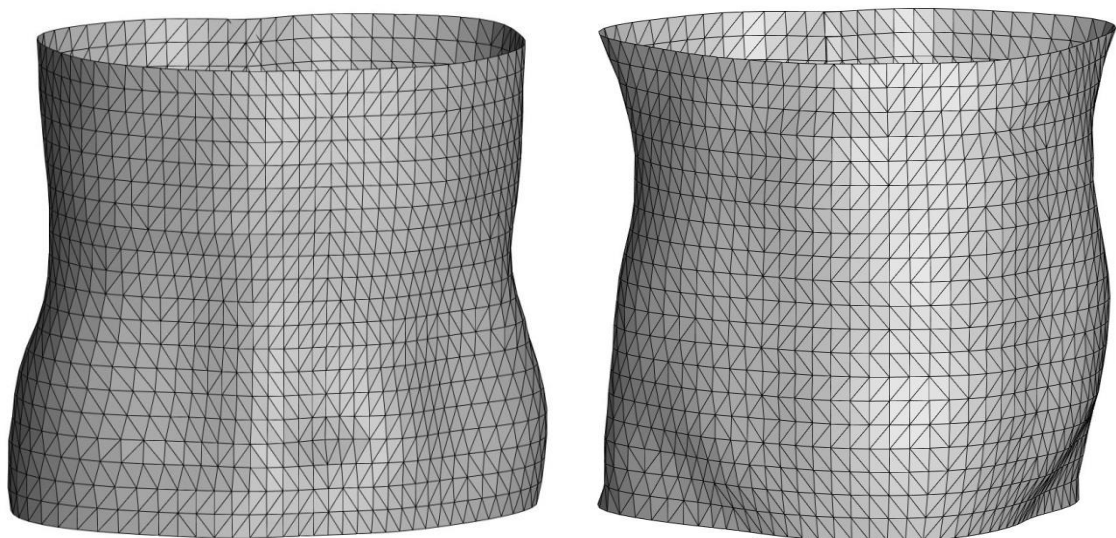


Figure 3.11. Torso shapes of two individuals with the effects of non-shape variation - location, rotation and scale - removed.

3.3.5 Dimensionality reduction

As discussed in Chapter Two, classical implementations of geometric morphometrics methods obtain shape variables by superimposing biologically meaningful, homologous bony landmark configurations using a process known as Generalised Procrustes Analysis (GPA) (183,184). However, a disadvantage of these traditional landmark-based geometric morphometric methods is that certain organisms provide insufficient numbers of homologous anatomical landmarks to describe their external shape. This is particularly apparent when assessing human morphology, which has almost no visible bony anatomical landmarks that are homologous between individuals, but is instead made up of smooth contours and surfaces. In response to this, sliding semi-landmark methods have been developed, whereby a number of points are digitised along an outline and optimally positioned to enable the analysis of 2D or 3D outline curves and surfaces (171,172).

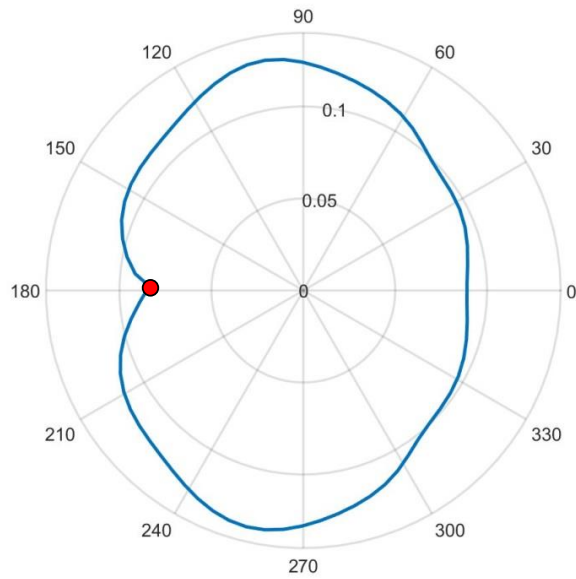
Initial experiments were conducted to explore the use of semi-landmark based analyses for assessing human torso shape. The first iteration utilised the uniformly spaced points around each of the torso outline curves extracted during the scaling operation in Section 3.3.4 as semi-landmarks. The second iteration extracted data point slices from the torso segment based on the three cardinal planes (sagittal, frontal and transverse) (212), in an attempt to reduce the dimensionality of data describing external torso shape. In each of these iterations, a generalised Procrustes analysis (GPA) (184) using the sliding semi-landmark method (189,213) was carried out to obtain sets of shape variables for each of the extracted outline curves for each participant. The landmark configurations of all outlines were superimposed into a common coordinate system to create a mean shape for the sample. This was achieved by translating the centroid of each outline to the origin and then scaling each outline to unit centroid size. The positions of semi-landmarks for each outline were optimally aligned with the corresponding semi-landmarks on the mean shape according to the minimum Procrustes distance criterion (213). This procedure included: calculating the vector tangent to the mean shape outline at each of its semi-landmark points, as well as the vector perpendicular to this tangent passing through each of the semi-landmark points. This was followed by repositioning the corresponding semi-landmark on each outline in the sample at the intersection point between the perpendicular vector and

the outline curve. Finally, the individual shape variables were found by calculating the Euclidean distance from the centroid to each of the semi-landmark points around each profile outline. Though these semi-landmarks were found to be able describe the external shape of the extracted torso outline profiles, it was evident that there were no homologous bony structures for them to be placed relative to. This meant that their placement around the boundaries of the outline curves could only be considered as arbitrary. It has been stated in previous geometric morphometric studies that homology must guide the placement of any landmark or semi-landmark protocol, since it is the differences in these landmark locations that describe variations in shape within the sample (33). As a result, it was decided that a semi-landmark based analysis was not the optimal solution for assessing external human shape.

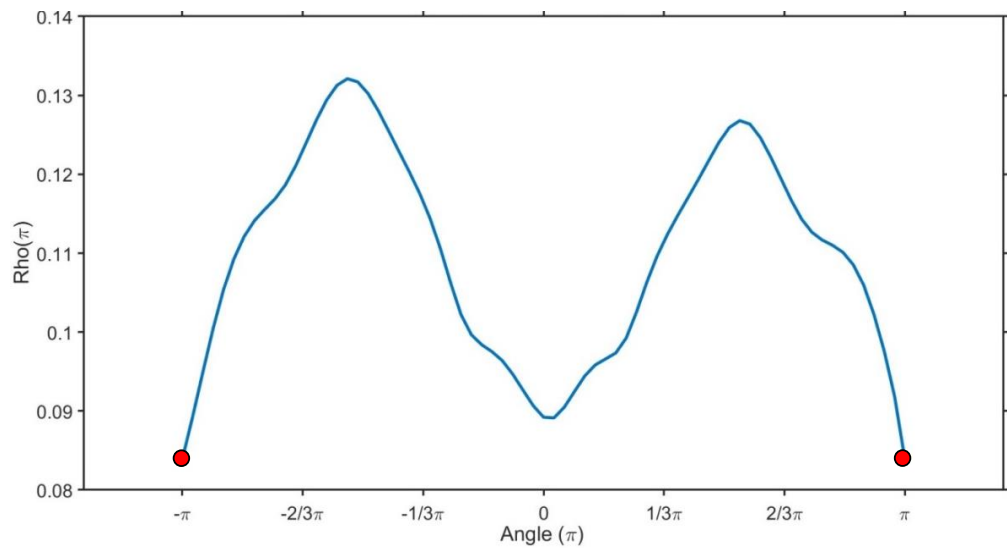
Following these initial semi-landmark based analyses, an alternative outline-based method was investigated using Fourier coefficients extracted from the cubic smoothing splines obtained for each scaled shape profile extracted in Section 3.3.4 to evaluate human torso shape. These methods were based on a previous study by Zahn and Roskies (195). Fourier coefficients were obtained using the following steps:

- The Cartesian coordinate points of each torso shape profile calculated in Section 3.3.4 were converted to a polar coordinate system (Figure 3.12a).
- The polar coordinates within each profile were then plotted as a continuous signal waveform (Figure 3.12b).
- The signal data was then inputted to the fast-Fourier transform (FFT) algorithm in MATLAB (version 9.2, Mathworks, USA) to extract the spatial frequency components within each outline curve (Figure 3.12c). The FFT computes the discrete Fourier transform (DFT) of an input signal by decomposing its sequence of values into components of different frequencies, thereby converting the signal from its original domain (either time or space) to a representation in the frequency domain (214).

a)



b)



c)

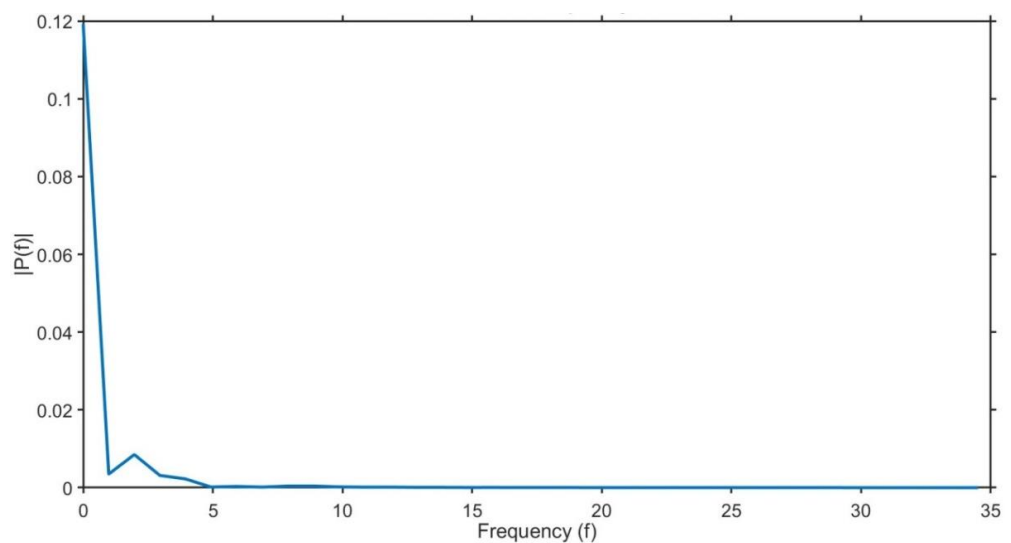


Figure 3.12. Extraction of Fourier descriptors from torso outlines. a) Polar coordinates of a typical torso shape outline; b) Polar coordinates of the torso shape outline plotted as a signal waveform, red dots showing the corresponding start and end points on the polar diagram; c) Representation of the torso shape outline in the frequency domain.

Figure 3.12c illustrates how the majority of the frequency content within a typical torso outline appears to be contained within the first few Fourier coefficients. The DFT is commonly used within digital signal processing as a method of data compression. The selection of the required number of coefficients is task-dependent and relies on the geometrical complexity of the measured signal waveform (215). However, previous studies suggest that Fourier coefficients of high frequencies are assumed to represent unnoticeable, low amplitude noise within the input signal waveform, which can be removed without affecting the shape of the original curve (195). An iterative procedure was conducted to determine the lowest number of Fourier coefficients that were required to reconstruct the original torso outline curves extracted from torso 3D imaging data. The root mean square error (RMSE) was calculated between the original and the reconstructed outline curves along the length of the torso to quantify the information loss caused by using different numbers of Fourier coefficients. Figure 3.13 shows how the RMSE for all outlines along the length of the torso converges asymptotically to zero as the number of Fourier coefficients used in reconstruction is increased.

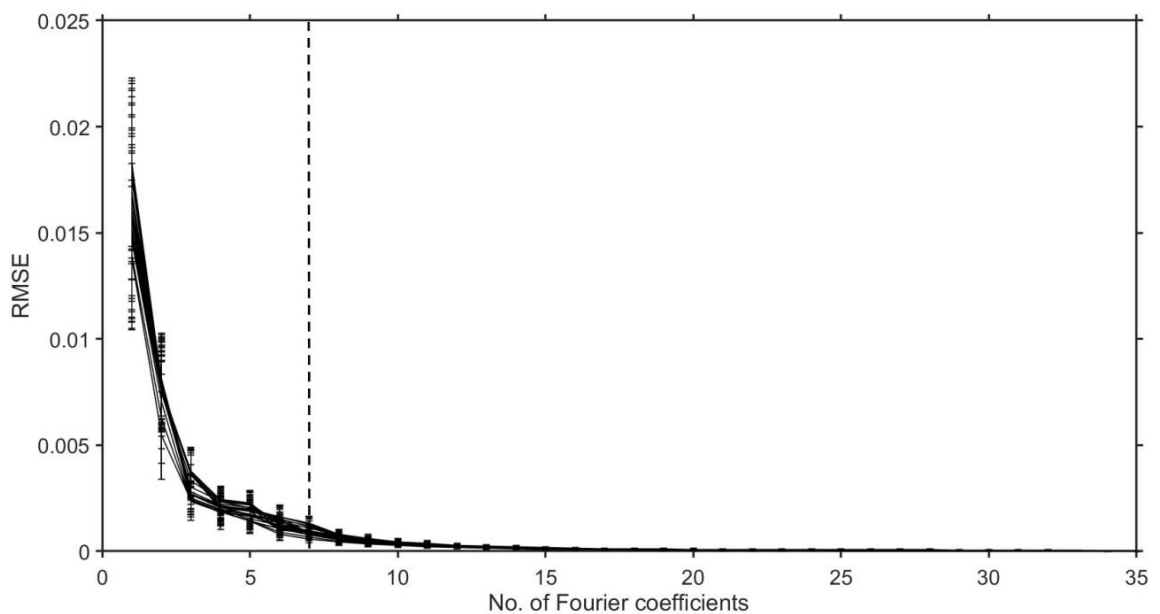


Figure 3.13. Average root mean square error (RMSE) between the original and reconstructed torso outlines for all extracted shape profiles along the length of the torso segment for all participants.

Vertical dotted line shows the initial cut-off point for the number of Fourier coefficients used to reconstruct the original curve, though has been shown to depend on the complexity of the input curve. Initially, 7 Fourier coefficients was chosen as a sufficient number of coefficients to reconstruct the original curves, since it is past the elbow of the RMSE curve and has almost converged to zero, shown as a dotted line in Figure 3.13. However, upon visual

inspection when only 7 Fourier coefficients were used to reconstruct the original torso outline curve this resulted in shape details being lost (Figure 3.14). In comparison, when the number of Fourier coefficients used to reconstruct the original curve was increased to 10, it was possible to recreate all of the features of each original torso shape outline, without any loss of shape information (Figure 3.14). This is due to the reduced standard deviation in RMSE values for reconstructed outlines when using a greater number of Fourier coefficients. This procedure reduced the total number of variables representing each participant to 210 complex Fourier coefficients, which describe the external shape features of the 21 torso outlines extracted from the 3D imaging data. Thus any potential redundancy in the variables required to describe the external shape of the human torso is reduced.

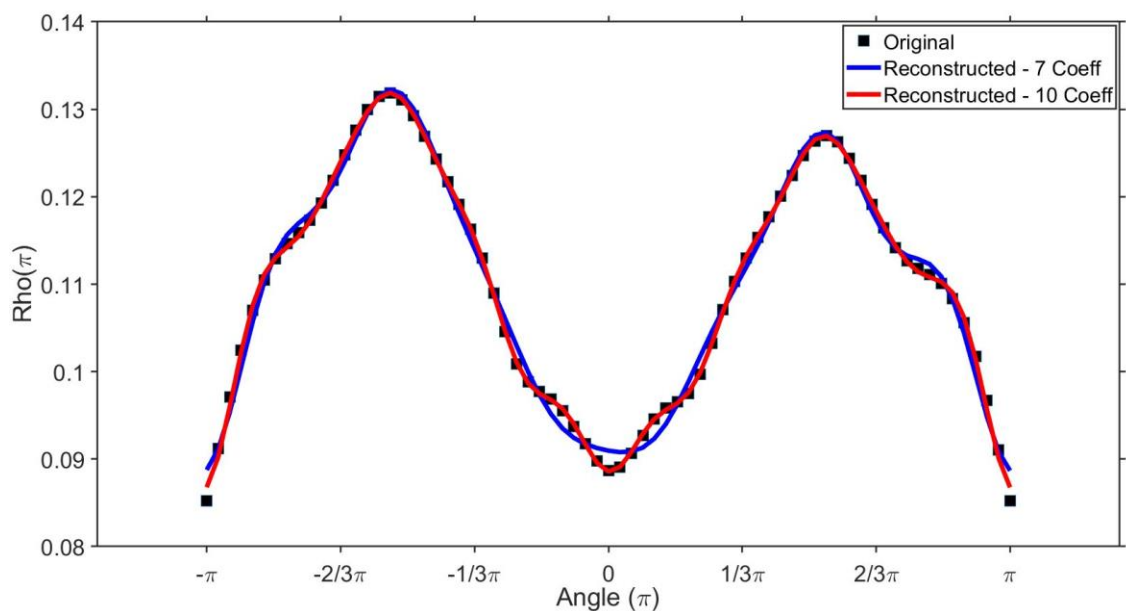


Figure 3.14. Visual comparison between an original torso outline curve (black markers) and reconstructed torso outline curves using 7 Fourier coefficients (blue) and 10 Fourier coefficients (red).

3.3.6 Shape feature detection

The obtained Fourier coefficients, which efficiently describe an individual's external torso shape, can be utilised to analyse variations in body shape within a sample of participants using multivariate analyses, such as principal components analysis (PCA). PCA reduces the dimensionality of a dataset, consisting of a large number of interrelated variables, while retaining as much of the variation present within the data as possible (171), and has been used previously to capture variations in body shape from 3D imaging data (23,170,172). PCA transforms an original dataset into a new set

of variables, principal components (PCs), which are uncorrelated and ordered so that the first few retain the majority of the variation present within the original variables. After the variation in the original variables has been described in terms of the PCs, the orthogonal projections of each individual relative to these new axes are determined. These principal component scores represent the distance of each individual from the sample mean in the directions of the identified PCs. As described, each PC represents progressively less variance, with many higher order PCs representing such small proportions of the total variance it can be assumed that they do not represent biologically meaningful information. A common method for determining how many PCs to omit from subsequent analysis is based on an established criterion of the amount of total variance within the sample that needs to be explained (e.g. 95%), or to only interpret those components that represent more than a certain amount of variance (e.g. 1%) (210). Previous studies by Ruto et al. (170) and Ng et al. (23) have demonstrated that body shape variations are subtle, requiring a greater number of principal components to describe them fully. Consequently, it was decided that for this programme of research only PCs that accounted for more than 1% of the total variance would be included in subsequent analysis.

PCA was thus conducted to investigate its potential for detecting independent features of torso shape variation within the extracted Fourier coefficients of the participant sample. This produced 9 PCs that captured over 90% of the total variation within the sample, with each PC representing at least 1% of total variance. These PCs were transformed back into the original data space and reconstructed as meshed surfaces to visualise the variations in torso shape they represent (Figure 3.15). Figure 3.15a shows the average torso shape calculated from all participants in the sample and the corresponding radar diagram representing the average scores for each of the first 5 PCs. Figure 3.15b shows the normalised maximum and minimum deviations from the average torso shape geometry along each of the first 5 PCs. Blue and red regions represent areas that protrude less, or more from the average torso, respectively. These 9 PCs create a feature vector which describes the torso shape characteristics of an individual, and will be the manner in which human shape is characterised throughout this programme of research. These PCs are analysed further in Chapter Five, to determine whether shape anthropometrics can complement manual anthropometric techniques currently used in practice.

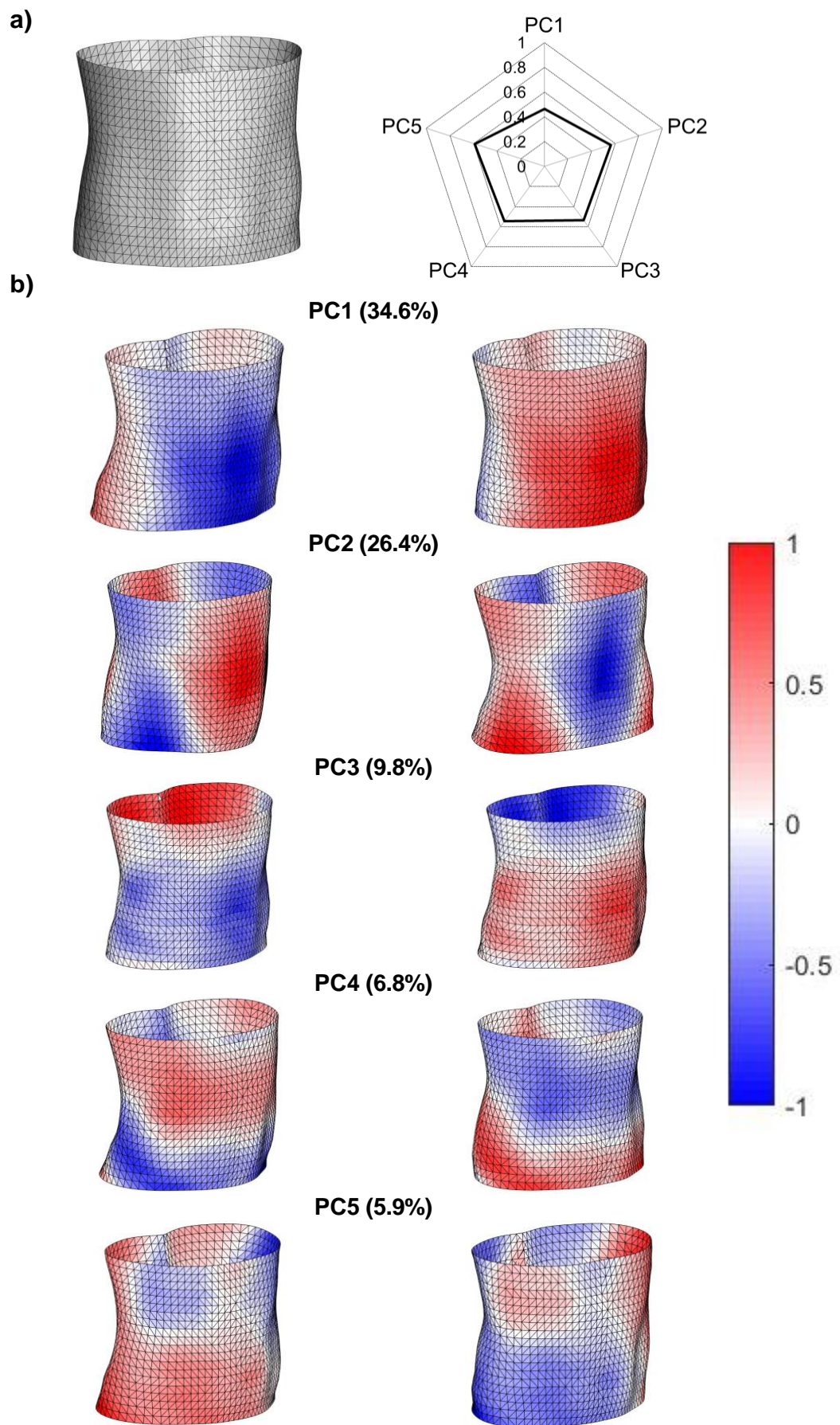


Figure 3.15. Extracted torso shape features; (a) Average torso shape; (b) Maximum and minimum deviations from the sample mean along the first 5 principal components and their explained variance. Blue and red regions represent areas that protrude less, or more than the average torso, respectively.

3.4 Chapter summary

This chapter detailed the development of methods to be used throughout this programme of research. This included procedures for locating anatomical landmarks that define the body segment of interest and acquiring 3D imaging data of the human torso. In addition, data post-processing algorithms were developed to implement geometric morphometric methods of analysis and extract numeric parameters that describe the external shape features of the human torso.

The locations of manually palpated anatomical landmarks were used to define the torso segment region of interest for this research. The locations of these anatomical landmarks were then used to create a local coordinate system at the centre of each 3D image, enabling subsequent alignment and segmentation. As identified in Chapter Two, a potential limitation of using a manual approach for locating anatomical landmarks is human error, both in the researcher palpating the landmarks and participant postural variations. The effect of these potential sources of error and the test-retest reliability of the procedures developed in this chapter will be evaluated further in Chapter Four. In addition, manual palpation and digitisation of landmarks used in the current iteration of the procedure would be feasible for characterising variations within small participant samples, but may not be suitable when assessing larger cohorts. Therefore an area of potential further work could be the automation of methods to enable more efficient data processing.

Procedures were also developed to remove variations in scale, location and orientation from acquired 3D imaging data, enabling the analysis of scale-invariant morphological features according to geometric morphometrics and shape theory. A quick and effective method for segmenting acquired 3D imaging data was also developed. However, this current implementation would not be suitable for analysing multiple body segments or the shape of the human body as a whole. This is a limitation of the current procedure and represents an area of potential further work. In addition, a procedure for characterising human torso shape as complex Fourier coefficients was developed. Though this method appears suitable for describing a typical human torso segment, other body segments, such as hands or feet, may not be able to be described sufficiently using this technique and would require further consideration.

The developed procedure to be used throughout the subsequent investigations in this programme of research can be summarised in a sequence of analytical steps (Figure 3.16).

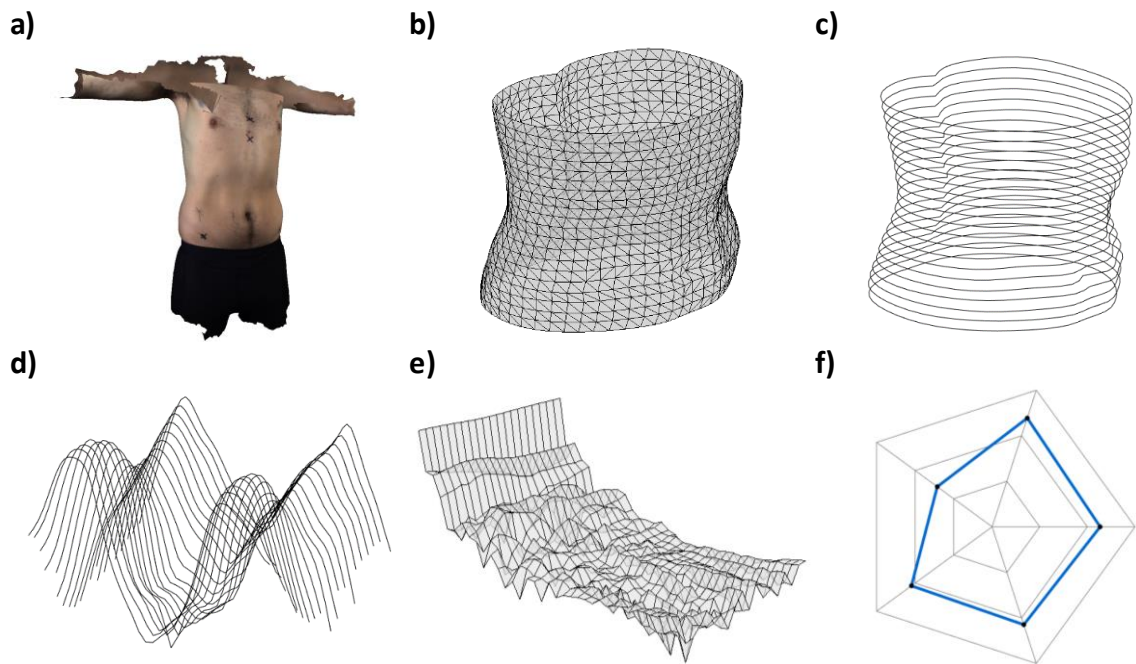


Figure 3.16. Analytical procedure for extracting shape features from torso 3D imaging data; a) Acquire and digitise 3D geometry of an individual; b) Segment, scale and rotate torso segment; c) Extract transverse data slice profiles; d) Obtain signal waveform from profiles; e) Extract frequency content from signals; f) Detect shape principal components from Fourier coefficients.

Chapter 4 - Test-retest reliability and observer error for shape anthropometrics

4.1 Introduction

Previous studies have evaluated the accuracy and precision of 3D imaging devices compared to manual measurements (165,216), as well as the repeatability of scan-derived measures and landmark locations (137,217). As a result of these studies, international standards have been established which specify the required accuracy of 3D imaging systems used in anthropometry (140). However, it has been suggested that the primary sources of measurement error within anthropometric data collection are identification of anatomical landmarks and variability of participant posture (18,105), which are associated with human error - observers and participants. Anatomical landmarks are detectable skeletal points that identify the location of measurement sites used to define body segments and ensure anatomical correspondence between individuals (18,53). In addition, landmark locations are used for performing statistical analysis, reconstructing variations in human body shape and creating homologous models (105,172,218), as detailed in Chapter Three. Previous studies have shown that even with training there can be significant intra and inter-observer errors in landmark identification, which can contribute to errors in derived body measurements and 3D imaging data processing (55,105,106). The methods developed in this programme of research rely on manual palpation and digitisation of anatomical landmarks to define the torso segment and create local anatomical coordinate systems for each participant. Consequently, variability when identifying anatomical landmarks within 3D imaging data could significantly affect shape anthropometrics.

Variability of participant posture during 3D imaging can also have significant effects on the reliability and accuracy of extracted body dimensions and body shape analysis (18,145,152,219). Postures used for 3D imaging require participants to stand with their arms abducted, enabling the imaging device to view the lateral torso aspect, to aid in 3D model segmentation (140,166). However, it has been found that individuals cannot keep their upper limbs in identical positions for repeated imaging trials (219) and is a common source of random error in studies with human participants (107). Though posture variation is typically considered a factor caused by the participant, it is also related to the observer, since posture can be controlled if adequate instructions are provided during data collection (105). Variations in posture can influence the creation

of local anatomical coordinate systems and the angle of segmentation planes, leading to errors during scan data post-processing. Previous investigations have suggested that postural variations can be captured by individual PCs (152,172). If this is the case, it may be possible to isolate and remove the effects of postural variations from acquired 3D imaging data, improving the precision of extracted size and shape anthropometrics. It is acknowledged that there are other potential sources of error which could affect the test-retest reliability of body measurement, such as circadian variations (54), hydration level (220) and breathing cycle (17,144). However, procedures can be put in place to mitigate the effects of these additional sources of error - collecting measures at a similar time of day and asking participants to hold their breath at end-tidal expiration - and therefore such errors are not the focus of this investigation. The aim of this investigation was to determine the effect of measurement error and the reliability of developed methods for assessing torso shape to be used throughout this programme of research. The objectives were to:

- Examine the effects of principal sources of observer error when measuring body shape, whilst limiting external factors.
- Determine the test-retest reliability of developed methods for performing human torso shape measurement.
- Determine whether postural variations are captured by individual principal components, without affecting other components of body shape.

4.2 Methods

4.2.1 Assessment of observer error

Before evaluating the test-retest reliability of developed methods using human participants, a series of experiments were conducted using 3D images of a representative, non-deformable torso mannequin (Figure 4.1a). The torso mannequin, the same used in a previous study by Chiu et al. (221), was used to assess the effects of identified sources of measurement error - landmark location and posture - whilst limiting external factors typically associated with human measurement (e.g. hair and involuntary movement), which could affect the analytical procedure. During scanning the torso mannequin was placed on a raised platform to ensure it was positioned within the vertical centre of the calibrated volume of the 3dMDBody5 imaging system.

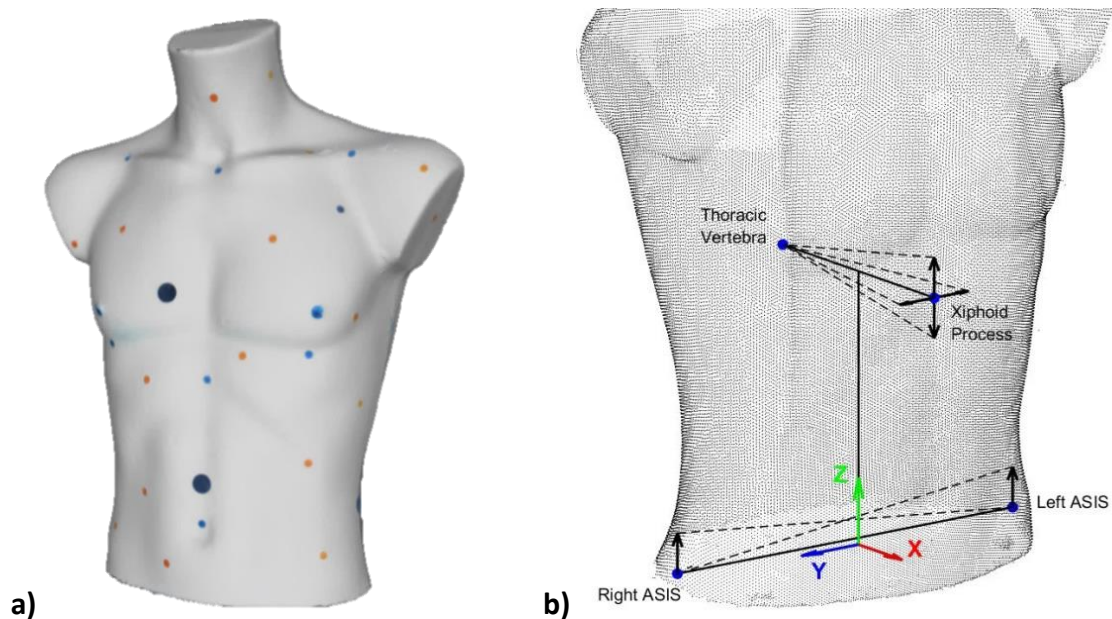


Figure 4.1. a) Non-deformable torso mannequin; b) Simulated errors in landmark locations on the surface of the torso mannequin and the subsequent effects on the vectors used to create the local coordinate system, shown as dashed lines

The tests conducted with the torso mannequin were as follows: 1) Repeated measures - six 3D scan images of the torso mannequin in a standard orientation within the capture volume were captured using the 3dMDbody5 system. This enabled an initial assessment of the repeatability of the developed analytical procedure when measuring a non-deformable object under standard conditions. 2) Posture/orientation - 3D images were collected of the torso mannequin after being manually rotated within the calibrated volume about the sagittal and transverse axes by approximately 30° , simulating side-side and forward-backward variations from the standard posture, respectively. This enabled the effectiveness of the scan alignment procedure (Section 3.3.2), to be assessed. 3) Landmark location - a single 3D image of the torso mannequin captured in the standard orientation was repeatedly digitised, with the coordinates of landmark points moved from their true position on the surface of the torso mannequin by 5, 10, 15 and 20 mm - typical intra-observer landmarking errors as found by Kouchi et al. (105). Figure 4.1b shows the direction of these simulated errors in landmark location and the subsequent effect on the local anatomical coordinate system within the torso segment. A single researcher manually digitised the locations of landmark points on the surface of the torso mannequin for all collected 3D scan images within KinAnthroScan, as detailed in Section 3.3.1. The root mean square error (RMSE) of the extracted outline curves was calculated to quantify the amount of measurement error in each experimental condition (Table 4.1). The RMSE for repeated

measures of the torso mannequin in the standard orientation was close to zero, suggesting that the analytical procedure was repeatable when measuring a non-deformable object under identical conditions. The RMSE for measures of the torso mannequin when manually adjusted into extreme orientations was also close to zero, suggesting that the scan alignment procedures, described in Section 3.3.2, were not affected by changes in orientation of a non-deformable body within the scan volume. However, the RMSE of shape measures for the torso mannequin increased with increasing movements of landmarks from their correct location.

Table 4.1. RMSE of shape measures for the torso mannequin in different conditions.

Experimental condition		RMSE (mean(SD))
Repeat measures		5.551e-04(7.021e-05)
Changes in torso orientation		7.568e-04(1.450e-04)
Changes in landmark location:	5 mm	0.002(0.001)
	10 mm	0.004(0.002)
	15 mm	0.007(0.003)
	20 mm	0.009(0.003)

4.2.2 Participants

Through convenience sampling, 29 recreationally active male volunteers participated in this study to determine the intra and inter-session reliability of human torso shape measurement (Table 4.2). All participants were required to be over the age of 18 years and able to stand unaided, as all data were collected while standing and provide written informed consent. During data collection participants were asked to wear non-compressive, form fitting shorts. Upon arrival, each participant's standing stature and body mass were acquired using a Leicester height stadiometer (Marsden, UK) and digital weight scales (Conair, UK), respectively. All procedures were approved by Sheffield Hallam University Research Ethics Committee, reference number ER10868123 (Appendix 3).

Table 4.2. Summary characteristics of participants.

Descriptive	Mean \pm SD	Min.	Max.	95% CI
Age (years)	37 \pm 14	21	78	[32, 42]
Stature (cm)	177.5 \pm 6.9	163.4	192.9	[175.0, 180.0]
Mass (kg)	85.7 \pm 18.4	65.9	152.1	[79.0, 92.4]
BMI (kg/m ²)	27.1 \pm 4.9	20.9	43.3	[25.3, 28.9]

SD, Standard deviation; 95% CI, 95% Confidence Interval; LB, Lower bound; UB, Upper bound

4.2.3 Research protocol

Each participant attended two separate 30 minute data collection sessions, at approximately the same time on consecutive days. During each data collection session

three 3D scan images of the participant were collected using the 3dMDbody5 imaging system. Thus, a total of six 3D images were acquired for each participant in the study. The locations of the anatomical landmarks, defined in Section 3.2.1, were manually palpated by a level one ISAK anthropometrist (the author) and marked with a cross on the skin using a fine-tipped surgical marker (e.g. Viscot 1451), to ensure correct identification of landmarks in the 3D images. The same level one ISAK anthropometrist performed this procedure across all participants. For torso imaging, participants were asked to hold their breath at end-tidal expiration and adopt the scanning pose, described in Section 3.2.3, throughout the short scanning duration. The configuration and calibration procedure of the 3dMDbody5 hybrid stereo photogrammetry surface imaging system was performed according to manufacturer's guidelines at the start of each data collection session, using the procedures described in Section 3.2.3.

4.2.4 3D imaging data post-processing

All 3D images of human participants were digitised by a single researcher within KinAnthroScan (the author), as detailed in Section 3.3.1. Mean intra-observer digitisation errors were 0.72, 0.78, 0.84 and 0.79 mm for the ASIS right, ASIS left, xiphoid process and posterior landmarks, respectively. Digitisation error was quantified as the Euclidean distance between the coordinates of digitised landmark locations made by the same researcher for each landmark, similar to Kouchi et al. (105). Mean digitisation error for each landmark was calculated from three repeated digitisations of all 29 participants' 3D imaging data. Following digitisation of all collected 3D images, the remaining stages of the developed methods were performed: segmenting 3D imaging data; alignment and scaling of torso scan data; extraction of shape profiles; and extraction of Fourier coefficients describing torso shape.

4.2.5 Statistical analysis

Test-retest reliability of torso shape measurement

Both the intra and inter-session reliability of extracted torso shape Fourier coefficients were assessed by calculating the intra-class correlation coefficient (ICC) (222,223), using a two-way mixed-effects model with single measures accuracy (ICC (A,1)) and a two-way mixed-effects model with the mean of multiple measures accuracy (ICC (A,k)), respectively. ICC is an established method of assessing clinical reliability, enabling the results from this study to be compared to previously published values (222), as well as

determining the likely acceptance of the procedures presented in this programme of research. The procedure for calculating ICC had to be modified to account for the nature of the measures used in this study. Typically, reliability of body measures are assessed using scalar outcome measures, such as girth or volume. However, the measures obtained using methods developed in Chapter Three represent human torso shape as 210 complex Fourier coefficients, which describe the frequency content within extracted outline curves from 3D imaging data. As a result, to study the reliability of torso shape measures obtained using this procedure requires all of this complex shape information to be evaluated. Smith et al. (224) developed a method for assessing variance of shapes, which enable the reliability of multivariate measures to be evaluated. The classical formulation for calculating the variance of a set of scalar observations, $X = \{x_i\}_{i=1}^N$, is expressed as,

$$\sigma^2 = VAR(X) = \frac{1}{N} \sum_{i=1}^N d(x_i, \mu_X)^2 \quad \text{Equation 4.1}$$

Where, $d(x_i, \mu_X) = |x_i - \mu_X|$, is a metric quantifying the distance between any two values and μ_X is the sample mean. Similarly, for a set of shapes, $S = \{s_i\}_{i=1}^N$, the variance is,

$$\sigma_s^2 = VAR(S) = \frac{1}{N} \sum_{i=1}^N d(s_i, \mu_S)^2 \quad \text{Equation 4.2}$$

Where the mean shape is defined as the average across all shapes in a sample,

$$\mu_S = \frac{1}{N} \sum_{i=1}^N s_i \quad \text{Equation 4.3}$$

The shape distance, d , in equation 4.2 is a metric function that quantifies the difference between any two shapes as a scalar value, $d(a, b) = \|a - b\|_1$. This shape distance provides a mapping from the multi-dimensional shape space to a scalar, non-negative distance, representing total absolute shape difference. This provides the same functionality as distance used in the classical variance formulation (Equation 4.1) and can be used in subsequent calculations of ICC for multivariate shape. According to this methodology, shape can be described by any type of continuous variable, of any dimension, which has been suggested as being suitable for assessing 3D imaging data (224). For this investigation, shape distance was quantified as the sum of differences in polar coordinates between sampled points of corresponding torso outline curves extracted from 3D imaging data of participants torso segments (Figure 4.2).

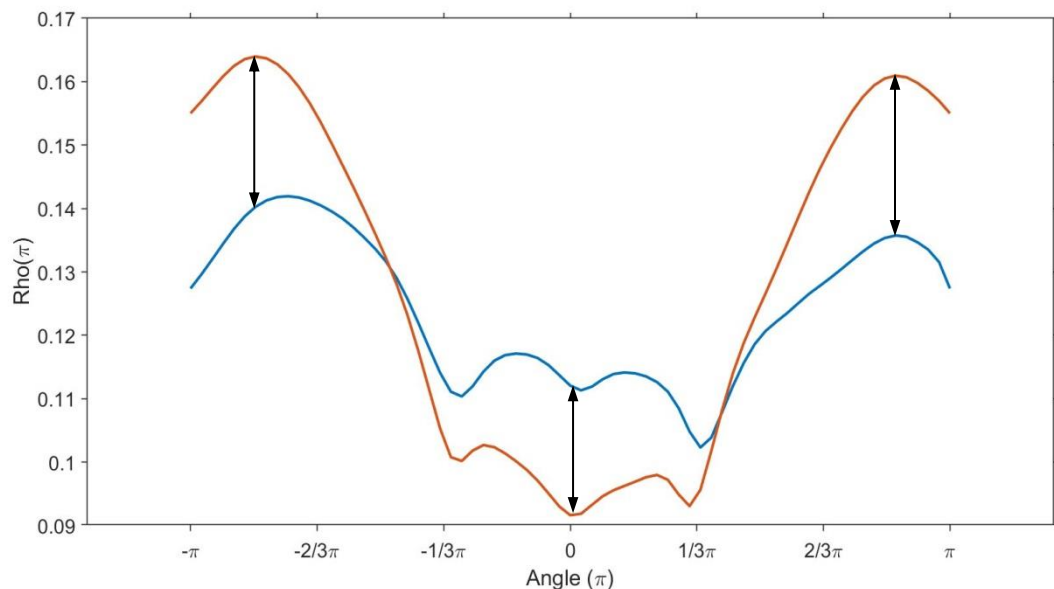


Figure 4.2. Examples of measured differences in polar coordinates between two corresponding torso outline curves, obtained from repeated measures of a single participant.

To evaluate test-retest reliability using ICC with multiple scores from the same rater, a two-way mixed-effects model is the most appropriate, as it is not reasonable to generalise the results of one rater to a larger population of raters (222) and repeated measures cannot be regarded as randomised samples (223). In addition, absolute agreement should always be chosen for test-retest reliability studies (223). The reliability of repeat measures within each session represents a context where a single measure would be performed, thus requiring single measure accuracy. In contrast, the reliability of shape measures between data collections on consecutive days is a context where measures would be averaged for each participant, thus requiring accuracy based on the mean of multiple measures. As a result, the within-session reliability of torso shape measures was calculated using a two-way mixed-effects model with single measures accuracy (ICC (A,1)), while the between-session reliability was calculated using a two-way mixed-effects model with the mean of multiple measures accuracy (ICC (A,k)). ICC values were calculated using the same approach for both: differences between individual data slices along the length of the torso segment; and for all slices along the torso as a whole.

A limitation of ICC is that it only provides a relative measure of reliability which offers little assistance in interpreting changes between repeat tests (225). The minimum detectable change (MDC) is an absolute measure of reliability, which accounts for various sources of variability in defining a confidence interval in units of the measure being assessed (225,226). The MDC was used to determine how much of a change in

polar coordinates would represent a true change in torso shape between repeated measures, not due to random error in the measurement. MDC was assessed based on the shape distance, d , between repeat measures of participants in each data collection session. This was performed using the ICC and standard deviation (σ) values from each session to calculate the standard error of measurement (SEM) and MDC, as follows:

$$SEM = \sigma \sqrt{(1 - ICC)} \quad \text{Equation 4.4}$$

$$MDC = 1.96 SEM \sqrt{2} \quad \text{Equation 4.5}$$

Assessing principal components of postural variation

Using the results of the PCA presented in Section 3.3.6, the Fourier coefficient data obtained from participants in this investigation were transformed into 9 PCs to determine whether postural variations are captured as individual components, without affecting other aspects of body shape. Histograms and Q-Q plots were visually inspected and a Shapiro-Wilks test was conducted to assess the normality of all shape PCs. One-way repeated measures MANOVA analyses were conducted to evaluate whether there were significant differences between repeat measures of individuals and whether posture variations were captured by individual PCs. One-way repeated measures MANOVA assesses differences in multiple dependent variables over time or between treatments, where participants have been measured at all time points (227). Separate analyses were performed to assess the variance of each shape PC, both within each data collection session and between the averages of both sessions. The within-participant standard deviation, S_w , otherwise known as the standard error of measurement, was calculated as the root mean square error term from the MANOVA, to assess variations in the PC scores between repeat measures of participants. Statistical analyses were performed within SPSS (IBM SPSS Statistics 24.0).

4.3 Results

4.3.1 Test-retest reliability of shape measures - ICC

Estimated ICCs for measures of the whole torso were 0.917 and 0.927 for sessions 1 and 2, respectively. This suggests high test-retest reliability of the developed analytical procedure for repeat measures within a data collection session. ICCs of shape measures for individual slices along the length of the torso segment ranged between 0.884-0.972 and 0.898-0.966 for sessions 1 and 2, respectively. The lowest ICCs were

observed for slices within the inferior region of the torso segment, suggesting higher reliability of shape measures for slices within the superior torso region (Table 4.3). Distances between measured outline curves demonstrated a MDC of 17.635 and 15.524, for sessions 1 and 2, respectively.

Table 4.3. ICCs for torso shape measurements within each data collection session, assessing the torso as a whole and for individual slices along the length of the torso segment.

	ICC(A,1)	F	df1	df2	Sig.	95% CI [LB, UB]
<u>Session 1</u>						
Whole Torso	0.917	33.977	28	57.968	> 0.001	[0.854, 0.957]
Slice 1	0.901	27.706	28	57.266	> 0.001	[0.827, 0.948]
Slice 2	0.895	26.060	28	57.219	> 0.001	[0.817, 0.945]
Slice 3	0.889	24.675	28	57.365	> 0.001	[0.808, 0.942]
Slice 4	0.886	23.841	28	57.466	> 0.001	[0.802, 0.940]
Slice 5	0.884	23.529	28	57.455	> 0.001	[0.799, 0.939]
Slice 6	0.894	25.913	28	57.628	> 0.001	[0.815, 0.945]
Slice 7	0.906	29.565	28	57.805	> 0.001	[0.835, 0.951]
Slice 8	0.913	32.489	28	57.953	> 0.001	[0.848, 0.955]
Slice 9	0.920	35.486	28	57.992	> 0.001	[0.858, 0.958]
Slice 10	0.920	35.944	28	57.903	> 0.001	[0.859, 0.959]
Slice 11	0.931	42.492	28	57.418	> 0.001	[0.878, 0.965]
Slice 12	0.938	48.177	28	56.376	> 0.001	[0.890, 0.968]
Slice 13	0.937	47.648	28	55.366	> 0.001	[0.887, 0.968]
Slice 14	0.940	51.028	28	53.071	> 0.001	[0.892, 0.969]
Slice 15	0.943	53.470	28	53.484	> 0.001	[0.897, 0.971]
Slice 16	0.953	64.797	28	55.242	> 0.001	[0.915, 0.976]
Slice 17	0.960	74.518	28	56.711	> 0.001	[0.927, 0.979]
Slice 18	0.967	89.892	28	57.811	> 0.001	[0.940, 0.983]
Slice 19	0.970	99.181	28	57.879	> 0.001	[0.946, 0.985]
Slice 20	0.972	105.748	28	57.443	> 0.001	[0.948, 0.986]
Slice 21	0.972	110.351	28	56.131	> 0.001	[0.950, 0.986]
<u>Session 2</u>						
Whole Torso	0.927	40.863	28	54.664	> 0.001	[0.869, 0.962]
Slice 1	0.916	34.112	28	57.933	> 0.001	[0.853, 0.957]
Slice 2	0.911	31.908	28	57.940	> 0.001	[0.844, 0.954]
Slice 3	0.902	28.920	28	57.968	> 0.001	[0.830, 0.949]
Slice 4	0.898	27.386	28	57.999	> 0.001	[0.822, 0.947]
Slice 5	0.900	27.899	28	57.999	> 0.001	[0.825, 0.948]
Slice 6	0.907	30.326	28	57.968	> 0.001	[0.837, 0.951]
Slice 7	0.908	30.852	28	57.982	> 0.001	[0.839, 0.952]
Slice 8	0.911	31.725	28	57.977	> 0.001	[0.843, 0.954]
Slice 9	0.914	33.041	28	57.907	> 0.001	[0.848, 0.955]
Slice 10	0.925	39.027	28	57.423	> 0.001	[0.868, 0.962]
Slice 11	0.933	44.123	28	56.732	> 0.001	[0.881, 0.966]
Slice 12	0.935	46.152	28	55.982	> 0.001	[0.885, 0.967]
Slice 13	0.938	49.106	28	54.190	> 0.001	[0.889, 0.968]
Slice 14	0.946	57.190	28	51.263	> 0.001	[0.901, 0.972]
Slice 15	0.956	71.115	28	49.872	> 0.001	[0.919, 0.978]
Slice 16	0.964	85.978	28	52.265	> 0.001	[0.933, 0.982]
Slice 17	0.966	91.265	28	55.129	> 0.001	[0.939, 0.983]
Slice 18	0.969	95.595	28	57.569	> 0.001	[0.943, 0.984]
Slice 19	0.965	82.579	28	57.995	> 0.001	[0.936, 0.982]
Slice 20	0.965	84.395	28	57.994	> 0.001	[0.937, 0.982]
Slice 21	0.966	85.593	28	57.967	> 0.001	[0.938, 0.982]

CI, confidence interval; ICC, intraclass correlation coefficient; LB, Lower bound; UB, Upper bound.

The ICC for shape measures of the whole torso was 0.905, suggesting high test-retest reliability of human torso shape measures on consecutive days. ICCs of shape measures for individual slices along the length of the torso segment ranged between 0.845-0.967. Similarly, estimated ICCs were lower in the inferior torso region compared to the superior region between sessions (Table 4.4).

Table 4.4. ICCs for torso shape measurements between repeat data collection sessions, assessing the torso as a whole and for individual slices along the length of the torso segment.

	ICC(A,k)	F	df1	df2	p	95% CI
Whole Torso	0.905	11.205	28	26.095	> 0.001	[0.795, 0.956]
Slice 1	0.863	7.608	28	27.471	> 0.001	[0.708, 0.935]
Slice 2	0.862	7.546	28	27.822	> 0.001	[0.708, 0.935]
Slice 3	0.855	7.117	28	28.079	> 0.001	[0.692, 0.931]
Slice 4	0.845	6.726	28	27.729	> 0.001	[0.672, 0.927]
Slice 5	0.851	7.140	28	26.340	> 0.001	[0.682, 0.930]
Slice 6	0.865	7.975	28	24.986	> 0.001	[0.706, 0.937]
Slice 7	0.883	9.322	28	23.760	> 0.001	[0.742, 0.946]
Slice 8	0.897	10.730	28	23.056	> 0.001	[0.771, 0.953]
Slice 9	0.907	11.845	28	22.767	> 0.001	[0.791, 0.957]
Slice 10	0.911	12.334	28	23.718	> 0.001	[0.804, 0.959]
Slice 11	0.918	13.247	28	24.387	> 0.001	[0.820, 0.962]
Slice 12	0.924	14.337	28	24.222	> 0.001	[0.833, 0.965]
Slice 13	0.925	14.397	28	24.445	> 0.001	[0.834, 0.965]
Slice 14	0.928	15.021	28	25.193	> 0.001	[0.844, 0.967]
Slice 15	0.944	19.483	28	24.605	> 0.001	[0.878, 0.974]
Slice 16	0.955	24.198	28	24.724	> 0.001	[0.902, 0.979]
Slice 17	0.966	30.454	28	27.291	> 0.001	[0.926, 0.984]
Slice 18	0.967	30.900	28	28.577	> 0.001	[0.930, 0.984]
Slice 19	0.967	29.883	28	28.975	> 0.001	[0.930, 0.984]
Slice 20	0.967	29.899	28	28.842	> 0.001	[0.930, 0.984]
Slice 21	0.966	29.060	28	28.901	> 0.001	[0.928, 0.984]

CI, confidence interval; ICC, intraclass correlation coefficient; LB, Lower bound; UB, Upper bound.

4.3.2 Assessing components of postural variation - MANOVA

Figure 4.3 shows the within-participants standard deviation (s_w) values of all identified torso shape PCs, both within each data collection session and between the average measures of both sessions. Within-participant variation was similar between repeat measures in both data collection sessions, while greater within-participant variations were observed for measures between data collection sessions. Figure 4.3 also shows that though PC1 exhibited the highest s_w , sources of measurement error caused variations in all identified torso shape PCs.

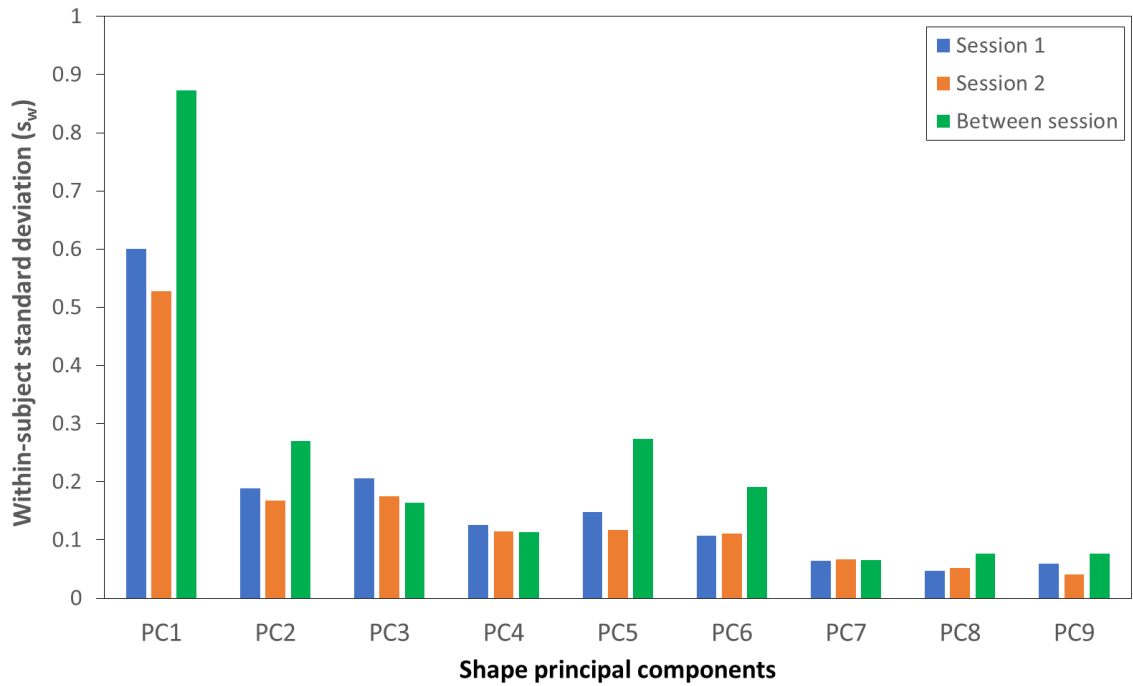


Figure 4.3. Within-participant standard deviation (s_w) values for all identified torso shape principal components, both within each data collection session and between sessions.

The multivariate test statistics for each of the one-way repeated measures MANOVA analyses are shown in Table 4.5. Using Wilks' statistic, it was found that observed differences in the identified torso shape PCs were not statistically significant ($p > 0.05$), either between repeat measures within each data collection session, or between the average shape PCs of both sessions.

Table 4.5. Results of one-way repeated measures MANOVA, for repeated shape measures within each data collection session and between the averages of both sessions.

	Wilks' Lambda (Λ)	F	Hypothesis df.	Error df.	Sig.
Session 1	0.669	1.187	18	96	0.287
Session 2	0.676	1.153	18	96	0.316
Between sessions	0.682	1.037	9	20	0.446

Figure 4.4 demonstrates differences in torso shape PCs caused by variations in posture between two repeat measures of an individual within a single data collection session. Small differences caused by changes in posture between repeat measures can be seen on the anterior torso aspect (Figure 4.4a), while more obvious differences can be seen on the posterior aspect (Figure 4.4b). Figure 4.4c shows the corresponding radar diagram, demonstrating the changes in each of the first 9 shape PCs between the two measurements. Shape PC1 captures the largest differences between measures, however, there are also changes observed in all identified torso shape PCs as a result of postural variations.

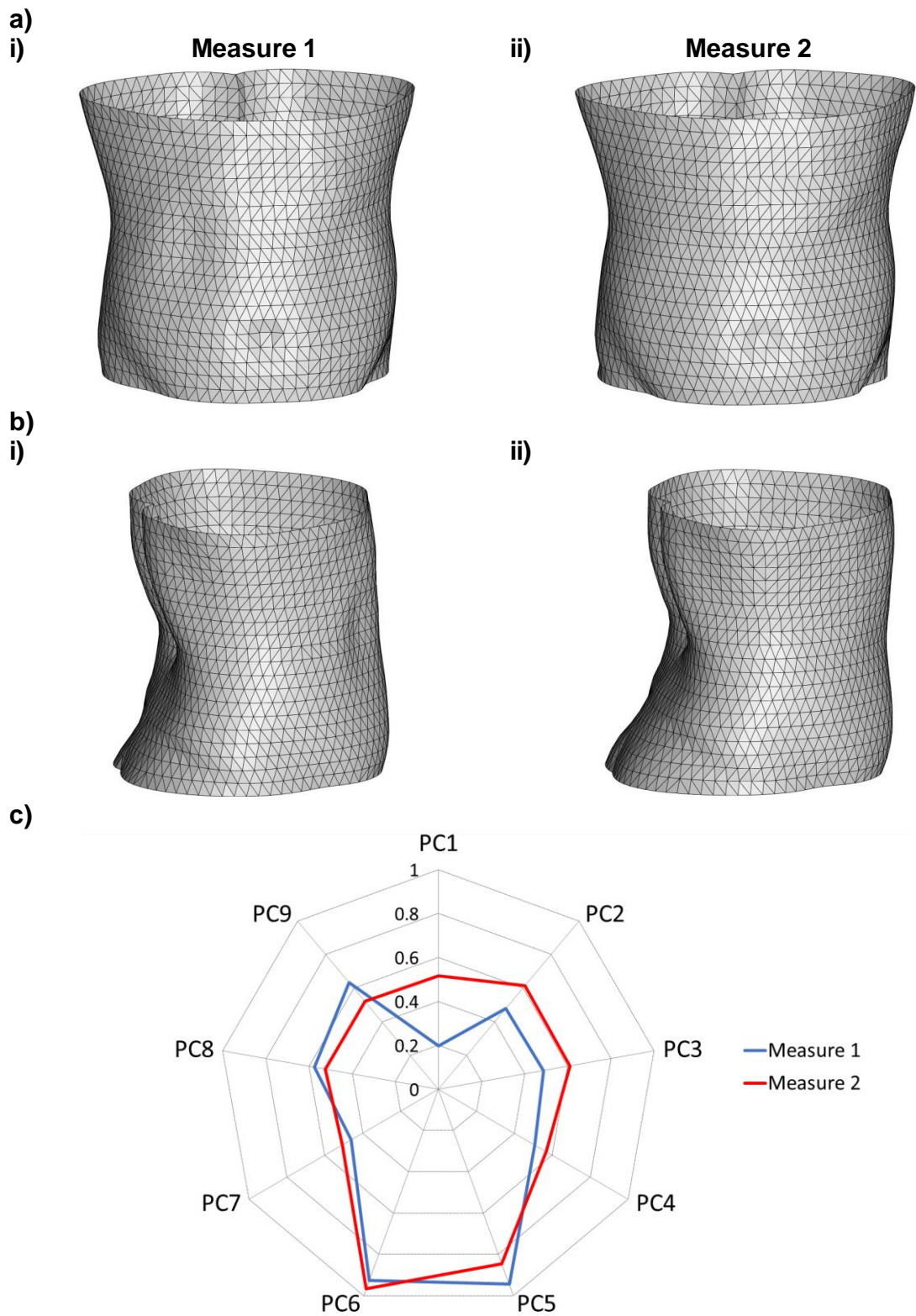


Figure 4.4. Comparison of torso shape PC's from two repeat measures of participant #25 within data collection session 1. a) front profile i) measure 1, ii) measure 2, b) side profile, i) measure 1, ii) measure 2, c) Radar diagram comparing shape principal components from measure 1 (blue) and measure 2 (red).

4.4 Discussion

Shape measurement methods, detailed in Chapter Three, rely on manually identifying the location of anatomical landmarks and acquiring 3D images of participants in a specified posture. Both landmark identification and participant posture have been shown to be the primary sources of measurement error in anthropometric data collection (18,105,219). The aim of this investigation was to determine the effect of these sources of measurement error and the reliability of developed methods for assessing human torso shape to be used throughout this programme of research.

Initial experiments with a non-deformable torso mannequin demonstrated that shape measures produce consistent results when performed under identical experimental conditions. In this controlled scenario, where the only potential source of error between repeat measures was intra-observer digitisation error (<1 mm), the same results were achieved. Similarly, when the orientation of the non-deformable torso mannequin was altered within the scan volume, the analytical procedure also produced almost identical results. This suggests that if landmarks are identified correctly on a non-deformable body the same results are obtained. However, it was found that landmarking errors, typical of manual techniques (105), cause inaccuracies in scan alignment and subsequent shape measures, illustrating the importance of minimising landmarking errors when evaluating human participants. Requiring investigators to be at least ISAK level 1 accredited anthropometrists can help ensure reliable manual identification of anatomical landmarks.

Myer (228) suggested that in situations where the true value of a given variable is not known, or when there is no widely accepted gold standard measurement system, researchers should seek to evaluate the reliability of measures. Since methods developed in Chapter Three produce novel measures of shape, which have not previously been used to evaluate the human body from an anthropometric perspective, the test-retest reliability of torso shape measures was evaluated. Previous studies have suggested that measurement systems with an ICC > 0.7 (229) are acceptable for use within clinical environments (230). In this investigation, measures of torso shape were found to have an average intra-session ICC of 0.922 and an inter-session ICC of 0.905. This suggests high test-retest reliability of torso shape measures, both within and between sessions, and would likely be accepted by practitioners. The

estimated reliability of measures taken during the second session (0.927) was slightly higher compared to those taken in the first session (0.917), though this difference was within the 95% confidence interval for each session. This suggests that there was not a significant change in measurement reliability associated with systematic bias due to learning effects, as has been observed in previous investigations (107).

ICC values were found to be lower for data slices within the inferior torso segment region compared to slices within the superior torso region. This is likely due to the centre of the local coordinate system being defined by the xiphoid process and the thoracic vertebra at the superior torso boundary, improving alignment of the torso segment in this region. Previous studies have shown that the xiphoid and vertebra landmarks are palpated more reliably than the ASIS landmarks (105,106), due to greater accumulations of adipose tissue in the lower torso region, causing difficulties in landmark palpation and marking (204,205). Also, because of greater amounts of adipose tissue typically being located in the inferior torso region, postural changes would likely lead to greater deformation and changes in lower torso shape compared to the superior torso. Shape measure reliability was shown to reduce between data collections compared to within sessions. This is most likely due to postural changes being compounded by errors in palpated landmark locations, as well as other external factors, such as hydration level (220), which may also have affected torso shape. Thus, it is important that external sources of measurement error are controlled as much as possible to ensure test-retest reliability of shape measurement.

The MDC was calculated to determine the smallest true differences in shape that can be detected using the developed method (226). The results of this study suggest that shape measures demonstrated an average MDC of 16.580 for overall differences between polar coordinates of torso outline curves. For comparison, the average measured shape difference between individuals in this study was 306.428. Though this MDC value cannot be interpreted as easily as scalar measures, such as girth or volume, this study suggests that a change greater than this value would represent a true change in an individual's torso shape, which is not attributable to measurement error. Further longitudinal studies are required to determine the amount of shape change that could be produced by an exercise or dietary intervention and whether the developed method could monitor those changes over time effectively.

It has previously been suggested that postural variation effects are captured by individual PCs and can be removed from acquired 3D imaging data during post-processing (152,172). Between repeat measures in each data collection session in this study, the locations of landmarks on each participant's torso surface were not moved. This means that the only potential sources of random measurement error within each data collection session were: digitisation of landmarks, shown to have almost no effect on shape; and variations in posture. The results of this investigation show that although shape PC1 demonstrated the largest within-participant differences, each of the other identified shape principal components were also affected by postural variations. This suggests that random variations in posture between repeat measures affect all identified shape PCs, rather than being isolated to a single component as previously suggested. The cause of these changes in all shape PCs is likely because the human torso is deformable. Consequently, when a participant alters their posture the soft tissues within their torso will deform, causing changes to multiple aspects of body shape, rather than along a single component. Instead it must be assumed that all shape PCs obtained using this method will include elements of postural variation, which must therefore be controlled as much as possible during data collection. However, this investigation has shown that though shape PCs change due to posture variations, the differences between repeat measures, either within or between sessions, are not statistically significant and would not affect statistical inferences made about participants in a cross-sectional study.

4.4.1 Limitations

This study has limitations that require consideration. Throughout this investigation, care was taken to limit the influence of postural sway upon the reliability of shape anthropometrics. Though the ICC results suggest that this was successful, some participants were able to adopt the defined scanning pose more reliably than others. This was due to either the effectiveness of instructions provided to participants, suggested as being a factor affecting reliability (105), or simply the inability of individuals to keep their upper limbs in identical positions for repeated scanning trials without the aid of a positioning device (219). Consequently, future studies should consider the use of postural aids (154) to reduce the effects of postural variability during scanning and increase the precision of shape measures. In addition, this

investigation only evaluated the reliability of shape measures performed on the torso segment. It is unknown whether the reliability of measures demonstrated within this investigation would be achieved when measuring other body segments, or the human body as a whole. Further research would be required to confirm this. Finally, the participant cohort analysed in this investigation only captured a narrow selection of body shapes and sizes that exist in the wider population. Further study is required to assess larger participant samples to determine whether the findings of this investigation are representative of the wider population, across a more extensive range of body types.

4.5 Conclusion

The results of this investigation suggest that although sources of random measurement error, such as landmark location and posture, do affect shape anthropometrics, the methods developed in Chapter Three have high test-retest reliability suitable for use within clinical applications. Future investigations should evaluate the use of shape anthropometrics in longitudinal studies to determine whether shape measures can successfully track changes in health and body composition following exercise or dietary interventions.

Chapter 5 - Complementing traditional anthropometrics with shape anthropometrics

5.1 Introduction

Traditional manual anthropometrics are used extensively in medical practice and epidemiological studies to provide proxies for nutritional status within the population and derive indicators of health risk. In addition, individual variations in body composition, such as ratios of fat to lean tissue and distributions of adipose tissue between central and peripheral depots, manifest outwardly as variations in physique ('body build') and shape (3,69,95). As a result, indices such as the body mass index (BMI), waist girth and the waist-hip ratio (WHR) are used to assess these variations in external human body dimensions to assess physical health (2,21,55). Of these, BMI is most commonly used in current practice to determine the healthy weight range for individuals based on their height. However, BMI fails to distinguish between quantities of muscle and body fat, which are of different density, and therefore is prone to misclassifying muscular individuals as being overweight or obese (231,232). Size measures, such as sagittal diameter, waist girth or waist girth divided by stature^{0.5} (WHT.5R) have been found to demonstrate improved correlations with quantities of abdominal visceral fat and greater associations with metabolic disease risks compared to BMI (50,72). Relative measures, such as the WHR, provide information about the size of the abdomen relative to the rest of the body, so has been used as a proxy of torso shape and central obesity, defined as excess fat around the abdominal region (50). However, these relatively simple approaches to assessing human morphology only utilise a small number of manual anthropometrics, which are prone to human error and limited by their simplicity, as they do not fully describe the complex three-dimensional (3D) variations in human body shape (4,19–21).

Skinfold thickness measures are another manual anthropometric technique which have been shown to be an accurate approach for measuring subcutaneous fat at a given location and measuring total subcutaneous fat from the sum of several skinfold sites (91). Studies often use the sum-of-skinfold thicknesses taken from around the waist as a measure of central subcutaneous adiposity to assess the efficacy of anthropometrics used in clinical practice (76). Predictive equations have previously been developed based on combinations of anthropometrics and approximate interrelationships among subcutaneous fat, visceral fat and whole body density.

Recent studies have also investigated the use of 3D imaging to predict body fat distribution (23,233,234). However, biological variations such as age, sex and body type (235) make estimations of visceral fat using anthropometric techniques difficult (73).

This chapter details a preliminary exploration into the use of developed methods for assessing variations in human torso shape within a small sample of participants. The aim of this study was to investigate whether shape anthropometrics can complement manual anthropometric techniques in the assessment of human morphology and the estimation of subcutaneous central adiposity. The objectives were to:

- Demonstrate the application of developed methods for extracting scale-invariant features of human body shape from 3D imaging data.
- Compare traditional manual anthropometrics and shape anthropometrics extracted from 3D imaging when assessing variations in human morphology.
- Determine whether shape anthropometrics can complement manual anthropometric techniques in estimating sum-of-skinfold thickness around the waist of human participants.

5.2 Methods

5.2.1 Participants

3D imaging data and manual body measures of 43 male participants (age 33 ± 12 years, height 179.8 ± 7.2 cm, weight 82.9 ± 16.2 kg), described in Chapter Three were analysed in this investigation. All participant data, procedures and documents were approved by the Sheffield Hallam University Research Ethics Committee, reference number ER5855905, as detailed in Section 3.2.1.

5.2.2 Experimental protocol

Bony landmark palpation

The locations of bony anatomical landmarks required for manual anthropometric procedures (53) were manually palpated and marked by an accredited level 1 anthropometrist (the author). Landmarks required for data post-processing were marked with a cross on the skin using a fine-tipped surgical marker (e.g. Viscot 1451),

to ensure correct identification of landmarks in the acquired 3D images, as detailed in Section 3.2.2.

Manual measurement

Upon arrival each participant was asked to remove clothing on their upper body, wearing only a pair of form fitting, non-compressive lycra shorts throughout the duration of the data collection. All manual measures were obtained according to ISO 7250-1:2017 anthropometric standards (138) and standard ISAK procedures by an accredited level 1 anthropometrist (the author) to minimise human error in measurement (53). Manual anthropometrics collected from participants included: stature, body mass, waist and hip girth. Anthropometrics of weight status were calculated as follows: BMI = mass/stature²; WHR = waist girth/hip girth; WHT.5R = waist girth/stature^{0.5}. Three skinfold sites in close proximity to the measured waist girth were used as the measure of subcutaneous central adiposity, similar to a recent study by Nevill et al. (76). The three skinfold sites, shown in Figure 2.3, and their definitions were: 1) the iliac crest: a near-horizontal fold superior to the iliac crest; 2) supraspinale: an oblique fold at approximately 45° at the intersection of a line from the anterior superior iliac spine (ASIS) to the anterior axillary fold and a line from the iliac crest; 3) abdominal: a vertical fold 5 cm lateral to the navel. The stature and mass of each participant was measured using a Leicester height stadiometer (Marsden, UK) and digital weight scales (Conair, UK). All girth and skinfold measures were acquired using a basic anthropometric tape measure (Lufkin Executive Thinline 2m, W606PM) and Harpenden skinfold caliper (Baty International, UK), respectively. The summary characteristics of the participant's manual measures are presented in Table 5.1.

Table 5.1. Summary characteristics of participant manual measurements.

Descriptive	Mean ± SD	Min.	Max.	95% CI [LB, UB]
Age (years)	33 ± 12	18	62	[29, 36]
Stature (cm)	179.8 ± 7.2	165.4	193.5	[177.2, 181.6]
Mass (kg)	82.9 ± 16.2	50.9	139.4	[78.1, 87.7]
Waist Girth (cm)	86.1 ± 10.19	67.3	116.6	[83.0, 89.1]
Hip Girth (cm)	100.4 ± 7.3	82.4	120.4	[98.2, 102.5]
BMI (kg.m ⁻²)	25.7 ± 4.2	17.9	38.3	[24.4, 26.9]
Waist-hip-ratio (WHR)	0.86 ± 0.07	0.75	1.04	[0.83, 0.88]
Waist by height ^{0.5} (WHT.5R)	0.64 ± 0.08	0.52	0.84	[0.62, 0.67]
Iliac crest skinfold thickness (mm)	17.4 ± 9.4	3.9	42.0	[14.6, 20.2]
Supraspinale skinfold thickness (mm)	11.7 ± 6.6	3.6	29.6	[9.7, 13.7]
Abdominal skinfold thickness (mm)	22.9 ± 11.6	4.3	44.4	[19.4, 26.3]
Sum-of-skinfold thickness (mm)	52.0 ± 26.3	11.8	101.6	[44.1, 59.8]

SD = Standard deviation; 95% CI = 95% Confidence Interval; LB = Lower bound; UB = Upper bound

3D imaging

3D imaging data of all participants was captured using the 3dMDbody5 surface imaging system. For torso scanning, participants were asked to hold their breath at end-tidal expiration and adopt the scanning pose, described in Section 3.2.3, throughout the short scanning duration. The configuration and calibration procedure of the 3dMDbody5 hybrid stereo photogrammetry surface imaging system was performed according to manufacturer's guidelines at the start of each data collection session, using the procedures described in Section 3.2.3.

5.2.3 3D imaging data post-processing

All 3D images of participants were digitised by a single researcher (the author) within KinAnthroScan, as detailed in Section 3.3.1. Following digitisation of all collected 3D images, the remaining stages of the analytical procedure detailed in Chapter Three were carried out: segmentation of 3D imaging data to remove coordinate points not related to the torso; alignment and scaling of torso segment geometry; extraction of shape profiles along the length of the segment; extraction of Fourier coefficients describing external torso shape; and principal components analysis to detect independent features of torso shape exhibiting the most variation within the sample.

5.2.4 Statistical analysis

To ensure the selection of suitable statistical analysis procedures the parametric nature of all variables were first explored within SPSS (IBM SPSS Statistics 24.0). Histograms and Q-Q plots were visually inspected and a Shapiro-Wilks test was conducted to assess the normality of all variables. All body size measures, skinfold measures and derived indices were converted into standardised z-scores, ensuring that they were comparable by providing a common scale in units of standard deviations from the mean value of each measure of the cohort. Pearson correlation coefficients were calculated to explore associations between manual anthropometrics, derived indices and identified body shape PCs. *P* values <0.05 were considered statistically significant.

Linear regression analyses were conducted to investigate the strength of associations between surface anthropometrics and skinfolds taken from the waist region of the torso segment; both individual skinfolds and the sum of all skinfolds. Three different

types of regression models were created: 1) Size-only models, separate regression models for each anthropometric index (BMI, WHR, waist girth and WHT.5R) and a combination of manual size measures (height, mass, waist and hip girth) were used as input variables; 2) Shape-only model, a stepwise regression model which used the first 9 torso shape principal components as input variables to determine which contribute to the estimation of skinfold thickness; 3) Combined models, which included size measures, derived indices and torso shape PCs as input variables. Each multiple regression model was assessed for multicollinearity between input variables using variance inflation factor (VIF) and tolerance (1/VIF) collinearity statistics, as well as for independence of errors using the Durbin-Watson test statistic. If the largest VIF value was greater than 10 for any given regression model then there was cause for concern (236), while tolerance values below 0.2 could indicate potential issues in the model associated with multicollinearity (237). Similarly, for any two observations the residual terms should be uncorrelated or independent. Therefore, if the Durbin Watson value differed significantly from 2 this would suggest dependence of errors between input variables in the model (227). If any of the calculated regression models demonstrated concerning levels of collinearity or dependence of errors it could be assumed that this model was biased and unreliable in the estimation of skinfold thickness. Statistical analyses were performed using SPSS software (version 24.0, IBM, USA).

5.3 Results

5.3.1 Torso shape features within cohort

As described in Section 3.3.6, PCA produced 9 components that captured over 90% of the total body shape variation for participants within the sample. Figure 3.15 in Section 3.3.6 visualises the reconstructed meshed surfaces of the average torso within the sample, as well as the deviations in torso shape from the average along each of the first 5 PCs.

5.3.2 Correlations between size and shape measures

Pearson correlations between size measures, derived indices and shape PCs are presented in Table 5.2. Waist girth measures were strongly correlated with hip girth, body mass and derived indices, BMI, WHR and WHT.5R. Hip girth was also strongly correlated with mass, BMI and WHT.5R, though only had weak correlation with WHR. Stature had moderate correlations with body mass and hip girth, but only weak

correlations with all other body size and shape measures, suggesting that central adiposity changes independently of body height. PC2 of shape was strongly correlated with waist girth, WHR and WHT.5R, and was also significantly correlated with BMI and other size measures. PC1, PC4, PC5 and PC6 had significant correlations with certain size measures and derived indices, while the remaining shape PCs were not significantly correlated with size measures. Due to the nature of PCA all extracted shape features were independent of each other and so were uncorrelated. Waist girth and WHT.5R had the strongest correlations with individual skinfold thickness measures and the sum-of-skinfold thickness, with several other size and shape measures also significantly correlated with both individual and sum-of-skinfold thickness measures. The strength of correlations between size and shape measures with individual skinfold thicknesses did fluctuate, with different measures being either more strongly associated with the supraspinale or iliac crest skinfold depending on the location around the waist where the size or shape measure was taken.

5.3.3 Regression analysis

Table 5.3 shows the results of linear regression analyses, evaluating the strength of associations between sum-of-skinfold measures taken from the torso segment and each of the commonly used derived indices identified in this study (BMI, WHR, waist girth and WHT.5R). All derived indices significantly improved the prediction of skinfold thickness. WHR had the weakest association, explaining 30.6 % of the variance in sum-of-skinfold thickness ($R^2 = 0.306$, $F(1,35) = 15.434$, $p < 0.01$), followed by BMI which explained 33.5% of variance ($R^2 = 0.335$, $F(1,35) = 17.605$, $p < 0.01$). Waist girth ($R^2 = 0.522$, $F(1,35) = 38.270$, $p < 0.01$) and WHT.5R ($R^2 = 0.522$, $F(1,35) = 38.258$, $p < 0.01$) had the strongest associations, both explaining 52.2% of the variance in sum-of-skinfold thickness measures. Table 5.4 shows the results of the multiple regression analyses for the size-only, the shape-only model and the combined models. The size-only model, which included all manual body size measures, explained 68.9% of the variance in sum-of-skinfold thickness ($R^2 = 0.689$, $F(1,32) = 17.690$, $p < 0.01$). However, the collinearity statistics suggest that there are serious concerns with this regression model. The tolerance values for mass and hip girth were both below 0.2 and the VIF values for these measures were 17.281 and 11.484, respectively, suggesting high levels of multicollinearity between individual size measures. In addition, the Durbin-Watson

statistic for this model was 2.387, suggesting that the residual error terms of adjacent observations within the sample were correlated when size measures were combined as input variables, which raise concerns about this regression model. Using stepwise regression for the shape-only model, it was shown that PC2, PC4, PC1 and PC3, in order of their strength of association, contributed significantly to the regression model, explaining 74.2% of the variance in skinfold thickness ($R^2 = 0.742$, $F(1,32) = 22.96$, $p < 0.01$). The Durbin Watson test statistic for this model was close to 2 suggesting independence of errors, while all VIF values for this model were below 10 and all tolerance statistics are above 0.2, suggesting that there was no collinearity between shape PCs. The results of the combined regression models show that integrating shape principal components with commonly used derived indices improved the estimation of skinfold thickness, with the WHT.5R and shape model explaining 76.5% of the variance in skinfold thickness. The Durbin Watson test statistic for all models was close to 2 suggesting independence of errors for all combined models. All VIF values for all models were below 10 and all tolerance statistics are above 0.2 suggesting that there was not concerning levels of collinearity within the data.

Table 5.5 shows the results of linear regression analyses, evaluating the strength of associations between the individual skinfolds (abdominal, supraspinale and iliac crest) taken from around the torso segment and each of the commonly used derived indices identified in this study (BMI, WHR, waist girth and WHT.5R). All derived indices significantly improved the prediction of the individual skinfolds. However it was observed that the strength of association varied between the derived indices and the different skinfolds. For example, all derived indices had the strongest association with the supraspinale skinfold, while they had the weakest association with the abdominal skinfold. Table 5.6 shows the results of the multiple regression analyses for the size-only, the shape-only model and the combined models in the estimation of the individual skinfolds. Similarly the different regression models were able to explain varying amounts of variance in the individual skinfolds. The size-only model, which included all manual body size measures, explained 61.3, 71.0 and 61.7% of the variance in the abdominal, supraspinale and iliac crest skinfolds, respectively. However, as with the sum-of-skinfolds model, the collinearity statistics suggest that there are serious concerns with these regression models, with high levels of multicollinearity between individual size measures.

Table 5.2. Pearson correlation coefficients between skinfolds, size measures, anthropometric indices and shape PCs.

	Size measures				Derived Indices			Shape principal components								
	Stature	Mass	Waist girth	Hip girth	BMI	WHR	WHT.5R	PC1	PC2	PC3	PC4	PC5	PC6	PC7	PC8	PC9
Sum-of-skinfolds	0.02	0.51*	0.72*	0.58*	0.58*	0.55*	0.72*	-0.30	0.55*	-0.27	-0.5*	0.046	-0.21	-0.12	0.11	0.14
Abdominal	0.04	0.43*	0.65*	0.51*	0.49*	0.51*	0.65*	-0.27	0.51*	-0.23	-0.49*	0.01	-0.31	-0.12	0.11	0.17
Supraspinale	-0.1	0.51*	0.74*	0.57*	0.63*	0.57*	0.76*	-0.25	0.62*	-0.29	-0.48*	0.09	-0.16	-0.1	0.12	0.01
Iliac crest	0.08	0.54*	0.71*	0.60*	0.58*	0.52*	0.70*	-0.34*	0.48*	-0.27	-0.46*	0.05	-0.11	-0.11	0.1	0.18
Stature		0.47*	0.12	0.46*	0.054	-0.26	-0.06	0.11	-0.26	-0.17	-0.31	-0.002	0.27	0.25	0.09	0.18
Mass			0.83*	0.95*	0.90*	0.34*	0.75*	-0.23	0.48*	-0.19	-0.15	0.28	0.40*	-0.01	0.21	0.18
Waist girth				0.79*	0.89*	0.78*	0.98*	-0.32*	0.76*	-0.25	-0.14	0.05	0.08	-0.01	0.24	0.09
Hip girth					0.87*	0.23	0.70*	-0.26	0.41*	-0.14	-0.30	0.37*	0.27*	0.08	0.19	0.11
BMI						0.52*	0.89*	-0.32	0.67*	-0.14	-0.03	0.33*	0.27	-0.01	0.23	0.11
WHR							0.84*	-0.24	0.77*	-0.24	0.063	-0.28	-0.14	-0.31	0.19	0.03
WHT.5R								-0.34*	0.81*	-0.22	-0.09	0.05	0.03	-0.19	0.23	0.06

(**P* < 0.05; BMI, Body mass index; WHR, waist-hip ratio; sum-of-skinfolds = Iliac crest + supraspinale + abdominal skinfolds.

Table 5.3. Linear regression models showing associations between derived indices and sum-of-skinfold thickness.

Model	R ²	Regression Equation	Standardised β	F(1,35)	Sig.
BMI	0.335	SSF = 0.033 + 0.555*BMI	0.578	17.605	<0.001
WHR	0.306	SSF = -0.005 + 0.525*WHR	0.553	15.434	<0.001
Waist Girth	0.522	SSF = 0.019 + 0.695*Waist	0.723	38.270	<0.001
WHT.5R	0.522	SSF = 0.02 + 0.694*WHT.5R	0.723	38.258	<0.001

SSF: sum-of-skinfolds

Table 5.4. Multiple linear models showing associations between sum-of-skinfold thickness and 1) size measures; 2) shape PCs; 3) derived indices and shape PCs.

Model	R ²	Regression Equation	DW	Predictor	Standardised β	t	Sig.	Collinearity Statistics	
								Tolerance	VIF
Size Measures	0.689	SSF = 0.023 + (0.082*Stature) + (-1.578*Mass) + (1.067*Waist) + (1.210*Hip)	2.387	Stature	0.084	0.625	0.536	0.534	1.874
				Mass	-1.640	-3.999	<0.001	0.058	17.281
				Waist	1.110	5.125	<0.001	0.207	4.820
				Hip	1.242	3.716	0.001	0.087	11.484
Shape PCs	0.742	SSF = 0.001 + (0.415*PC2) + (-0.787*PC4) + (-0.241*PC1) + (-0.402*PC3)	2.094	PC2	0.523	5.814	<0.001	0.998	1.002
				PC4	-0.526	-5.823	<0.001	0.991	1.009
				PC1	-0.350	-3.866	0.001	0.987	1.014
				PC3	-0.319	-3.530	0.001	0.991	1.009
BMI & Shape	0.748	SSF = 0.005 + (0.120*BMI) + (0.350*PC2) + (-0.778*PC4) + (-0.213*PC1) + (-0.376*PC3)	2.164	BMI	0.125	0.918	0.366	0.437	2.290
				PC2	0.441	3.475	0.002	0.504	1.984
				PC4	-0.520	-5.729	<0.001	0.986	1.014
				PC1	-0.310	-3.083	0.004	0.803	1.245
WHR & Shape	0.743	SSF = -0.001 + (0.073*WHR) + (0.368*PC2) + (-0.793*PC4) + (-0.228*PC1) + (-0.377*PC3)	1.993	PC3	-0.298	-3.198	0.003	0.934	1.071
				WHR	0.077	0.461	0.648	0.294	3.396
				PC2	0.464	2.966	0.006	0.338	2.960
				PC4	-0.530	-5.768	<0.001	0.981	1.020
Waist girth & Shape	0.758	SSF = 0.003 + (0.250*Waist) + (0.262*PC2) + (-0.726*PC4) + (-0.182*PC1) + (-0.311*PC3)	2.010	PC1	-0.331	-3.318	0.002	0.830	1.205
				PC3	-0.299	-2.963	0.006	0.813	1.230
				Waist	0.260	1.457	0.155	0.246	4.067
				PC2	0.331	2.082	0.046	0.309	3.233
WHT.5R & Shape	0.765	SSF = 0.002 + (0.341*WHT.5R) + (0.192*PC2) + (-0.731*PC4) + (-0.158*PC1) + (-0.291*PC3)	2.006	PC4	-0.485	-5.214	<0.001	0.902	1.109
				PC1	-0.265	-2.492	0.018	0.690	1.448
				PC3	-0.247	-2.431	0.021	0.757	1.321
				WHT.5R	0.355	1.745	0.091	0.183	5.450
				PC2	0.242	1.324	0.195	0.227	4.412
				PC4	-0.488	-5.416	<0.001	0.934	1.070
				PC1	-0.229	-2.047	0.049	0.607	1.646
				PC3	-0.231	-2.283	0.029	0.743	1.345

SSF = sum-of-skinfolds; VIF: variance inflation factor; DW: Durbin-Watson

Table 5.5. Linear models showing associations between derived indices and individual skinfold thickness measures.

Skinfold	Model	R ²	Regression Equation	Standardised β	F(1,35)	Sig.
Abdominal	BMI	0.236	Ab = -9.35 + 1.26*BMI	0.486	10.8	0.002
	WHR	0.264	Ab = -51.6 + 86.9*WHR	0.513	12.5	0.001
	Waist Girth	0.420	Ab = -37.853 + 0.708*Waist	0.648	25.3	<0.001
	WHT.5R	0.417	Ab = -38.0 + 95.0*WHT.5R	0.645	25.0	<0.001
Supraspinale	BMI	0.401	Sup = -12.285 + 0.941*BMI	0.633	23.4	<0.001
	WHR	0.326	Sup = -35.5 + 55.1*WHR	0.571	16.9	<0.001
	Waist Girth	0.542	Sup = -27.677 + 0.459*Waist	0.736	41.4	<0.001
	WHT.5R	0.575	Sup = -29.1 + 63.7*WHT.5R	0.758	47.3	<0.001
Iliac crest	BMI	0.332	Ilia = -13.62 + 1.22*BMI	0.576	17.4	<0.001
	WHR	0.266	Ilia = -43.3 + 70.9*WHR	0.516	12.7	0.001
	Waist Girth	0.501	Ilia = -36.483 + 0.628*Waist	0.708	35.2	<0.001
	WHT.5R	0.484	Ilia = -35.8 + 83.1*WHT.5R	0.696	32.8	<0.001

Ab: Abdominal; Sup: Supraspinale; Ilia: Iliac crest.

Table 5.6. Multiple linear models showing associations between individual skinfold thickness and 1) size measures; 2) shape PCs; 3) derived indices & shape PCs.

Model	R ²	Regression Equation	DW	Predictor	Standardised β	t	Sig.	Collinearity Statistics	
								Tolerance	VIF
Size Measures	0.613	Ab = -223.79 + (0.26*Stature) + (-1.25*Mass) + (1.26*Waist) + (1.96*Hip)	2.28	Stature	0.166	1.10	0.279	0.53	1.87
				Mass	-1.815	-3.97	<0.001	0.06	17.28
				Waist	1.150	4.76	<0.001	0.21	4.82
				Hip	1.269	3.41	0.002	0.09	11.48
	0.710	Sup = -83.90 + (-0.10*Stature) + (-0.55*Mass) + (0.62*Waist) + (1.06*Hip)	2.21	Stature	-0.109	-0.840	0.407	0.53	1.87
				Mass	-1.410	-3.561	0.001	0.06	17.28
				Waist	0.988	4.725	<0.001	0.21	4.82
				Hip	1.198	3.712	<0.001	0.09	11.48
	0.617	Ilia = -154.62 + (0.14*Stature) + (-0.77*Mass) + (0.89*Waist) + (1.35*Hip)	2.62	Stature	0.110	0.733	0.469	0.53	1.87
				Mass	-1.367	-3.006	0.005	0.06	17.28
				Waist	0.998	4.155	<0.001	0.21	4.82
				Hip	1.072	2.891	0.007	0.09	11.48

Shape PCs	0.641	Ab = 22.90 + (4.44*PC2) + (-8.86*PC4) + (-2.47*PC1) + (-4.03*PC3)	2.25	PC2	0.483	4.56	<0.001	0.998	1.01
				PC4	-0.511	-4.81	<0.001	0.991	1.01
				PC1	-0.310	-2.91	0.007	0.987	1.01
				PC3	-0.276	-2.60	0.014	0.991	1.01
	0.776	Sup = 11.72 + (3.09*PC2) + (-4.98*PC4) + (-1.36*PC1) + (-2.76*PC3)	1.92	PC2	0.590	7.05	<0.001	0.998	1.01
				PC4	-0.503	-5.99	<0.001	0.991	1.01
				PC1	-0.298	-3.54	0.001	0.987	1.01
				PC3	-0.331	-3.94	<0.001	0.991	1.01
	0.660	Iliac = 17.38 + (3.39*PC2) + (-6.87*PC4) + (-2.51*PC1) + (-3.79*PC3)	2.30	PC2	0.455	4.41	<0.001	0.998	1.01
				PC4	-0.488	-4.71	<0.001	0.991	1.01
				PC1	-0.388	-3.73	<0.001	0.987	1.01
				PC3	-0.319	-3.08	0.004	0.991	1.01
BMI & Shape	0.641	Ab = 21.76 + (0.04*BMI) + (4.33*PC2) + (-8.85*PC4) + (-2.43*PC1) + (-3.99*PC3)	2.25	BMI	0.017	0.105	0.917	0.437	2.29
				PC2	0.472	3.116	0.004	0.504	1.98
				PC4	-0.510	-4.711	<0.001	0.986	1.01
				PC1	-0.305	-2.540	0.016	0.803	1.25
	0.791	Sup = 4.739 + (0.273*BMI) + (2.461*PC2) + (-4.892*PC4) + (-1.089*PC1) + (-2.506*PC3)	1.95	PC3	-0.273	-2.457	0.020	0.934	1.07
				BMI	0.184	1.480	0.149	0.437	2.29
				PC2	0.470	4.063	<0.001	0.504	1.98
				PC4	-0.495	-5.985	<0.001	0.986	1.01
	0.677	Iliac = 6.602 + (0.422*BMI) + (2.418*PC2) + (-6.742*PC4) + (-2.100*PC1) + (-3.399*PC3)	2.45	PC1	-0.239	-2.614	0.014	0.803	1.25
				PC3	-0.301	-3.543	0.001	0.934	1.07
				BMI	0.199	1.290	0.207	0.437	2.29
				PC2	0.324	2.255	0.031	0.504	1.98
				PC4	-0.479	-4.659	<0.001	0.986	1.01
				PC1	-0.324	-2.847	0.008	0.803	1.25
				PC3	-0.287	-2.714	0.011	0.934	1.07

WHR & Shape	0.645	Ab = 6.82 + (18.72*WHR) + (3.67*PC2) + (-8.96*PC4) + (-2.26*PC1) + (-3.62*PC3)	2.13	WHR	0.111	0.561	0.579	0.294	3.40
				PC2	0.399	2.168	0.038	0.338	2.96
				PC4	-0.517	-4.786	<0.001	0.981	1.02
				PC1	-0.284	-2.417	0.022	0.830	1.20
				PC3	-0.248	-2.089	0.045	0.813	1.23
	0.776	Sup = 12.52 + (-0.93* WHR) + (3.13*PC2) + (-4.97*PC4) + (-1.37*PC1) + (-2.78*PC3)	1.93	WHR	-0.010	-0.062	0.951	0.294	3.40
				PC2	0.598	4.089	<0.001	0.338	2.96
				PC4	-0.503	-5.865	<0.001	0.981	1.02
				PC1	-0.300	-3.220	0.003	0.830	1.20
				PC3	-0.334	-3.541	0.001	0.813	1.23
	0.662	Iliac = 7.01 + (12.08* WHR) + (2.89*PC2) + (-6.94*PC4) + (-2.38*PC1) + (-3.52*PC3)	2.22	WHR	0.088	0.457	0.651	0.294	3.40
				PC2	0.388	2.160	0.039	0.338	2.96
PC4				-0.493	-4.678	<0.001	0.981	1.02	
PC1				-0.367	-3.200	0.003	0.830	1.20	
PC3				-0.297	-2.564	0.015	0.813	1.23	
Waist girth & Shape	0.649	Ab = 6.02 + (0.20*Waist) + (3.22*PC2) + (-8.37*PC4) + (-2.01*PC1) + (-3.31*PC3)	2.17	Waist	0.180	0.837	0.409	0.246	4.07
				PC2	0.350	1.831	0.077	0.309	3.23
				PC4	-0.483	-4.311	<0.001	0.902	1.11
				PC1	-0.252	-1.065	0.058	0.690	1.45
				PC3	-0.226	-1.852	0.074	0.757	1.32
	0.784	Sup = 2.40 + (0.11* Waist) + (2.42*PC2) + (-4.71*PC4) + (-1.10*PC1) + (-2.36*PC3)	1.88	Waist	0.174	1.032	0.310	0.246	4.07
				PC2	0.461	3.072	0.004	0.309	3.23
				PC4	-0.476	-5.414	<0.001	0.902	1.11
				PC1	-0.241	-2.398	0.023	0.690	1.45
				PC3	-0.283	-2.948	0.006	0.757	1.32
	0.696	Iliac = -11.84 + (0.34* Waist) + (1.28*PC2) + (-6.03*PC4) + (-1.70*PC1) + (-2.53*PC3)	2.34	Waist	0.383	1.917	0.065	0.246	4.07
				PC2	0.171	0.961	0.344	0.309	3.23
PC4				-0.428	-4.105	<0.001	0.902	1.11	
PC1				-0.262	-2.202	0.035	0.690	1.45	
PC3				-0.213	-1.873	0.070	0.757	1.32	

WHT.5R & Shape	0.652	Ab = 0.22 + (35.29* WHT.5R) + (2.70*PC2) + (-8.42*PC4) + (-1.82*PC1) + (-3.16*PC3)	2.16	WHT.5R	0.240	0.969	0.340	0.183	5.45
				PC2	0.293	1.319	0.197	0.227	4.41
				PC4	-0.486	-4.430	<0.001	0.934	1.07
				PC1	-0.229	-1.681	0.103	0.607	1.65
				PC3	-0.217	-1.763	0.088	0.743	1.35
	0.798	Sup = -6.88 + (28.95* WHT.5R) + (1.66*PC2) + (-4.62*PC4) + (-0.82*PC1) + (-2.05*PC3)	1.84	WHT.5R	0.345	1.831	0.077	0.183	5.45
				PC2	0.317	1.873	0.071	0.227	4.41
				PC4	-0.467	-5.594	<0.001	0.934	1.07
				PC1	-0.180	-1.743	0.091	0.607	1.65
				PC3	-0.246	-2.624	0.013	0.743	1.35
	0.698	Iliac = -17.61 + (54.45* WHT.5R)+(0.70*PC2) + (-6.20*PC4) + (-1.51*PC1) + (-2.45*PC3)	2.36	WHT.5R	0.456	1.976	0.057	0.183	5.45
				PC2	0.094	0.455	0.652	0.227	4.41
PC4				-0.440	-4.309	<0.001	0.934	1.07	
PC1				-0.233	-1.835	0.076	0.607	1.65	
PC3				-0.206	-1.802	0.081	0.743	1.35	

Ab: Abdominal; Sup: Supraspinale; Iliac: Iliac crest; VIF: variance inflation factor; DW: Durbin-Watson

Using stepwise regression for the shape-only model, it was shown that PC2, PC4, PC1 and PC3, in order of their strength of association, contributed significantly to the regression model, explaining 64.1, 77.6 and 66.0% of the variance in the abdominal, supraspinale and iliac crest skinfold, respectively. The results of the different combined regression models show that integrating shape principal components with commonly used derived indices also improved the estimation of the individual skinfolds, though the strength of association varied with the different skinfolds. For example, the WHT.5R and shape model explained 65.2, 79.8 and 69.8% of the variance in the abdominal, supraspinale and iliac crest skinfold, respectively. This suggests that measures of size and shape used in combination can explain fat distribution in different areas of the torso with greater accuracy.

5.4 Discussion

It has been suggested that more sophisticated shape indexes, measured using 3D imaging, can surpass manual measures in epidemiology and clinical practice for classifying and health monitoring of individuals (2). The aim of this study was to investigate whether shape anthropometrics can complement existing anthropometric techniques in the assessment of variations in human morphology and the estimation of subcutaneous central adiposity.

Shape features identified in this study characterise deviations in torso shape that exist within the participant cohort and are invariant to the effects of scale, location and orientation. The information used to characterise individuals in this investigation differs from that used in previous studies by Loffler-Wirth et al. (19) and Pleuss et al. (122). In these studies, large numbers of simple measures, such as lengths and girths and their ratios, were extracted from 3D imaging data and normalised with respect to height. Machine learning processes were then used to find clusters of participants based on these simple measures. However, though these previous approaches to body measurement (19,122) have identified clusters of individuals within large cohorts, the primary differences between clusters have typically been variations in the lengths and girths of body segments. In contrast, the approach used in this investigation has been shown to identify differences in scale-invariant shape features that are not captured using traditional anthropometric techniques. There have been recent studies which have also used principal components analysis (PCA) to detect variations in torso 3D

imaging data similar to this investigation, such as Ruto et al. (170) and Ng et al. (23). However, the imaging data in both these investigations were not scaled to uniform size. As a result some variations observed within these studies were related to differences in overall body height and size, as well as variations in scale-invariant body shape. Though the size of the participant cohorts used in previous studies were larger than in this investigation, the PCA procedure identified the same number of components to describe 95% of the variation present within the cohort. This suggests that shape information inherent within 3D imaging data includes subtle variations requiring a greater number of principal components to describe them fully, as opposed to size measures which can be described in a smaller number of components (122). Though it is currently unknown what all of the shape PCs identified in this investigation represent in terms of physical health, they could be used to reveal variations in internal fat distributions which cannot be captured by existing anthropometrics, as has been suggested by Ng et al. (23). This investigation has demonstrated an effective method of capturing and quantifying additional information about human morphology. If it can be shown that the additional information contained within shape anthropometrics is related to health risk factors, they could provide more effective tools for assessing human morphological variations within a population.

External body shape is determined by its skeletal structure and the distributions of fat and muscle mass along its length (3,238). It has previously been found that the distribution of body fat, especially visceral fat accumulation in the abdominal region, represent the most significant metabolic consequences (12,233,238). However, the ability of current anthropometric approaches, such as BMI, to determine body fat mass has been questioned repeatedly in previous studies (238,239). Though the BMI was not originally developed for use specifically as an index of fatness, it has been utilised for this purpose because it is a readily obtained metric (238). However, accumulations of visceral fat do not correlate with total body mass and are therefore not detectable using BMI (235). Measures such as waist girth and WHT.5R, which utilise measures of body size, have been found to demonstrate improved correlations with quantities of abdominal adiposity and therefore are used as surrogates of central obesity (76). Regression analyses were conducted to investigate whether torso shape PCs identified in this investigation contain additional information that can complement these existing anthropometric techniques in the estimation of subcutaneous central adiposity. In this

study it has been shown that shape PCs explained 74.2 % of the variance in sum-of-skinfold thickness, compared to 52.2 % explained by existing derived indices, waist girth and WHT.5R. However, when waist girth and WHT.5R were combined with torso shape PCs they were able to explain 75.8 % and 76.5 % of the variance in sum-of-skinfold thickness, respectively. These results agree with those of Nevill et al. (76), which found that WHT.5R was the most sensitive of existing derived indices to changes in abdominal adiposity, however, the addition of scale-invariant measures of body shape can improve this prediction still further. These results are promising for a study conducted on a small cohort. However, the issue of sample size and the number of predictor variables when performing regression analyses is an important consideration to ensure a reliable regression model is obtained, due to the estimate of R being dependent on these factors as well as the size of the effect. Several different rules for this have been proposed, the most common of which being the need for 10 observations for each predictor included in the model (227). In addition, Miles and Shevlin (240) propose that in order to find a large effect with a high level of power, a sample size of 50 is required to include 5 predictor variables. In this study, the participant sample size was 43 and 5 predictor variables were used in the combined size and shape regression models, suggesting that the reliability of the developed regression models could be questioned and is a limitation of this study. Though the addition of greater numbers of predictor variables will always improve the accuracy of a regression model, the torso shape features extracted using developed analytical procedures are independent and describe different aspects of human form. This is contrary to individual manual measures of body size (stature, mass, waist and hip girth), which have been shown to exhibit high levels of collinearity, preventing them being from combined in the same regression model without causing bias in the estimation of model coefficients. For this reason, indices, such as BMI, WHR and WHT.5R, are often used as a way to combine measures of body size to create proxies of body shape, reducing the complexity of human morphology to a single value. However, this investigation has shown that distinct features of body shape can be measured directly, providing additional information that can be used to complement existing derived techniques in the estimation of central adiposity.

It is acknowledged that anthropometric proxies of adiposity, such as waist girth, WHT.5R and measures of shape, will only be able to reliably capture variations in

subcutaneous adiposity. This is due partly because subcutaneous adiposity accounts for the large majority of total body fat mass (>80%), and because it sits just below the skin layer on the surface of the body and therefore is closely associated with superficial topography (73,241). Though the focus of much body composition measurement and health research has been on the detection of visceral adiposity, the role of subcutaneous adiposity and its contribution to insulin resistance has often been overlooked until recently. Adverse metabolic effects, such as insulin resistance or dyslipidemia dependent on abdominal adiposity, are likely to result from both dysfunctional abdominal subcutaneous and visceral adipose tissue accumulation. Since abdominal subcutaneous adiposity has much greater mass than visceral adiposity it has the potential to contribute to insulin resistance through the release of free-fatty acids (95). As a result, the additional information provided by shape measures has the potential to play a major role in both epidemiological studies of risk of the metabolic syndrome. Shape may be able to identify morphological features that relate to variations in subcutaneous adipose tissue quantities in different regions of the body that are associated to cardio-metabolic health risks; both in the torso, as well as low amounts of subcutaneous thigh fat which has been shown to be an independent risk factor for unfavourable glucose and lipid levels (79). Further study is required to establish these relationships, as well as the effects on shape measurement caused by underlying health issues, such as edema, which could obscure relationships between body shape and its composition.

5.4.1 Limitations

This study has several limitations that require consideration. First, due to the exploratory nature of this investigation only a small sample of participants was considered, which only captured a narrow selection of body shapes and sizes, and may have affected the reliability of results obtained from both the PCA and multiple linear regressions used in this study. Therefore, further study is required to assess a larger sample of individuals, exhibiting a more extensive range of body size and shape, to determine whether the findings of this investigation are representative of the wider population. In addition, this study only considered relationships between external body measures and quantities of central subcutaneous adiposity. However, as outlined in Chapter Two, the susceptibility of individuals to obesity-related metabolic

complications is not necessarily caused by overall fat mass, but depends on the distribution of body fat and the ability of subcutaneous adipose tissue to expand, preventing the deposition of fat in other organs (12). This concept of adipose tissue expandability varies considerably between individuals and has been suggested as being an explanation of the distinct metabolic risk profiles exhibited within the population. Consequently, though shape features identified in this study are related to quantities of subcutaneous fat, the lack of medical assessments, such as MRI scans of visceral adipose tissue volume or oral glucose tolerance tests (OGTT), prevent relationships between body shape and cardio-metabolic risk factors to be investigated.

5.5 Conclusion

This investigation has demonstrated the application of developed methods for extracting scale-invariant features from 3D imaging data, which characterise an individual's body shape. This characterisation of shape has been shown to contain information that is absent from measures used in current anthropometric practice. In addition, these identified shape features can complement traditional anthropometrics when explaining variations in quantities of subcutaneous abdominal adiposity. Further investigation is warranted to apply the developed methods to characterise a large cohort of several thousand participants and identify patterns of variation across a wider range of body shapes. In addition, future studies should investigate relationships that exist between body shape, distributions of body fat and associated health risks, such as diabetes and cardiovascular disease.

Chapter 6 - Allometry of human morphology within a large population-based cohort

6.1 Introduction

The results of Chapter Five demonstrated that scale-invariant features of body shape extracted from 3D imaging data can identify variations in human morphology that cannot be captured using traditional anthropometric techniques. In addition, these shape anthropometrics were shown to complement traditional anthropometrics when explaining variations in quantities of subcutaneous abdominal adiposity, measured using skinfold callipers. However, a limitation of this study was the size of the participant cohort that only captured a narrow selection of body shapes and sizes and is therefore not representative of the diverse body types that exist in the wider population. Previous literature has suggested that methods of 3D body classification require several thousand participants in order to be robust (19) and that estimates of allometry between size and shape are weak if a sample only includes a limited range of body sizes (181). Previous studies have used 3D imaging to assess variations in external dimensions of the human body and categorise distinguishable clusters of individuals into body types within large cohorts (19,122). However, these studies have used a specific definition of shape, based on the ratios and relative proportions of 1D size measures, such as lengths and girths. Though large numbers of size measures can be rapidly obtained, this approach discards the shape information captured by 3D imaging systems which describe human morphology.

As outlined in Chapter Two, allometry investigates the dependence of a body's shape on its size and is commonly used in anthropology and evolutionary biology to assess morphological variations within species (181,201,242). Allometric scaling suggests that when body size is altered its shape must also change in a compensatory fashion to preserve function and is generally considered the null hypothesis in studies of allometry (202). Though many studies have found that allometry is a dominant factor contributing to morphological variation within species (201,242), there are aspects of shape variation resulting from other environmental and ecological factors which cannot be explained by changes in size (181,202,203). Geometric morphometrics and size-correction can be used to partition shape variation of biological organisms into an allometric component, which is explained by variations in size, and a non-allometric component, which cannot be explained by changes in size (181). This chapter details

an investigation of allometry between measures of torso size and shape within a large population-based cohort. The aim of this study was to determine whether shape anthropometrics provide additional information regarding variations in human morphology that cannot be captured by existing anthropometric techniques. The objectives were to:

- Characterise the size and shape of individuals within a large cohort.
- Critically compare information provided by measures of size and shape regarding variations in human morphology.
- Determine the degree of allometric scaling and inter-dependence between measures of torso size and shape.
- Perform size-correction to identify non-allometric variations in torso shape which cannot be explained by existing anthropometric techniques.

6.2 Methods

6.2.1 Participants

Body size measures and 3D imaging data of participants analysed in this study were provided by the Leipzig Research Center for Civilization Diseases (LIFE). LIFE-Adult is a population-based cohort study, which collected extensive phenotype data of over 10,000 individuals from the city of Leipzig, Germany, with full details found in a publication by Loeffler et al. (11). LIFE-Adult covers a main age range between 40-79 years of age, with deep phenotyping in participants above the age of 60, and only a subset of participants aged between 18-39 years. During recruitment citizens were sent an invitation letter containing an information leaflet about the study, a response form and a postage-paid return envelope. Interested persons were scheduled for an appointment at the LIFE study centre and received a lump sum of 20 EUR per visit to cover their travel expenses. Basic characteristics of the LIFE-Adult participants are shown in Table 6.1. As a prerequisite to enrolment, written informed consent was obtained from all participants. The study was approved by the institutional ethics board of the Medical Faculty of the University of Leipzig and the responsible data protection officer. A formal agreement to access the LIFE-Adult cohort was approved by the LIFE Consortium and the Medical Faculty of the University of Leipzig (Appendix 4). All procedures and documents for this study were approved by the Sheffield Hallam University Research Ethics Committee, reference number ER13534279 (Appendix 4).

Table 6.1. Basic characteristics of participants in LIFE-Adult cohort.

Descriptive	Mean \pm SD	Male		Female		
		Min.	Max.	Mean \pm SD	Min.	Max.
n	4,578			5,086		
Age (years)	58 \pm 13	18	81	57 \pm 12	19	80
Stature (cm)	176.1 \pm 7.3	150.5	206.5	164.0 \pm 7.0	141.6	188.4
Mass (kg)	86.0 \pm 14.5	49.6	174.7	72.1 \pm 14.3	40.0	182.8
BMI (kg/m ²)	27.6 \pm 4.2	16.5	50.2	27.0 \pm 5.3	16.2	55.6
WHR	0.99 \pm 0.07	0.74	1.21	0.87 \pm 0.07	0.65	1.16

SD, Standard deviation.

6.2.2 Data acquisition

3D images of participants within the LIFE-Adult cohort were acquired by researchers at Leipzig University using a commercial Vitus Smart XXL 3D laser scanner (Human Solutions GmbH, Germany), with 3 mm vertical and 1 mm horizontal resolution at 27 measurement points per square centimetre of the body surface. 3D imaging was carried out in accordance with ISO 20685-1:2018 standards (140). Participants were asked to undress down to underwear and stockings and to remove any hair accessories and jewellery. Longer hair was required to be hidden under a tight-fitting bathing cap in a way not substantially changing the shape of the head. The 7th neck vertebra had to be exposed and ears had to be uncovered. Participants were advised to stand with feet shoulder-width apart with thighs not touching below the crotch, if possible, and weight distributed equally on both feet. Participants were asked to assume an upright and relaxed posture, standing as naturally as possible with arms slightly spread and elbows bent. They were asked to make fists, thumbs outside and pointing forward, with their eyes kept open during scanning, but not following the laser beam. 140 body size measures (lengths, girths, angles and aggregated measures) were automatically extracted from each acquired 3D image using Anthroscan ScanWorX 2.9.9b software (Human Solutions GmbH, Germany). Extracted body measures were based on the location of anatomical landmarks determined by proprietary automatic landmark identification algorithms within the Anthroscan ScanWorX software.

6.2.3 Pre-processing of extracted size measures

140 direct and indirect size measurements were provided alongside the 3D images of each participant. Direct measures include: length measures of body segments and distance measures between anatomical landmarks; girth measures of body segments and aggregated body characteristics: body mass index (BMI), waist-hip ratio (WHR), waist-height ratio (WHtR). Indirect quantities refer to those given relative to

predefined reference lines or planes, which are not part of the 3D image, such as distance to vertical. Body size measures were extracted automatically from the 3D images using proprietary algorithms within the Anthroscan ScanWorX software, in accordance with ISO 20685-1:2018 (140). Automatic methods enable large numbers of body measures to be rapidly extracted from 3D imaging data; however, they do not always correspond directly with measures acquired using manual techniques. Previous studies conducted by researchers at Leipzig University have shown that these automatically extracted body measures demonstrate good agreement with manual body measures (overall concordance correlation coefficient (OCCC) > 0.77) (55).

Removal of participants with missing measurements

Not all size measures could be estimated for all participants in the cohort, due to errors in the automatic landmark identification algorithms within the ScanWorX software. As a result, of the original 9,664 participants in the raw data matrix, 455 participants that were missing body size measures were removed from the analysis. It was decided that participants missing excessive volumes of size measures would negatively impact the allometric analysis. The resulting data matrix consisted of 34 body size measures (Table 6.2) for 9,209 participants (4,405 male, 4,804 female).

Normalisation of body size measures

When performing multivariate analyses with variables measured on different scales, such as clustering, PCA and multiple regression, variables are often standardised to aid interpretation (243). To facilitate comparisons between individuals of differing heights, measures of each participant were normalised by dividing all extracted torso size measures of each participant by their height as performed in Loeffler-Wirth et al. (19). Finally, these height normalised torso size measures were converted into z-scores, providing a common scale in units of standard deviations to enable subsequent stages of analysis. However, it has previously been shown that body proportions, such as segment lengths and girths, increase disproportionately with increased body height (244). Thus, to understand how each extracted body size measure would truly be expected to change with increased height, linear models were created using ordinary least squares regression to estimate the scaling exponent power, β_i , in the allometric models:

$$\text{Body Measure}_i = \alpha_i H^{\beta_i} \quad \text{Equation 6.1}$$

Where i represents measure i , α is a constant, and H represents height in metres.

These models were log-transformed:

$$\ln(\text{Body Measure}_i) = \ln(\alpha_i H^{\beta_i}) \quad \text{Equation 6.2}$$

By applying logarithms, Equation 6.2 becomes:

$$\ln(\text{Body Measure}_i) = \ln(\alpha_i) + \beta_i \ln(H) \quad \text{Equation 6.3}$$

If $y_i = \ln(\text{Body Measure}_i)$, $x = \ln(H)$ and an error term is added, the linear model becomes:

$$y = \ln(\alpha_i) + \beta_i x + \varepsilon_i \quad \text{Equation 6.4}$$

The estimated body size measure powers (reported as mean \pm SE) are shown in Table 6.2.

Table 6.2. Estimated coefficients of linear models for allometric height normalisation for participants in LIFE-Adult cohort.

Size Measure	Males (n = 4,405)		Females (n = 4,804)	
	$\ln(\alpha)$	β	$\ln(\alpha)$	β
Weight	3.52 \pm 0.03	1.64 \pm 0.05	3.75 \pm 0.03	1.04 \pm 0.06
Waist girth	4.62 \pm 0.03	-0.01 \pm 0.04	4.47 \pm 0.03	-0.48 \pm 0.05
Belly circ.	4.56 \pm 0.02	0.12 \pm 0.04	4.61 \pm 0.02	-0.09 \pm 0.04
Bust chest girth	4.54 \pm 0.02	0.25 \pm 0.03	4.71 \pm 0.02	-0.17 \pm 0.04
Buttock girth	4.4 \pm 0.01	0.42 \pm 0.03	4.62 \pm 0.02	0.10 \pm 0.03
High hip girth	4.54 \pm 0.02	0.15 \pm 0.04	4.62 \pm 0.02	-0.06 \pm 0.04
High waist girth	4.6 \pm 0.02	0.01 \pm 0.04	4.7 \pm 0.02	-0.46 \pm 0.05
Hip girth	4.41 \pm 0.01	0.43 \pm 0.03	4.61 \pm 0.02	0.15 \pm 0.03
Middle hip	4.51 \pm 0.02	0.21 \pm 0.04	4.72 \pm 0.02	-0.17 \pm 0.04
Torso width waist	3.85 \pm 0.03	-0.03 \pm 0.06	3.93 \pm 0.03	-0.36 \pm 0.06
Under bust circ.	4.52 \pm 0.02	0.2 \pm 0.03	4.61 \pm 0.02	-0.26 \pm 0.04
Waistband	4.44 \pm 0.02	0.26 \pm 0.04	4.55 \pm 0.02	0.00 \pm 0.04
Distance neck - hip	3.6 \pm 0.01	0.93 \pm 0.01	3.55 \pm 0.01	0.99 \pm 0.01
Side upper torso left	2.58 \pm 0.02	1.11 \pm 0.04	2.55 \pm 0.02	1.18 \pm 0.04
Side upper torso right	2.57 \pm 0.02	1.10 \pm 0.04	2.48 \pm 0.02	1.28 \pm 0.04
Cross shoulder	3.77 \pm 0.01	0.26 \pm 0.02	3.85 \pm 0.01	-0.02 \pm 0.03
Across front width	3.69 \pm 0.02	0.17 \pm 0.04	3.79 \pm 0.02	-0.14 \pm 0.04
Width armpits	3.71 \pm 0.02	0.25 \pm 0.04	3.89 \pm 0.02	-0.17 \pm 0.05
Across back width	3.54 \pm 0.02	0.36 \pm 0.03	3.56 \pm 0.02	0.18 \pm 0.04
Neck - waist	3.34 \pm 0.01	0.78 \pm 0.02	3.38 \pm 0.01	0.67 \pm 0.02
Neck left - waist back	3.45 \pm 0.01	0.76 \pm 0.02	3.48 \pm 0.01	0.63 \pm 0.02
Neck right - waist back	3.45 \pm 0.01	0.74 \pm 0.02	3.48 \pm 0.01	0.61 \pm 0.02
Across back width	2.82 \pm 0.03	0.82 \pm 0.05	2.75 \pm 0.02	0.99 \pm 0.05
Waist - high hip back	0.55 \pm 0.05	2.21 \pm 0.1	-0.65 \pm 0.09	4.36 \pm 0.17
Waist - buttock	2.36 \pm 0.02	1.13 \pm 0.03	2.18 \pm 0.02	1.50 \pm 0.04
Waistband - buttock	2.15 \pm 0.05	0.58 \pm 0.08	2.48 \pm 0.02	0.50 \pm 0.05
Crotch length	4.14 \pm 0.01	0.58 \pm 0.02	4.13 \pm 0.01	0.45 \pm 0.03
Crotch length front	3.51 \pm 0.02	0.51 \pm 0.03	3.42 \pm 0.02	0.39 \pm 0.03
Crotch length rear	3.39 \pm 0.01	0.64 \pm 0.02	3.45 \pm 0.01	0.51 \pm 0.02
Waist - buttock (L)	2.37 \pm 0.02	1.12 \pm 0.03	2.15 \pm 0.02	1.53 \pm 0.04
Waist - buttock (R)	2.36 \pm 0.02	1.13 \pm 0.03	2.15 \pm 0.02	1.55 \pm 0.04
Waistband-buttock (L)	1.66 \pm 0.06	0.99 \pm 0.11	2.33 \pm 0.03	0.67 \pm 0.06
Waistband-buttock (R)	1.66 \pm 0.06	1.00 \pm 0.11	2.32 \pm 0.03	0.69 \pm 0.06
Torso length	2.88 \pm 0.01	1.04 \pm 0.02	2.86 \pm 0.01	1.11 \pm 0.02

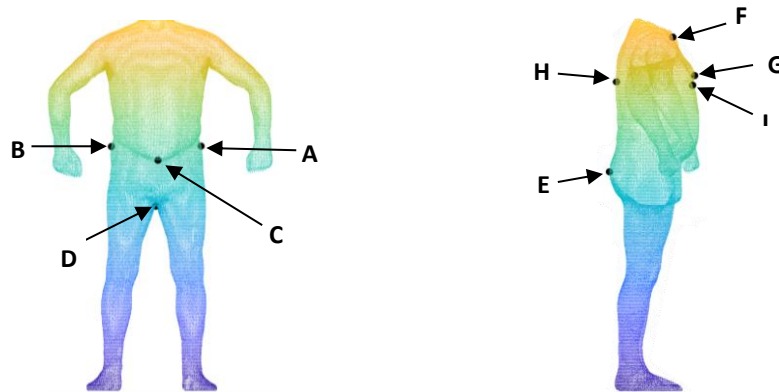
Results are displayed as X \pm SE.

6.2.4 3D imaging data post-processing

Data processing algorithms described in Chapter Three, were used to process the 3D imaging data. These scripts had to be modified to account for the differences in anatomical landmark locations marked on the 3D images of participants in the LIFE-Adult cohort. Previously in Chapters Three, Four and Five, bony anatomical landmarks were manually palpated and marked on the skin of each participant during data collection, and then digitised during post-processing. However, as described in Section 6.2.2, landmarks within the LIFE-Adult 3D images were identified automatically by proprietary software, which did not always correspond to the manually palpated landmarks, defined in Chapter Three. An investigation was therefore conducted, using a subset of 100 participants from the LIFE-Adult cohort, to determine whether landmarks identified by Anthroscan software could be used to process 3D images as in Chapter Three, Four and Five.

Identification of inferior and superior boundaries of the torso segment

Previously the inferior torso segment boundary was defined at the height of the anterior superior iliac spine (ASIS) markers, while the superior torso segment boundary was defined at the height of the xiphoid process. However, locating these anatomical points requires manual palpation and therefore were not identified by the automatic landmarking algorithms within the ScanWorX software. Examination of landmarks identified by the ScanWorX software highlighted several possible alternatives that could be used to define the inferior and superior boundaries of the torso segment. Figure 6.1 shows a typical 3D image from the LIFE-Adult dataset, with alternative landmarks for the inferior and superior torso segment boundaries also presented. Exploration of these alternative landmarks indicated that several were unreliably identified; either they were not identified or were identified incorrectly on the 3D image.



Landmark ID	Anatomical Landmark	Superior/ Inferior	Landmark ID	Anatomical Landmark	Superior/ Inferior
A	'3D Waistband Left'	Inferior	E	Buttock ('11330')	Inferior
B	'3D Waistband Right'	Inferior	F	'Neck Front'	Superior
C	'3D Waistband Front'	Inferior	G	'Breast Front'	Superior
D	'Crotch Center'	Inferior	H	'Scapula Point'	Superior
			I	'Midriff Girth'	Superior

Figure 6.1. Typical 3D body scan provided by the Vitus XXL Smart Laser Scanner and selected anatomical landmarks identified within the software.

Of the potential inferior anatomical landmarks, identification of the ScanWorX point '11330' (buttock height) was the most reliable. The location of this landmark corresponds to the gluteal (hip) girth location, defined by ISAK guidelines as: *"The gluteal girth is taken at the level of the greatest posterior protuberance of the buttocks."* (53) (p84). This landmark is lower than the ASIS markers used in previous chapters to define the inferior boundary of the torso segment. However, its ease of identification within the 3D images and its agreement with ISAK anthropometric guidelines made this landmark suitable for use as the inferior boundary of the torso segment. Of the potential superior anatomical landmarks, only the ScanWorX 'Neck Front' landmark was reliably identified. However, the 'Neck Front' landmark was considerably higher than the xiphoid process landmark used as the superior boundary of the torso segment previously. If this landmark was used as the superior boundary of the torso segment then the participant shoulder and armpit areas would be within the region of interest, introducing complications into the data processing stage. However, since the buttock and neck landmarks both provided reliably identified points within the 3D images it was posited that it would be possible to calculate proportional distances along the length of the 3D images to define the inferior and superior boundaries of the torso segment.

An investigation was conducted, using 3D imaging data of 90 participants with manually palpated landmarks, presented in Chapters Three, Four and Five, to determine the proportionate distance of the xiphoid process landmark along the length of the torso segment. It was determined that the xiphoid process landmark was $60 \pm 1.5\%$ of the proportionate vertical distance between the buttock and neck height locations (Figure 6.2). It is possible that these differences between the manually palpated xiphoid location and the calculated location could influence the results of subsequent analysis of torso variation. However, it has been shown that trained anthropometrists exhibit intra-observer errors of approximately 5 mm when manually palpating the xiphoid process landmark (106), which may also contribute to these differences in location. It was decided that this method was sufficient for determining the inferior and superior boundaries of the torso segment.

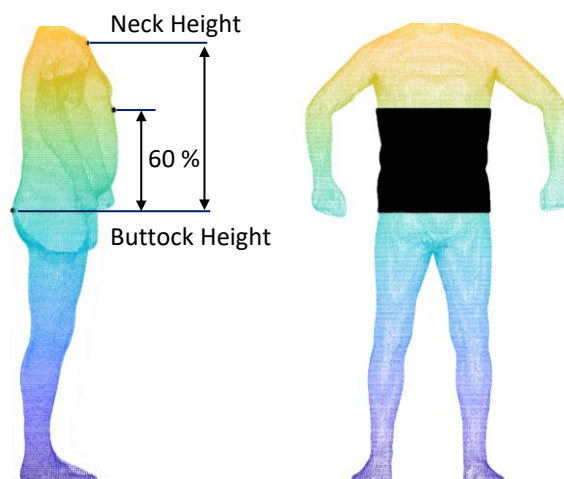


Figure 6.2. Determining the superior and inferior boundaries of the torso segment of interest.

Creating local anatomical coordinate system

The orientations of images acquired by the Vitus Smart XXL 3D laser imaging system are based on the Vitus coordinate system (Figure 6.3a), consequently if participants were not scanned facing in the frontal direction of the scanner differences in orientation in the acquired imaging data were present (Figure 6.3b). A local anatomical co-ordinate system was therefore required to remove differences in location and orientation between participants in the LIFE-Adult cohort. As described in Chapter Three, the centre of each torso image was defined as the midpoint between the xiphoid process and the 9th thoracic vertebra landmarks, with the vector between these used as the sagittal axis. However, as these palpated anatomical landmarks were

not present in the LIFE-Adult 3D imaging data, an alternative method to create a local co-ordinate system was required.

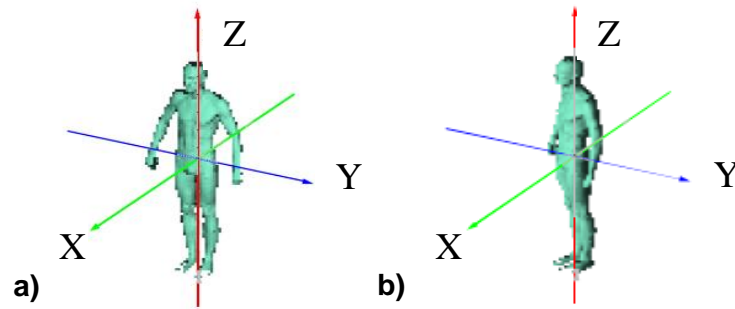


Figure 6.3. Vitus scanner coordinate system. a) Correct positioning of participant; b) Incorrect positioning of participant.

Initial alignment of the 3D images was required to ensure that the anterior and posterior aspects of the torso segment of each participant were facing in the positive and negative directions on the x-axis for further processing, respectively. This was achieved by aligning the vector between the left and right shoulder landmarks, identified by the ScanWorX software, with the x-axis of the global coordinate system. A slice of data points was extracted from each 3D image at the estimated xiphoid process location, which contained features present on the surface of the torso that could be used to define the local coordinate system (Figure 6.4a). The inferior-superior z component of all raw data points within this slice was disregarded, considering the planar dimensions of all data points only in the x-y plane (Figure 6.4b). The local maxima and minima of the extracted point slice data along the x-axis were then identified on the posterior and anterior aspects of the torso, respectively (Figure 6.4b). These localised peaks in the point slice data were assumed to correspond to the approximate locations of the xiphoid process and vertebra landmarks, which would otherwise be manually palpated. Experimentation with the subset of 100 3D images from the LIFE-Adult cohort demonstrated that these simple features could be identified reliably for all individuals. As a result, the centre of each torso segment could then be defined as the midpoint between the identified anterior and posterior landmarks, in the same manner as described in Section 3.3.2.

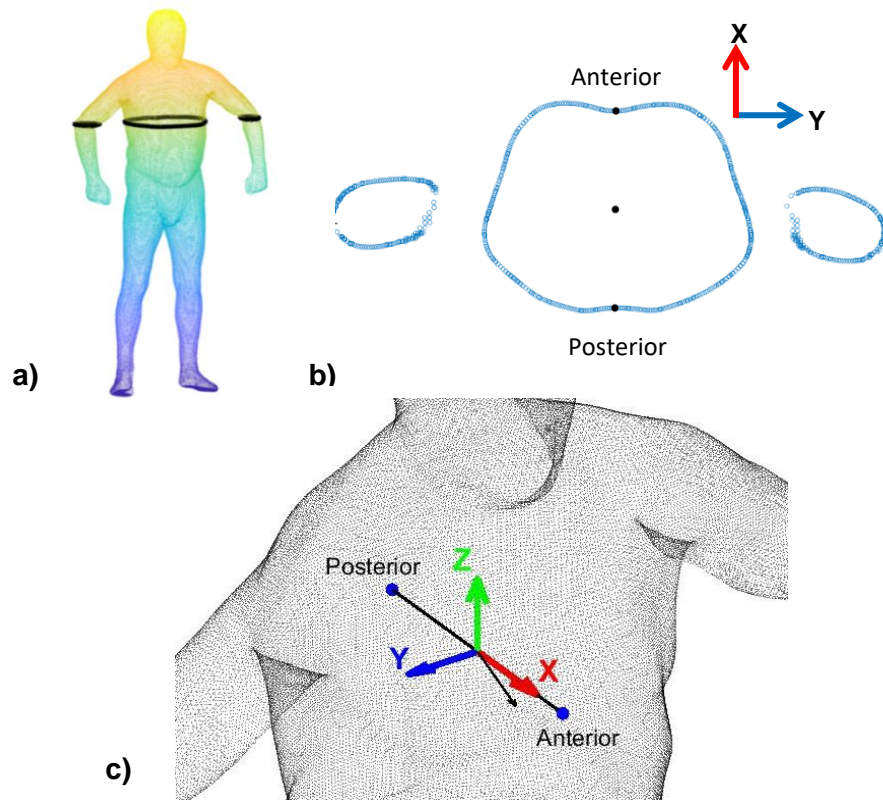


Figure 6.4. Creating local coordinate system torso segment. a) Extract cross-sectional slice from 3D image; b) Identification of anterior, posterior and midpoint landmarks in slice; c) Creation of coordinate system within torso segment.

As described in Section 3.3.2, a vector from the anterior landmark to the posterior landmark identified on the surface of the 3D image was defined the sagittal axis of the local coordinate system. In the absence of anatomical landmarks on the lateral aspect of the torso segment, the cross product of the sagittal axis and an angled vector on the x-y plane was used to define the longitudinal axis, assuming that the participant was stood parallel to the global vertical axis. This is a limitation, since it has been shown in Chapter Four that a participants' posture during imaging can vary considerably in the lateral direction. Finally, the transverse axis was defined as being perpendicular to the plane formed by the sagittal and longitudinal axes (Figure 6.4c). This anatomical axis system ensured differences in translation and orientation between participants were removed during data processing.

Torso shape feature detection

Following alignment, the remaining stages of the analytical procedure detailed in Chapter Three were carried out: segmenting the 3D images to remove coordinate points not related to the torso region of interest; extracting features of torso shape variation. For this, 25 separate 2mm thick bands of 3D coordinate points were extracted from each torso segment point cloud, at proportionate distances along their

length to account for the increase in the region of interest. The centroid size of all extracted data point slices were scaled by a single scale factor to ensure that all torso segments were of uniform overall size, removing differences in scale. The first 10 frequency coefficients present within each data slice were then extracted using a fast-Fourier transform algorithm, reducing the total number of variables representing each participant to 250 complex Fourier coefficients. Finally, a principal components analysis (PCA) was carried out to detect independent features of torso shape that exhibited the highest variation within the LIFE-Adult cohort. PCA was carried out for all participants in the LIFE-Adult cohort, both male and female, to capture all possible torso shape variations present within the sample. This enabled differences between males and females for each of the identified shape features to be evaluated.

6.2.5 Statistical analysis

To ensure the selection of suitable statistical analysis procedures the parametric nature of all variables were first explored within SPSS (IBM SPSS Statistics 24.0). Histograms and Q-Q plots were visually inspected and a Shapiro-Wilks test was conducted to assess the normality of all extracted size measures and shape features. Previous studies have shown that there are underlying sexual dimorphisms in adipose tissue biology and deposition, caused by genetic and hormonal factors, which cause differences in body size and shape between males and females (65,66). Consequently, sex-specific means and standard deviations for each torso shape principal component and size measure were calculated. Independent t-tests were conducted to determine if there were statistically significant differences between male and female participants in all 34 traditional anthropometrics (listed in Tables 6.3 & 6.4) and shape PC's. Pearson's product-moment correlations, r , were used to assess linear relationships between individual size measures, as well as between measures of size and shape. P-values < 0.001 were considered statistically significant, because with large sample sizes statistical tests will often demonstrate significant differences when using a typical alpha level (0.05) (245). The coefficient of determination, R^2 , was also calculated as a measure of effect size, to assess the practical importance of correlations between individual variables independent of sample size (245). Correlations and effect sizes were calculated within SPSS (IBM SPSS Statistics 24.0). In addition, mutual information ($I(X,Y)$) - a non-parametric measure of total dependence between random variables

(246) - was calculated to assess whether there was any degree of dependence, either linear or nonlinear, between measures of size and shape. Mutual information was calculated within MATLAB (version 9.2, Mathworks, USA) using kernel estimates of mutual information (247).

Allometry is typically assessed by a multivariate regression of shape variables onto a measure of size, to determine the expected change in shape per unit increase in size (181). For this investigation, allometry was examined using partial least squares regression (PLSR) models to determine how much the variance in each identified torso shape principal component depends on traditional anthropometrics extracted from 3D imaging data. Originally proposed by Wold (248), PLSR is a generalisation of multiple linear regression (MLR) that combines elements of linear regression and factor analysis. PLSR is particularly useful for this analysis, because unlike MLR it can perform analysis with a large number of strongly collinear predictor variables (249), which has been shown to be the case with measures of body size (2,122). PLSR reduces the predictor (x) and response (y) variables to principal components. The y-component scores are then predicted from the x-components creating several latent factors, which in turn are used to predict the raw y-variable (250). PLSR is reported to be more efficient than PCA as it takes the response variable into account (251). According to Wold et al. (248) if y variables are correlated they should be analysed together, however, if the y variables are independent, separate PLSR models should be created for each. Since the torso shape principal components are orthogonal, separate PLSR models were created for each shape principal component with all torso size measures used as predictor variables. PLSR analyses were conducted within MATLAB (version 9.2, Mathworks, USA) using the plsregress MATLAB library.

The mean squared prediction error (MSEP) by 10-fold cross-validation was calculated to determine the number of components required for each PLSR model, preventing overfitting of the model to ensure the same data are not used to fit a model and estimate prediction error. The importance of each size measure within each PLSR model was determined using the variable importance in projection (VIP) statistic. VIP is the weighted sum of squares of the PLSR-weights, with the weights calculated from the amount of y-variance of each PLSR component (248,252). Wold (248) previously suggested that predictor variables demonstrating a $VIP \geq 0.8$ can be considered to

significantly contribute to the model with high predictive power. VIP's were calculated within MATLAB (version 9.2, Mathworks, USA) using libPLS (253) MATLAB library.

Stepwise MLR analyses were performed to determine how much variance in traditional anthropometrics could be explained by the torso shape PCs. As demonstrated in Chapter Five, shape PCs are uncorrelated and can be combined as predictor variables within a single MLR model, without multicollinearity reducing the precision of the coefficient estimates of the regression model (236,254). Separate MLR models were created to estimate each individual size measure from combinations of the torso shape PCs. The predictor variable that had the strongest correlation with the outcome variable was entered into the model first and was retained if it contributed significantly to the model. Subsequent predictor variables that had the highest semi-partial correlations with the outcome variable were then added, but were only retained if they contributed significantly to the model (254). MLR analyses were executed within SPSS (IBM SPSS Statistics 24.0).

Sex-specific allometric models were created to assess the inter-dependence of measures of torso size and shape within the LIFE-Adult cohort. For this, PLSR models were created to estimate changes in each torso shape PC from unit changes in torso size, using coefficients from the previously calculated PLSR models. Changes in torso shape were estimated across the entire range of torso size measures within the LIFE-Adult cohort, with height measures constant at 180 cm and 160 cm for the male and female allometric models, respectively.

6.3 Results

6.3.1 Torso shape features within LIFE-Adult cohort

PCA produced 9 PCs that captured 90.6 % of the total torso shape variation within the LIFE-Adult cohort (Figure 6.5). PCs which accounted for less than 1% of the total variance in torso shape were removed from the analysis. Figure 6.5 shows the maximum deviations from the average torso shape of the sample along each of these PCs. Blue and red regions on the images represent areas that protrude less, or more than the average torso shape of the cohort, respectively. The torso shape features identified within the LIFE-Adult cohort resemble those identified in Chapter Five, such as variations in anterior-posterior weighting (PC1), abdominal roundness (PC3), lateral asymmetry (PC4) and mass distributions along the length of the torso segment (PC2).

PC's 2, 5 and 7 in the LIFE-Adult cohort clearly represent differences between male and female body shapes.

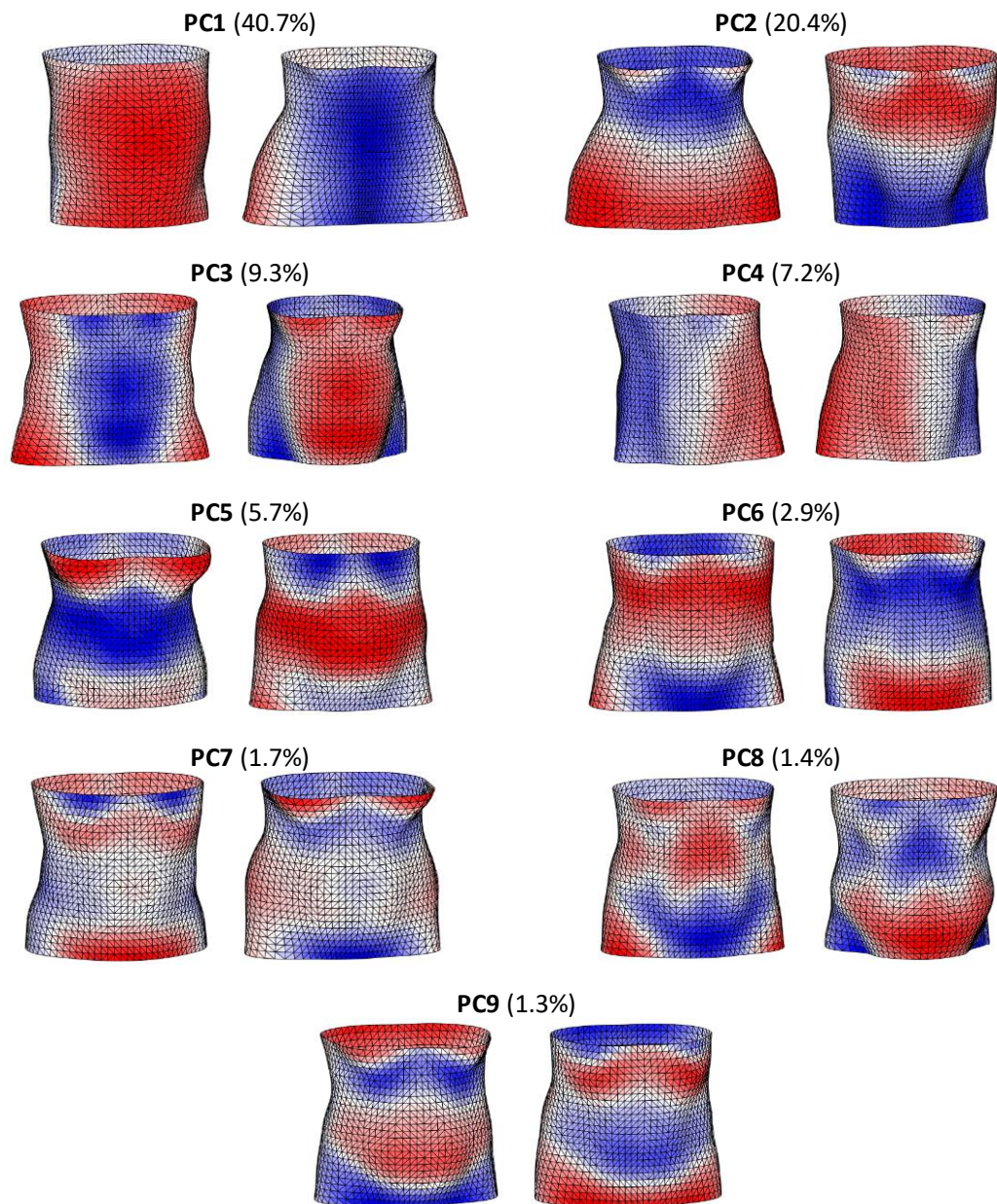


Figure 6.5. First 9 principal components capturing 90.6 % of variation in torso shape in the LIFE-Adult cohort, shown as the maximum positive (left) and negative (right) deviations from the sample mean. Blue and red regions represent areas that protrude less, or more than the average torso, respectively.

Statistical difference testing found significant differences between males and females for all size and shape anthropometrics collected in this study (Appendix 4). Figure 6.6 shows the mean torso shapes for males and females within the LIFE-Adult cohort, demonstrating clear differences in mass distribution between male and female body shapes. Males have mass located more centrally along the torso segment, while

females have more mass in the lower torso and in the bust region. As a result, all subsequent analyses were stratified by sex.

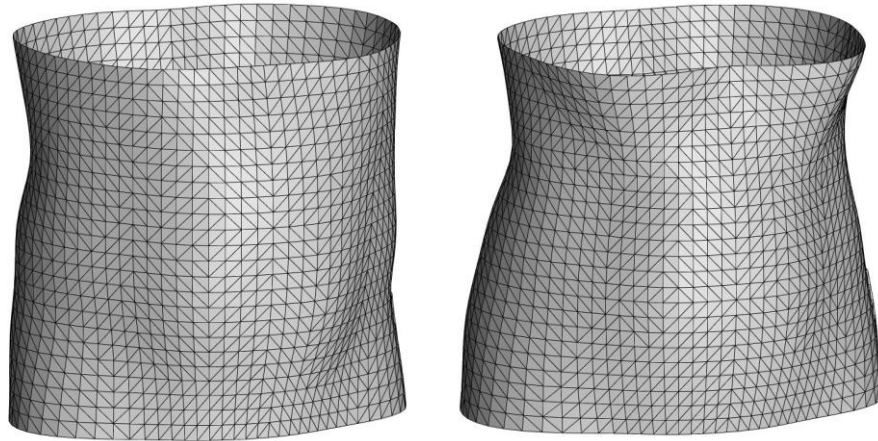


Figure 6.6. Average torso shape of male (left) and female (right) participants in the LIFE-Adult cohort.

6.3.2 Relationships between size and shape measures

There were moderate to strong correlations between the majority of extracted size anthropometrics, for both male and female participants (Appendix 4). In particular, individual torso girth measures were strongly correlated with each other and with body weight and torso width measures. These correlations were statistically significant ($p < 0.01$) and had medium to large effect sizes. However, girth measures were less strongly correlated with torso length and distance measures, such as side upper torso length and waist-buttock distance. Though these correlations were statistically significant ($p < 0.01$), they only demonstrated small effect sizes. Shape PC3 was strongly correlated with torso girth measures and demonstrated moderate to strong correlations with body weight and torso width measures, for both male and female participants. These correlations were statistically significant ($p < 0.01$) and demonstrated medium to large effect sizes. Shape PC's 1, 2 and 5 demonstrated weak to moderate correlations with torso girth and width size measures, suggesting reasonable linear relationships between these measures. However, though these correlations were statistically significant ($p < 0.01$), they only demonstrated small to medium effect sizes. The remaining shape PCs demonstrated only weak to no linear correlations with traditional anthropometrics. In addition, according to calculated mutual information primarily linear dependence was observed between measures of body size and shape, with low amounts of nonlinear dependence.

6.3.3 Regression analysis

Predicting shape from size - Partial Least Squares Regression (PLSR)

Size measures explained between 3.2-84.4% and between 4.3-72.7% of shape PC variation for male and female participants, respectively. Between 44-65% of predictor size measures used within each PLSR model demonstrated VIP values ≥ 0.8 for males (Table 6.3), while 41-82% of size measures had VIP values ≥ 0.8 for females (Table 6.4), with different combinations of size measures contributing to the prediction of shape.

Table 6.3. Variable importance in projection statistic scores and predicted variance in male PLSR models.

Size Measure	Shape PCs								
	PC1	PC2	PC3	PC4	PC5	PC6	PC7	PC8	PC9
Shape explained by size:	64.9%	57.9%	84.4%	3.2%	66.5%	42.5%	56.8%	15.2%	38.3%
Weight	0.76	0.62	1.01*	1.20*	0.52	0.69	0.63	0.82*	0.43
Waist girth	1.15*	1.17*	1.26*	0.40	0.80*	0.89*	1.30*	0.96*	0.78
Belly circ.	1.01*	0.63	1.38*	0.33	1.29*	0.63	1.50*	0.73	0.38
Bust chest girth	1.03*	1.66*	1.30*	0.28	2.15*	1.37*	0.73	0.94*	0.82*
Buttock girth	0.90*	1.91*	1.19*	0.48	0.56	0.90*	1.34*	1.03*	1.57*
High hip girth	0.95*	0.52	1.44*	0.34	1.32*	0.56	1.41*	0.94*	0.28
High waist girth	1.23*	1.33*	1.17*	0.50	0.59	0.90*	1.07*	0.84*	0.80*
Hip girth	0.95*	1.97*	1.21*	0.32	0.53	0.99*	1.42*	1.34*	1.58*
Middle hip	0.89*	0.55	1.59*	0.48	1.28*	0.51	0.88*	1.26*	0.70
Torso width waist	2.39*	1.19*	1.11*	0.53	1.39*	2.02*	1.00*	0.98*	0.76
Under bust circ.	1.05*	1.62*	1.39*	0.58	2.36*	0.74	0.82*	0.97*	0.84*
Waistband	0.88*	1.09*	1.27*	0.41	0.93*	1.03*	0.79	1.48*	0.74
Distance neck - hip	0.63	0.56	0.31	0.71	0.51	1.16*	0.83*	1.23*	1.33*
Side upper torso left	0.49	0.52	0.53	0.49	0.87*	0.37	0.49	0.39	0.80*
Side upper torso right	0.47	0.54	0.50	1.54*	0.79	0.55	0.49	0.52	0.71
Cross shoulder	0.76	0.73	1.11*	0.50	1.07*	0.76	0.56	0.60	0.37
Across front width	0.67	0.70	0.86*	0.54	0.93*	0.41	0.57	0.70	0.72
Width armpits	1.30*	0.98*	0.90*	0.83*	1.39*	0.60	0.47	0.54	0.20
Across back width	0.87*	0.85*	1.13*	0.65	1.02*	0.82*	0.60	0.71	1.11*
Neck - waist	0.51	0.40	0.50	0.81*	0.88*	0.83*	0.64	0.51	1.01*
Neck left - waist back	0.59	0.41	0.52	1.07*	0.96*	1.01*	0.62	0.63	0.94*
Neck right - waist back	0.68	0.54	0.52	0.81*	0.90*	1.03*	0.60	0.47	0.93*
Across back width	0.56	0.54	0.32	0.55	0.69	0.65	0.76	0.44	1.24*
Waist - high hip back	0.53	0.40	0.40	0.92*	0.48	1.21*	0.80*	1.21*	0.59
Waist - buttock	1.56*	1.39*	0.75	1.49*	0.50	1.59*	0.88*	1.24*	1.34*
Waistband - buttock	1.19*	1.65*	1.30*	0.81*	0.81*	1.87*	1.24*	1.54*	2.14*
Crotch length	1.01*	0.57	1.25*	0.33	0.64	0.55	1.29*	0.78	0.80*
Crotch length front	0.91*	0.59	1.21*	0.80*	0.71	0.65	1.42*	1.33*	1.72*
Crotch length rear	1.45*	0.94*	1.15*	0.97*	0.70	0.53	1.26*	1.31*	0.86*
Waist - buttock (L)	0.64	0.60	0.50	2.80*	0.41	1.23*	0.79	1.13*	0.55
Waist - buttock (R)	0.66	0.66	0.54	2.65*	0.43	1.21*	0.79	1.20*	0.61
Waistband-buttock (L)	1.04*	1.02*	0.67	1.04*	0.75	1.00*	1.48*	0.91*	1.28*
Waistband-buttock (R)	1.05*	1.06*	0.69	0.58	0.78	1.02*	1.52*	1.10*	1.29*
Torso length	0.84*	0.50	0.54	1.17*	0.59	1.14*	1.00*	1.41*	0.50

*Variable importance in projection (VIP) values ≥ 0.8 , shown in grey fields.

Table 6.4. Variable importance in projection statistic scores and predicted variance in female PLSR models.

	Shape PCs								
	PC1	PC2	PC3	PC4	PC5	PC6	PC7	PC8	PC9
Shape explained by size:	65.6%	51.1%	72.7%	4.3%	62.2%	29.5%	57.0%	7.3%	35.1%
Size Measure									
Weight	0.82*	0.88*	1.10*	1.02*	0.54	0.95*	0.83*	1.24*	0.76
Waist girth	1.03*	0.89*	1.13*	0.82*	0.81*	0.94*	0.87*	0.80*	0.80*
Belly circ.	0.94*	0.63	1.21*	0.84*	0.99*	0.90*	1.41*	0.51	0.94*
Bust chest girth	1.08*	1.57*	1.20*	1.03*	2.01*	1.10*	0.62	0.30	1.65*
Buttock girth	0.88*	1.59*	1.22*	0.76	0.58	1.01*	1.16*	0.67	1.46*
High hip girth	0.91*	0.47	1.30*	0.82*	0.92*	0.84*	1.46*	0.49	0.59
High waist girth	1.13*	1.21*	1.05*	0.85*	0.67	0.75	0.59	0.33	0.85*
Hip girth	0.89*	1.73*	1.29*	0.76	0.55	1.27*	1.27*	0.44	1.53*
Middle hip	0.95*	0.50	1.50*	0.78	0.65	0.76	0.78	0.46	0.52
Torso width waist	1.75*	1.33*	0.97*	0.92*	1.31*	1.10*	0.76	1.84*	1.29*
Under bust circ.	1.09*	1.57*	1.34*	1.02*	0.91*	0.73	1.03*	1.88*	0.47
Waistband	1.04*	0.48	1.11*	0.80*	0.94*	1.24*	1.57*	0.58	0.64
Distance neck - hip	0.87*	0.61	0.46	0.46	1.17*	0.71	0.65	1.15*	1.41*
Side upper torso left	0.53	0.51	0.44	0.43	0.51	0.83*	0.63	0.76	0.44
Side upper torso right	0.60	0.51	0.45	1.01*	0.63	1.03*	0.60	0.66	0.50
Cross shoulder	0.91*	0.74	1.11*	0.99*	0.90*	0.70	0.62	0.94*	0.73
Across front width	0.83*	0.79	0.92*	0.69	0.75	0.78	0.61	1.33*	0.99*
Width armpits	0.94*	0.95*	0.90*	1.22*	0.85*	0.82*	0.76	0.91*	0.46
Across back width	1.02*	0.65	1.14*	0.88*	0.99*	0.55	0.60	0.35	1.20*
Neck - waist	0.48	0.67	0.56	0.56	0.47	0.92*	0.83*	0.35	1.06*
Neck left - waist back	0.60	0.59	0.61	0.97*	0.68	1.29*	0.73	0.60	0.41
Neck right - waist back	0.66	0.73	0.61	1.12*	0.71	1.32*	0.75	0.74	0.42
Across back width	0.58	0.61	0.26	0.68	0.38	0.86*	0.78	1.07*	0.87*
Waist - high hip back	0.95*	0.70	0.62	0.51	1.64*	1.11*	0.86*	1.01*	0.64
Waist - buttock	1.48*	1.51*	0.97*	0.48	1.38*	1.40*	0.87*	0.54	1.31
Waistband - buttock	1.35*	2.05*	1.31*	0.82*	0.83*	0.98*	0.46	0.57	0.73
Crotch length	0.81*	0.64	1.29*	0.77	0.71	0.63	1.89*	0.78	0.85*
Crotch length front	0.96*	0.70	1.19*	0.73	0.62	0.68	1.88*	2.27*	1.53*
Crotch length rear	1.28*	0.98*	1.29*	0.81*	0.82*	0.55	1.87*	1.55*	1.07*
Waist - buttock (L)	0.99*	0.67	0.86*	2.39*	1.47*	1.32*	0.79	0.58	0.69
Waist - buttock (R)	1.02*	0.72	0.95*	1.90*	1.46*	1.15*	0.75	0.55	0.85*
Waistband-buttock (L)	1.10*	0.96*	0.52	1.41*	0.87*	0.79	0.47	0.71	0.85*
Waistband-buttock (R)	1.12*	1.01*	0.57	0.98*	0.87*	0.70	0.47	0.83*	0.84*
Torso length	1.23*	0.90*	0.70	1.25*	1.78*	1.90*	0.91*	1.80*	1.94*

*Variable importance in projection (VIP) values ≥ 0.8 , shown in grey fields.

Predicting size from shape - Multiple Linear Regression (MLR)

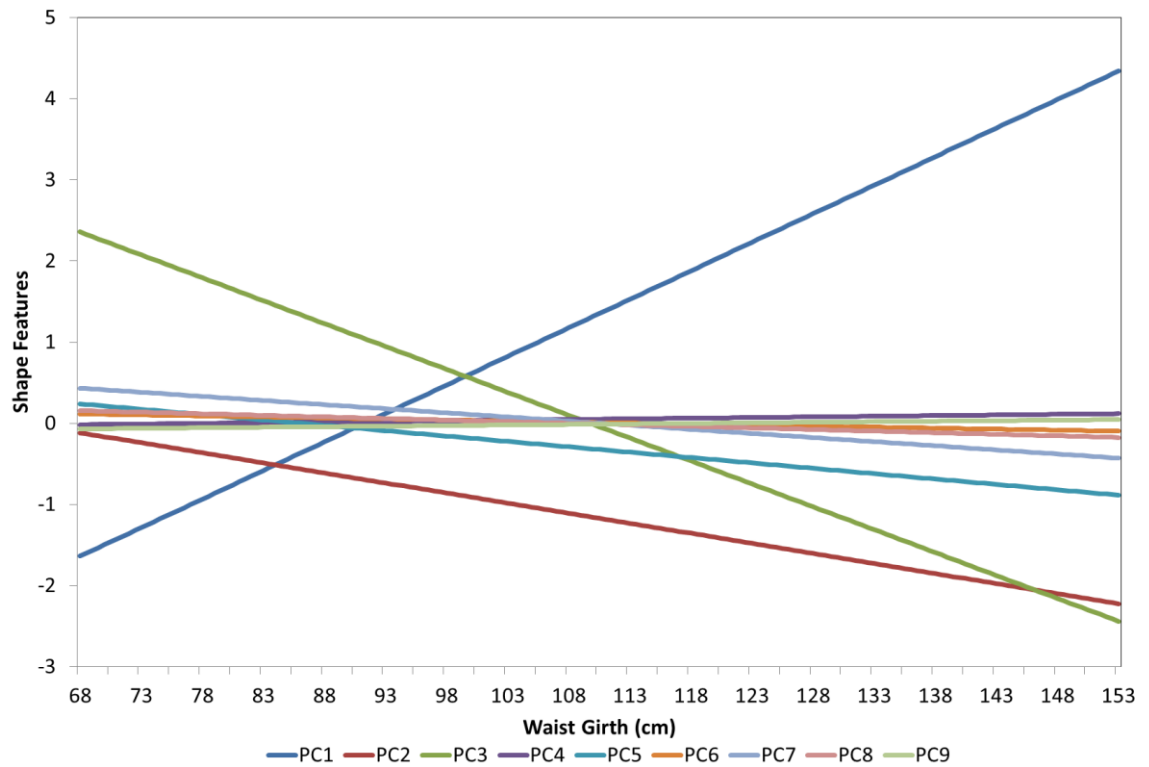
Combinations of shape PCs explained between 5.8-82.8% and between 4.8-80.1% of the variance in torso size measures for male and female participants, respectively. Similar to the PLSR models, the results of the MLR analysis demonstrate that though shape anthropometrics can predict some of the variation in torso size measures, there are residual components of torso size variation which cannot be explained by torso shape.

6.3.4 Allometric model between torso size and shape measures in LIFE-Adult cohort

Shape variations explained by changes in size

Figures 6.7 and 6.8 present the predicted (allometric) variations in all identified torso shape features corresponding to unit changes in waist girth measures for males and females, respectively.

a)



b)

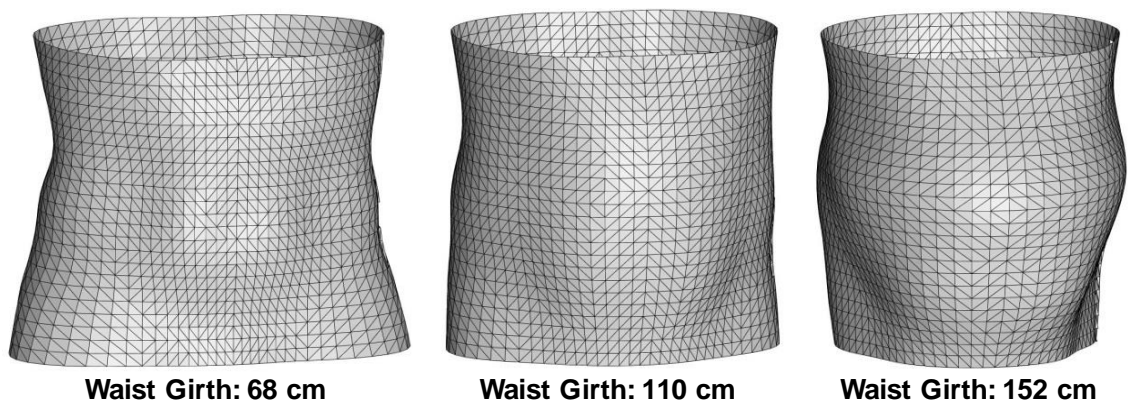


Figure 6.7. Allometric scaling between size and shape measures for male participants. a) Predicted changes in shape features using PLSR models; b) Reconstructed allometric torso shapes for males with waist girths of 68, 110 and 152 cm.

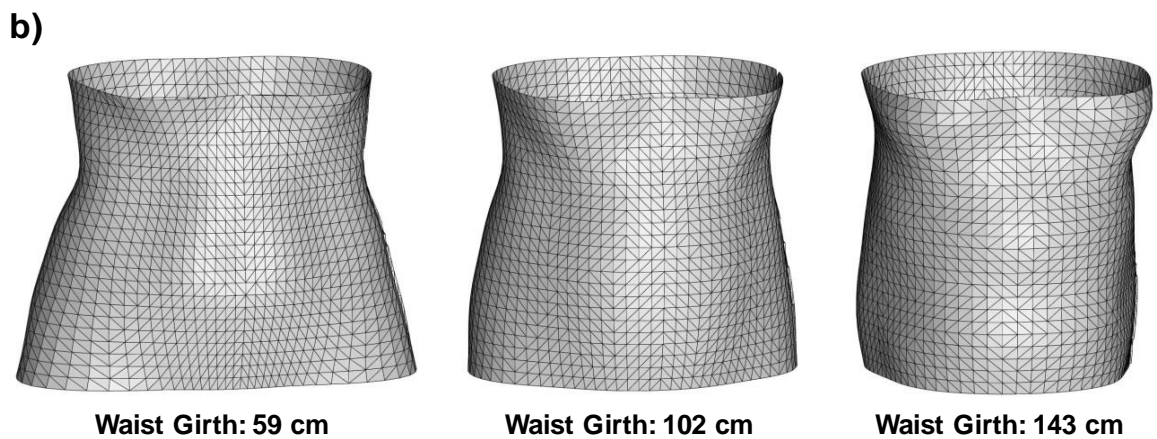
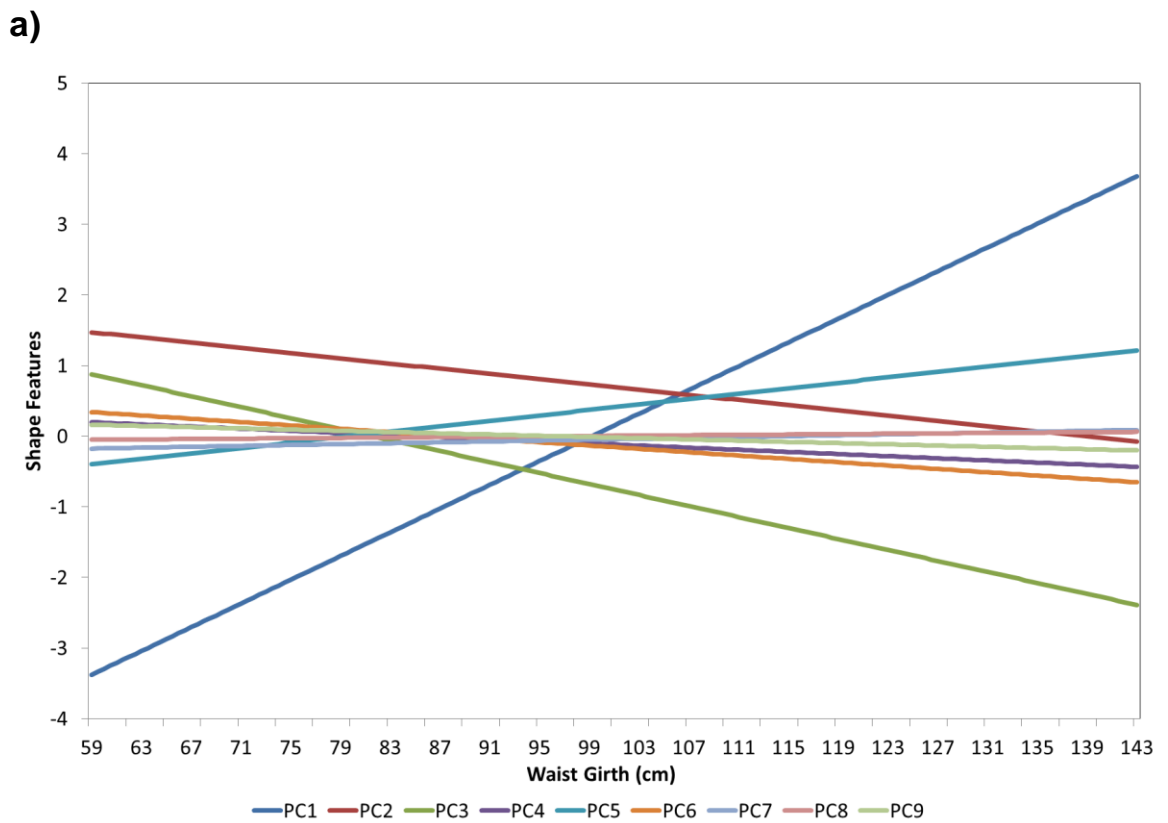


Figure 6.8. Allometric scaling between size and shape measures for female participants. a) Predicted changes in shape features using PLSR models; b) Reconstructed allometric torso shapes for females with waist girths of 59, 102 and 143 cm.

There are strong allometric relationships between torso size and shape PCs 1, 2, 3 and 5, with increases in torso size corresponding to considerable changes in these shape features for both males and females (Figure 6.7a & 6.8a). These predicted changes in torso shape are visualised as reconstructed torso meshes for the smallest, mean and largest waist girth values within the LIFE-Adult cohort for males (Figures 6.7b) and females (Figure 6.8b). Increases in torso size correspond to greater mass and increased curvature on the anterior aspect of the torso segment for both males and females. Though, as described in Section 6.3.1, males appear to exhibit these changes primarily

in the central region of the torso, while females exhibit these changes initially in the lower torso and bust region. However, at the largest torso sizes changes in shape also occur across the rest of the anterior aspect of the torso segment for female participants.

Shape variations unexplained by changes in size

Figures 6.9a and 6.10a show the predicted torso shapes for individuals with the 50th percentile waist girth measure according to the developed allometric models, for males (100 cm) and females (91 cm), respectively. Figures 6.9b and 6.10b show examples of observed torso shapes for individuals within the LIFE-Adult cohort who all have waist girth measures at the 50th percentile. Although these individuals all have the same waist girth they differ considerably from the predicted torso shape, due to non-allometric variations which cannot be explained by changes in size measures. Figures 6.9c and 6.10c show boxplots displaying the amount of residual (non-allometric) shape variation present in the developed PLSR models for each torso shape PC for male and female participants, respectively. These residuals represent size-corrected shape variables, which are uncorrelated with changes in the size measures used as predictor variables in the PLSR models. Outliers were observed for each of the shape PCs, representing the extreme variations in torso shape from the mean of the sample that were unexplained by allometric scaling, with PC4 and PC8 exhibiting the greatest amount of unexplained shape variation. The values of the non-allometric deviations from the predicted torso shape for each of the observed participants are also shown in the boxplots in Figures 6.9c and 6.10c for males and females, respectively.

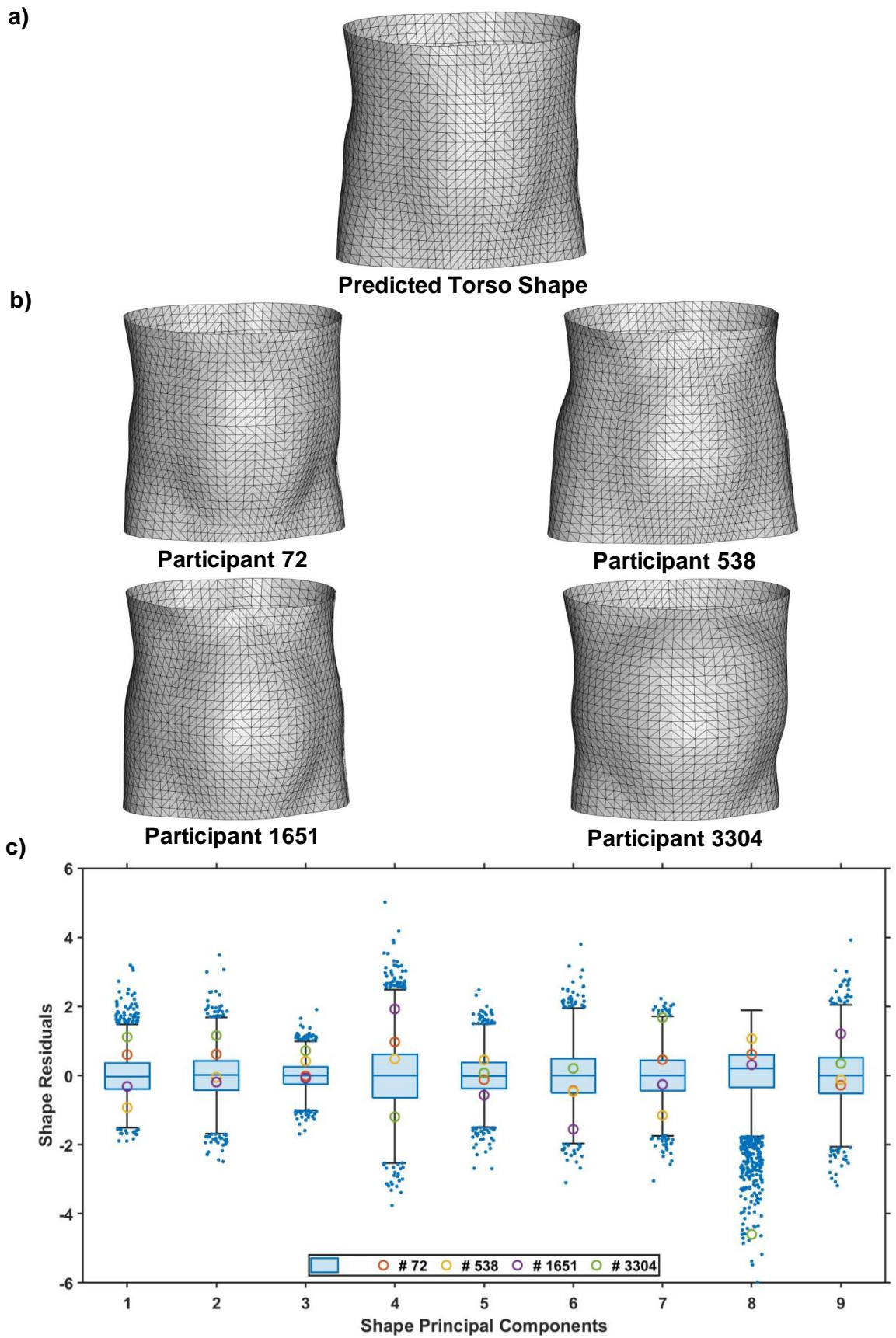


Figure 6.9. Non-allometric male torso shape variation. a) Predicted torso shape for males with waist girth 100 cm; b) Examples of observed torso shapes of males with waist girth 100 cm; c) Boxplots showing the amount of residual variation for each shape principal component in PLSR model, with deviations from the predicted torso shape displayed by the participants in b).

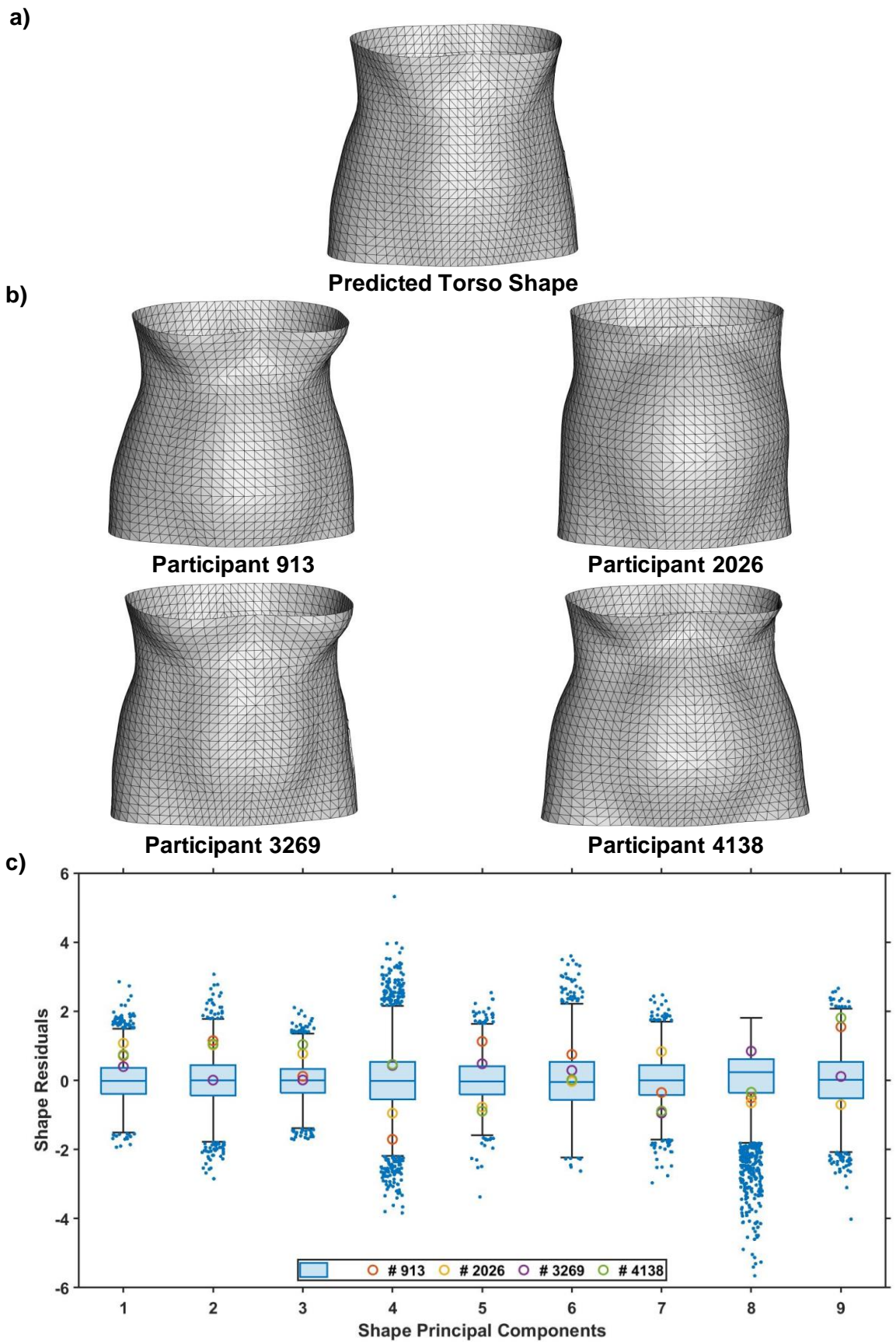


Figure 6.10. Non-allometric female torso shape variation. a) Predicted torso shape for females with waist girth 91 cm; b) Examples of observed torso shapes of females with waist girth 91 cm; c) Boxplots showing the amount of residual variation for each shape principal component in PLSR model, with deviations from the predicted torso shape displayed by the participants in b).

6.4 Discussion

Allometry is the study of relationships between measures of body size and shape, and is commonly used to assess morphological variations within species (181). Previous investigations have found that several developmental processes and morphological traits change with body size, due to allometric scaling (201,202,242). However, there are also non-allometric aspects of shape variation which cannot be explained by changes in body size, due to factors such as environment, phylogenetic heritable traits and individual morphological variation (181,202,203). Thus, if variations in human torso shape cannot be fully explained by existing anthropometric techniques this would suggest that additional measures are required to evaluate all aspects of human morphology in practice. The aim of this study was to determine whether shape anthropometrics provide additional information regarding variations in human morphology that cannot be captured by existing anthropometric techniques.

Previous investigations which have used 3D imaging to perform anthropometric assessments, have typically only obtained traditional anthropometrics of body size in order to analyse variations within the population (2,19,122). Though this approach enables a thorough characterisation of body size, it discards body shape information captured by 3D imaging systems. As a result, this has limited analyses within the discipline of anthropometry to only consider relationships between body size measures and derived indices, without considering allometric relationships between size and shape. The results of this investigation agree with those of previous biological studies (2,19,122), demonstrating that measures of an organisms size are strongly linearly correlated, suggesting that aspects of torso size increase proportionally. However, this form of analysis does not consider variations in other morphological traits which cannot be captured by measures of body size and it has been suggested that more sophisticated shape measures could provide additional information regarding human morphology that complement existing anthropometrics (2).

Recent investigations have also utilised statistical methods, such as PCA, to identify features of body shape variation directly from 3D imaging data (170), which have been used to improve predictions of body composition (23) and refine methods for apparel sizing (173). These studies have typically used Pearson's correlation coefficients to determine whether there are linear relationships between torso shape PCs and

traditional anthropometrics. The results of this investigation reiterate those of previous studies (23,170), finding that certain torso shape PCs demonstrate moderate to strong correlations with individual measures of body size. For example, shape PC3 in this investigation was found to be strongly correlated with torso girth measures and body weight. This suggests that there are proportions of human torso shape variation which are related to changes in size. However, assessing the relationships between individual size measures and features of shape in this way is limited, in that correlations can only evaluate the linear dependence between variables. Whereas, the shape features identified in this study represent complex, scale-invariant features, such as curvatures and contours, present on the external surface of the human body, which may not be dependent on changes in size. Though morphological traits often increase with body size, to identify shape variations which are not related to size it is necessary to perform some kind of size-correction analysis.

Geometric morphometric studies of allometry typically utilise regression analyses to evaluate allometric scaling between size and shape, as well as to partition total observed shape variation into both predicted and residual components (181). The predicted component represents allometric shape variation, which can be explained by changes in size, while the residual component represents non-allometric shape variation, which size measures cannot explain. Previous geometric morphometric studies have found that allometry can account for large proportions of total shape variation within different species (181,201–203). The results of this investigation agree with these previous studies of allometry, with large proportions of observed torso shape variation explained by changes in size measures. For example, torso size measures explained over 50% of the variation in each of shape PC's 1, 2, 3 and 5, for both males and females. VIP values for size measures used in the PLSR models, demonstrated that torso girth measures contributed most to the prediction of shape. This suggests that size-related changes in these torso shape features are explained primarily by changes in girths, which could explain why girth measures and their ratios are often used as proxies of abdominal shape. These size-related changes in torso shape represent the allometric components of shape variation which can already be explained by existing anthropometric techniques. However, the results of this

investigation also showed that significant proportions of all identified torso shape PCs cannot be explained by changes in body size according to allometric scaling.

Certain shape PCs, such as PC4 and PC8, were found to represent subtle, localised variations on the torso surface, which were almost completely unexplained by changes in torso size. Even torso shape PCs which demonstrate changes with increases in body size according to allometric scaling, such as PC's 1, 2, 3 and 5, contain information about body shape that cannot be explained by existing anthropometric techniques, represented as residual error in the PLSR models. Currently, practitioners conducting clinical and population-based health screenings rely upon traditional anthropometrics and derived indices, to estimate quantities of abdominal visceral adiposity and classify individuals according to their associated cardio-metabolic health risk (12,73). However, it is acknowledged that these existing anthropometric techniques are confounded by levels of subcutaneous fat and can only identify overall changes in body size or provide proxies of central obesity (241). Though it is currently unknown what the non-allometric variations in torso shape PCs represent in terms of physical health, the additional information provided might identify subtle surface morphological features that are related to body fat distributions and associated health risks. Further study is required to establish these relationships.

Also, it has been shown that the non-allometric variations from the predicted torso shape are randomly distributed throughout the entire range of torso sizes within the LIFE-Adult cohort (Appendix 4). This indicates that the expected unexplained variations in each of the shape PCs can be assumed to be equal for individuals of any torso size. This means that individuals classed as having different cardio-metabolic risk, according to traditional anthropometrics, could exhibit the same torso shape features which would go unnoticed by existing measurement techniques. As a result, the ability to measure variations in body shape could enable clinical practitioners to perform more effective population-level diagnoses of cardio-metabolic health risk, not possible using current size-based anthropometric techniques. Similarly, apparel designers rely almost entirely on the use of linear body size measures when creating clothing sizing systems and designing garments (35). However, the results of this study demonstrate that if designers only use traditional anthropometrics when establishing sizing standards, there will be variations in body shape that cannot be accounted for, leading to

considerable proportions of their target populations being dissatisfied with the fit of mass produced clothing. These results further illustrate the wealth of information regarding body shape and weight distribution which cannot be captured by measurements used in current anthropometric practice.

6.4.1 Limitations

This study has limitations that require consideration. First, the data for some participants in the LIFE-Adult cohort could not be analysed (455 of 9,664) due to missing size measures resulting from anatomical landmarks not being successfully identified by the Anthroscan ScanWorX software. This potentially limited the range of body shapes and sizes assessed in this investigation. Further study is therefore required to investigate improved methods of landmark identification during data post-processing to help improve the effectiveness of automatic digital anthropometric techniques. Second, though the LIFE-Adult cohort is one of the largest collections of 3D imaging data currently available, containing equal proportions of male and female participants that represent an extensive range of body shapes and sizes, the dataset has a lack of ethnic diversity since the cohort is of central European origin. This is significant, since it has been established that different ethnic groups vary in their cardio-metabolic risk, with several components of body composition variability that differ across ethnic groups (fat/lean ratio, fat distribution, lean mass composition and metabolism, and adipose tissue biology) increasingly linked with cardio-metabolic risk (63,95,255). In addition, only 400 participants in the LIFE-Adult cohort were under the age of 40 years old. Further study is required to assess individuals from a more extensive range of ages and ethnicities to determine whether these allometric relationships are representative of the wider population. Finally, in this investigation body size measures of each participant were normalised by being divided by body height, as in a previous study of the LIFE-Adult cohort (19). This method of normalisation adjusts measures for body height and assumes that the size of different parts of the body scale linearly with height. However, this was an inappropriate method of height normalisation, since it has been shown previously that regional body lengths and girths do not all scale linearly with body height, but in fact scale disproportionately with increased height (244). In future studies, scaling exponents should be determined for body size measures across all regions of the body, rather

than simply dividing my height to achieve more precise normalisation of body size, as demonstrated in Section 6.2.3.

6.5 Conclusion

The results of this investigation suggest that geometric morphometric methods of shape analysis can identify non-allometric variations in human morphology which cannot be identified by existing size-based digital anthropometric techniques. These results further demonstrate the need for more comprehensive body measurement tools which characterise human body shape and its underlying mass distribution. Future research should further evaluate the benefits of improved body measurement in different applications, such as obesity classification and epidemiology.

Chapter 7 - Application of shape anthropometrics for obesity categorisation.

7.1 Introduction

The results of Chapter Six suggest that shape anthropometrics can identify non-allometric variations in human morphology that cannot be captured by current techniques. Though these results demonstrate that some features of body shape are independent of size, the value of shape anthropometrics as an effective tool remains unknown. Derived health indices are used extensively in epidemiological studies and health screening - the most prolific of which being BMI. As discussed in Chapter Two, obesity is defined using BMI according to the World Health Organization (WHO) (60). However, it has been shown that obesity is a heterogeneous condition; whereby people with the same BMI can have distinct cardiovascular and metabolic risk profiles, making true health risk difficult to determine (12,62). Categorising individuals using BMI in isolation can result in some receiving treatment which is unnecessary, while others are subsequently missed. Susceptibility to adverse metabolic and cardiovascular diseases has been shown not to be determined solely by total body fat mass, but in fact depends on the distribution of adiposity (12,64) and amounts of lean mass and organ size (69), which is also affected by ethnicity, sex and age-associated variability. Additional proxies of abdominal or central obesity, such as waist girth (WC) and waist-hip ratio (WHR) have been suggested as being a means of refining obesity classification and assessing cardio-metabolic risk (73,74). The WHO and previous literature have shown that combining BMI with a measure of central obesity can improve the capabilities of anthropometric techniques in the prediction of disease risk (61,74,256). However, it has also been suggested that more sophisticated measures of body shape could provide additional information to improve population-level obesity categorisation (2). The aim of this investigation was to demonstrate that there are variations in body shape within existing obesity classifications, which provide additional information compared to anthropometrics currently used in practice. The objectives were to:

- Categorise participants within the LIFE-Adult cohort according to existing World Health Organisation (WHO) obesity classification guidelines and torso shape.
- Determine the level of agreement between existing anthropometric classifications of overall and central obesity, and body shape-based clusters.

- Demonstrate that within existing classifications there are variations in body shape parameters which cannot be identified by current anthropometric techniques.

7.2 Methods

7.2.1 Participants

3D body scan data and anthropometrics of 9,565 participants from the LIFE-Adult cohort were analysed in this study. Summary characteristics of participants analysed in this investigation are shown in Table 7.1. All participant data adheres to the same ethical procedures detailed in Section 6.2.1.

Table 7.1. Sample characteristics (mean \pm standard deviation).

Descriptive	Male	Female
No. of participants	4,538	5,027
Age (years)	58 \pm 13	57 \pm 12
Stature (cm)	176.1 \pm 7.3	164.0 \pm 7.0
Mass (kg)	88.8 \pm 18.2	76.8 \pm 16.9
BMI (kg/m ²)	27.6 \pm 4.2	27.1 \pm 5.6
Waist Girth (cm)	101.1 \pm 12.4	92.1 \pm 14.0
WHR	0.99 \pm 0.07	0.87 \pm 0.07

7.2.2 Data processing

Size measures required for this investigation included: stature, mass, waist and hip girth. External torso shape PCs were extracted from the 3D scan data of participants, as described in Section 6.2.4.

Extracted measures of body size were used to calculate indices of weight status and central obesity in order to categorise participants according to WHO recommended guidelines (61). Participants were stratified into the following BMI categories: underweight (BMI < 18.5 kg/m²); normal weight (BMI 18.5 - 24.9 kg/m²); overweight (BMI 25.0 - 29.9 kg/m²); obese (BMI \geq 30.0 kg/m²). Participants were also stratified according to WHO established sex-specific cut-off points for waist girth (WC) and waist-hip ratio (WHR), beyond which cardiovascular disease (CVD) risk is augmented or substantially increased (61). According to the WHO (61) population groups can be categorised by WC and WHR into one of the following risk levels:

- Level I: Low risk - Males (WC \leq 94 cm or WHR < 0.90) and females (WC \leq 80 cm or WHR < 0.85) are deemed to have the lowest level of risk, with less than 10 % of individuals in this category likely to present any indicative health risk factors.

- Level II: Increased risk - Males ($94 < WC \leq 102$ cm) and females ($80 < WC \leq 88$ cm) have an increased level of risk, with 80 % of individuals in this category highly likely to present at least one indicative health risk factor. Providing them with health advice or other appropriate action is deemed essential.
- Level III: High risk - Males ($WC > 102$ cm or $WHR \geq 0.90$) and females ($WC > 88$ cm or $WHR \geq 0.85$). Everyone in this category is certain to present at least one indicative health risk factors, with these individuals deemed to demonstrate double the level of risk compared to those in the low-risk group.

Agglomerative hierarchical clustering using the Ward linkage algorithm (257), was performed to categorise participants in the LIFE-Adult cohort that exhibited similar torso shape characteristics. Clusters were based on the pairwise Euclidean distances, d , between individuals, according to their scores on first nine shape PCs, identified in Section 6.3.1. Three hierarchical shape clusters were selected to correspond to the number of health risk categories defined by existing anthropometric classification methods according to the WHO (61). Hierarchical clustering was conducted within MATLAB (version 9.2, Mathworks, USA).

7.2.3 Data analysis

All anthropometric indices and shape measures were converted into sex-specific z-scores; measures were first centralised with respect to their mean value and then divided by their standard deviation. Pearson's product-moment correlations (r) were used to assess linear relationships between existing indices and extracted shape anthropometrics. Pearson's chi-square tests for independence (258) were used to examine the association between existing obesity classifications and identified body shape clusters. The chi-square statistic (χ^2) was used to determine whether there was a statistically significant association between existing classification methods and shape clusters. The null hypothesis was that classifications of individuals according to the different anthropometric and shape-based techniques were independent of each other. However, if χ^2 was significant ($p < 0.05$), the null hypothesis could be rejected and would provide confidence that there is an association between the different classification methods. All correlation and chi-squared tests were conducted within SPSS (IBM SPSS Statistics 24.0).

Graphic analyses of age-associated variability in torso shape between standard BMI categories is presented, as well as shape variations within combined risk classifications, based on both overall and central obesity. For this second demonstration, BMI = 22 kg/m² represented normal weight, BMI = 26 kg/m² represented overweight and BMI = 30 kg/m² represented obese, similar to previous studies (74). WHR is used in clinical practice to relate waist circumference to the overall body shape and is considered an effective proxy of central obesity (82). The 10th and 90th percentiles of WHR values in the LIFE cohort were selected to represent individuals classed as low and high risk, these values were 0.89 and 1.08 for male, and 0.78 and 0.95 for female participants.

7.3 Results

Dendrograms of the three hierarchical clusters for male and female participants within the LIFE-Adult cohort, according to their torso shape PCs are shown in Figures 7.1a and 7.2a, respectively. Figures 7.1b and 7.2b visualise the centroids of the identified clusters as reconstructed torsos for males and females, respectively.

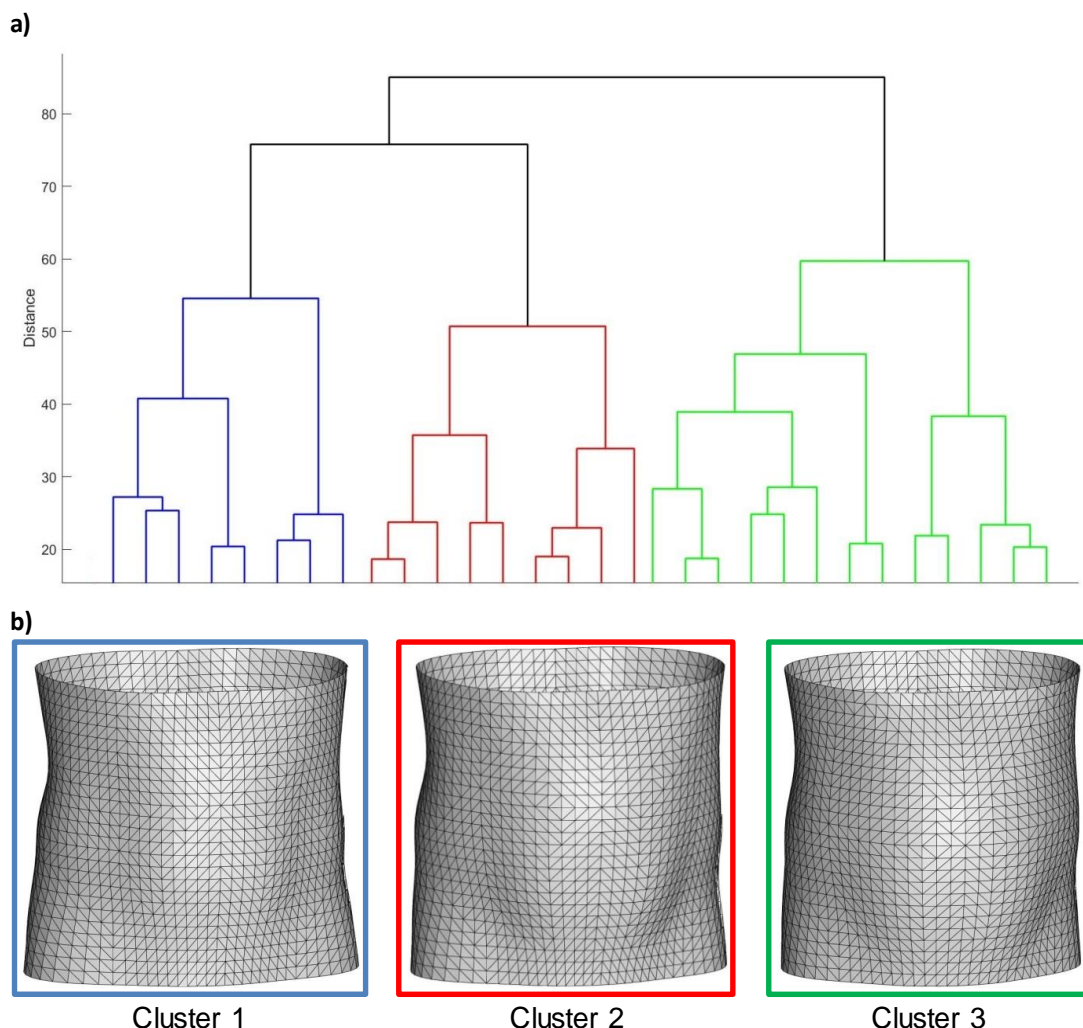


Figure 7.1. Hierarchical clustering of male participants in LIFE cohort according to shape. a) Dendrogram showing cluster 1 (blue), cluster 2 (red) and cluster 3 (green); b) Reconstructed torsos of cluster centroids and their deviations from the average male torso.

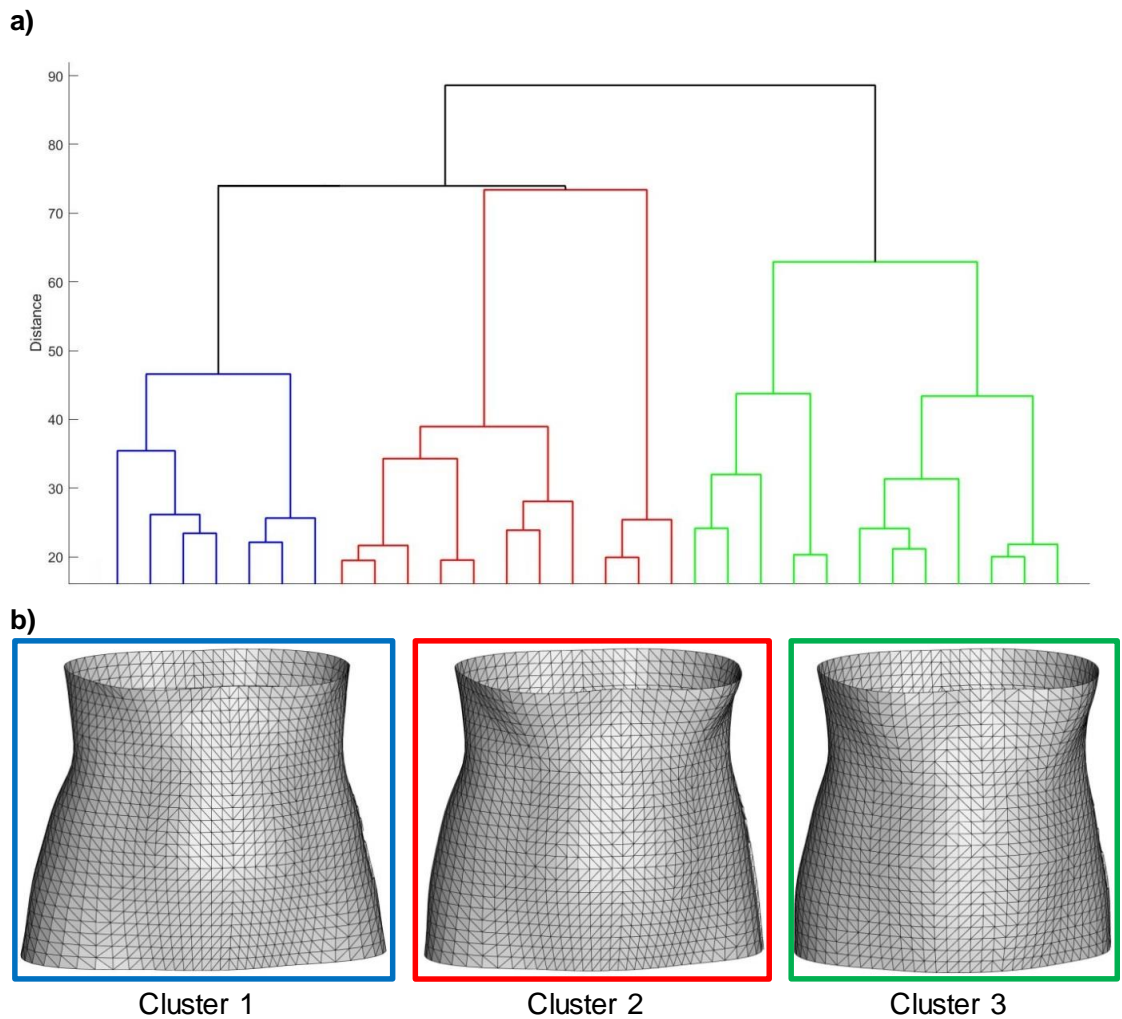


Figure 7.2. Hierarchical clustering of female participants in LIFE cohort according to shape. a) Dendrogram showing cluster 1 (blue), cluster 2 (red) and cluster 3 (green); b) Reconstructed torsos of cluster centroids and their deviations from the average female torso.

Associations between existing classifications and body shape clusters

Correlation testing demonstrated statistically significant ($p \leq 0.05$), positive correlations between existing indices (BMI, WC and WHR) (Appendix 5). For example, there was strong positive correlations between BMI and waist girth for males and females ($r = 0.91$, $R^2 = 0.83$, $p < 0.001$). There was also moderate positive correlation between BMI and WHR among males ($r = 0.62$, $R^2 = 0.39$, $p < 0.001$), but only weak positive correlation among females ($r = 0.44$, $R^2 = 0.19$, $p < 0.001$). In addition, existing indices demonstrated statistically significant ($p \leq 0.05$), moderate to strong correlations with shape PC1 and PC3, but only weak to no correlations with the remaining shape PCs for male and female participants.

The results of chi-square testing between existing classifications are presented in Table 7.2. This shows the percentage of participants within each BMI classification that are categorised at each level of cardio-metabolic health risk, according to WC and WHR. There was a statistically significant ($p < 0.001$) association between BMI classification and central obesity indices WC and WHR (Figure 7.3). However, these results also demonstrate considerable overlap between classifications, with 69.1% and 40.8% of male and female participants classed as normal weight according to BMI classed as having high risk of metabolic complications according to WHR, respectively. At the same time, 40.3% of female participants classed as overweight or obese were also classed as having low risk of metabolic complications according to WHR.

Table 7.2. Chi-square (χ^2) results showing percentage of participants within each BMI classification at each risk level according to WC and WHR.

Central Obesity Index	BMI Classification			χ^2	df	Sig.	Φ_c
	Normal Weight	Overweight	Obese				
Males (n = 4538)							
<u>WC (cm)</u>							
Low Risk	79.4%	14.9%	0.2%	3349.82	4	<.001	0.608
Increased Risk	18.7%	43.5%	1.9%				
High Risk	1.9%	41.6%	97.9%				
<u>WHR</u>							
Low Risk	30.9%	4.4%	0.4%	745.21	2	<.001	0.405
High Risk	69.1%	95.6%	99.6%				
Females (n = 5027)							
<u>WC</u>							
Low Risk	52.6%	1.9%	0.0%	3126.98	4	<.001	0.558
Increased Risk	33.6%	16.7%	0.2%				
High Risk	13.9%	81.4%	99.8%				
<u>WHR</u>							
Low Risk	59.2%	25.4%	14.9%	798.30	2	<.001	0.399
High Risk	40.8%	74.6%	85.1%				

Table 7.3 shows the results of chi-square testing between existing individual anthropometric classifications (BMI, WC and WHR) and clusters based on torso shape. This shows the percentage of participants within each of the BMI, WC and WHR classification groups that are represented by each shape cluster. There was a statistically significant ($p < 0.001$) association between existing classifications and shape clusters (Figure 7.3). However, it can also be seen that there are individuals representing each of the identified shape clusters within every weight/health risk category according to existing anthropometric classifications methods.

Table 7.3. Chi-square (χ^2) results showing percentage of participants within each BMI, WC and WHR classification within each shape cluster.

Existing Classifications	Shape Cluster			χ^2	df	Sig.	Φ_c
	Cluster 1	Cluster 2	Cluster 3				
Males (n = 4538)							
<u>BMI</u>							
Normal Weight	70.1%	19.3%	10.7%	961.95	4	<.001	0.326
Overweight	40.9%	43.2%	15.9%				
Obese	16.0%	37.7%	46.3%				
<u>WC</u>							
Low Risk	79.4%	12.8%	7.8%	1283.32	4	<.001	0.376
Increased Risk	44.0%	40.4%	15.6%				
High Risk	18.1%	46.7%	35.2%				
<u>WHR</u>							
Low Risk	94.3%	1.6%	4.0%	600.96	2	<.001	0.364
High Risk	36.6%	39.2%	24.2%				
Females (n = 5027)							
<u>BMI</u>							
Normal Weight	46.6%	43.0%	10.4%	1846.92	4	<.001	0.429
Overweight	14.6%	47.5%	37.9%				
Obese	2.2%	20.1%	77.8%				
<u>WC</u>							
Low Risk	64.0%	30.9%	5.1%	1802.59	4	<.001	0.423
Increased Risk	31.0%	51.9%	17.1%				
High Risk	7.5%	37.6%	54.9%				
<u>WHR</u>							
Low Risk	47.4%	33.2%	19.4%	874.69	2	<.001	0.417
High Risk	11.3%	42.2%	46.5%				

Table 7.4 shows the results of chi-square testing between combined classifications (BMI & WC, and BMI & WHR) and clusters based on torso shape, demonstrating the percentage of participants within these combined classification groups that are represented by each shape cluster. There was a statistically significant ($p < 0.001$) association between these combined classifications and shape clusters (Figure 7.3). Though, there are individuals representing each of the identified shape clusters within several of the combined weight/health risk categories according to existing anthropometric classifications methods.

Table 7.4. Chi-square (χ^2) results showing the percentage of participants within combined classifications (BMI & WC, and BMI & WHR) that are within each shape cluster.

Combined Indices		Shape Cluster			χ^2	df	Sig.	Φ_c
		Cluster 1	Cluster 2	Cluster 3				
Males (n = 4538)								
<u>BMI & WC</u>								
Normal Weight	Low Risk	79.1%	11.8%	9.1%	1522.47	16	<.001	0.410
	Increased Risk	37.4%	44.9%	17.7%				
	High Risk	20.0%	72.0%	8.0%				
Overweight	Low Risk	81.2%	14.9%	3.9%				
	Increased Risk	46.2%	38.9%	14.9%				
	High Risk	21.3%	57.5%	21.1%				
Obese	Low Risk	0.0%	50.0%	50.0%				
	Increased Risk	54.5%	27.3%	18.2%				
	High Risk	15.3%	37.8%	46.8%				
<u>BMI & WHR</u>								
Normal Weight	Low Risk	94.9%	1.3%	3.8%	1231.23	10	<.001	0.368
	High Risk	59.0%	27.3%	13.8%				
Overweight	Low Risk	93.6%	2.1%	4.3%				
	High Risk	38.4%	45.1%	16.4%				
Obese	Low Risk	60.0%	20.0%	20.0%				
	High Risk	15.9%	37.7%	46.4%				
Females (n = 5027)								
<u>BMI & WC</u>								
Normal Weight	Low Risk	64.10%	31.00%	5.00%	2363.58	16	<.001	0.485
	Increased Risk	32.50%	53.10%	14.30%				
	High Risk	16.10%	63.40%	20.50%				
Overweight	Low Risk	68.80%	21.90%	9.40%				
	Increased Risk	29.00%	48.30%	22.80%				
	High Risk	10.40%	48.00%	41.60%				
Obese	Low Risk	-	-	-				
	Increased Risk	0.00%	0.00%	100.0%				
	High Risk	2.20%	20.10%	77.70%				
<u>BMI & WHR</u>								
Normal Weight	Low Risk	60.50%	33.20%	6.30%	2234.61	10	<.001	0.471
	High Risk	26.50%	57.30%	16.20%				
Overweight	Low Risk	28.70%	41.50%	29.80%				
	High Risk	9.80%	49.60%	40.70%				
Obese	Low Risk	6.50%	13.50%	80.00%				
	High Risk	1.40%	21.20%	77.40%				

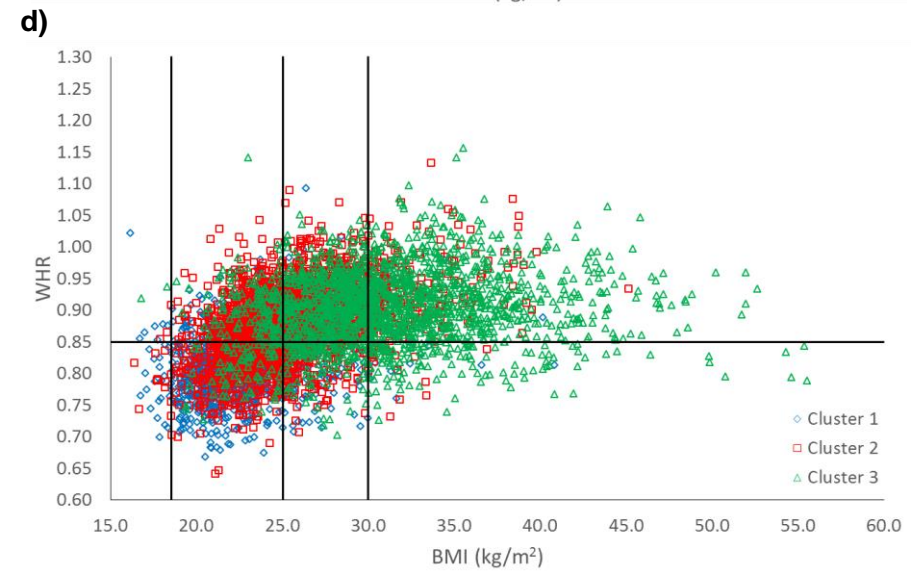
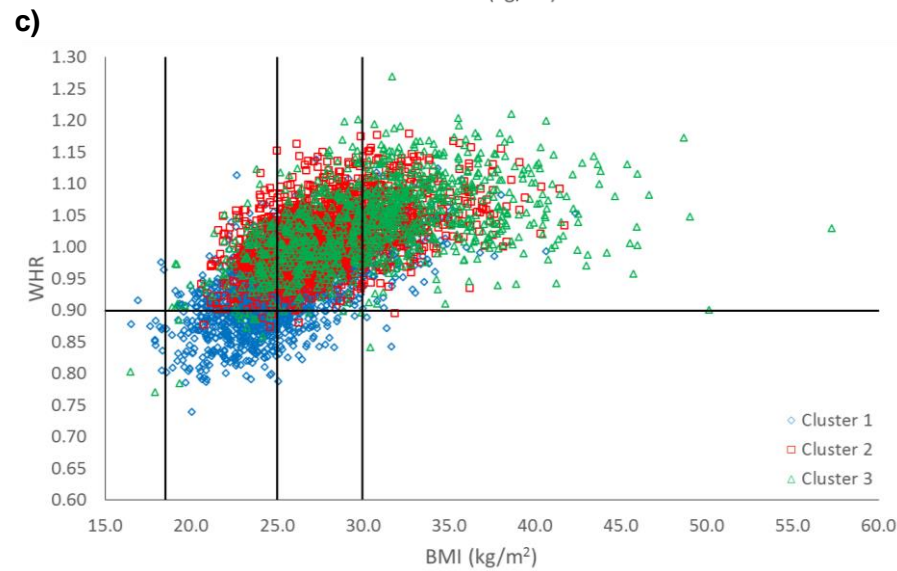
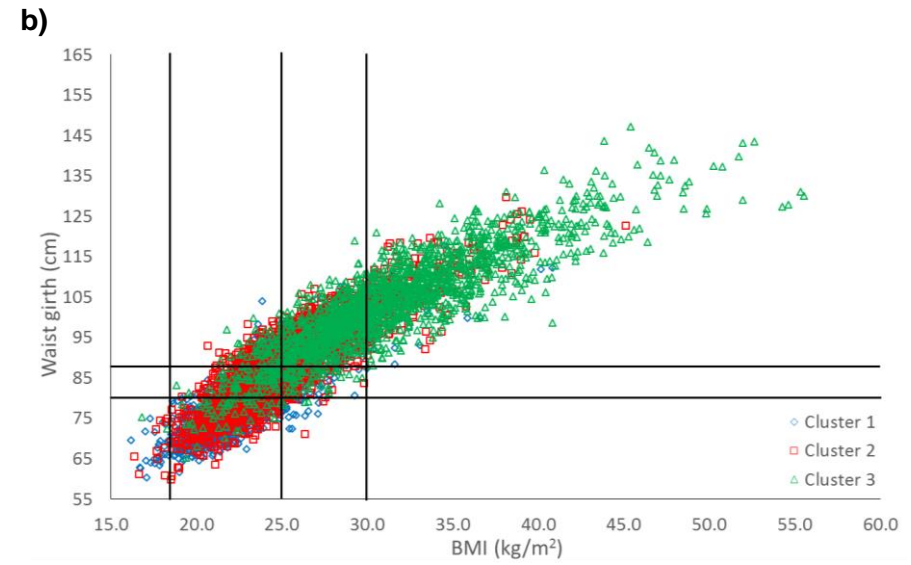
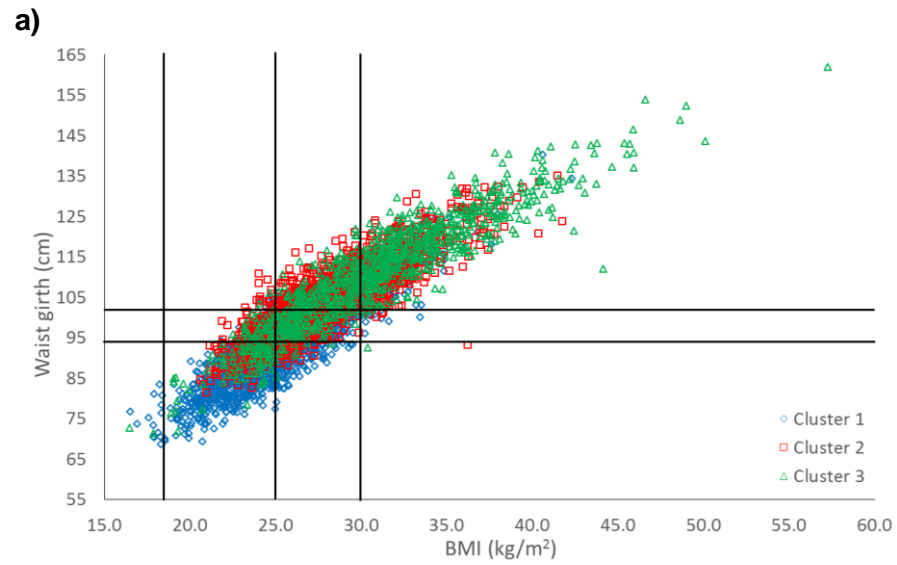


Figure 7.3. Associations between current indices and shape. BMI vs WC vs Shape: a) male, b) female; BMI vs WHR vs Shape: c) male, d) female.

Age-associated torso shape variations within BMI categories

Graphic analysis of age-associated variations within BMI categories for all shape PC's (1-9) was conducted (Appendix 5), with selected plots presented here. Figures 7.4a and 7.4b present plots by age of shape PC1 for males and females, respectively. Shape PC1 which captures variations in anterior-posterior weighting (Section 6.3.1), increased across the BMI categories in males and females. Age also appeared to have a strong effect on this trend, though both trends appeared stronger in females. Older groups of obese women, exhibited values of shape PC1 similar to that of older overweight males, and higher values than that of all younger males.

Figures 7.5a and 7.5b present similar plots of shape PC5 for males and females, respectively. Age appeared to have very little effect on shape PC5 for males, with very little difference between age groups, whereas age demonstrated a strong effect for females. PC5 describes differences in mass accumulation between the bust and abdominal region of the torso, and appears to be strongly influenced by age, with older females exhibiting higher values for PC5 across BMI categories.

Figures 7.6a and 7.6b present plots of shape PC6 for males and females, respectively. Similar to PC5, age appears to have a stronger effect on shape PC6 for females than for males, with PC6 describing differences in mass accumulation between the lower and upper abdomen. However, for both males and females there appears to be greater age-associated variation in PC6 for underweight individuals, with values converging for overweight and obese individuals.

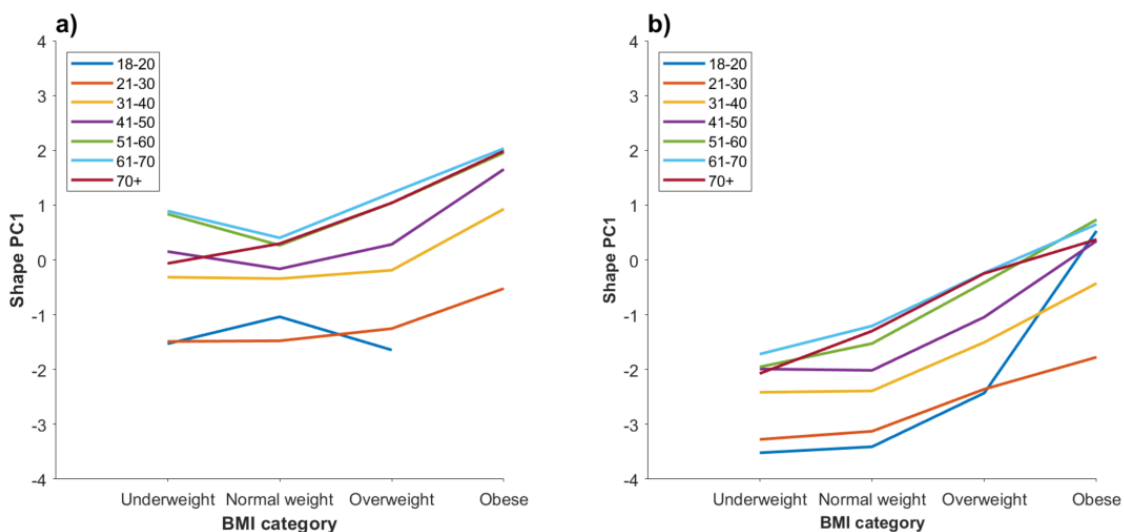


Figure 7.4. Shape PC1 by BMI category and age group in a) males and b) females.

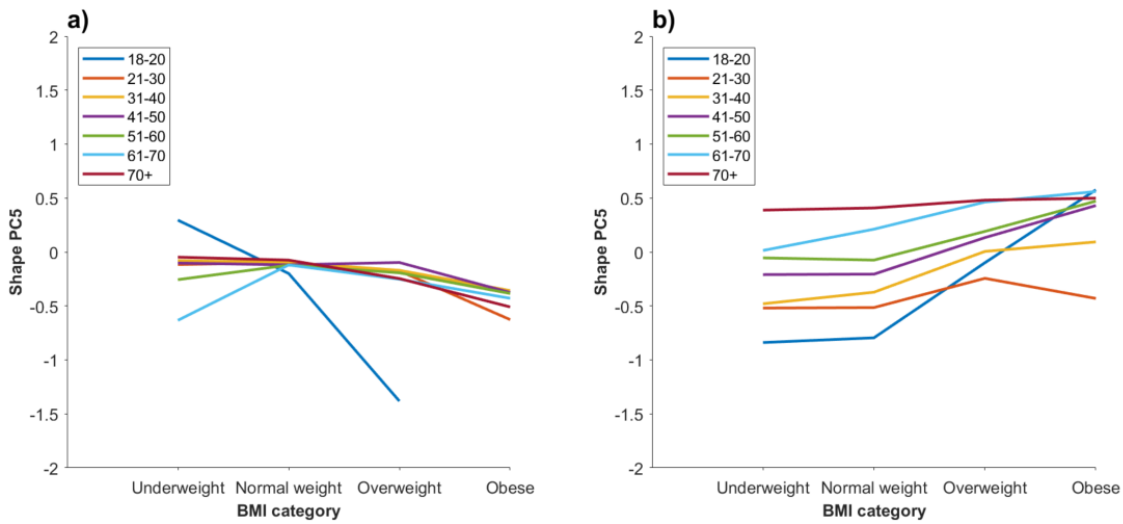


Figure 7.5. Shape PC5 by BMI category and age group in a) males and b) females.

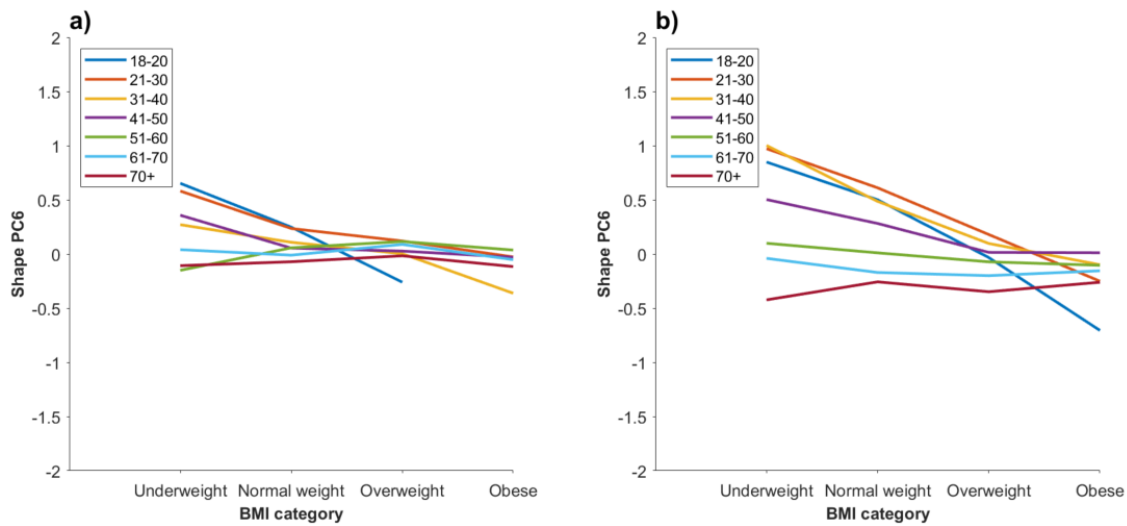


Figure 7.6. Shape PC6 by BMI category and age group in a) males and b) females.

Observed torso shape variations within combined risk classifications

Figures 7.7 and 7.8 show representative torso shapes of each of the three shape clusters observed within the combined weight/health risk classifications according to BMI and WHR, for males and females, respectively.

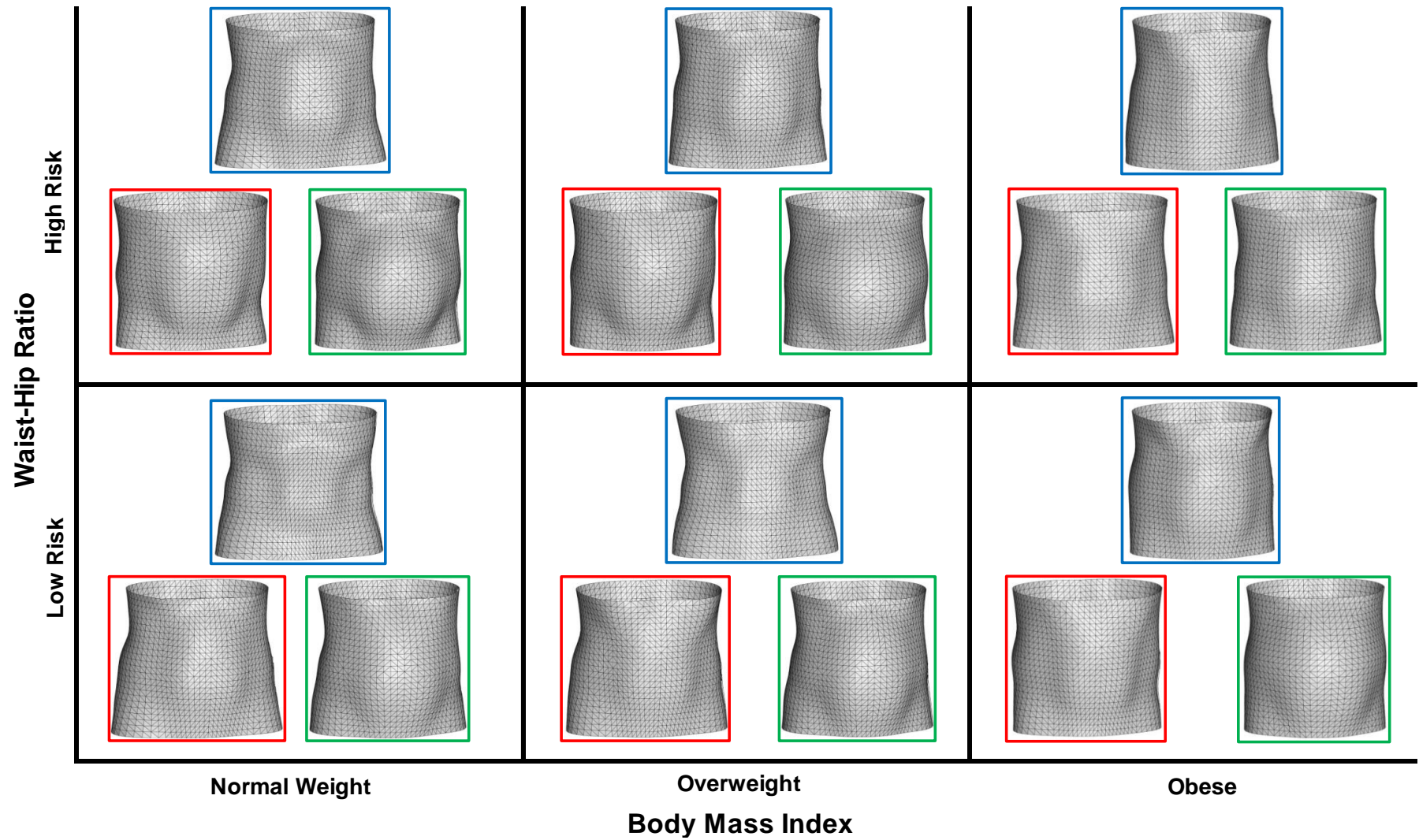


Figure 7.7. Male torso shape variations within combined BMI and WHR obesity/risk classifications, with representative torsos of shape cluster 1 (blue), cluster 2 (red) and cluster 3 (green).

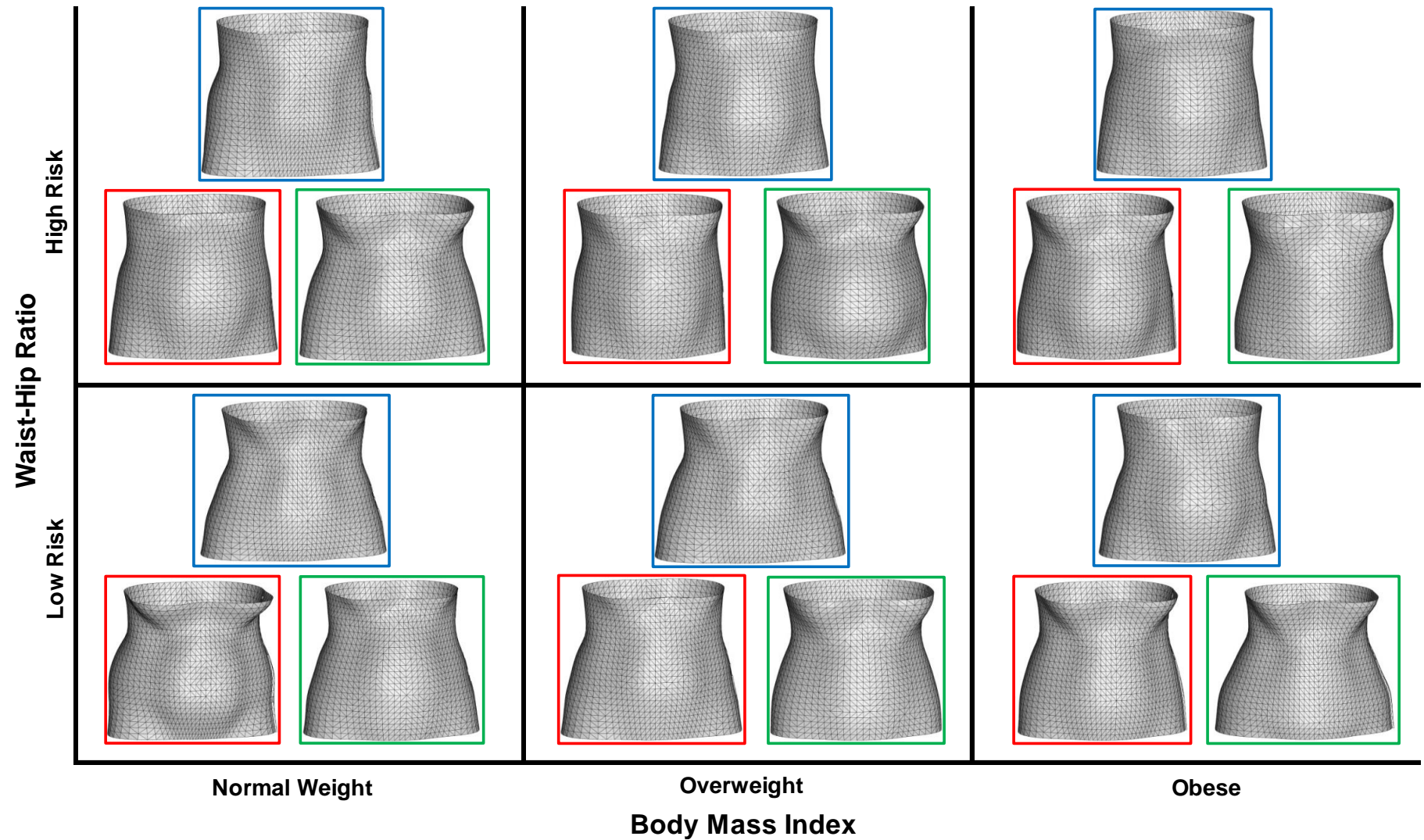


Figure 7.8. Female torso shape variations within combined BMI and WHR obesity/risk classifications, with representative torsos of shape cluster 1 (blue), cluster 2 (red) and cluster 3 (green).

7.4 Discussion

It has been suggested that more sophisticated shape anthropometrics, acquired using 3D imaging, can surpass manual measures in epidemiology and clinical practice for classification of individuals in the population (2). The aim of this investigation was to demonstrate that there are variations in torso shape within existing obesity classifications that can provide additional information regarding human morphology, compared to indices currently used in practice.

Though BMI is the accepted means of monitoring the prevalence of obesity at the population-level, previous studies have suggested that combining measures of central obesity, such as WC and WHR, with BMI will provide improved means of stratifying individuals in the assessment of metabolic disease risk associated with obesity (12,74,241). The results of this investigation agree with those of previous studies, demonstrating that though BMI and waist girth are strongly correlated at the population level, individual waist girth measures can vary considerably at any given BMI value, causing differences in classification between the two methods. The implications of these variations in waist girth within BMI categories are significant, since it has been shown that differences in waist girth in both obese and non-obese individuals are associated with variations in quantities of both adipose tissue (241) and lean mass (77), each of which contribute to differences in metabolic load and metabolic capacity, respectively (63). Similar relationships were observed between BMI and WHR. The majority of individuals classed as obese according to BMI were also classed as having high risk of metabolic complications according to WHR; however, measures of WHR were also shown to vary considerably within BMI classifications. It has previously been suggested that individuals, classed as being normal weight according to BMI, but exhibiting central obesity according to WC or WHR, have up to 60% greater risk of mortality compared to obese individuals without central obesity (74). This suggests that by combining BMI with indices of central obesity, such as WC and WHR, it is possible to identify obesity subgroups within BMI categories, such as metabolically healthy and obese, or metabolically unhealthy and normal weight which would otherwise be missed if using BMI alone (62,73,74).

Existing indices of central obesity provide relatively simple proxies of fat distribution and body shape, reducing the complexity of human form down to a single value that

can be obtained and interpreted easily by practitioners and patients. However, previous studies have suggested that more sophisticated indices of body shape could surpass the use of body girths in obesity assessment and health monitoring, providing finer morphological distinctions in body characteristics (2,19). Principal components of torso shape identified within the LIFE-Adult cohort in Chapter Six have been shown to capture subtle variations in torso shape, which cannot be explained by measures of body size currently used in practice. When assessed at the population level it has been shown that there is a statistically significant association between existing anthropometric classifications and body shape clusters, suggesting that overall the largest individuals in the population differ from the smallest individuals in terms of their torso shape. However, the results of this investigation also demonstrate that there are variations in body shape that existing classification methods cannot identify.

First, it has been shown that certain aspects of torso shape can vary considerably across the adult lifespan independently of BMI, particularly for females with increasing age being associated with greater accumulations of mass in the abdomen, as demonstrated in a previous study by Wells et al. (67). The reason for this being that as females get older their reproductive biology undergoes significant changes, which changes how mass is distributed around their body, most notably characterised by greater amounts of fat mass being deposited in the abdomen rather than in the lower body, subsequently causing a reduction in sexual dimorphisms in body shape observed in younger adults (65,66,68). In addition, though it has been suggested that combining BMI with a measure of central obesity can improve the capabilities of anthropometry in the prediction of disease risk, even when indices of overall and central obesity are combined there are still significant amounts of variation within these classification groups that cannot currently be identified. Conversely, there are clusters of individuals within the sample that exhibit similar torso shape features, but are represented across all BMI weight categories and across all WC and WHR metabolic risk classifications. For example, when combining BMI with WHR, individuals classed as having either low and high risks of metabolic complications, within each of the normal weight, overweight or obese weight categories, were shown to represent all three identified shape clusters. In addition, individuals classed as normal weight with low risk of metabolic complications were shown to exhibit the same torso shape features as individuals who were classed as obese with a high risk of metabolic complications. This suggests that

there are a greater number of dimensions in which the torso shape of individuals can vary than can currently be identified by existing anthropometric classification techniques. Though it is currently unknown what this additional information regarding torso shape variation represents in terms of human health, these results further illustrate the wealth of information regarding body shape and weight distribution cannot be captured by measurements used in current practice.

The findings of this investigation further demonstrate the potential for misclassification of individuals using existing simple anthropometrics and how more sophisticated measures could complement existing methods of obesity classification. Indices of central obesity have been shown to be associated with accumulations of visceral and deep superficial adipose tissue and can identify subgroups of abdominally obese individuals within BMI classifications. However, even when measures, such as WC and WHR, are used in combination with BMI to refine health risk classification they have still been shown to be insensitive to variations in mass distribution and shape related to age, sex and ethnicity (61,63,67,73,241). Traditional anthropometrics have typically been considered a relatively unsophisticated approach to assessing body composition and health risk, with contemporary studies instead using more direct imaging approaches, such as magnetic resonance imaging (MRI) or computed tomography (CT) scanning to assess fat distribution. However, despite their high accuracy, MRI and CT are not ideal for routine practice due to their high cost and harmful radiation exposure, meaning anthropometry remains the most practical solution. This investigation has shown that shape measures are able to identify differences in human morphology between individuals who would be otherwise be classed as having the same level of health risk. However, further study with more diverse populations is required to establish whether there are key features of body shape which reveal variations in mass distribution that are also associated with sex, age and ethnicity. Establishing these relationships would enable the development of a new health index can identify individuals at risk of cardio-metabolic issues, without having to undergo expensive and potentially harmful radiographic imaging procedures.

7.4.1 Limitations

As discussed in Chapter Six, though the LIFE-Adult cohort is one of the largest collections of 3D body scan data currently available, the dataset has a limited age range and lack of ethnic diversity. In particular, there was only a small subset of data for younger adults (<40 years), which could have affected the assessment of age-associated shape variations. As such, further study is required to assess individuals from a wider range of ages and ethnicities to determine whether the findings of this investigation can be generalised to the wider population.

7.5 Conclusion

The results of this investigation suggest that in the categorisation of individuals, measures of body shape can identify variations in external human form that cannot be captured by existing anthropometric techniques. These results further demonstrate the need for more comprehensive body measurement tools which characterise external body shape and its underlying mass distribution. Future research should investigate relationships between body shape, body composition and associated health risks for specific groups of individuals to improve population-level diagnostics.

Chapter 8 - Overall discussion

8.1 Introduction

The aim of this programme of research was to determine whether shape anthropometrics can complement existing anthropometric techniques in the assessment of human morphology. This research was motivated by previous literature, which has suggested that external human form is dependent on its internal anatomical structures and the belief that an individual's body shape is a direct indicator of physical health (1–3). Though there have been significant advances in 3D imaging technology since the end of the 20th century, practitioners and researchers in areas such as healthcare (123,127) and apparel sizing (13,14), still rely predominantly on traditional anthropometric techniques to assess human body shape. However, manual anthropometrics are prone to human error and limited by their simplicity, as they do not fully describe the complex variations present on the surface of the body (4,19–21). Even studies which have utilised 3D imaging devices to acquire anthropometrics have typically used a specific definition of body shape, based on the ratios and relative proportions of 1D anthropometrics, such as waist girth and stature. This approach discards the shape information captured by 3D imaging systems and is a common misconception within anthropometry literature (28). Geometric morphometrics are established methods within the fields of anthropology and evolutionary biology to analyse variations in shape and its covariation with other variables (29). Though these methods have been used extensively to analyse biological shape (32,33), few studies have investigated how geometric morphometrics can complement existing anthropometric techniques in the assessment of human morphology. This chapter summarises the findings of this programme of research in relation to each specified objective, as well as the primary contributions to knowledge, practical implications, limitations, potential areas for further research and overall conclusions.

8.2 Summary of work

8.2.1 Objective One: *Review published literature regarding existing anthropometric techniques and quantitative methods for analysing the shape of biological organisms.*

This was achieved in Chapter Two through a review of previous literature within the field of anthropometry, in particular: the foremost scientific fields and applications which require measures of human body size and shape; existing techniques for

acquiring anthropometrics; as well as other quantitative methods for analysing the shape of biological organisms. Previous literature suggests researchers are critical of manual anthropometric techniques, due to their susceptibility to observer error and the limited information which they can provide regarding human morphology. 3D imaging systems have been shown to acquire both traditional and more complex anthropometrics with minimal physical contact between the researcher and the participant. However, there are potential sources of measurement error when using digital anthropometric techniques, such as anatomical landmark identification and postural variation, which need to be considered. Though 3D imaging technology is well established, the methods and metrics used to analyse human shape information is not, with the majority of previous studies typically extracting traditional anthropometrics from acquired point cloud data. Consequently, further research into how sophisticated methods of shape analysis can complement existing anthropometric techniques in the assessment of human morphology was warranted.

8.2.2 Objective Two: Develop analytical procedures for extracting scale-invariant features of human body shape from 3D imaging data.

This was achieved in Chapter Three, which detailed the development of methods to be used throughout this programme of research to enable the assessment of human morphology. This included establishing methods for defining the torso segment region of interest according to the location of anatomical landmarks and the acquisition of 3D imaging data of the human torso. In addition, analytical procedures were developed to segment acquired 3D geometries, perform Procrustes superimposition to implement geometric morphometric methods and to extract numeric parameters describing scale-invariant features of the human torso. These methods were evaluated in Chapter Five, which investigated how shape anthropometrics obtained using these methods could complement traditional anthropometrics in the assessment of human morphology and the estimation of subcutaneous central adiposity within a small cohort. Shape anthropometrics acquired using the developed method were shown to capture scale-invariant features which are absent from traditional measures used in current anthropometric practice. In addition, anthropometrics currently used in practice were shown to explain up to 52.2% of variance in waist skinfold thickness measures, while a combined regression model using size and shape anthropometrics explained 76.5 % of

variation. This initial investigation suggested that more sophisticated methods of analysis could be used to complement traditional anthropometric techniques.

8.2.3 Objective Three: *Determine the test-retest reliability of developed methods for acquiring measures of body shape and the effect of identified sources of measurement error.*

This was achieved in Chapter Four, which investigated the effects of potential sources of measurement error within the developed analytical procedures, as well as the reliability of obtained shape anthropometrics. The results of this investigation suggest that although sources of measurement error, such as landmark location and posture, do affect shape anthropometrics, the developed method had high test-retest reliability (ICC > 0.9), suitable for use within clinical applications. It was also determined that variations in a participants posture affects all identified shape PCs, rather than being isolated to a single component as has been suggested in previous literature. This is likely due to the human torso being a deformable object, meaning that when a participant's posture changes between repeat measures multiple aspects of their torso segment will deform and consequently change in shape. However, these changes in torso shape caused by variations in posture have been shown to not be statistically significant. Future investigations should evaluate these developed methods in longitudinal studies to determine whether shape measures can reliably monitor changes in body composition following treatment interventions.

8.2.4 Objective Four: *Critically evaluate the degree of allometric scaling between measures of body size and shape, as well as identifying nonallometric variations in torso shape which cannot be explained by existing anthropometric techniques.*

This was achieved in Chapter Six, which investigated allometry between measures of torso size and shape extracted from 3D imaging data of individuals and whether shape anthropometrics provide additional information which cannot be captured by existing anthropometric techniques. Size and shape anthropometrics were extracted from a large cohort of participants (n = 9,209 (4,405 male, 4,804 female)) collected in the LIFE-Adult study. The results of this investigation suggest that although certain shape PCs demonstrate allometric scaling, there are significant proportions of shape variation which cannot be explained by changes in size and existing anthropometric techniques. In addition, it has been shown that these nonallometric deviations from the predicted

torso shape according to allometry are randomly distributed throughout the entire range of torso sizes and can be assumed to be equal for individuals of any torso size. These results further illustrate the wealth of information regarding body shape and weight distribution which cannot be captured by measurements used in current anthropometric practice.

8.2.5 Objective Five: *Determine how body shape measurement can complement anthropometric techniques currently used in population-based studies and obesity assessment.*

This was achieved in Chapter Seven, which investigated whether there are variations in body shape within existing obesity classifications that can provide additional information compared to anthropometric techniques currently used in practice. Participants within the LIFE-Adult cohort were first categorised into obesity and cardio-metabolic health risk classification groups, according to WHO recommended guidelines for BMI, WC and WHR. In addition, participants were separately grouped according to their torso shape PCs using hierarchical clustering. Chi-square statistical testing was then performed to determine whether there were associations between existing classification methods and clusters of individuals based on their shape. The results of this investigation suggest that when assessed at the population level there is a statistically significant association between existing anthropometric classifications and body shape clusters, suggesting that the largest individuals are different in shape from the smallest individuals. However, it was also shown that within current classification groups there are individuals who exhibit significant variations in torso shape which are not identified by existing anthropometric techniques. Simultaneously, there are clusters of individuals within the cohort that exhibit similar torso shape features, but are represented across different BMI weight categories and WC/WHR metabolic risk classifications. This suggests that shape anthropometrics can identify subtle variations in human morphology which are not captured by existing anthropometric techniques and could complement population-level diagnostics of cardio-metabolic health risk.

8.3 Contribution to knowledge

This programme of research makes several contributions to the body of knowledge within the field of anthropometry regarding the objective measurement of human body shape. First, a novel analytical procedure has been developed which uses

methods from geometric morphometrics and statistical shape analysis to extract shape anthropometrics from 3D imaging data of the human torso. This method has been shown to be an effective technique for capturing and quantifying morphological information from the surface of the human torso, which is absent from existing anthropometric techniques. In addition, these independent features of body shape can be used in combination with existing anthropometrics to improve the estimation of subcutaneous abdominal adiposity.

This programme of research has also identified potential sources of measurement error within the developed analytical procedures when acquiring shape anthropometrics and has determined their effect on the test-retest reliability of shape measurement. Principally, errors in anatomical landmark identification can adversely affect the results of shape measurement, requiring investigators to be ISAK level 1 accredited anthropometrists to ensure reliable palpation if using manual landmarking techniques. In addition, variations in a participant's posture can affect the acquisition of shape anthropometrics due to deformations of the human torso and should be controlled during the collection of 3D imaging data through proper instructions or postural aids in future studies.

This research has established a database of body shape information, which characterises the morphological features of participants within the LIFE-Adult cohort that can be used in future anthropometric studies. This research has identified non-allometric variations in torso shape within a population-based cohort which cannot be explained by traditional anthropometric techniques currently used in practice. This contributes to improving current understanding of how human morphology can vary for people of different sizes throughout the population and between individuals. In addition, this research has demonstrated the potential for misclassification of individuals using indices, such as BMI, WC or WHR, and how more sophisticated shape anthropometrics can complement existing methods of obesity and health risk classification. Though indices of central obesity have been shown to be associated with accumulations of visceral adipose tissue and can identify subgroups of abdominally obese individuals within BMI classifications they remain confounded by levels of subcutaneous fat and factors such as age, sex and ethnicity. This research has shown that there are individuals who would be classed as being low risk according to WC and

WHR, that exhibit the same shape features as individuals who are classed as having high risk of metabolic complications. The additional information about human morphology contained within shape anthropometrics may be able to identify subtle, localised features on the surface of the body that reveal variations in body fat distribution and associated cardio-metabolic health risks that cannot be captured by existing anthropometric techniques. The knowledge gained throughout this programme of research informs future studies investigating relationships between human morphology and body composition, as well as the development of tools to improve the diagnostic and predictive capabilities of measures used in practice.

8.4 Practical applications

The primary contributions to knowledge of this programme of research offer practical applications in a range of fields, including healthcare, apparel sizing and kinanthropometry.

8.4.1 Healthcare

Currently, healthcare practitioners conducting population-level health screenings rely upon size anthropometrics and derived indices, such as BMI, WC and WHR, to estimate quantities of abdominal visceral adiposity and classify individuals according to their associated cardio-metabolic health risks (12,73). However, it is acknowledged that existing anthropometric techniques are confounded by levels of subcutaneous fat, age, sex and ethnicity (61,73,241), and can only identify overall changes in body size or provide proxies of central obesity (241). The findings of this research further demonstrate the potential for misclassification of individuals using existing classification methods. It has been shown that individuals classed as having low levels of risk can exhibit the same shape characteristics as individuals classed as being at high risk of cardio-metabolic complications. In addition, individuals who are the same size according to traditional anthropometrics and are within the same health risk classification group can vary considerably in body shape. Though it is currently unknown what these scale-invariant shape variations represent in terms of human health, the additional information provided by shape anthropometrics may be able to identify subtle features on the surface of the human body that reveal variations in body fat distribution and associated health risks that cannot be captured by existing anthropometric techniques. Clinical nutritionists primarily use anthropometrics such

as, weight, BMI, WC and WHR to monitor longitudinal changes in a patient's health, following either exercise or nutritional interventions (3,114). Similarly, these simple anthropometrics are also used to monitor the development and growth of children and adolescents, and is recognised as an important indicator of proper development (55,56). However, the findings of this research suggest that traditional anthropometric techniques are unable to identify non-allometric variations in human morphology which change independently of increases in body size. The ability to identify these deviations from the allometric trend within the population could be used to: differentiate between normal physiological and pathological developments in children as they grow; or determine whether a change in an overweight individual's weight following a diet or exercise programme corresponds to changes in their quantities of muscle or fat.

8.4.2 Apparel

Another key application of the findings of this research is within apparel sizing and ecommerce. It is accepted within the apparel industry that in order to design and manufacture well-fitting clothing both effective measurements and in-depth understanding of body shapes and sizes within the target population is required (35). However, this presents a significant design challenge, due to large variations in body dimensions within the general population and major demographic changes in developed countries. Individuals vary in their size, shape and body proportions, with these characteristics also varying according to sex, age, nationality and ethnicity (14,157). In addition, consumers' body size and shape characteristics have changed significantly in recent years, resulting from changes in nutrition, healthcare and more sedentary lifestyles (13,157). Standard garment sizing systems have been developed in many countries and are based on the concept of dividing the population into subgroups of individuals who are similar in relevant body dimensions (157). However, many consumers deviate from these standard dimensions, highlighting the need for more comprehensive anthropometrics that can capture as wide a range of body sizes and shapes as possible (117,259). The findings of this programme of research suggest that combining shape anthropometrics with traditional anthropometrics could enable clothing retailers and manufacturers to gain a better understanding of the morphological variations that exist within their target markets when conducting large-

scale anthropometric surveys. This improved understanding of variations within the population could enable the development of sizing systems which cater for individuals that would normally deviate from standard dimensions used in mass produced, ready-to-wear (RTW) garments. In addition, recent growths in ecommerce, combined with the inclusion of depth sensing 3D imaging technology within modern smartphones (260) has facilitated the development of phone-based 3D scanning apps that provide virtual try-on and garment sizing recommendations (120). More sophisticated shape anthropometrics could enable online customers to receive improved garment size and style recommendations based on their inputted 3D imaging data and clothing fit preferences, as well as the development of custom-fit clothing that accounts for variations in their body size and shape.

8.4.3 Kinanthropometry

The findings of this programme of research also have several applications within sport and kinanthropometry. First, shape anthropometrics could enable researchers and practitioners to perform more comprehensive descriptive assessments of elite performers within a specific sport, enabling researchers and practitioners to identify subtle features that differentiate them from the general population. Though anthropometrics are not the only factor determining sporting success, the ability to describe additional physical attributes of elite athletes could assist in the creation of more sophisticated talent identification criteria when assessing the future potential of young athletes. Shape anthropometrics could also enable researchers to perform comprehensive applied assessments, to evaluate whether characteristics of elite athletes are related to biomechanical and physiological measures of sporting performance. For example, previous studies have compared the anthropometric and physiological characteristics of elite mountain bikers and road cyclists to examine differences in their power-to-weight characteristics (261). Determining relationships between shape anthropometrics and performance could provide coaches with easily obtained measures that can be used to optimise training programmes and monitor performance. In addition, the findings of this research could provide sports practitioners with improved tools for monitoring longitudinal changes in an athlete's body size and shape in relation to changes in their performance following a period of intense training, as well as understanding the stability of measures during or between

seasons (15,164). Similarly, longitudinal changes within specific athletic populations in response to factors such as rule changes, and technological advancements in equipment within that sport could be assessed with greater specificity. For example, it has been shown that changes in a specific athletic populations' anthropometrics can differ significantly from changes within the general population; such as the height of elite jockeys and gymnasts remaining relatively constant despite height increases in the general population (262).

8.5 Limitations

Limitations have been identified in each chapter of this programme of research; however, there are three that warrant further consideration. First, the analytical procedures developed during this programme of research were only designed to evaluate the shape of the torso segment in isolation. In its current implementation the proposed method is unable to analyse other body segments, such as the arms and legs, or the shape of the human body as a whole. The rationale for only assessing the torso segment during this research was that the torso has the greatest potential for differences in size and shape between participants, due to considerable variations in the types and amounts of tissue present. However, this is a limitation of the current procedure and represents an area of potential further work to extend the findings of this research to the rest of the body.

Second, the LIFE-Adult dataset analysed during this research contains one of the largest collections of 3D imaging data currently available, representing an extensive range of body shapes and sizes. However, by design this study focused specifically on inhabitants of the city of Leipzig in Germany, causing the LIFE-Adult dataset to have a distinct lack of ethnic diversity, being primarily of central European origin. This lack of ethnic diversity is a common issue within nutrition and biomedical research, with current knowledge and understanding regarding health risk being dominated by studies of Europeans within industrialised countries, or of different ethnic groups within these same environments (255,263). However, chronic disease risk has become increasingly prevalent around the world, with the majority of those suffering chronic diseases living in low- and middle-income countries, where both ethnic profile and environmental conditions differ significantly from those studied in research studies. From the evidence that does exist, it has been demonstrated that body composition

and associated chronic disease risk differ systematically across ethnic groups (69). Previous studies have demonstrated that both the amount and distribution of adipose tissue vary between ethnic groups, with African Americans having low levels of visceral fat compared to Europeans, while South Asians have higher total body fat content for a given BMI and greater amounts of visceral fat. In addition, differences in birth weight between ethnic groups lead to reduced amounts of muscle mass and organ size, while brain growth and adiposity levels are preserved. These ethnic differences in body build and organ size persist into later life, with lower amounts of lean mass observed in South Asian individuals compared to Europeans, with evidence suggesting that individuals with smaller organs have reduced metabolic capacity to maintain homeostasis (63,69). In addition to variations in the amount and distribution of adipose tissue, ethnic groups also vary in the level of metabolic impact these factors cause. For example, it has been shown that associations between adipose tissue and insulin resistance were stronger in South Asians compared to those of African/Caribbean or European ethnicity. This suggests that excess levels of adiposity appear to be more damaging for some ethnic groups compared to others, with some populations having greater risk of metabolic complications for a given mass of body fat, such as South Asians in the UK, African and Hispanic Americans in the US and aboriginal populations in Australia. However, understanding these relationships presents a significant research challenge since ethnic-associated variability is complex, with several biological and cultural components contributing to chronic disease risk, not just variations in body composition (255). Additional factors could contribute to these observed ethnic variations include: living environment, dietary habits, likelihood of smoking, physical activity levels, as well as long-term racial prejudices and psychosocial stresses which may elevate metabolic load through chronic activation of the stress response. These ethnic variations increase the complexity of assessing variations in human body shape still further, with further research required to understand how these differences between ethnic groups are expressed as variations in body shape, and whether shape anthropometrics can be used to identify to an individual's cardio-metabolic risk regardless of ethnicity.

Finally, during this programme of research shape anthropometrics were extracted from 3D imaging data acquired using either a 3dMDbody5 stereo photogrammetry imaging system, or a Vitus Smart XXL 3D laser scanner. Both of these represent high

cost, high accuracy 3D imaging systems. It is possible that the high cost of these 3D imaging systems may limit the transferability and practical implications of the findings and recommendations reported within this body of work.

8.6 Future research

Several areas of further research have been highlighted through this programme of research. First, practitioners conducting clinical and population-level health screenings currently rely upon manual anthropometrics and derived indices, such as the BMI and WHR, to classify individuals according to their cardio-metabolic health risks. However, the findings of this research have shown that existing techniques can only identify overall changes in body size and allometric changes in body shape. Whereas, it has shown that shape anthropometrics, measured directly from the surface of the body can identify subtle, non-allometric variations in human morphology, which could complement existing techniques in the characterisation of human morphology and the estimation of body composition. It is posited that the additional information provided by shape anthropometrics identified during this programme of research can identify localised, morphological variations on the surface of the body that relate to distributions of body fat and associated health risks, such as diabetes and cardiovascular disease. Further research is required to establish these relationships and to improve current understanding of associations between human morphology and health risk. This could enable clinical practitioners to perform more effective population-level diagnoses of cardio-metabolic health risk, not possible using current anthropometric techniques. In addition, as discussed in Section 8.5, the majority of previous research has taken place in multi-ethnic countries such as the UK, USA and Australia and therefore comparatively little is known about chronic disease profiles in other human populations. Therefore, larger, more representative cohorts are needed, as well as cohorts from low- and middle-income countries to improve understanding of the ethnic heterogeneity of cardio-metabolic profiles, as well as the enhanced disease risk of migrants from different ethnic backgrounds.

Second, the procedures for evaluating shape anthropometrics developed during this research are limited to only analysing the shape of the torso segment only and are not able to analyse the human body as a whole. Further research should address this limitation and investigate adapting current methods to enable analysis of the entire

human body. This could be achieved either by: assessing the shape of individual body segments similar to current methods and combining them; or investigating a new procedure which can identify scale-invariant features across the entire body surface. Finally, further research should investigate the use of low-cost tools to acquire shape anthropometrics from the surface of the body, enabling all practitioners to assess human morphology without relying on expensive 3D imaging devices. These low-cost tools could either be physical objects, allowing practitioners to manually measure body shape features such as curvature and simple ratios, or smartphone-based scanning apps, which are able to capture shape anthropometrics to a required level of accuracy.

8.7 Conclusions

The findings of this programme of research demonstrate how geometric morphometrics analysis methods can identify shape anthropometrics which complement traditional anthropometric techniques in the assessment of human morphology. It has been shown that sophisticated shape anthropometrics can improve estimations of subcutaneous abdominal adiposity and the potential for misclassification of individuals using existing obesity and health risk classification methods. This programme of research contributes to current understanding of human morphological variation, which could inform the development of tools to improve the capabilities of anthropometrics used in applications, such as healthcare, apparel sizing and kinanthropometry.

Chapter 9 - References

1. Utkualp N, Ercan I. Anthropometric measurements usage in medical sciences. *Biomed Res Int.* 2015;2015.
2. Wells JCK, Treleaven P, Cole TJ. BMI compared with 3-dimensional body shape: The UK National Sizing Survey. *Am J Clin Nutr.* 2007;85(2):419–25.
3. Jones PRM, Rioux M. Three-dimensional surface anthropometry: Applications to the human body. *Opt Lasers Eng.* 1997;28(2):89–117.
4. Tsang B, Chan CK, Taylor G, Tsang B, Taylor KC. Kinanthropometry study of the physique of disciplined personnel. *Int J Cloth Sci Technol.* 2000;12(2):144–60.
5. Heath BH, Carter JEL. The Heath-Carter Anthropometric Somatotype - Instruction Manual. 2007;(March):185–219.
6. Carter JEL, Heath BH. *Somatotyping: Development and Applications.* Cambridge University Press; 1990. (Cambridge Studies in Biological and Evolutionary Anthropology).
7. Sheldon WH. The varieties of human physique: An introduction to constitutional psychology. *J Am Med Assoc.* 1940;115(15):1303.
8. Ercan İ, Prof A. Statistical Shape Analysis and Usage in Medical Sciences : Review. 2012;4(1).
9. Oxford Dictionaries. *Concise Oxford English Dictionary.* Oxford University Press; 2008.
10. Treleaven, Philip JW. 3D body scanning and healthcare applications. *Cloth Appear Fit.* 2004;40(7):135–68.
11. Loeffler M, Engel C, Ahnert P, Alfermann D, Arelin K, Baber R, et al. The LIFE-Adult-Study: Objectives and design of a population-based cohort study with 10,000 deeply phenotyped adults in Germany. *BMC Public Health.* 2015;15(1):1–14.
12. Piché ME, Poirier P, Lemieux I, Després JP. Overview of Epidemiology and Contribution of Obesity and Body Fat Distribution to Cardiovascular Disease: An Update. *Prog Cardiovasc Dis.* 2018;61(2):103–13.
13. Treleaven P. Sizing us up. *IEEE Spectr.* 2004;41(April):29–31.
14. Simmons KP, Istook CL. Body measurement techniques. Vol. 7, *Journal of Fashion Marketing and Management: An International Journal.* 2003. 306-332 p.
15. Bullas A, Choppin S, Heller B, Clarkson S, Wheat J. Kinanthropometry

- Applications of Depth Camera Based 3D Scanning Systems in Cycling :
Repeatability and Agreement with Manual Methods. 5th Int Conf 3D Body
Scanning Technol. 2014;44(October):21–2.
16. Stewart A. Kinanthropometry - The interdisciplinary discipline. *J Sports Sci.* 2007;25(4):373.
 17. Schranz N, Tomkinson G, Olds T, Daniell N. Three-dimensional anthropometric analysis: Differences between elite Australian rowers and the general population. *J Sports Sci.* 2010;28(5):459–69.
 18. Bragança S, Arezes P, Carvalho M, Ashdown SP. Current state of the art and enduring issues in anthropometric data collection. *Dyna.* 2016;83(197):22–30.
 19. Löffler-Wirth H, Willscher E, Ahnert P, Wirkner K, Engel C, Loeffler M, et al. Novel anthropometry based on 3D-bodyscans applied to a large population based cohort. *PLoS One.* 2016;11(7):1–20.
 20. Soileau L, Bautista D, Johnson C, Gao C, Zhang K, Li X, et al. Automated anthropometric phenotyping with novel Kinect-based three-dimensional imaging method: Comparison with a reference laser imaging system. *Eur J Clin Nutr.* 2016;70(4):475–81.
 21. Wells JCK, Ruto A, Treleaven P. Whole-body three-dimensional photonic scanning: A new technique for obesity research and clinical practice. *Int J Obes.* 2008;32(2):232–8.
 22. Price GM, Uauy R, Breeze E, Bulpitt CJ, Fletcher AE. Weight, shape, and mortality risk in older persons: elevated waist-hip ratio, not high body mass index, is associated with a greater risk of death. *Am J Clin Nutr.* 2006 Aug 1;84(2):449–60.
 23. Ng BK, Sommer MJ, Wong MC, Pagano I, Nie Y, Fan B, et al. Detailed 3-dimensional body shape features predict body composition, blood metabolites, and functional strength: the Shape Up! studies. *Am J Clin Nutr.* 2019;1–11.
 24. Douros I. Calculating the Curvature Shape Characteristics of the Human Body from 3D Scanner Data. 2004;(June).
 25. Schranz N, Tomkinson G, Olds T, Petkov J, Hahn AG. Is three-dimensional anthropometric analysis as good as traditional anthropometric analysis in predicting junior rowing performance? *J Sports Sci.* 2012;30(12):1241–8.
 26. Bullas AM. The importance of complex anthropometrics in the assessment of cyclists. 2017.

27. Barnes R. The Body Volume Index (BVI): Using 3D Scanners to Measure and Predict Obesity. 2010;1(October):19–20.
28. Lee DR, Sallee GT. A Method of Measuring Shape. *Geogr Rev.* 1970 Oct;60(4):555.
29. Bookstein FL. *Morphometric tools for landmark data: geometry and biology.* Cambridge Univ Press. 1991;10:435.
30. Small CG. *The Statistical Theory of Shape.* New York, NY: Springer New York; 1996. (Springer Series in Statistics).
31. Kendall DG. Shape manifolds, procrustean metrics, and complex projective spaces. *Bull London Math Soc.* 1984;16(2):81–121.
32. Adams DC, Rohlf FJ, Slice DE. Geometric morphometrics: Ten years of progress following the “revolution.” *Ital J Zool.* 2004;71(1):5–16.
33. Adams D, Rohlf JL, Slice D. A field comes of age: geometric morphometrics in the 21 st century. *Hystrix, Ital J Mammal.* 2013;24(1):7–14.
34. Pavlova A V., Saunders FR, Muthuri SG, Gregory JS, Barr RJ, Martin KR, et al. Statistical shape modelling of hip and lumbar spine morphology and their relationship in the MRC National Survey of Health and Development. *J Anat.* 2017;231(2):248–59.
35. Gupta D. Anthropometry and the design and production of apparel: an overview. In: *Anthropometry, Apparel Sizing and Design.* Elsevier; 2014. p. 34–66.
36. Carr DJ, Wilson CA, Laing RM. Anthropometric methods for the successful design of military clothing and equipment. *Advances in Military Textiles and Personal Equipment.* Woodhead Publishing Limited; 2012. 49-63 p.
37. Albrizio A. Biometry and anthropometry: from Galton to constitutional medicine. *J Anthropol Sci.* 2007;85:101–23.
38. Quételet A. *Sur l’homme et le développement de ses facultés, ou, Essai de physique sociale.* Bachelier; 1835. (Sur l’homme et le développement de ses facultés, ou, Essai de physique sociale).
39. Quetelet A. *Anthropométrie ou Mesure des différentes facultés de l’homme.* C. Muquardt; 1870.
40. Timothy O. Body Composition and Sports Performance. In: *Olympic Textbook of Science in Sport.* Wiley-Blackwell; 2009. p. 129–45.

41. Stewart AD. Kinanthropometry and body composition: a natural home for three-dimensional photonic scanning. *J Sport Sci.* 2010;28(5):455–7.
42. Bullas AM, Choppin S, Heller B, Wheat J. Validity and repeatability of a depth camera-based surface imaging system for thigh volume measurement. *J Sports Sci.* 2016;34(20):1–7.
43. Clarkson S, Choppin S, Hart J, Heller B, Wheat J. Calculating body segment inertia parameters from a single rapid scan using the Microsoft Kinect. *3rd Int Conf 3D Body Scanning Technol.* 2012;(October):153–63.
44. Abbott A, Collins D, Martindale RJJ, Sowerby K. Talent identification and development: an academic review. Sport University of Edinburgh. 2002.
45. Brunkhorst L, Kielstein H. Comparison of anthropometric characteristics between professional triathletes and cyclists. *Biol Sport.* 2013 Nov 25;30(4):269–73.
46. Health NRC. Diet and Health. Washington, D.C.: National Academies Press; 1989.
47. Wells JCK, Fewtrell MS. Measuring body composition. *Arch Dis Child.* 2006;91(7):612–7.
48. Borga M, West J, Bell JD, Harvey NC, Romu T, Heymsfield SB, et al. Advanced body composition assessment: From body mass index to body composition profiling. *J Investig Med.* 2018;66(5):887–95.
49. Duren DL, Sherwood RJ, Czerwinski SA, Lee M, Choh AC, Siervogel RM, et al. Body composition methods: Comparisons and interpretation. *J Diabetes Sci Technol.* 2008;2(6):1139–46.
50. Lee JJ. Assessment of Body Composition : Total , Central , and Regional Adiposity via Stereovision Body Imaging. 2014.
51. Hume PA, Ackland T. Physical and Clinical Assessment of Nutritional Status. In: *Nutrition in the Prevention and Treatment of Disease.* Elsevier; 2017. p. 71–84.
52. Bretschneider T, Koop U, Schreiner V, Wenck H, Jaspers S. Validation of the body scanner as a measuring tool for a rapid quantification of body shape. *Ski Res Technol.* 2009 Aug;15(3):364–9.
53. Stewart AD, Marfell-Jones M, Olds T, Al. E. International standards for anthropometric assessment. *Low Hutt, New Zeal Int Soc Adv Kinanthropometry.* 2011;125f.
54. Reilly T, Tyrrell A, Troup JDG. Circadian Variation in Human Stature. *Chronobiol*

- Int. 1984 Jan 7;1(2):121–6.
55. Kuehnappel A, Ahnert P, Loeffler M, Broda A, Scholz M. Reliability of 3D laser-based anthropometry and comparison with classical anthropometry. *Sci Rep*. 2016;6(May):1–11.
 56. Loeffler-Wirth H, Vogel M, Kirsten T, Glock F, Poulain T, Körner A, et al. Body typing of children and adolescents using 3D-body scanning. *PLoS One*. 2017;12(10):1–11.
 57. MacMahon S, Baigent C, Duffy S, Rodgers A, Tominaga S, Chambless L, et al. Body-mass index and cause-specific mortality in 900 000 adults: Collaborative analyses of 57 prospective studies. *Lancet*. 2009;373(9669):1083–96.
 58. WHO. Physical status: the use and interpretation of anthropometry. Report of a WHO Expert Committee. Vol. 854, World Health Organization technical report series. 1995. p. 1–452.
 59. Goodpaster BH, Krishnaswami S, Harris TB, Katsiaras A, Kritchevsky SB, Simonsick EM, et al. Obesity, Regional Body Fat Distribution, and the Metabolic Syndrome in Older Men and Women. 2005;165.
 60. World Health Organisation. Obesity: preventing and managing the global epidemic Report of a WHO Consultation (WHO Technical Report Series 894). 2000.
 61. World Health Organisation (WHO). WHO | Waist Circumference and Waist–Hip Ratio. Report of a WHO Expert Consultation. Geneva, 8-11 December 2008. 2008;(December):8–11.
 62. Neeland IJ, Poirier P, Després JP. Cardiovascular and Metabolic Heterogeneity of Obesity: Clinical Challenges and Implications for Management. *Circulation*. 2018;137(13):1391–406.
 63. Wells JCK. Ethnic variability in adiposity, thrifty phenotypes and cardiometabolic risk: Addressing the full range of ethnicity, including those of mixed ethnicity. *Obes Rev*. 2012 Dec;13(SUPPL.2):14–29.
 64. Kissebah AH, Vydelingum N, Murray R, Evans DJ, Kalkhoff RK, Adams PW. Relation of Body Fat Distribution to Metabolic Complications of Obesity. *J Clin Endocrinol Metab*. 1982 Feb;54(2):254–60.
 65. Karastergiou K, Smith SR, Greenberg AS, Fried SK. Sex differences in human adipose tissues – the biology of pear shape. *Biol Sex Differ*. 2012;3(1):13.

66. Brown LM, Gent L, Davis K, Clegg DJ. Metabolic impact of sex hormones on obesity. *Brain Res.* 2010 Sep;1350:77–85.
67. Wells JCK, Cole TJ, Treleaven P. Age-variability in body shape associated with excess weight: The UK national sizing survey. *Obesity.* 2008 Feb;16(2):435–41.
68. Wells JCK. Sexual dimorphism of body composition. *Best Pract Res Clin Endocrinol Metab.* 2007 Sep;21(3):415–30.
69. Wells JCK. *The Metabolic Ghetto: An Evolutionary Perspective on Nutrition, Power Relations and Chronic Disease.* Cambridge University Press; 2016.
70. Jaeschke L, Steinbrecher A, Pischon T. Measurement of waist and hip circumference with a body surface scanner: Feasibility, validity, reliability, and correlations with markers of the metabolic syndrome. *PLoS One.* 2015;10(3):1–16.
71. Rosenzweig JL, Bakris GL, Berglund LF, Hivert M-F, Horton ES, Kalyani RR, et al. Primary Prevention of ASCVD and T2DM in Patients at Metabolic Risk: An Endocrine Society* Clinical Practice Guideline. *J Clin Endocrinol Metab.* 2019;104(9):3939–85.
72. Nevill AM, Duncan MJ, Lahart IM, Sandercock GR. Scaling waist girth for differences in body size reveals a new improved index associated with cardiometabolic risk. *Scand J Med Sci Sport.* 2017;27(11):1470–6.
73. Swainson MG, Batterham AM, Tsakirides C, Rutherford ZH, Hind K. Prediction of whole-body fat percentage and visceral adipose tissue mass from five anthropometric variables. *PLoS One.* 2017;12(5):1–12.
74. Coutinho T, Goel K, Corrêa De Sá D, Carter RE, Hodge DO, Kragelund C, et al. Combining body mass index with measures of central obesity in the assessment of mortality in subjects with coronary disease: Role of “normal weight central obesity.” *J Am Coll Cardiol.* 2013;61(5):553–60.
75. Goh LGH, Dhaliwal SS, Welborn TA, Lee AH, Della PR. Anthropometric measurements of general and central obesity and the prediction of cardiovascular disease risk in women: A cross-sectional study. *BMJ Open.* 2014;4(2).
76. Nevill AM, Stewart AD, Olds T, Duncan MJ. A new waist-to-height ratio predicts abdominal adiposity in adults. *Res Sport Med.* 2020;28(1):15–26.
77. Jensen SM, Mølgaard C, Ejlerskov KT, Christensen LB, Michaelsen KF, Briend A.

- Validity of anthropometric measurements to assess body composition, including muscle mass, in 3-year-old children from the SKOT cohort. *Matern Child Nutr.* 2015;11(3):398–408.
78. Snijder MB, Dekker JM, Visser M, Yudkin JS, Stehouwer CDA, Bouter LM, et al. Larger thigh and hip circumferences are associated with better glucose tolerance: The Hoorn Study. *Obes Res.* 2003;11(1):104–11.
 79. Snijder MB, Visser M, Dekker JM, Goodpaster BH, Harris TB, Kritchevsky SB, et al. Low subcutaneous thigh fat is a risk factor for unfavourable glucose and lipid levels, independently of high abdominal fat. The Health ABC Study. *Diabetologia.* 2005 Feb;48(2):301–8.
 80. VAGUE J. The Degree of Masculine Differentiation of Obesity. *Am J Clin Nutr.* 1956 Jan 1;4(1):20–34.
 81. Hall G, Campus SP, Kingdom U. Points of View. 2003;52(5):724–9.
 82. National Institute for Health and Clinical Excellence (NICE). Section 2: Identification And Classification - Evidence Statements and Reviews. *Obes Full Guidel.* 2006;(December):196–248.
 83. Wang J, Thornton JC, Bari S, Williamson B, Gallagher D, Heymsfield SB, et al. Comparisons of waist circumferences measured at 4 sites. *Am J Clin Nutr.* 2003;77(2):379–84.
 84. Office IS. ISO 8559-1:2017 Size designation of clothes - Part 1: Anthropometric definitions for body measurement. 2017.
 85. Office IS. ISO 8559-2:2017 Size designation of clothes — Part 2: Primary and secondary dimension indicators. 2017.
 86. Office IS. ISO 8559-3:2018 Size designation of clothes — Part 3: Methodology for the creation of body measurement tables and intervals. 2018.
 87. Office IS. ISO 18890:2018 Clothing — Standard method of garment measurement. 2018.
 88. Akhtar M. Different girth measurement of human body [Internet]. 2020 [cited 2020 Aug 6]. Available from: <https://www.slideshare.net/MohammadAkhtar/different-girth-measurement-of-human-body>
 89. Day JAP. Bilateral symmetry and reliability of upper limb measurements. In: *Perspectives in kinanthropometry.* Champaign, IL: Human Kinetics; 1986. p.

- 257–61.
90. Chumlea WC, Wisemandle W, Guo SS, Siervogel RM. Relations between frame size and body composition and bone mineral status. *Am J Clin Nutr.* 2002 Jun 1;75(6):1012–6.
 91. Lohman TG. Skinfolts and body density and their relation to body fatness: a review. *Hum Biol.* 1981 May;53(2):181–225.
 92. Durnin JVGA, Womersley J. Body fat assessed from total body density and its estimation from skinfold thickness: measurements on 481 men and women aged from 16 to 72 Years. *Br J Nutr.* 1974;32(1):77–97.
 93. Ackland T, Lohman T, Sundgot-Borgen J, Maughan R, Meyer N, Stewart A, et al. Current status of body composition assessment in sport. *Sport Med.* 2012;42(3):227–49.
 94. Goossens GH. The Metabolic Phenotype in Obesity: Fat Mass, Body Fat Distribution, and Adipose Tissue Function. *Obes Facts.* 2017;10(3):207–15.
 95. Dulloo AG, Jacquet J, Solinas G, Montani JP, Schutz Y. Body composition phenotypes in pathways to obesity and the metabolic syndrome. *Int J Obes.* 2010 Dec 1;34:S4–17.
 96. Müller W, Lohman TG, Stewart AD, Maughan RJ, Meyer NL, Sardinha LB, et al. Subcutaneous fat patterning in athletes: Selection of appropriate sites and standardisation of a novel ultrasound measurement technique: Ad hoc working group on body composition, health and performance, under the auspices of the IOC Medical Commission. *Br J Sports Med.* 2016;50(1):45–54.
 97. Sheldon WH, Stevens SS, Tucker WB. The varieties of human physique. *The varieties of human physique.* Oxford, England: Harper; 1940. xii, 347-xii, 347.
 98. Sheldon W. *Atlas of Men: A Guide for Somatotyping the Adult Male at All Ages.* *J Am Med Assoc.* 1954 Nov 27;156(13):1294.
 99. Rosenbaum R. The great ivy league nude posture photo scandal. *The New York Times Magazine.* 1995 Jan;26.
 100. Olds T, Daniell N, Petkov J, David Stewart A. Somatotyping using 3D anthropometry: A cluster analysis. *J Sports Sci.* 2013;31(9):936–44.
 101. Eston R, Reilly T. *Kinanthropometry and Exercise Physiology Laboratory Manual: Tests, Procedures and Data, Third Edition: Volume One: Anthropometry.* Taylor & Francis; 2009.

102. Stewart A, Ledingham R, Williams H. Variability in body size and shape of UK offshore workers: A cluster analysis approach. Vol. 58, *Applied Ergonomics*. 2017. p. 265–72.
103. Sicotte M, Ledoux M, Zunzunegui M-V, Ag Aboubacrine S, Nguyen V-K. Reliability of anthropometric measures in a longitudinal cohort of patients initiating ART in West Africa. *BMC Med Res Methodol*. 2010 Dec 22;10(1):102.
104. Maylia E, Fairclough JA, Nokes LDM, Jones MD. Can Thigh Girth Be measured Accurately? A Preliminary Investigation. *J Sport Rehabil*. 1999;8(1):43–9.
105. Kouchi M, Mochimaru M. Errors in landmarking and the evaluation of the accuracy of traditional and 3D anthropometry. *Appl Ergon*. 2011;42(3):518–27.
106. Schwartz C, Fedrigo T, Bruls O, Cescotto S, Denoel V, Croisier JL, et al. Reproducibility and repeatability of upper limb landmarks palpation for junior operators. In: XXIII congress of the International Society of Biomechanics. Brussels; 2011.
107. Atkinson G, Nevill AM. Measurement Error (Reliability) in Variables Relevant to Sports Medicine. 1998;26(4):217–38.
108. Stewart AD. Kinanthropometry and body composition: A natural home for three-dimensional photonic scanning. *J Sports Sci*. 2010;28(5):455–7.
109. Ulijaszek SJ, Kerr DA. Anthropometric measurement error and the assessment of nutritional status. *Br J Nutr*. 1999 Sep 9;82(3):165–77.
110. Kroemer KHE, Kroemer HJ, Kroemer-Elbert KE. Engineering physiology: bases of human factors/ergonomics. Van Nostrand Reinhold; 1997. (Occupational Health and Safety Series).
111. Montagu MFA, Brožek J. A handbook of anthropometry. Springfield: Charles C Thomas Publisher; 1960.
112. Lovesey EJ. A Method for Determining Facial Contours by Shadow Projection. RAE; 1966. (RAE/TR-66192).
113. Jones PRM, West GM, Harris DH, Read JB. The loughborough anthropometric shadow scanner (LASS). *Endeavour*. 1989 Jan;13(4):162–8.
114. Heymsfield SB, Bourgeois B, Ng BK, Sommer MJ, Li X, Shepherd JA. Digital anthropometry: A critical review. *Eur J Clin Nutr*. 2018;72(5):680–7.
115. Daanen HAM, Ter Haar FB. 3D whole body scanners revisited. *Displays*. 2013;34(4):270–5.

116. Hamad M, Thomassey S, Bruniaux P. A new sizing system based on 3D shape descriptor for morphology clustering. *Comput Ind Eng.* 2017;113:683–92.
117. Bougourd J, Treleaven P. National size and shape surveys for apparel design. *Anthropometry, Apparel Sizing and Design.* Woodhead Publishing Limited; 2014. 141-166 p.
118. Gill S. A review of research and innovation in garment sizing, prototyping and fitting. *Text Prog.* 2015;47(1):1–85.
119. Jurca A, Žabkar J, Džeroski S. Analysis of 1.2 million foot scans from North America, Europe and Asia. *Sci Rep.* 2019;9(1):1–10.
120. NetVirta. Smartphone-based 3D body scanning app. [Internet]. 2020. Available from: <https://www.netvirta.com/>
121. D'Apuzzo N. Book of Abstracts 11th International Conference and Exhibition on 3D Body Scanning and Processing Technologies. In: 11th International Conference and Exhibition on 3D Body Scanning and Processing Technologies. Lugano; 2020. p. 17–8.
122. Pleuss JD, Talty K, Morse S, Kuiper P, Scioletti M, Heymsfield SB, et al. A machine learning approach relating 3D body scans to body composition in humans. *Eur J Clin Nutr.* 2019;73(2):200–8.
123. Wells JCK. Three-dimensional optical scanning for clinical body shape assessment comes of age. *Am J Clin Nutr.* 2019;(9):1–3.
124. HERCA Group. Facts and figures concerning the use of Full body scanners using X-Rays for security reason. *Herca.* 2010;(June):1–12.
125. Robinette KM, Daanen HAM. Precision of the CAESAR scan-extracted measurements. *Appl Ergon.* 2006 May;37(3):259–65.
126. Daanen HAM, Brunsmann MA, Robinette KM. Reducing movement artifacts in whole body scanning. In: *Proceedings International Conference on Recent Advances in 3-D Digital Imaging and Modeling (Cat No97TB100134).* IEEE Comput. Soc. Press; p. 262–5.
127. Treleaven P, Wells J. 3D Body Scanning and Healthcare Applications. *Computer (Long Beach Calif).* 2007 Jul;40(7):28–34.
128. Tzou C-HJ, Artner NM, Pona I, Hold A, Placheta E, Kropatsch WG, et al. Comparison of three-dimensional surface-imaging systems. *J Plast Reconstr Aesthetic Surg.* 2014 Apr;67(4):489–97.

129. 3dMD. Body Scanning Systems [Internet]. 2020. Available from:
http://www.3dmd.com/static-3dmd_systems/
130. Sarbolandi H, Lefloch D, Kolb A. Kinect range sensing: Structured-light versus Time-of-Flight Kinect. *Comput Vis Image Underst.* 2015 Oct;139:1–20.
131. D'Apuzzo N. Recent Advances in 3D Full Body Scanning With Applications To Fashion and Apparel. *Opt 3-D Meas Tech IX, Vienna, Austria.* 2009;2.
132. Hollander MHJ, Kraeima J, Meesters AML, Delli K, Vissink A, Jansma J, et al. Reproducibility of 3D scanning in the periorbital region. *Sci Rep.* 2021 Dec;11(1).
133. Besl PJ, McKay ND. A method for registration of 3-D shapes. *IEEE Trans Pattern Anal Mach Intell.* 1992 Feb;14(2):239–56.
134. Chiu C-Y, Thelwell M, Senior T, Choppin S, Hart J, Wheat J. Comparison of depth cameras for three-dimensional reconstruction in medicine. *Proc Inst Mech Eng Part H J Eng Med.* 2019;233(9).
135. Chatterjee A, Govindu VM. Noise in Structured-Light Stereo Depth Cameras: Modeling and its Applications. 2015;
136. Horaud R, Hansard M, Evangelidis G, Ménier C. An overview of depth cameras and range scanners based on time-of-flight technologies. *Mach Vis Appl.* 2016 Oct 16;27(7):1005–20.
137. Kouchi M, Mochimaru M, Bradtmiller B, Daanen H, Li P, Nacher B, et al. A protocol for evaluating the accuracy of 3D body scanners. *Work.* 2012;41(SUPPL.1):4010–7.
138. Office IS. ISO 7250-1:2017(en) Basic human body measurements for technological design — Part 1: Body measurement definitions and landmarks. 2017.
139. Office IS. ISO 15535:2012 - General requirements for establishing anthropometric databases. 2012.
140. Office IS. ISO 20685-1:2018(en) - 3-D scanning methodologies for internationally compatible anthropometric databases — Part 1: Evaluation protocol for body dimensions extracted from 3-D body scans. 2018.
141. Han H, Nam Y, Choi K. Comparative analysis of 3D body scan measurements and manual measurements of size Korea adult females. *Int J Ind Ergon.* 2010;40(5):530–40.
142. Clarkson S, Wheat J, Heller B, Webster J, Choppin S. Distortion Correction of

- Depth Data from Consumer Depth Cameras. 44(0).
143. Glock F, Vogel M, Naumann S, Kuehnappel A, Scholz M, Hiemisch A, et al. Validity and intraobserver reliability of three-dimensional scanning compared with conventional anthropometry for children and adolescents from a population-based cohort study. *Pediatr Res.* 2017 May 4;81(5):736–44.
 144. Clarkson S, Wheat J, Heller B, Choppin S. Assessing the suitability of the Microsoft Kinect for calculating person specific body segment parameters
Assessing the Suitability of the Microsoft Kinect for Calculating Person Specific Body Segment Parameters. In: 4th IEEE Workshop on Consumer Depth Cameras for Computer Vision, Zurich, Switzerland. 2014.
 145. Kouchi M. Anthropometric methods for apparel design: body measurement devices and techniques. In: *Anthropometry, Apparel Sizing and Design.* Elsevier; 2014. p. 67–94.
 146. Olds T, Honey F. In: Marfell-Jones, M., Stewart, A. and Olds, T., eds. *Kinanthropometry IX: Proceedings of the 9th International Conference of the International Society for the Advancement of Kinanthropometry.* Taylor & Francis; 2006. 1-14 p.
 147. Sims RE, Marshall R, Gyi DE, Summerskill SJ, Case K. Collection of anthropometry from older and physically impaired persons: Traditional methods versus TC2 3-D body scanner. *Int J Ind Ergon.* 2012 Jan;42(1):65–72.
 148. Ben Azouz Z, Shu C, Mantel A. Automatic Locating of Anthropometric Landmarks on 3D Human Models. In: *Third International Symposium on 3D Data Processing, Visualization, and Transmission (3DPVT'06).* IEEE; 2006. p. 750–7.
 149. Leong I-F, Fang J-J, Tsai M-J. Automatic body feature extraction from a marker-less scanned human body. *Comput Des.* 2007 Jul;39(7):568–82.
 150. Lu J, Wang M. Automated anthropometric data collection using 3D whole body scanners. *Expert Syst Appl.* 2008 Jul;35(1–2):407–14.
 151. Human Solutions. Vitronic Vitus XXL 3D Laser Scanner [Internet]. 2020. Available from: <https://www.human-solutions.com/>
 152. Daanen HAM, Psikuta A. 3D body scanning. Vol. 1, *Automation in Garment Manufacturing.* Elsevier Ltd; 2018. 237-252 p.
 153. Tomkinson GR, Shaw LG. Quantification of the postural and technical errors in asymptomatic adults using direct 3D whole body scan measurements of

- standing posture. *Gait Posture*. 2013;37(2):172–7.
154. Schwarz-Müller F, Marshall R, Summerskill S. Development of a positioning aid to reduce postural variability and errors in 3D whole body scan measurements. *Appl Ergon*. 2018;68(March 2017):90–100.
 155. ShapeGB. ShapeGB [Internet]. 2020. Available from: shapegb.org
 156. Zakaria N, Ruznan WS. Developing apparel sizing system using anthropometric data: Body size and shape analysis, key dimensions, and data segmentation. 2nd ed. *Anthropometry, Apparel Sizing and Design*. Elsevier Ltd.; 2019. 91-121 p.
 157. Chun J. International apparel sizing systems and standardization of apparel sizes. *Anthropometry, Apparel Sizing and Design*. Woodhead Publishing Limited; 2014. 274-304 p.
 158. Zakaria N. Children and teenagers body sizes and shapes analyses. *Clothing for Children and Teenagers*. 2016. 53-103 p.
 159. Tucker GR, Alexander JK. Estimation of body surface area of extremely obese human subjects. *J Appl Physiol*. 1960;15:781–4.
 160. Crawford JD, Terry ME, Rourke GM. Simplification of drug dosage calculation by application of the surface area principle. *Pediatrics*. 1950;5(5):783–90.
 161. Yu C-Y, Lo Y-H, Chiou W-K. The 3D scanner for measuring body surface area: a simplified calculation in the Chinese adult. *Appl Ergon*. 2003 May;34(3):273–8.
 162. Lin J Der, Chiou WK, Weng HF, Tsai YH, Liu TH. Comparison of three-dimensional anthropometric body surface scanning to waist-hip ratio and body mass index in correlation with metabolic risk factors. *J Clin Epidemiol*. 2002;55(8):757–66.
 163. Rahman SA, Adjero D. Surface-based body shape index and its relationship with all-cause mortality. *PLoS One*. 2015;10(12):1–21.
 164. Rønnestad BR, Hansen EA, Raastad T. Effect of heavy strength training on thigh muscle cross-sectional area, performance determinants, and performance in well-trained cyclists. *Eur J Appl Physiol*. 2010;108(5):965–75.
 165. Clarkson S, Wheat J, Heller B, Choppin S, Clarkson S, Wheat J, et al. Assessment of a Microsoft Kinect-based 3D scanning system for taking body segment girth measurements : a comparison to ISAK and ISO standards segment girth measurements : a comparison to ISAK and ISO standards. *J Sports Sci*. 2016;34(11):1006–14.
 166. Wang J, Gallagher D, Thornton JC, Yu W, Horlick M, Pi-Sunyer FX. Validation of a

- 3-dimensional photonic scanner for the measurement of body volumes, dimensions, and percentage body fat. *Am J Clin Nutr.* 2006;83(4):809–16.
167. Wilson JP, Kanaya AM, Fan B, Shepherd JA. Ratio of Trunk to Leg Volume as a New Body Shape Metric for Diabetes and Mortality. *PLoS One.* 2013;8(7):1–11.
 168. Schranz N, Tomkinson G, Olds T, Petkov J, Hahn AG. Is three-dimensional anthropometric analysis as good as traditional anthropometric analysis in predicting junior rowing performance? *J Sports Sci.* 2012;30(12):1241–8.
 169. Lu Y, Mcquade S, Hahn JK. 3D Shape-based Body Composition Prediction Model Using Machine Learning. In: the 40th Annual International Conference of the IEEE Engineering in Medicine and Biology Society (EMBC'18). 2018. p. 2–5.
 170. Ruto A, Lee M, Buxton B. Comparing principal and independent modes of variation in 3D human torso shape using PCA and ICA. *ICA Res Netw.* 2006;3–6.
 171. Jolliffe IT. *Principal Component Analysis, Second Edition.* *Encycl Stat Behav Sci.* 2002;30(3):487.
 172. Allen B, Curless B, Popović Z. The space of human body shapes. In: *ACM SIGGRAPH 2003 Papers on - SIGGRAPH '03.* New York, New York, USA: ACM Press; 2003. p. 587.
 173. Song HK, Ashdown SP. Categorization of lower body shapes for adult females based on multiple view analysis. *Text Res J.* 2011;81(9):914–31.
 174. Pei J, Park H, Ashdown SP. Female breast shape categorization based on analysis of CAESAR 3D body scan data. *Text Res J.* 2019;89(4):590–611.
 175. Dai H, Smith WAP, Pears N, Duncan C. Symmetry-Factored Statistical Modelling of Craniofacial Shape. In: *2017 IEEE International Conference on Computer Vision Workshops (ICCVW).* IEEE; 2017. p. 786–94.
 176. Dai H, Pears N, Smith W, Duncan C. Statistical Modeling of Craniofacial Shape and Texture. *Int J Comput Vis.* 2020;128(2):547–71.
 177. Darwin C. *On the origins of species by means of natural selection.* London: Murray. 1859;247.
 178. Thompson DW. XXVII.—Morphology and Mathematics. *Trans R Soc Edinburgh.* 1916;50(4):857–895.
 179. James Rohlf F, Marcus LF. A revolution morphometrics. *Trends Ecol Evol.* 1993;8(4):129–32.
 180. Gelvartas J. Geometric morphometrics. *Ital J Zool.* 2013;1–4.

181. Klingenberg CP. Size, shape, and form: concepts of allometry in geometric morphometrics. *Dev Genes Evol.* 2016;226(3):113–37.
182. Cooke SB, Terhune CE. Form, Function, and Geometric Morphometrics. *Anat Rec.* 2015;298(1):5–28.
183. Gower JC. Generalized procrustes analysis. *Psychometrika.* 1975 Mar;40(1):33–51.
184. Rohlf FJ, Slice D. Extensions of the Procrustes Method for the Optimal Superimposition of Landmarks. *Syst Zool.* 1990;39(1):40.
185. Baab KL, McNulty KP, Rohlf FJ. The shape of human evolution: A geometric morphometrics perspective. *Evol Anthropol.* 2012;21(4):151–65.
186. Slice DE, Olmstead R. Landmark Coordinates Aligned by Procrustes Analysis Do Not Lie in Kendall's Shape Space. *Syst Biol.* 2001;50(1):141–9.
187. Goodall C. Procrustes Methods in the Statistical Analysis of Shape. *J R Stat Soc Ser B.* 1991 Jan;53(2):285–321.
188. Bookstein FL. Landmark methods for forms without landmarks: Morphometrics of group differences in outline shape. *Med Image Anal.* 1997;1(3):225–43.
189. Gunz P, Mitteroecker P. Semilandmarks: A method for quantifying curves and surfaces. *Hystrix.* 2013;24(1):103–9.
190. Huanca Ghislazoni L, Lione R, Cozza P, Franchi L. Measuring 3D shape in orthodontics through geometric morphometrics. *Prog Orthod.* 2017;18(1).
191. D'Amore DC. Illustrating ontogenetic change in the dentition of the Nile monitor lizard, *Varanus niloticus*: A case study in the application of geometric morphometric methods for the quantification of shape-size heterodonty. *J Anat.* 2015;226(5):403–19.
192. Navarro P, Ramallo V, Cintas C, Ruderman A, de Azevedo S, Paschetta C, et al. Body shape: Implications in the study of obesity and related traits. *Am J Hum Biol.* 2020;32(2):1–10.
193. Sheets HD, Covino KM, Panasiewicz JM, Morris SR. Comparison of geometric morphometric outline methods in the discrimination of age-related differences in feather shape. *Front Zool.* 2006;3:15.
194. Jaranilla L, Chavez J, Rosales Carandang JS. Outline Based Geometric Morphometric Analysis in Describing Shape Variation in Suckermouth Armoured Catfishes (*Pterygoplichthys* spp.): Basis for the Development of Automated

- Species Identification System. In: International Conference on Agricultural, Ecological and Medical Sciences (AEMS-2014) Feb 6-7, 2014 Bali (Indonesia). International Institute of Chemical, Biological & Environmental Engineering; 2014.
195. Zahn CT, Roskies RZ. Fourier descriptors for plane closed curves. *IEEE Trans Comput.* 1972;C-21(3):269–81.
 196. Attneave F. Some informational aspects of visual perception. *Psychol Rev.* 1954;61(3):183–93.
 197. Kuhl FP, Giardina CR. Elliptic Fourier features of a closed contour. Vol. 18, *Computer Graphics and Image Processing.* 1982. p. 236–58.
 198. Rohlf FJ. Relationships among eigenshape analysis, Fourier analysis, and analysis of coordinates. *Math Geol.* 1986;18(8):845–54.
 199. Ferson S, Rohlf FJ, Koehn RK. Measuring Shape Variation of Two-Dimensional Outlines. *Syst Zool.* 1985;34(1):59–68.
 200. Cosgriff RL. Identification of shape. 1960.
 201. Murta-Fonseca RA, Fernandes DS. The skull of *Hydrodynastes gigas* (Duméril, Bibron & Duméril, 1854) (Serpentes: Dipsadidae) as a model of snake ontogenetic allometry inferred by geometric morphometrics. *Zoomorphology.* 2016;135(2):233–41.
 202. Openshaw GH, Keogh JS. Head shape evolution in monitor lizards (*Varanus*): Interactions between extreme size disparity, phylogeny and ecology. *J Evol Biol.* 2014;27(2):363–73.
 203. McCoy MW, Bolker BM, Osenberg CW, Miner BG, Vonesh JR. Size correction: Comparing morphological traits among populations and environments. *Oecologia.* 2006;148(4):547–54.
 204. Wicke J, Dumas GA. Influence of the Volume and Density Functions Within Geometric Models for Estimating Trunk Inertial Parameters. 2010;26–31.
 205. Dumas A, Costigan PA, Wicke J. Trunk density profile estimates from dual X-ray absorptiometry. 2008;41:861–7.
 206. Yeadon MR. The simulation of aerial movement-ii. a mathematical inertia model of the human body. 1989;(February):67–74.
 207. Muscolino JE. *The Muscle and Bone Palpation Manual with Trigger Points, Referral Patterns and Stretching.* Mosby/Elsevier; 2008.

208. Paul SM, Chamberlin AP, Hatt C, Nayak A V., Danoff J V. Reliability, validity, and precision of an active stereophotogrammetry system for three-dimensional evaluation of the human torso. *Med Eng Phys.* 2009 Dec;31(10):1337–42.
209. Ustinova KI, Perkins J. Gaze and viewing angle influence visual stabilization of upright posture. *Brain Behav.* 2011 Sep;1(1):19–25.
210. Zelditch ML, Swiderski DL, Sheets HD. *Geometric Morphometrics for Biologists: A Primer.* Elsevier Academic Press; 2012. (Academic Press).
211. de Boor C. *A Practical Guide to Splines (Applied Mathematical Sciences).* Springer-Verlag New York; 1978.
212. Braddom RL. *Physical Medicine and Rehabilitation E-Book.* Elsevier Health Sciences; 2010.
213. Sheets HD, Kim K, Mitchell CE. A combined landmark and outline-based approach to ontogenetic shape change in the Ordovician trilobite *Triarthrus becki*. In: Elewa AMT, editor. *Morphometrics: Applications in Biology and Paleontology.* Berlin, Heidelberg: Springer Berlin Heidelberg; 2004. p. 67–82.
214. Heideman M, Johnson D, Burrus C. Gauss and the history of the fast fourier transform. *IEEE ASSP Mag.* 1984 Oct;1(4):14–21.
215. Kardamakias AA, Mouchtaris A, Pasadakis N. Linear predictive spectral coding and independent component analysis in identifying gasoline constituents using infrared spectroscopy. *Chemom Intell Lab Syst.* 2007 Oct;89(1):51–8.
216. Jun-Ming Lu, Wang M-JJ. The Evaluation of Scan-Derived Anthropometric Measurements. *IEEE Trans Instrum Meas.* 2010 Aug;59(8):2048–54.
217. Kouchi M, Mochimaru M. Evaluation of Accuracy in Traditional and 3D Anthropometry. In 2008.
218. Mochimaru M, Kouchi M. Statistics for 3D Human Body Forms. *Proc Hum Factors Ergon Soc Annu Meet.* 2000 Jul 5;44(38):852–5.
219. Chiu CY, Pease DL, Sanders RH. The effect of pose variability and repeated reliability of segmental centres of mass acquisition when using 3D photonic scanning. *Ergonomics.* 2016;59(12):1673–8.
220. Popkin BM, D’Anci KE, Rosenberg IH. Water, hydration, and health. *Nutr Rev.* 2010 Aug;68(8):439–58.
221. Chiu CY, Thelwell M, Senior T, Choppin S, Hart J, Wheat J. Comparison of depth cameras for three-dimensional reconstruction in medicine. *Proc Inst Mech Eng*

- Part H J Eng Med. 2019;233(9):938–47.
222. Shrout PE, Fleiss JL. Intraclass correlations: uses in assessing rater reliability.1. Shrout PE, Fleiss JL: Intraclass correlations: uses in assessing rater reliability. Psychol Bull 1979, 86:420–8. Psychol Bull. 1979;86(2):420–8.
 223. Koo TK, Li MY. A Guideline of Selecting and Reporting Intraclass Correlation Coefficients for Reliability Research. J Chiropr Med. 2016 Jun;15(2):155–63.
 224. Smith TB, Smith N. Agreement and reliability statistics for shapes. PLoS One. 2018;13(8):1–11.
 225. Darter BJ, Rodriguez KM, Wilken JM. Test–Retest Reliability and Minimum Detectable Change Using the K4b 2 : Oxygen Consumption, Gait Efficiency, and Heart Rate for Healthy Adults During Submaximal Walking. Res Q Exerc Sport. 2013 Jun;84(2):223–31.
 226. Haley SM, Fragala-Pinkham MA. Interpreting change scores of tests and measures used in physical therapy. Phys Ther. 2006 May;86(5):735–43.
 227. Field AP. Discovering Statistics Using SPSS. Third. Sage Publications Ltd.; 2009.
 228. Myer L. Impact of measurement error in the study of sexually transmitted infections. Sex Transm Infect. 2004 Aug 1;80(4):318–21.
 229. de Vet HCW, Terwee CB, Knol DL, Bouter LM. When to use agreement versus reliability measures. J Clin Epidemiol. 2006;59(10):1033–9.
 230. Munro BH. Statistical methods for health care research. 4th ed. . Philadelphia: Lippincott Williams and Wilkins; 2000.
 231. McAuley PA, Blair SN. Obesity paradoxes. J Sports Sci. 2011;29(8):773–82.
 232. Ruderman N, Chisholm D, Pi-Sunyer X, Schneider S. The metabolically obese, normal-weight individual revisited. Diabetes. 1998;47(5):699–713.
 233. Lee JJ, Freeland-Graves JH, Pepper MR, Yao M, Xu B. Predictive equations for central obesity via anthropometrics, stereovision imaging and MRI in adults. Obesity. 2014;22(3):852–62.
 234. Lu Y, Hahn JK. Shape-based three-dimensional body composition extrapolation using multimodality registration. In: Angelini ED, Landman BA, editors. Medical Imaging 2019: Image Processing. SPIE; 2019. p. 64.
 235. Stefan N, Kantartzis, Konstantinos, Machann, Jurgen, Schick, Fritz, Thamer, Claus, Rittig, Kilian, et al. Identification and Characterization of Metabolically Benign Obesity in Humans. Arch Intern Med. 2008 Aug 11;168(15):1609.

236. Myers RH. Classical and Modern Regression with Applications. PWS-KENT; 1990. (Bookware Companion Series).
237. Menard S. Applied Logistic Regression Analysis. 2455 Teller Road, Thousand Oaks California 91320 United States of America: SAGE Publications, Inc.; 2002.
238. Nuttall FQ. Body Mass Index: Obesity, BMI, and Health: A Critical Review. *Nutr Today*. 2015;50(3):117–28.
239. Heymsfield SB, Scherzer R, Pietrobelli A, Lewis CE, Grunfield C. Body Mass Index as a Phenotypic Expression of Adiposity: Quantitative Contribution of Muscularity in a Population-Based Sample. *Int J Obes*. 2011;33(12):1363–73.
240. Miles J, Shevlin M. Applying Regression and Correlation: A Guide for Students and Researchers. SAGE Publications; 2001.
241. Després JP. Body fat distribution and risk of cardiovascular disease: An update. *Circulation*. 2012;126(10):1301–13.
242. Klingenberg CP. Evolution and development of shape: integrating quantitative approaches. *Nat Rev Genet*. 2010 Sep 10;11(9):623–35.
243. Everitt B, Hothorn T. An Introduction to Applied Multivariate Analysis with R. New York, NY: Springer New York; 2011.
244. Watts K, Hwaung P, Grymes J, Cottam SH, Heymsfield SB, Thomas DM. Allometric models of adult regional body lengths and circumferences to height: Insights from a three-dimensional body image scanner. *Am J Hum Biol*. 2020 May 1;32(3).
245. Sullivan GM, Feinn R. Using Effect Size—or Why the P Value Is Not Enough. *J Grad Med Educ*. 2012 Sep;4(3):279–82.
246. Smith R. A mutual information approach to calculating nonlinearity. *Stat*. 2015;4(1):291–303.
247. Mikhail. Kernel estimate for (Conditional) Mutual Information. MATLAB Central File Exchange; 2020.
248. Wold S, Sjöström M, Eriksson L. PLS-regression: A basic tool of chemometrics. *Chemom Intell Lab Syst*. 2001;58(2):109–30.
249. Wold S, Ruhe A, Wold H, Dunn, III WJ. The Collinearity Problem in Linear Regression. The Partial Least Squares (PLS) Approach to Generalized Inverses. *SIAM J Sci Stat Comput*. 1984 Sep;5(3):735–43.
250. Bastien P, Vinzi VE, Tenenhaus M. PLS generalised linear regression. *Comput*

- Stat Data Anal. 2005 Jan;48(1):17–46.
251. Maitra S, Yan J. Principle Component Analysis and Partial Least Squares: Two Dimension Reduction Techniques for Regression. *Appl Multivar Stat Model.* 2008;79–90.
 252. Farrés M, Platikanov S, Tsakovski S, Tauler R. Comparison of the variable importance in projection (VIP) and of the selectivity ratio (SR) methods for variable selection and interpretation. *J Chemom.* 2015;29(10):528–36.
 253. Li HD, Xu QS, Liang YZ. libPLS: An integrated library for partial least squares regression and linear discriminant analysis. *Chemom Intell Lab Syst.* 2018;176:34–43.
 254. Field AP. *Discovering statistics using SPSS : (and sex and drugs and rock “n” roll).* Los Angeles [i.e. Thousand Oaks, Calif.]; London: SAGE Publications; 2009.
 255. Duggan CP, Kurpad A, Stanford FC, Sunguya B, Wells JC. Race, ethnicity, and racism in the nutrition literature: An update for 2020. *Am J Clin Nutr.* 2020 Dec 1;112(6):1409–14.
 256. Wilson OWA, Zou ZH, Bopp M, Bopp CM. Comparison of obesity classification methods among college students. *Obes Res Clin Pract.* 2019;13(5):430–4.
 257. Ward JH. Hierarchical Grouping to Optimize an Objective Function. *J Am Stat Assoc.* 1963 Mar;58(301):236–44.
 258. Pearson K. On the criterion that a given system of deviations from the probable in the case of a correlated system of variables is such that it can be reasonably supposed to have arisen from random sampling. London, Edinburgh, Dublin *Philos Mag J Sci.* 1900 Jul 21;50(302):157–75.
 259. Sabina O, Emilia F, Manuela A, Alexandra M, Georgeta P, Adrian S. Applied 3D virtual try-on for bodies with atypical characteristics. *Procedia Eng.* 2015;100(January):672–81.
 260. Company F. The next iPhone will get a “world facing” 3D camera. [Internet]. 2020. Available from: [https://www.fastcompany.com/90474966/the-next-iphone-will-get-a-world-facing-3d-camera#:~:text=iPhones already feature depth cameras \(TrueDepth\) on their fronts.&text=The iPhone 11 Pro and,ultra-wide-angle lens](https://www.fastcompany.com/90474966/the-next-iphone-will-get-a-world-facing-3d-camera#:~:text=iPhones already feature depth cameras (TrueDepth) on their fronts.&text=The iPhone 11 Pro and,ultra-wide-angle lens).
 261. Lee H, Martin DT, Anson JM, Grundy D, Hahn AG. Physiological characteristics of successful mountain bikers and professional road cyclists. *J Sports Sci.* 2002

Jan;20(12):1001–8.

262. Ackland T, Mazza J. Introduction. In: Kinanthropometry in Aquatic Sports. Champaign, IL: Human Kinetics; 1994. p. 8–10.
263. Wells JCK. Promoting ethnic parity in health, leaving behind “race”: A challenge for the global community in 2020. Vol. 112, American Journal of Clinical Nutrition. Oxford University Press; 2020. p. 505–6.

Chapter 10 - Appendices

Appendix 1

A.1.1 Anthropometrics included in the restricted and full ISAK profiles

Type	No.	Site	Restricted	Full
Basic	1	Mass	X	X
	2	Stature	X	X
	3	Sitting height		X
	4	Arm span		X
Skinfolds	5	Triceps	X	X
	6	Subscapular	X	X
	7	Biceps	X	X
	8	Iliac crest	X	X
	9	Supraspinale	X	X
	10	Abdominal	X	X
	11	Front thigh	X	X
	12	Medial calf	X	X
Girths	13	Head		X
	14	Neck		X
	15	Arm (relaxed)	X	X
	16	Arm (flexed and tensed)	X	X
	17	Forearm (maximum)		X
	18	Wrist (distal styloids)		X
	19	Chest (mesosternale)		X
	20	Waist (minimum)	X	X
	21	Gluteal (hips)	X	X
	22	Thigh (1cm gluteal fold)		X
	23	Thigh (mid-troch-tib. lat.)		X
	24	Calf (maximum)	X	X
25	Ankle (minimum)		X	
Lengths	26	Acromiale-radiale		X
	27	Radiale-styilion		X
	28	Midstyliion-dactylion		X
	29	Iliospinale height		X
	30	Trochanterion height		X
	31	Trochanterion-tibiale laterale		X
	32	Tibiale laterale height		X
	33	Tibiale mediale-sphyriion tibiale		X
Breadths	34	Biacromial		X
	35	A-P abdominal depth		X
	36	Biliocristal		X
	37	Foot length		X
	38	Transverse chest		X
	39	A-P chest depth		X
	40	Humerus	X	X
	41	Bi-styloid		X
	42	Femur	X	X

Appendix 2

A.2.1 Research ethics approval

Comparison of Cost-effective 3D Photonic Scanning Techniques for Anthropometric Measurements

Ethics Review ID: ER5855905

Workflow Status: Approved with Advisory Comments

Type of Ethics Review Template: All other research with human participants

Primary Researcher / Principal Investigator

Chuang-Yuan Chiu
(Sports Engineering Research Group)

Converis Project Application::

Q1. Is this project: i) Staff research

Other SHU Investigator

Alice Bullas
Simon Choppin
Michael Thelwell
(Sports Engineering Research Group),(Health and Wellbeing),(Sports Engineering Research Group)

Q3b. External Investigator Details: Professor Ross Sanders, The University of Sydney

Q4. Proposed Start Date of Data Collection: 05/02/2018

Q5. Proposed End Date of Data Collection : 31/07/2018

Q6. Will the research involve any of the following:

i) Participants under 5 years old: No

ii) Pregnant women: No

iii) 5000 or more participants: No

iv) Research being conducted in an overseas country: No

Q7. If overseas, specify the location:

Q8. Is the research externally funded?: No

Q9. Will the research be conducted with partners and subcontractors?: No

Q10. Does the research involve one or more of the following?

i. Patients recruited because of their past or present use of the NHS or Social Care: No

ii. Relatives/carers of patients recruited because of their past or present use of the NHS or Social Care: No

iii. Access to data, organs, or other bodily material of past or present NHS patients: No

iv. Foetal material and IVF involving NHS patients: No

v. The recently dead in NHS premises: No

vi. Participants who are unable to provide informed consent due to their incapacity even if the project is not health related: No

vii. Prisoners or others within the criminal justice system recruited for health-related research: No

A.2.2 Participant consent form



PARTICIPANT CONSENT FORM

Comparison of Cost-effective 3D Photonic Scanning Techniques for Anthropometric Measurements:

Please answer the following questions by ticking the response that applies

- | | YES | NO |
|--|--------------------------|--------------------------|
| 1. I have read the Information Sheet for this study and have had details of the study explained to me. | <input type="checkbox"/> | <input type="checkbox"/> |
| 2. My questions about the study have been answered to my satisfaction and I understand that I may ask further questions at any point. | <input type="checkbox"/> | <input type="checkbox"/> |
| 3. I understand that I am free to withdraw from the study without giving a reason for my withdrawal. | <input type="checkbox"/> | <input type="checkbox"/> |
| 4. I understand that I can decline to answer any questions in the study without any consequences to my future treatment by the researcher. | <input type="checkbox"/> | <input type="checkbox"/> |
| 5. I agree to provide information to the researchers under the conditions of confidentiality set out in the Information Sheet. | <input type="checkbox"/> | <input type="checkbox"/> |
| 6. I wish to participate in the study under the conditions set out in the Information Sheet. | <input type="checkbox"/> | <input type="checkbox"/> |
| 7. I consent to the information collected for the purposes of this research study, once anonymised (so that I cannot be identified), to be used for any other research purposes. | <input type="checkbox"/> | <input type="checkbox"/> |
| 8. I agree to dress into a close-fit suit and be touched by a measurer | <input type="checkbox"/> | <input type="checkbox"/> |
| 9. I agree to be measured manually with palpation and callipers, etc. | <input type="checkbox"/> | <input type="checkbox"/> |
| 10. I agree to have my photograph taken. | <input type="checkbox"/> | <input type="checkbox"/> |
| 11. I understand that my name will not be linked to the photograph(s). | <input type="checkbox"/> | <input type="checkbox"/> |
| 12. I understand that I will not be given credit for my appearance in photograph(s). | <input type="checkbox"/> | <input type="checkbox"/> |
| 13. I give the project team permission to: | | |
| - use my photograph(s) in printed material (e.g. reports, leaflets, newspaper articles, news releases) | <input type="checkbox"/> | <input type="checkbox"/> |
| - use my photograph(s) in presentations (e.g. at conferences or seminars) | <input type="checkbox"/> | <input type="checkbox"/> |
| - use my data in future relevant research | <input type="checkbox"/> | <input type="checkbox"/> |

14. I agree to be contacted about future studies.

Participant's Signature: _____ Date: _____

Participant's Name (Printed): _____

Contact details: _____

Researcher's Name (Printed): _____

Researcher's Signature: _____

Researcher's contact details:
(Name, address, contact number of investigator)

Please keep your copy of the consent form and the information sheet together.

PARTICIPANT INFORMATION SHEET

Comparison of Cost-effective 3D Photonic Scanning Techniques for Anthropometric Measurements

(1) What is this study about?

You are invited to take part in a research study about understanding your body size, shape and composition. We will use data obtained from standard body measurement and 3D body scanning techniques.

You have been invited to participate in this study because you are aged over 18 years and we think you might be interested in learning about your body size, shape and composition. This Participant Information Sheet tells you about the research study. Knowing what is involved will help you decide if you want to take part in the research. Please read this sheet carefully and ask questions about anything that you don't understand or want to know more about.

Participation in this research study is voluntary.

By giving your consent to take part in this study you are telling us that you:

- ✓ Understand what you have read.
- ✓ Agree to take part in the research study as outlined below.
- ✓ Agree to the use of your personal information as described.

You will be given a copy of this Participant Information Statement to keep.

(2) What will the study involve for me?

You will need to change into a close-fitting suit (e.g. swimming suit, two-piece for female; tri-pants with sports top) with a polyester cap. You will also be asked to remove any jewellery, watches or other accessories. It is highly recommended that you bring your own jacket, robe, or bath towel to keep you warm between each test. Private changing facilities are provided. Males will be required to take off their shirts. As you might be measured by a researcher of a different gender, you can invite a chaperone to accompany with you during the tests.

During the tests, your body will be measured by experienced operators and well-trained anthropometrists (someone who has been trained in body measurement). There will be a series of assessments in a test session including baseline information, manual assessment, image capturing, and 3D body scanning.

Some tests involve taking measurements of the body using a tape measure, and calipers. Others will involve you remaining still in a standing position while we capture images of your body. All tests will be conducted in a private, enclosed space. Details of these assessments are below.

Baseline information

We will ask you for your gender and birthday.

Manual assessment

This will involve a light manipulation of the body and marking certain points on your body with a pen (specific 'bony-landmarks'). Tape measures, callipers and segmometers will be used to

assess lengths, breadths, heights and girths of the body. Callipers will be used to assess skinfolds (a light pinch of the skin to judge underlying fat content).

3D body scanning

3D body scanning requires markers placed on bony anatomical landmarks points. In the body scanning test, you will be scanned by three body scanning systems. You will stand inside a booth and attempt to keep still while being scanned. Being scanned will take less than a minute for each system.

(3) Where will this take place?

All test will be conduct at Sheffield Hallam University, Collegiate Campus.

(4) How much of my time will the study take?

You can choose only one test session or attend repeated test sessions described above if you like. The whole process for each test session will take around 1 hour.

(5) Who can take part in the study?

If you are age above 18, able-bodied (people without amputations or missing limbs), you are eligible for all assessments.

(6) Do I have to be in the study? Can I withdraw from the study once I've started?

Being in this study is completely voluntary and you do not have to take part. Your decision whether to participate will not affect your current or future relationship with the researchers or anyone else at the Sheffield Hallam University.

If you decide to take part in the study and then change your mind later, you are free to withdraw at any time. You can do this by informing Dr. Chuang-Yuan Chiu (c.chiu@shu.ac.uk). Also, you are free to opt out of ant test or stop any test at any time. If you do opt out of any tests you will still be allowed to participate in the other tests.

If you decide to withdraw from the study, we will not collect any more information from you. Any information that we have already collected, however, will be kept in our study records in coded form (i.e. you are not identified) and may be included in the study results.

(7) Are there any risks or costs associated with being in the study?

There is no cost for the test assessments and the tests will take place in the weekdays during the office hours (8AM-6PM). You might need to spend time and cover your cost for your travel.

(8) Are there any benefits associated with being in the study?

If you wish, you will receive the test results after conducting all assessments which will help you understand your body size, shape and composition. If you attend more than one test sessions, you can track the change in your body shape and body composition.

(9) What will happen to information about me that is collected during the study?

By providing your consent, you are allowing us to collect personal information for the purposes of this research study. Your information will only be used for the purposes outlined in this Participant Information Statement, unless you consent otherwise.

Your information including anthropometric data and (3D) images will be stored electronically with a code as an identifier rather than your name. The recordings will be accessible only to the researchers and protected by a password. The images will be applied to generate your 3D human model and possibly used in publication or presentation to illustrate the testing process. We will hide or blur your face or use a virtual face to replace your face in the relevant figures and images which might show your identification. We will not disclose your personal information or identity. Your 3D human model and the captured image will be used only for the research purpose.

Your information will be stored securely and your identity/information will be kept strictly confidential, except as required by law. Study findings may be published. Your face will be obscured in all images. The information will be kept in a confidential locked file and can be accessed for a period of 20 years. After 20 years, electronic data will be deleted from the hard discs and the paper materials will be shredded.

(10) Can I tell other people about the study?

Yes. You are permitted to tell other people about the program but should not tell them your results or ask other participants about their results.

(11) What if I would like further information about the study?

If you would like to know more at any stage, please feel free to ask any of researchers, operators or recorders during the sessions. If you wish to know more before giving consent, you can e-mail Dr. Chuang-Yuan Chiu (c.chiu@shu.ac.uk)

(12) Will I be told the results of the study?

If you wish, we can provide your personal results of body size and body composition.

Appendix 3

A.3.1 Research ethics approval.

Understanding Body Shapes from Rapid Approaches

Ethics Review ID: ER10868123

Workflow Status: Application Approved

Type of Ethics Review Template: All other research with human participants

Primary Researcher / Principal Investigator

Chuang-Yuan Chiu
(Advanced Wellbeing Research Centre)

Converis Project Application::

Q1. Is this project: i) Staff research

Other SHU Investigator

Alice Bullas
Simon Choppin
Raimonds Ciems
Michael Thelwell
(Centre for Sports Engineering Research),(Health and Wellbeing),(Advanced Wellbeing Research Centre),(Health and Wellbeing)

Q4. Proposed Start Date of Data Collection: 01/02/2019

Q5. Proposed End Date of Data Collection : 31/12/2019

Q6. Will the research involve any of the following:

- i) Participants under 5 years old: No
- ii) Pregnant women: No
- iii) 5000 or more participants: No
- iv) Research being conducted in an overseas country: No

Q7. If overseas, specify the location:

Q8. Is the research externally funded?: No

Q9. Will the research be conducted with partners and subcontractors?: No

Q10. Does the research involve one or more of the following?

- i. Patients recruited because of their past or present use of the NHS or Social Care: No
- ii. Relatives/carers of patients recruited because of their past or present use of the NHS or Social Care: No
- iii. Access to data, organs, or other bodily material of past or present NHS patients: No
- iv. Foetal material and IVF involving NHS patients: No
- v. The recently dead in NHS premises: No
- vi. Participants who are unable to provide informed consent due to their incapacity even if the project is not health related: No
- vii. Prisoners or others within the criminal justice system recruited for health-related research: No
- viii. Prisoners or others within the criminal justice system recruited for non-health-related research: No

PARTICIPANT INFORMATION SHEET

Title of Project: Estimating Somatotypes from Rapid Approaches

(1) What is this study about?

You are invited to take part in a research study about understanding your body shape and composition. We will collect your data from standard body measurement, bioelectrical impedance analysis (e.g. Body composition analyser of Tanita or InBody) and 3D body scanning techniques.

You have been invited to participate in this research study because you are aged over 18 years and we think you might be interested in learning about your body shape and composition. This participant information sheet tells you about this research study. Knowing what is involved will help you decide whether you want to take part in the research. Please read this sheet carefully and ask questions about anything that you don't understand or want to know more about.

Participation in this research study is voluntary.

By giving your consent to take part in this study you are telling us that you:

- ✓ Understand what you have read.
- ✓ Agree to take part in the research study as outlined below.
- ✓ Agree to the use of your personal information as described.

You will be given a copy of this Participant Information Statement to keep.

(2) What will the study involve for me?

You will need to change into a close-fitting suit (e.g. swimming suit, two-piece for female; tri-pants with sports top) and might have to wear a polyester cap. You might also be asked to remove any jewellery, watches or other accessories. It is highly recommended that you bring your own jacket, robe, or bath towel to keep you warm between each test. Private changing facilities are provided. Males will be required to take off their shirts. As you might be measured by a researcher of a different gender, you can invite a chaperone to accompany you during the tests.

During the tests, your body will be measured by experienced operators and well-trained anthropometrists (someone who has been trained in body measurement). There will be a series of assessments in a test session including baseline information, manual assessment, bioelectrical impedance analysis, and/or 3D body scanning.

Some tests involve taking measurements of the body using a tape measure, and calipers. Others will involve pose in different pre-defined postures (e.g. stand straight, put hands of their head, abduct arms and/or legs slightly, self-rotation on one spot, etc) while we capture images of your body or take body fat measurements. All tests will be conducted in a private, enclosed space. Details of these assessments are below.

Baseline information

We will ask for your gender, date of birth and sport status (e.g. sports ages, training frequencies, sports types).

Manual assessment

This will involve a light manipulation of the body and marking certain points on your body with a felt-tipped pen (specific 'bony-landmarks'). Tape measures, callipers and segmometers will be

used to assess lengths, breadths, heights and girths of the body. Callipers will be used to assess skinfolds (a light pinch of the skin to judge underlying fat content).

Bioelectrical impedance analysis

If you would like to attend bioelectrical impedance analysis, please do not eat, shower or do any strenuous exercise before the test (at least three hours). Please maintain your normal water intake. You might be asked to clean your feet and hand before the bioelectrical impedance analysis. During the test, you will have to stand on the monitor. Your feet (and/or hands) should be placed on (and/or hold) the electrodes.

3D body scanning

3D body scanning might require that markers are placed on bony anatomical landmark points. In the body scanning test, you will be scanned by one or multiple body scanning systems. You will have to pose in pre-defined posture or movement while being scanned. You might be asked to hold your breath during the scanning (around 10-15 seconds). Being scanned will take less than a minute in each instance.

(3) Where will this take place?

All tests will be conducted at Sheffield Hallam University, Collegiate Campus.

(4) How much of my time will the study take?

You can choose only one test session or attend repeated test sessions described above if you like. The whole process for each test session will take around 1 hour.

(5) Who can take part in the study?

If you are age above 18, able-bodied (people without amputations or missing limbs), not pregnant, without metal allergies, without pacemakers or other mechanical implants, you are eligible for all assessments.

(6) Do I have to be in the study? Can I withdraw from the study once I've started?

Being in this study is completely voluntary and you do not have to take part. Your decision whether to participate will not affect your current or future relationship with the researchers or anyone else at the Sheffield Hallam University.

If you decide to take part in the study and then change your mind later, you are free to withdraw at any time. You can do this by informing Dr Chuang-Yuan Chiu (c.chiu@shu.ac.uk). Also, you are free to opt out of any test or stop any test at any time. If you do opt out of any tests you will still be allowed to participate in the other tests.

If you decide to withdraw from the study, we will not collect any more information from you. Any information that we have already collected, however, will be kept in our study records in a coded form (i.e. you are not identified) and may be included in the study results.

(7) Are there any risks or costs associated with being in the study?

There is no cost for the test assessments and the tests will take place on the weekdays during the office hours (8AM-6PM). You might need to spend time and cover your cost for your travel.

(8) Are there any benefits associated with being in the study?

If you wish, you will receive the test results after conducting all assessments which will help you understand your body shape and composition. If you attend more than one test sessions, you can track the change in your body shape and body composition.

(9) What will happen to information about me that is collected during the study?

By providing your consent, you are allowing the research team to collect personal information for the purposes of this research study. Your information will only be used for the purposes outlined in this participant information sheet unless you consent otherwise.

Your information including anthropometric data and (3D) images will be stored electronically with a code as an identifier rather than your name. The recordings will be accessible to the researchers and protected by a password. The images will be applied to generate your 3D human model and possibly used in publication or presentation to illustrate the testing process. We will hide or blur your face or use a virtual face to replace your face in the relevant figures and images which might show your identification. We will not disclose your personal information or identity. Your 3D human models and the captured images will be used for the research purpose.

Only researchers in the research team (listed below) can access both your identity and information. Your raw anonymous data could be supplied to our collaborated researchers. We will make sure to replace your name with numbers and hide or blur your face before supplying your data to the external researchers.

Your information will be stored securely, and your identity/information will be kept strictly confidential, except as required by law. Study findings may be published. Your face will be hidden or obscured in all images. Your paper data will be retained until the project finish. The paper data will be shredded securely after taking a scanned copy. Your electronic data will be retained until all relevant research is complete and it will then be deleted from the hard disks.

(10) Are there any possible risks or disadvantaged in taking part.

The tests have a very low risk of physical injury. A well-trained anthropometrist will be conducted all the manual anthropometric measurement. The test will not be taken during increased blood flow such as after exercise, showering or sauna use. This should avoid breaking the participants' skin and extravasation. Some trip injury might happen since the participants might not be aware of cables and level differences. Thus, we will give clear instructions and make participants aware of the cables, level differences to avoid trip injury. The test of bioelectrical impedance analysis could generate some issues for pregnant participants or people with metal allergies, pacemakers or other mechanical implants. Please let the researcher know if you have these conditions so the researcher will not conduct the bioelectrical impedance analysis with you.

(11) Can I tell other people about the study?

Yes. You are permitted to tell other people about the program but should not tell them your results or ask other participants about their results.

(12) What if I would like further information about the study?

If you would like to know more at any stage, please feel free to ask the researchers, operators or recorders during the sessions. If you wish to know more before giving consent, you can e-mail Dr Chuang-Yuan Chiu (c.chiu@shu.ac.uk)

(13) Will I be told the results of the study?

If you wish, we can provide your personal results of body shape and body composition.

(14) The legal basis for research for studies

The University undertakes research as part of its function for the community under its legal status. Data protection allows us to use personal data for research with appropriate safeguards in place under the legal basis of **public tasks that are in the public interest**. A full statement of your rights can be found at <https://www.shu.ac.uk/about-this-website/privacy-policy/privacy-notices/privacy-notice-for-research>. However, all University research is reviewed to ensure that participants are treated appropriately and their rights respected. This study was approved by UREC with Convens number ER10868123. Further information at <https://www.shu.ac.uk/research/ethics-integrity-and-practice>

Research Team Details:

Investigator:

Chuang-Yuan Chiu (c.chiu@shu.ac.uk)

Co-investigator:

Simon Choppin (s.choppin@shu.ac.uk)

Alice Bullas (a.bullas@shu.ac.uk)

Michael Thelwell (Michael.J.Thelwell@student.shu.ac.uk)

Raimonds Ciems (Raimonds.Ciems@student.shu.ac.uk)

<p>You could contact the Data Protection Officer if:</p> <ul style="list-style-type: none">• you have a query about how your data is used by the University• you would like to report a data security breach (e.g. if you think your personal data has been lost or disclosed inappropriately)• you would like to complain about how the University has used your personal data <p>DPO@shu.ac.uk</p>	<p>You could contact the Head of Research Ethics (Professor Ann Macaskill) if:</p> <ul style="list-style-type: none">• you have concerns with how the research was undertaken or how you were treated <p>a.macaskill@shu.ac.uk</p>
--	--

Postal address: Sheffield Hallam University, Howard Street, Sheffield S1 1WB Telephone: 0114 225 5555

A.3.3 Participant consent form



PARTICIPANT CONSENT FORM

Title of Project: Estimating Somatotypes from Rapid Approaches

Please answer the following questions by ticking the response that applies

- | | YES | NO |
|--|--------------------------|--------------------------|
| 1. I have read the participant information sheet for this study and have had details of the study explained to me. | <input type="checkbox"/> | <input type="checkbox"/> |
| 2. My questions about the study have been answered to my satisfaction and I understand that I may ask further questions at any point. | <input type="checkbox"/> | <input type="checkbox"/> |
| 3. I understand that I am free to withdraw from the study without giving a reason for my withdrawal. | <input type="checkbox"/> | <input type="checkbox"/> |
| 4. I understand that I can decline to answer any questions in the study without any consequences to my future treatment by the researcher. | <input type="checkbox"/> | <input type="checkbox"/> |
| 5. I agree to provide information to the researchers under the conditions of confidentiality set out in the participant information sheet. | <input type="checkbox"/> | <input type="checkbox"/> |
| 6. I wish to participate in the study under the conditions set out in the participant information sheet. | <input type="checkbox"/> | <input type="checkbox"/> |
| 7. I consent to the information collected for the purposes of this research study, once anonymised (so that I cannot be identified), to be used for any other research purposes. | <input type="checkbox"/> | <input type="checkbox"/> |
| 8. I agree to dress into a close-fit suit and be touched by a measurer. | <input type="checkbox"/> | <input type="checkbox"/> |
| 9. I agree to be measured manually with palpation and callipers, etc. | <input type="checkbox"/> | <input type="checkbox"/> |
| 10. I agree to be measured by a body composition analyser. | <input type="checkbox"/> | <input type="checkbox"/> |
| 11. I agree to have my photograph taken. | <input type="checkbox"/> | <input type="checkbox"/> |
| 12. I understand that my name will not be linked to the photograph(s). | <input type="checkbox"/> | <input type="checkbox"/> |
| 13. I understand that I will not be given credit for my appearance in the photograph(s). | <input type="checkbox"/> | <input type="checkbox"/> |
| 14. I give the project team permission to: | | |
| - use my photograph(s) in printed material (e.g. reports, leaflets, newspaper articles, news releases) | <input type="checkbox"/> | <input type="checkbox"/> |

- use my photograph(s) in presentations (e.g. at conferences or seminars)

- use my data in future relevant research

15. I agree to be contacted about future studies.

Participant's Signature: _____ Date: _____

Participant's Name (Printed): _____

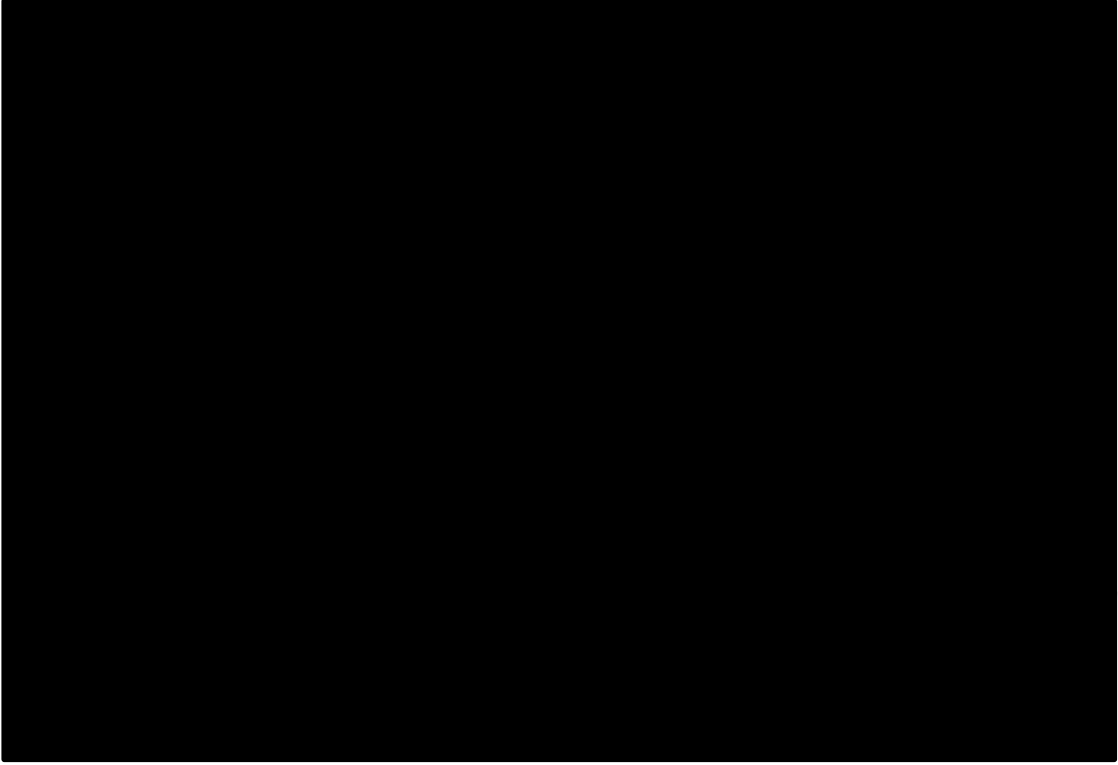

Contact Email: _____

Researcher's Name (Printed): _____

Researcher's Signature: _____

Appendix 4

A.4.1 Data sharing agreement with LIFE Consortium and Leipzig University.

<p>Signatures</p> <p>PROVIDER INFORMATION and AUTHORISED SIGNATURE</p> 
<p>RECIPIENT INFORMATION and AUTHORISED SIGNATURE</p> 

A.4.2 Research ethics approval.

Application of shape-based digital anthropometry for population clustering.

Ethics Review ID: ER13534279

Workflow Status: Application Approved

Type of Ethics Review Template: No human participants, human tissue or personal data

Primary Researcher / Principal Investigator

Michael Thelwell
(Health and Wellbeing)

Converis Project Application::

Q1. Is this project: ii) Doctoral research

Director of Studies

Simon Choppin
(Health and Wellbeing)

Supervisory Team

Alice Bullas
John Hart
Jonathan Wheat
(Advanced Wellbeing Research Centre),(Advanced Wellbeing Research Centre),(Advanced Wellbeing Research Centre)

Q3b. External Investigator Details: Dr. Peter Ahnert, Leipzig University

Q4. Proposed Start Date of Data Collection: 01/04/2019

Q5. Proposed End Date of Data Collection : 02/12/2019

Q6. Will the research involve any of the following:

- i) Participants under 5 years old:
 - ii) Pregnant women:
 - iii) 5000 or more participants:
 - iv) Research being conducted in an overseas country: Yes
- Q7. If overseas, specify the location: Leipzig, Germany

Q8. Is the research externally funded?: No

Q9. Will the research be conducted with partners and subcontractors?: Yes

Q9b. If yes, outline how you will ensure that their ethical policies are consistent with university policy: The data was collected previously by Leipzig University, with written informed consent obtained from all participants. This study was approved by the ethics board of the medical faculty of Leipzig University, with all data privacy and safety forms approved by a data protection officer.

A.4.3 Sex differences in size and shape measures.

Measure	Male	Female	p-value
	Mean (SD)	Mean (SD)	
Height (cm)	176.07 (7.34)	164.0 (6.97)	<0.001
Weight (kg)	85.97 (14.46)	72.13 (14.28)	<0.001
BMI (kg/m ²)	27.59 (4.19)	26.97 (5.27)	<0.001
WHR	0.99 (0.07)	0.87 (0.06)	<0.001
Waist Girth (cm)	100.99 (12.32)	91.76 (13.78)	<0.001
Belly Circ. (cm)	103.03 (11.86)	96.71 (11.78)	<0.001
Bust Chest Girth (cm)	107.91 (9.71)	102.01 (11.36)	<0.001
Buttock Girth (cm)	104.04 (7.88)	107.14 (10.78)	<0.001
High Hip Girth (cm)	102.98 (11.74)	98.69 (11.68)	<0.001
High Waist Girth (cm)	100.21 (11.72)	88.80 (13.13)	<0.001
Hip Girth (cm)	105.18 (7.85)	108.46 (10.49)	<0.001
Middle Hip (cm)	102.56 (11.20)	103.15 (12.36)	<0.001
Torso Width Waist (cm)	46.97 (7.34)	43.34 (7.40)	<0.001
Under Bust Circ. (cm)	103.15 (9.64)	89.07 (11.36)	<0.001
Waistband (cm)	98.78 (10.18)	95.22 (11.51)	<0.001
Distance Neck - Hip (cm)	61.66 (3.23)	56.90 (3.18)	<0.001
Side Upper Torso Length Left (cm)	24.90 (2.81)	23.13 (3.1)	<0.001
Side Upper Torso Length Right (cm)	24.47 (2.77)	22.77 (3.06)	<0.001
Cross Shoulder (cm)	50.24 (3.36)	46.62 (3.78)	<0.001
Across Front Width (cm)	44.05 (4.32)	41.54 (4.71)	<0.001
Width Armpits (cm)	47.05 (4.96)	45.37 (6.47)	<0.001
Across Back Width (cm)	42.48 (3.36)	38.71 (3.61)	<0.001
Neck - Waist Centre Back (cm)	43.80 (2.31)	40.77 (2.39)	<0.001
Neck Left - Waist Back (cm)	48.30 (2.78)	44.34 (2.74)	<0.001
Neck Right - Waist Back (cm)	48.05 (2.79)	44.18 (2.68)	<0.001
Distance Across Back Width (cm)	26.82 (3.61)	25.79 (3.45)	<0.001
Waist - High Hip Back (cm)	6.22 (1.51)	5.07 (2.1)	<0.001
Waist - Buttock (cm)	20.14 (1.72)	18.63 (2.3)	<0.001
Waistband - Buttock (cm)	12.18 (2.37)	15.44 (1.98)	<0.001
Crotch Length (cm)	87.41 (6.09)	77.93 (6.11)	<0.001
Crotch Length Front (cm)	44.70 (3.47)	37.30 (3.38)	<0.001
Crotch Length Rear (cm)	42.70 (2.97)	40.64 (3.09)	<0.001
Waist - Buttock Height Left (cm)	20.1 (1.68)	18.43 (2.32)	<0.001
Waist - Buttock Height Right (cm)	20.14 (1.7)	18.49 (2.38)	<0.001
Waistband - Buttock Height Left (cm)	9.63 (2.55)	14.53 (2.38)	<0.001
Waistband - Buttock Height Right (cm)	9.60 (2.58)	14.57 (2.41)	<0.001
Torso Length (cm)	32.14 (2.13)	30.13 (2.06)	<0.001
PC1	0.8548 (1.7198)	-0.7929 (2.1113)	<0.001
PC2	-0.9941 (1.1194)	0.9042 (1.176)	<0.001
PC3	0.3587 (1.0173)	-0.3185 (0.8644)	<0.001
PC4	0.0399 (0.7877)	-0.0338 (0.9612)	<0.001
PC5	-0.2286 (0.5389)	0.194 (0.9027)	<0.001
PC6	0.0274 (0.5056)	-0.0225 (0.6052)	<0.001
PC7	0.0745 (0.3467)	-0.0793 (0.4739)	<0.001
PC8	0.0188 (0.3541)	-0.0103 (0.4242)	<0.001
PC9	-0.0103 (0.3251)	0.0283 (0.3972)	<0.001

A.4.4 Pearson correlation and effect size - size measures male and female.

	Age	Weight	Waist Girth	Belly Circ.	Bust Chest Girth
Age		0.09(0.01)	0.46(0.21)	0.42(0.17)	0.3(0.09)
Weight	0.16(0.02) ²		0.8(0.63)	0.82(0.66)	0.79(0.63)
Waist Girth	0.46(0.21) ²	0.84(0.71) ²		0.99(0.98)	0.9(0.8)
Belly Circ.	0.39(0.15) ²	0.87(0.76) ²	0.98(0.95) ²		0.89(0.78)
Bust Chest Girth	0.38(0.14) ²	0.83(0.69) ²	0.94(0.88) ²	0.93(0.86) ²	
Buttock Girth	0.3(0.09) ²	0.88(0.78) ²	0.88(0.78) ²	0.91(0.83) ²	0.85(0.73) ²
High Hip Girth	0.39(0.15) ²	0.88(0.77) ²	0.97(0.94) ²	0.99(0.99) ²	0.92(0.85) ²
High Waist Girth	0.45(0.21) ²	0.84(0.71) ²	0.99(0.97) ²	0.97(0.93) ²	0.95(0.91) ²
Hip Girth	0.27(0.07) ²	0.87(0.76) ²	0.85(0.73) ²	0.89(0.79) ²	0.83(0.69) ²
Middle Hip	0.43(0.19) ²	0.87(0.75) ²	0.96(0.92) ²	0.97(0.94) ²	0.91(0.83) ²
Torso Width Waist	0.39(0.15) ²	0.75(0.56) ²	0.89(0.79) ²	0.87(0.76) ²	0.83(0.69) ²
Under Bust Circ.	0.4(0.16) ²	0.83(0.69) ²	0.94(0.89) ²	0.93(0.87) ²	0.96(0.92) ²
Waistband	0.42(0.18) ²	0.87(0.75) ²	0.97(0.94) ²	0.98(0.96) ²	0.93(0.87) ²
Distance Neck - Hip	-0.27(0.07) ²	-0.14(0.02) ²	-0.23(0.05) ²	-0.13(0.02) ²	-0.23(0.05) ²
Side Upper Torso Left	-0.2(0.04) ²	-0.17(0.03) ²	-0.18(0.03) ²	-0.17(0.03) ²	-0.2(0.04) ²
Side Upper Torso Right	-0.24(0.06) ²	-0.21(0.04) ²	-0.23(0.05) ²	-0.22(0.05) ²	-0.26(0.07) ²
Cross Shoulder	0.37(0.14) ²	0.64(0.41) ²	0.79(0.62) ²	0.78(0.6) ²	0.81(0.66) ²
Across Front Width	0.39(0.15) ²	0.54(0.3) ²	0.68(0.47) ²	0.67(0.45) ²	0.7(0.49) ²
Width Armpits	0.31(0.1) ²	0.59(0.35) ²	0.67(0.45) ²	0.68(0.46) ²	0.71(0.51) ²
Across Back Width	0.22(0.05) ²	0.55(0.31) ²	0.63(0.4) ²	0.63(0.4) ²	0.68(0.46) ²
Neck - Waist Centre Back	0.29(0.08) ²	0.37(0.14) ²	0.51(0.26) ²	0.48(0.23) ²	0.4(0.16) ²
Neck Left - Waist Back	0.33(0.11) ²	0.4(0.16) ²	0.54(0.29) ²	0.51(0.26) ²	0.42(0.18) ²
Neck Right - Waist Back	0.33(0.11) ²	0.4(0.16) ²	0.54(0.29) ²	0.51(0.26) ²	0.43(0.18) ²
Distance Across Back Width	0.12(0.01) ²	-0.05(0) ²	0.02(0) ²	0(0) ²	-0.07(0) ²
Waist - High Hip Back	-0.5(0.25) ²	-0.37(0.13) ²	-0.61(0.37) ²	-0.48(0.23) ²	-0.53(0.28) ²
Waist - Buttock	-0.5(0.25) ²	-0.32(0.1) ²	-0.57(0.32) ²	-0.43(0.18) ²	-0.48(0.23) ²
Waistband - Buttock	-0.16(0.03) ²	0.07(0) ²	0.03(0) ²	0.11(0.01) ²	0.01(0) ²
Crotch Length	0.24(0.06) ²	0.77(0.6) ²	0.71(0.5) ²	0.78(0.6) ²	0.75(0.56) ²
Crotch Length Front	0.26(0.07) ²	0.76(0.58) ²	0.73(0.53) ²	0.79(0.62) ²	0.77(0.6) ²
Crotch Length Rear	0.19(0.04) ²	0.7(0.49) ²	0.6(0.36) ²	0.68(0.46) ²	0.63(0.4) ²
Waist - Buttock Left	-0.47(0.22) ²	-0.42(0.18) ²	-0.65(0.42) ²	-0.51(0.26) ²	-0.55(0.3) ²
Waist - Buttock Right	-0.48(0.23) ²	-0.42(0.18) ²	-0.65(0.43) ²	-0.52(0.27) ²	-0.55(0.3) ²
Waistband - Buttock Left	-0.26(0.07) ²	-0.12(0.02) ²	-0.2(0.04) ²	-0.13(0.02) ²	-0.21(0.05) ²
Waistband - Buttock Right	-0.27(0.07) ²	-0.13(0.02) ²	-0.21(0.04) ²	-0.14(0.02) ²	-0.22(0.05) ²
Torso Length	-0.37(0.14) ²	-0.22(0.05) ²	-0.36(0.13) ²	-0.27(0.07) ²	-0.29(0.09) ²

²Female data

	Buttock Girth	High Hip Girth	High Waist Girth	Hip Girth	Middle Hip
Age	0.28(0.08)	0.41(0.17)	0.45(0.21)	0.23(0.05)	0.4(0.16)
Weight	0.8(0.64)	0.82(0.67)	0.8(0.63)	0.79(0.63)	0.82(0.67)
Waist Girth	0.86(0.74)	0.98(0.96)	1(0.99)	0.84(0.71)	0.96(0.92)
Belly Circ.	0.89(0.79)	1(0.99)	0.98(0.96)	0.87(0.76)	0.98(0.96)
Bust Chest Girth	0.82(0.68)	0.88(0.77)	0.91(0.83)	0.81(0.66)	0.86(0.74)
Buttock Girth		0.9(0.8)	0.86(0.73)	0.99(0.98)	0.92(0.84)
High Hip Girth	0.92(0.85) ²		0.97(0.94)	0.88(0.77)	0.99(0.97)
High Waist Girth	0.87(0.76) ²	0.96(0.92) ²		0.83(0.7)	0.95(0.9)
Hip Girth	0.99(0.99) ²	0.9(0.81) ²	0.85(0.71) ²		0.9(0.81)
Middle Hip	0.95(0.89) ²	0.98(0.95) ²	0.95(0.89) ²	0.93(0.86) ²	
Torso Width Waist	0.77(0.59) ²	0.86(0.74) ²	0.88(0.77) ²	0.74(0.55) ²	0.84(0.71) ²
Under Bust Circ.	0.86(0.74) ²	0.93(0.86) ²	0.97(0.93) ²	0.84(0.7) ²	0.91(0.83) ²
Waistband	0.89(0.79) ²	0.98(0.95) ²	0.96(0.93) ²	0.86(0.74) ²	0.96(0.91) ²
Distance Neck - Hip	-0.14(0.02) ²	-0.13(0.02) ²	-0.25(0.06) ²	-0.12(0.01) ²	-0.18(0.03) ²
Side Upper Torso Left	-0.17(0.03) ²	-0.17(0.03) ²	-0.21(0.04) ²	-0.17(0.03) ²	-0.17(0.03) ²
Side Upper Torso Right	-0.23(0.05) ²	-0.22(0.05) ²	-0.27(0.07) ²	-0.22(0.05) ²	-0.23(0.05) ²
Cross Shoulder	0.72(0.52) ²	0.77(0.59) ²	0.8(0.64) ²	0.7(0.49) ²	0.77(0.59) ²
Across Front Width	0.62(0.39) ²	0.67(0.45) ²	0.69(0.48) ²	0.6(0.36) ²	0.67(0.45) ²
Width Armpits	0.63(0.4) ²	0.67(0.45) ²	0.69(0.47) ²	0.61(0.38) ²	0.66(0.44) ²
Across Back Width	0.59(0.34) ²	0.62(0.39) ²	0.65(0.42) ²	0.57(0.32) ²	0.62(0.38) ²
Neck - Waist Centre Back	0.42(0.18) ²	0.48(0.23) ²	0.46(0.21) ²	0.41(0.17) ²	0.49(0.24) ²
Neck Left - Waist Back	0.46(0.21) ²	0.51(0.26) ²	0.49(0.24) ²	0.44(0.19) ²	0.53(0.28) ²
Neck Right - Waist Back	0.45(0.21) ²	0.51(0.26) ²	0.49(0.24) ²	0.44(0.19) ²	0.53(0.28) ²
Distance Across Back Width	-0.03(0) ²	0(0) ²	-0.02(0) ²	-0.03(0) ²	0.01(0) ²
Waist - High Hip Back	-0.43(0.19) ²	-0.48(0.23) ²	-0.57(0.33) ²	-0.41(0.16) ²	-0.54(0.29) ²
Waist - Buttock	-0.35(0.12) ²	-0.42(0.18) ²	-0.53(0.28) ²	-0.32(0.1) ²	-0.47(0.22) ²
Waistband - Buttock	0.18(0.03) ²	0.13(0.02) ²	0.01(0) ²	0.19(0.04) ²	0.12(0.02) ²
Crotch Length	0.83(0.69) ²	0.79(0.62) ²	0.74(0.55) ²	0.82(0.68) ²	0.78(0.61) ²
Crotch Length Front	0.79(0.63) ²	0.79(0.63) ²	0.77(0.59) ²	0.78(0.6) ²	0.78(0.61) ²
Crotch Length Rear	0.78(0.61) ²	0.69(0.47) ²	0.63(0.4) ²	0.78(0.61) ²	0.7(0.48) ²
Waist - Buttock Left	-0.44(0.2) ²	-0.51(0.26) ²	-0.6(0.36) ²	-0.41(0.17) ²	-0.56(0.32) ²
Waist - Buttock Right	-0.44(0.2) ²	-0.52(0.27) ²	-0.61(0.37) ²	-0.41(0.17) ²	-0.57(0.32) ²
Waistband - Buttock Left	0.01(0) ²	-0.11(0.01) ²	-0.23(0.05) ²	0.03(0) ²	-0.09(0.01) ²
Waistband - Buttock Right	0.01(0) ²	-0.11(0.01) ²	-0.23(0.05) ²	0.03(0) ²	-0.09(0.01) ²
Torso Length	-0.26(0.07) ²	-0.27(0.07) ²	-0.36(0.13) ²	-0.24(0.06) ²	-0.32(0.1) ²

²Female data

	Torso Width Waist	Under Bust Circ.	Waistband	Distance Neck - Hip	Side Upper Torso Left
Age	0.43(0.18)	0.36(0.13)	0.38(0.15)	-0.14(0.02)	-0.11(0.01)
Weight	0.63(0.4)	0.79(0.63)	0.81(0.66)	0.04(0)	-0.16(0.02)
Waist Girth	0.84(0.7)	0.93(0.86)	0.94(0.89)	-0.03(0)	-0.19(0.04)
Belly Circ.	0.82(0.68)	0.91(0.83)	0.96(0.93)	-0.02(0)	-0.19(0.04)
Bust Chest Girth	0.67(0.45)	0.98(0.95)	0.86(0.73)	-0.02(0)	-0.24(0.06)
Buttock Girth	0.69(0.48)	0.83(0.69)	0.94(0.87)	0.04(0)	-0.16(0.03)
High Hip Girth	0.81(0.66)	0.9(0.81)	0.97(0.94)	-0.05(0)	-0.19(0.04)
High Waist Girth	0.84(0.7)	0.94(0.89)	0.93(0.87)	-0.03(0)	-0.2(0.04)
Hip Girth	0.67(0.45)	0.81(0.66)	0.92(0.84)	0.04(0)	-0.16(0.02)
Middle Hip	0.8(0.63)	0.88(0.77)	-0.98(0.96)	-0.04(0)	-0.18(0.03)
Torso Width Waist		0.75(0.56)	0.77(0.6)	0.02(0)	-0.19(0.03)
Under Bust Circ.	0.84(0.71) ²		0.88(0.77)	-0.03(0)	-0.23(0.05)
Waistband	0.86(0.74) ²	0.93(0.87) ²		-0.04(0)	-0.18(0.03)
Distance Neck - Hip	-0.17(0.03) ²	-0.25(0.06) ²	-0.22(0.05) ²		0.4(0.16)
Side Upper Torso Left	-0.21(0.04) ²	-0.23(0.05) ²	-0.2(0.04) ²	0.41(0.17) ²	
Side Upper Torso Right	-0.25(0.06) ²	-0.28(0.08) ²	-0.25(0.06) ²	0.44(0.2) ²	0.55(0.3) ²
Cross Shoulder	0.65(0.42) ²	0.8(0.64) ²	0.77(0.6) ²	-0.15(0.02) ²	-0.28(0.08) ²
Across Front Width	0.69(0.48) ²	0.69(0.48) ²	0.67(0.45) ²	-0.14(0.02) ²	-0.32(0.1) ²
Width Armpits	0.75(0.56) ²	0.7(0.49) ²	0.67(0.45) ²	-0.17(0.03) ²	-0.48(0.23) ²
Across Back Width	0.46(0.22) ²	0.66(0.43) ²	0.63(0.39) ²	-0.11(0.01) ²	-0.13(0.02) ²
Neck - Waist Centre Back	0.44(0.2) ²	0.38(0.15) ²	0.45(0.2) ²	0.37(0.14) ²	0.27(0.07) ²
Neck Left - Waist Back	0.48(0.23) ²	0.42(0.18) ²	0.48(0.23) ²	0.28(0.08) ²	0.23(0.05) ²
Neck Right - Waist Back	0.48(0.23) ²	0.42(0.18) ²	0.48(0.23) ²	0.29(0.08) ²	0.22(0.05) ²
Distance Across Back Width	0.04(0) ²	-0.07(0) ²	-0.02(0) ²	0.31(0.09) ²	0.4(0.16) ²
Waist - High Hip Back	-0.49(0.24) ²	-0.51(0.26) ²	-0.54(0.29) ²	0.63(0.39) ²	0.12(0.01) ²
Waist - Buttock	-0.46(0.21) ²	-0.47(0.22) ²	-0.49(0.24) ²	0.63(0.4) ²	0.12(0.01) ²
Waistband - Buttock	0.02(0) ²	0(0) ²	-0.02(0) ²	0.48(0.23) ²	0.2(0.04) ²
Crotch Length	0.64(0.41) ²	0.77(0.59) ²	0.79(0.62) ²	-0.1(0.01) ²	-0.26(0.07) ²
Crotch Length Front	0.68(0.46) ²	0.8(0.64) ²	0.81(0.65) ²	-0.12(0.02) ²	-0.26(0.07) ²
Crotch Length Rear	0.52(0.27) ²	0.65(0.42) ²	0.68(0.47) ²	-0.05(0) ²	-0.24(0.06) ²
Waist - Buttock Left	-0.52(0.27) ²	-0.53(0.28) ²	-0.56(0.32) ²	0.6(0.36) ²	0.1(0.01) ²
Waist - Buttock Right	-0.53(0.28) ²	-0.54(0.29) ²	-0.57(0.32) ²	0.6(0.36) ²	0.1(0.01) ²
Waistband - Buttock Left	-0.19(0.04) ²	-0.23(0.05) ²	-0.24(0.06) ²	0.46(0.21) ²	0.2(0.04) ²
Waistband - Buttock Right	-0.19(0.04) ²	-0.23(0.05) ²	-0.25(0.06) ²	0.47(0.22) ²	0.2(0.04) ²
Torso Length	-0.27(0.07) ²	-0.33(0.11) ²	-0.34(0.11) ²	0.79(0.63) ²	0.31(0.1) ²

²Female data

	Side Upper Torso		Across Front		Across Back
	Right	Cross Shoulder	Width	Width Armpits	Width
Age	-0.14(0.02)	0.27(0.07)	0.37(0.14)	0.29(0.08)	0.13(0.02)
Weight	-0.13(0.02)	0.55(0.3)	0.39(0.15)	0.48(0.23)	0.52(0.27)
Waist Girth	-0.17(0.03)	0.71(0.5)	0.57(0.33)	0.6(0.36)	0.6(0.36)
Belly Circ.	-0.17(0.03)	0.7(0.48)	0.56(0.32)	0.59(0.35)	0.58(0.34)
Bust Chest Girth	-0.22(0.05)	0.75(0.56)	0.51(0.26)	0.6(0.36)	0.71(0.51)
Buttock Girth	-0.14(0.02)	0.66(0.43)	0.51(0.26)	0.56(0.31)	0.56(0.31)
High Hip Girth	-0.18(0.03)	0.69(0.47)	0.56(0.31)	0.59(0.35)	0.58(0.33)
High Waist Girth	-0.18(0.03)	0.71(0.51)	0.58(0.33)	0.61(0.37)	0.61(0.37)
Hip Girth	-0.13(0.02)	0.65(0.42)	0.5(0.25)	0.54(0.3)	0.55(0.31)
Middle Hip	-0.17(0.03)	0.67(0.45)	0.55(0.3)	0.58(0.33)	0.56(0.31)
Torso Width Waist	-0.17(0.03)	0.5(0.25)	0.63(0.39)	0.7(0.49)	0.33(0.11)
Under Bust Circ.	-0.21(0.04)	-0.73(0.53)	0.55(0.3)	0.63(0.39)	0.68(0.46)
Waistband	-0.17(0.03)	0.67(0.45)	0.55(0.3)	0.58(0.33)	0.56(0.31)
Distance Neck - Hip	0.44(0.19)	0.05(0)	0.07(0)	0.04(0)	0.03(0)
Side Upper Torso Left	0.51(0.26)	-0.27(0.07)	-0.16(0.03)	-0.34(0.12)	-0.21(0.04)
Side Upper Torso Right		-0.25(0.06)	-0.15(0.02)	-0.32(0.1)	-0.19(0.03)
Cross Shoulder	-0.32(0.1) ²		0.73(0.54)	0.67(0.44)	0.76(0.58)
Across Front Width	-0.34(0.11) ²	0.84(0.71) ²		0.9(0.8)	0.33(0.11)
Width Armpits	-0.49(0.24) ²	0.73(0.54) ²	0.89(0.79) ²		0.37(0.14)
Across Back Width	-0.17(0.03) ²	0.76(0.58) ²	0.48(0.23) ²	0.46(0.21) ²	
Neck - Waist Centre Back	0.24(0.06) ²	0.4(0.16) ²	0.36(0.13) ²	0.24(0.06) ²	0.25(0.06) ²
Neck Left - Waist Back	0.17(0.03) ²	0.4(0.16) ²	0.38(0.14) ²	0.27(0.07) ²	0.24(0.06) ²
Neck Right - Waist Back	0.19(0.03) ²	0.4(0.16) ²	0.38(0.14) ²	0.27(0.07) ²	0.24(0.06) ²
Distance Across Back Width	0.38(0.14) ²	0.01(0) ²	0.18(0.03) ²	-0.07(0.01) ²	-0.21(0.04) ²
Waist - High Hip Back	0.17(0.03) ²	-0.46(0.21) ²	-0.4(0.16) ²	-0.32(0.1) ²	-0.32(0.1) ²
Waist - Buttock	0.17(0.03) ²	-0.42(0.17) ²	-0.36(0.13) ²	-0.28(0.08) ²	-0.28(0.08) ²
Waistband - Buttock	0.21(0.04) ²	0.03(0) ²	0(0) ²	0.02(0) ²	0.04(0) ²
Crotch Length	-0.3(0.09) ²	0.62(0.38) ²	-0.55(0.3) ²	0.59(0.35) ²	0.52(0.27) ²
Crotch Length Front	-0.3(0.09) ²	0.64(0.41) ²	0.57(0.33) ²	0.61(0.38) ²	0.53(0.28) ²
Crotch Length Rear	-0.27(0.07) ²	0.53(0.28) ²	0.46(0.22) ²	0.5(0.25) ²	0.44(0.19) ²
Waist - Buttock Left	0.15(0.02) ²	-0.46(0.21) ²	-0.4(0.16) ²	-0.33(0.11) ²	-0.33(0.11) ²
Waist - Buttock Right	0.15(0.02) ²	-0.47(0.22) ²	-0.4(0.16) ²	-0.33(0.11) ²	-0.33(0.11) ²
Waistband - Buttock Left	0.23(0.05) ²	-0.14(0.02) ²	-0.15(0.02) ²	-0.14(0.02) ²	-0.09(0.01) ²
Waistband - Buttock Right	0.23(0.05) ²	-0.15(0.02) ²	-0.16(0.02) ²	-0.14(0.02) ²	-0.1(0.01) ²
Torso Length	0.36(0.13) ²	-0.25(0.06) ²	-0.24(0.06) ²	-0.19(0.04) ²	-0.13(0.02) ²

²Female data

	Neck - Waist Centre Back	Neck Left - Waist Back	Neck Right - Waist Back	Distance Across Back Width	Waist - High Hip Back
Age	0.28(0.08)	0.29(0.08)	0.3(0.09)	0.24(0.06)	-0.44(0.19)
Weight	0.17(0.03)	0.2(0.04)	0.18(0.03)	-0.11(0.01)	-0.03(0)
Waist Girth	0.29(0.09)	0.32(0.1)	0.3(0.09)	0.01(0)	-0.28(0.08)
Belly Circ.	0.28(0.08)	0.31(0.1)	0.3(0.09)	0(0)	-0.26(0.07)
Bust Chest Girth	0.14(0.02)	0.16(0.02)	0.15(0.02)	-0.17(0.03)	-0.14(0.02)
Buttock Girth	0.28(0.08)	0.3(0.09)	0.29(0.08)	-0.03(0)	-0.18(0.03)
High Hip Girth	0.28(0.08)	0.31(0.09)	0.29(0.08)	-0.01(0)	-0.28(0.08)
High Waist Girth	0.28(0.08)	0.3(0.09)	0.29(0.08)	-0.01(0)	-0.26(0.07)
Hip Girth	0.26(0.07)	0.29(0.08)	0.27(0.07)	-0.04(0)	-0.16(0.03)
Middle Hip	0.28(0.08)	0.31(0.1)	0.3(0.09)	-0.01(0)	-0.26(0.07)
Torso Width Waist	0.27(0.07)	0.31(0.1)	0.29(0.09)	0.11(0.01)	-0.2(0.04)
Under Bust Circ.	0.18(0.03)	0.19(0.04)	0.18(0.03)	-0.11(0.01)	-0.18(0.03)
Waistband	0.28(0.08)	0.32(0.1)	0.3(0.09)	0(0)	-0.27(0.08)
Distance Neck - Hip	0.56(0.31)	0.42(0.17)	0.42(0.18)	0.31(0.09)	0.76(0.57)
Side Upper Torso Left	0.34(0.11)	0.3(0.09)	0.27(0.07)	0.42(0.17)	0.23(0.05)
Side Upper Torso Right	0.34(0.12)	0.25(0.06)	0.32(0.1)	0.4(0.16)	0.27(0.07)
Cross Shoulder	0.25(0.06)	0.22(0.05)	0.22(0.05)	0.04(0)	-0.17(0.03)
Across Front Width	0.33(0.11)	0.33(0.11)	0.33(0.11)	0.41(0.17)	-0.2(0.04)
Width Armpits	0.19(0.04)	0.21(0.04)	0.2(0.04)	0.17(0.03)	-0.12(0.01)
Across Back Width	0.07(0.01)	0.04(0)	0.03(0)	-0.26(0.07)	-0.05(0)
Neck - Waist Centre Back		0.91(0.83)	0.9(0.81)	0.6(0.36)	-0.04(0)
Neck Left - Waist Back	0.92(0.84) ²		0.87(0.76)	0.55(0.3)	-0.13(0.02)
Neck Right - Waist Back	0.93(0.86) ²	0.9(0.81) ²		0.56(0.31)	-0.12(0.02)
Distance Across Back Width	0.52(0.27) ²	0.48(0.23) ²	0.49(0.24) ²		-0.08(0.01)
Waist - High Hip Back	-0.41(0.17) ²	-0.44(0.19) ²	-0.46(0.21) ²	-0.13(0.02) ²	
Waist - Buttock	-0.38(0.15) ²	-0.41(0.17) ²	-0.42(0.17) ²	-0.14(0.02) ²	0.97(0.94) ²
Waistband - Buttock	0.21(0.04) ²	0.18(0.03) ²	0.19(0.04) ²	0.1(0.01) ²	0.29(0.08) ²
Crotch Length	0.15(0.02) ²	0.2(0.04) ²	0.19(0.04) ²	-0.18(0.03) ²	-0.13(0.02) ²
Crotch Length Front	0.16(0.02) ²	0.2(0.04) ²	0.2(0.04) ²	-0.17(0.03) ²	-0.17(0.03) ²
Crotch Length Rear	0.13(0.02) ²	0.17(0.03) ²	0.16(0.03) ²	-0.17(0.03) ²	-0.07(0) ²
Waist - Buttock Left	-0.44(0.19) ²	-0.46(0.21) ²	-0.47(0.22) ²	-0.14(0.02) ²	0.97(0.94) ²
Waist - Buttock Right	-0.44(0.2) ²	-0.47(0.22) ²	-0.47(0.22) ²	-0.14(0.02) ²	0.97(0.94) ²
Waistband - Buttock Left	0.09(0.01) ²	0.06(0) ²	0.07(0) ²	0.09(0.01) ²	0.36(0.13) ²
Waistband - Buttock Right	0.09(0.01) ²	0.05(0) ²	0.07(0) ²	0.09(0.01) ²	0.37(0.13) ²
Torso Length	0(0) ²	-0.12(0.01) ²	-0.12(0.01) ²	0.07(0) ²	0.68(0.46) ²

²Female data

	Waist - Buttock	Waistband - Buttock	Crotch Length	Length Front	Crotch Length Rear
Age	-0.42(0.18)	-0.12(0.01)	0.23(0.05)	0.25(0.06)	0.19(0.04)
Weight	-0.03(0)	-0.07(0.01)	0.72(0.51)	0.68(0.47)	0.67(0.44)
Waist Girth	-0.23(0.05)	-0.1(0.01)	0.77(0.59)	0.76(0.58)	0.68(0.46)
Belly Circ.	-0.21(0.04)	-0.1(0.01)	0.79(0.63)	0.78(0.61)	0.71(0.5)
Bust Chest Girth	-0.11(0.01)	-0.09(0.01)	0.75(0.56)	0.73(0.54)	0.67(0.44)
Buttock Girth	-0.11(0.01)	0.06(0)	0.78(0.6)	0.73(0.53)	0.73(0.54)
High Hip Girth	-0.22(0.05)	-0.11(0.01)	0.8(0.64)	0.78(0.61)	0.72(0.52)
High Waist Girth	-0.22(0.05)	-0.11(0.01)	0.77(0.59)	0.77(0.59)	0.68(0.46)
Hip Girth	-0.09(0.01)	0.06(0)	0.77(0.6)	0.72(0.52)	0.74(0.54)
Middle Hip	-0.2(0.04)	-0.04(0)	0.81(0.65)	0.79(0.62)	0.73(0.53)
Torso Width Waist	-0.17(0.03)	-0.09(0.01)	0.65(0.42)	0.68(0.46)	0.52(0.27)
Under Bust Circ.	-0.15(0.02)	-0.11(0.01)	0.75(0.56)	0.75(0.56)	0.66(0.44)
Waistband	-0.22(0.05)	-0.05(0)	0.78(0.61)	0.76(0.57)	0.71(0.51)
Distance Neck - Hip	0.76(0.58)	0.39(0.16)	0.1(0.01)	0.09(0.01)	0.1(0.01)
Side Upper Torso Left	0.23(0.05)	0.16(0.02)	-0.15(0.02)	-0.16(0.02)	-0.12(0.01)
Side Upper Torso Right	0.27(0.08)	0.17(0.03)	-0.13(0.02)	-0.14(0.02)	-0.1(0.01)
Cross Shoulder	-0.12(0.01)	-0.04(0)	0.56(0.32)	0.56(0.31)	0.5(0.25)
Across Front Width	-0.16(0.03)	-0.06(0)	0.45(0.2)	0.45(0.21)	0.39(0.15)
Width Armpits	-0.09(0.01)	-0.05(0)	0.51(0.26)	0.52(0.27)	0.43(0.19)
Across Back Width	-0.02(0)	-0.01(0)	0.49(0.24)	0.47(0.22)	0.44(0.2)
Neck - Waist Centre Back	-0.01(0)	0.13(0.02)	0.15(0.02)	0.14(0.02)	0.14(0.02)
Neck Left - Waist Back	-0.1(0.01)	0.09(0.01)	0.17(0.03)	0.16(0.03)	0.15(0.02)
Neck Right - Waist Back	-0.1(0.01)	0.1(0.01)	0.16(0.03)	0.15(0.02)	0.15(0.02)
Distance Across Back Width	-0.08(0.01)	0.02(0)	-0.08(0.01)	-0.07(0)	-0.07(0.01)
Waist - High Hip Back	0.97(0.93)	0.39(0.15)	0.01(0)	0(0)	0.01(0)
Waist - Buttock		0.44(0.19)	0.07(0.01)	0.06(0)	0.09(0.01)
Waistband - Buttock	0.34(0.11) ²		-0.19(0.04)	-0.2(0.04)	-0.16(0.02)
Crotch Length	-0.05(0) ²	-0.02(0) ²		0.96(0.91)	0.93(0.86)
Crotch Length Front	-0.11(0.01) ²	-0.06(0) ²	0.95(0.91) ²		0.78(0.61)
Crotch Length Rear	0.03(0) ²	0.03(0) ²	0.94(0.88) ²	0.79(0.63) ²	
Waist - Buttock Left	0.95(0.91) ²	0.26(0.07) ²	-0.14(0.02) ²	-0.18(0.03) ²	-0.07(0.01) ²
Waist - Buttock Right	0.05(0) ²	0.27(0.07) ²	-0.14(0.02) ²	-0.19(0.03) ²	-0.08(0.01) ²
Waistband - Buttock Left	0.39(0.15) ²	0.85(0.72) ²	-0.19(0.04) ²	-0.23(0.05) ²	-0.13(0.02) ²
Waistband - Buttock Right	0.4(0.16) ²	0.85(0.72) ²	-0.19(0.04) ²	-0.23(0.05) ²	-0.13(0.02) ²
Torso Length	0.67(0.45) ²	0.37(0.14) ²	-0.16(0.03) ²	-0.18(0.03) ²	-0.13(0.02) ²

²Female data

	Buttock Left	Waist - Buttock Right	Waistband - Buttock Left	Waistband - Buttock Right	Torso Length
Age	-0.41(0.17)	-0.42(0.18)	-0.25(0.06)	-0.25(0.06)	-0.25(0.06)
Weight	-0.09(0.01)	-0.1(0.01)	-0.31(0.09)	-0.3(0.09)	-0.02(0)
Waist Girth	-0.28(0.08)	-0.3(0.09)	-0.41(0.17)	-0.41(0.16)	-0.16(0.03)
Belly Circ.	-0.26(0.07)	-0.28(0.08)	-0.41(0.17)	-0.41(0.17)	-0.15(0.02)
Bust Chest Girth	-0.13(0.02)	-0.15(0.02)	-0.33(0.11)	-0.32(0.1)	-0.04(0)
Buttock Girth	-0.17(0.03)	-0.18(0.03)	-0.17(0.03)	-0.17(0.03)	-0.1(0.01)
High Hip Girth	-0.28(0.08)	-0.3(0.09)	-0.42(0.17)	-0.41(0.17)	-0.17(0.03)
High Waist Girth	-0.26(0.07)	-0.29(0.08)	-0.41(0.16)	-0.4(0.16)	-0.15(0.02)
Hip Girth	-0.15(0.02)	-0.16(0.03)	-0.16(0.03)	-0.16(0.03)	-0.09(0.01)
Middle Hip	-0.27(0.07)	-0.29(0.08)	-0.36(0.13)	-0.35(0.12)	-0.17(0.03)
Torso Width Waist	-0.2(0.04)	-0.21(0.04)	-0.36(0.13)	-0.36(0.13)	-0.1(0.01)
Under Bust Circ.	-0.17(0.03)	-0.19(0.04)	-0.36(0.13)	-0.35(0.12)	-0.07(0)
Waistband	-0.27(0.07)	-0.29(0.08)	-0.33(0.11)	-0.32(0.1)	-0.17(0.03)
Distance Neck - Hip	0.78(0.6)	0.77(0.59)	0.37(0.14)	0.37(0.14)	0.75(0.56)
Side Upper Torso Left	0.24(0.06)	0.24(0.06)	0.21(0.04)	0.21(0.04)	0.23(0.05)
Side Upper Torso Right	0.27(0.07)	0.27(0.07)	0.21(0.04)	0.21(0.04)	0.25(0.06)
Cross Shoulder	-0.14(0.02)	-0.15(0.02)	-0.23(0.05)	-0.22(0.05)	-0.06(0)
Across Front Width	-0.18(0.03)	-0.18(0.03)	-0.21(0.04)	-0.21(0.05)	-0.08(0.01)
Width Armpits	-0.1(0.01)	-0.11(0.01)	-0.22(0.05)	-0.22(0.05)	-0.02(0)
Across Back Width	-0.03(0)	-0.05(0)	-0.17(0.03)	-0.17(0.03)	0.02(0)
Neck - Waist Centre Back	-0.02(0)	-0.03(0)	0.04(0)	0.04(0)	0.04(0)
Neck Left - Waist Back	-0.11(0.01)	-0.12(0.01)	0(0)	-0.01(0)	-0.11(0.01)
Neck Right - Waist Back	-0.1(0.01)	-0.12(0.01)	0(0)	0.01(0)	-0.1(0.01)
Distance Across Back Width	-0.06(0)	-0.07(0)	0.03(0)	0.03(0)	-0.02(0)
Waist - High Hip Back	0.98(0.96)	0.98(0.96)	0.43(0.19)	0.43(0.18)	0.82(0.67)
Waist - Buttock	0.96(0.93)	0.96(0.92)	0.44(0.19)	0.43(0.19)	0.8(0.65)
Waistband - Buttock	0.4(0.16)	0.4(0.16)	0.87(0.75)	0.86(0.74)	0.33(0.11)
Crotch Length	0.01(0)	-0.01(0)	-0.45(0.2)	-0.45(0.2)	0.03(0)
Crotch Length Front	0(0)	-0.01(0)	-0.47(0.22)	-0.46(0.21)	0.03(0)
Crotch Length Rear	0.01(0)	0(0)	-0.37(0.14)	-0.37(0.13)	0.02(0)
Waist - Buttock Left		0.99(0.99)	0.45(0.2)	0.44(0.2)	0.83(0.69)
Waist - Buttock Right	0.99(0.98) ²		0.46(0.21)	0.45(0.2)	0.83(0.69)
Waistband - Buttock Left	0.37(0.14) ²	0.37(0.13) ²		0.99(0.97)	0.36(0.13)
Waistband - Buttock Right	0.37(0.14) ²	0.38(0.14) ²	0.99(0.98) ²		0.35(0.12)
Torso Length	0.66(0.44) ²	0.66(0.44) ²	0.4(0.16) ²	0.4(0.16) ²	

²Female data

A.4.5 Pearson correlation and effect size - size and shape male participants.

Size measure	Shape principal components								
	PC1	PC2	PC3	PC4	PC5	PC6	PC7	PC8	PC9
Age	0.28(0.08)	-0.23(0.05)	-0.34(0.11)	0.06(0)	-0.1(0.01)	-0.07(0.01)	-0.33(0.11)	-0.08(0.01)	-0.06(0)
Weight	0.39(0.15)	-0.14(0.02)	-0.6(0.36)	-0.01(0.0)	-0.22(0.05)	-0.1(0.01)	-0.17(0.03)	-0.1(0.01)	0.04(0.0)
Waist Girth	0.53(0.28)	-0.3(0.09)	-0.74(0.55)	0.02(0.0)	-0.33(0.11)	-0.07(0.01)	-0.38(0.14)	-0.15(0.02)	0.02(0.0)
Belly Circ.	0.5(0.25)	-0.25(0.06)	-0.77(0.59)	0.02(0.0)	-0.38(0.14)	-0.08(0.01)	-0.38(0.14)	-0.17(0.03)	0.02(0.0)
Bust Chest Girth	0.45(0.2)	-0.32(0.1)	-0.54(0.29)	0.01(0.0)	-0.05(0.0)	-0.15(0.02)	-0.26(0.07)	-0.11(0.01)	0.11(0.01)
Buttock Girth	0.36(0.13)	-0.04(0.0)	-0.65(0.43)	0.02(0.0)	-0.26(0.07)	-0.16(0.03)	-0.07(0.01)	-0.18(0.03)	-0.09(0.01)
High Hip Girth	0.49(0.24)	-0.23(0.05)	-0.78(0.61)	0.02(0.0)	-0.38(0.14)	-0.1(0.01)	-0.36(0.13)	-0.19(0.03)	0.03(0.0)
High Waist Girth	0.54(0.29)	-0.31(0.1)	-0.71(0.51)	0.02(0.0)	-0.28(0.08)	-0.07(0.0)	-0.36(0.13)	-0.15(0.02)	0.02(0.0)
Hip Girth	0.33(0.11)	-0.03(0.0)	-0.63(0.4)	0.01(0.0)	-0.26(0.07)	-0.16(0.03)	-0.05(0.0)	-0.19(0.04)	-0.09(0.01)
Middle Hip	0.45(0.2)	-0.19(0.04)	-0.8(0.65)	0.01(0.0)	-0.38(0.14)	-0.1(0.01)	-0.29(0.08)	-0.2(0.04)	0.04(0.0)
Torso Width Waist	0.58(0.34)	-0.16(0.03)	-0.63(0.4)	0.01(0.0)	-0.36(0.13)	0.06(0.0)	-0.3(0.09)	-0.11(0.01)	0.06(0.0)
Under Bust Circ.	0.5(0.25)	-0.33(0.11)	-0.56(0.31)	0.02(0.0)	-0.06(0.0)	-0.12(0.02)	-0.29(0.09)	-0.12(0.01)	0.1(0.01)
Waistband	0.45(0.21)	-0.14(0.02)	-0.75(0.56)	0.02(0.0)	-0.34(0.12)	-0.17(0.03)	-0.27(0.07)	-0.21(0.05)	-0.03(0.0)
Distance Neck - Hip	-0.04(0.0)	0.03(0.0)	0.04(0.0)	-0.04(0.0)	-0.07(0.01)	0.23(0.05)	0.06(0.0)	0.17(0.03)	-0.09(0.01)
Side Upper Torso Length Left	-0.18(0.03)	0.02(0.0)	0.1(0.01)	-0.01(0.0)	0.02(0.0)	0.06(0.0)	0.02(0.0)	0.07(0.0)	-0.13(0.02)
Side Upper Torso Length Right	-0.17(0.03)	0.01(0.0)	0.1(0.01)	-0.04(0.0)	0.01(0.0)	0.1(0.01)	0.02(0.0)	0.09(0.01)	-0.12(0.01)
Cross Shoulder	0.37(0.13)	-0.19(0.04)	-0.41(0.16)	0.02(0.0)	-0.13(0.02)	-0.12(0.01)	-0.2(0.04)	-0.11(0.01)	0.05(0.0)
Across Front Width	0.25(0.06)	-0.21(0.04)	-0.38(0.14)	0.02(0.0)	-0.11(0.01)	-0.1(0.01)	-0.23(0.05)	-0.12(0.01)	-0.06(0.0)
Width Armpits	0.26(0.07)	-0.24(0.06)	-0.38(0.15)	0.0(0.0)	-0.03(0.0)	-0.08(0.01)	-0.2(0.04)	-0.09(0.01)	0.02(0.0)
Across Back Width	0.37(0.13)	-0.15(0.02)	-0.28(0.08)	0.0(0.0)	-0.06(0.0)	-0.07(0.01)	-0.12(0.02)	-0.06(0.0)	0.14(0.02)
Neck - Waist Centre Back	0.06(0.0)	-0.07(0.01)	-0.21(0.04)	0.02(0.0)	-0.24(0.06)	-0.14(0.02)	-0.16(0.02)	-0.03(0.0)	-0.11(0.01)
Neck Left - Waist Back	0.05(0.0)	-0.09(0.01)	-0.25(0.06)	0.04(0.0)	-0.27(0.07)	-0.19(0.04)	-0.14(0.02)	-0.08(0.01)	-0.11(0.01)
Neck Right - Waist Back	0.03(0.0)	-0.1(0.01)	-0.23(0.05)	0.02(0.0)	-0.25(0.06)	-0.19(0.04)	-0.14(0.02)	-0.06(0.0)	-0.12(0.01)
Distance Across Back Width	-0.06(0.0)	-0.02(0.0)	-0.04(0.0)	0.02(0.0)	-0.12(0.01)	-0.08(0.01)	-0.14(0.02)	-0.02(0.0)	-0.2(0.04)
Waist - High Hip Back	-0.13(0.02)	0.08(0.01)	0.22(0.05)	-0.07(0.0)	0.08(0.01)	0.32(0.1)	0.23(0.05)	0.19(0.04)	0.04(0.0)
Waist - Buttock	-0.22(0.05)	0.0(0.0)	0.12(0.01)	-0.08(0.01)	0.05(0.0)	0.37(0.14)	0.27(0.07)	0.21(0.04)	0.1(0.01)
Waistband - Buttock	-0.26(0.07)	0.02(0.0)	-0.02(0.0)	-0.04(0.0)	0.0(0.0)	0.19(0.03)	0.31(0.1)	0.11(0.01)	-0.02(0.0)
Crotch Length	0.35(0.12)	-0.18(0.03)	-0.69(0.48)	0.0(0.0)	-0.26(0.07)	0.01(0.0)	-0.08(0.01)	-0.13(0.02)	0.11(0.01)
Crotch Length Front	0.41(0.17)	-0.17(0.03)	-0.67(0.45)	-0.01(0.0)	-0.28(0.08)	0.03(0.0)	-0.09(0.01)	-0.15(0.02)	0.18(0.03)
Crotch Length Rear	0.23(0.05)	-0.18(0.03)	-0.63(0.39)	0.01(0.0)	-0.2(0.04)	-0.01(0.0)	-0.05(0.0)	-0.09(0.01)	0.02(0.0)

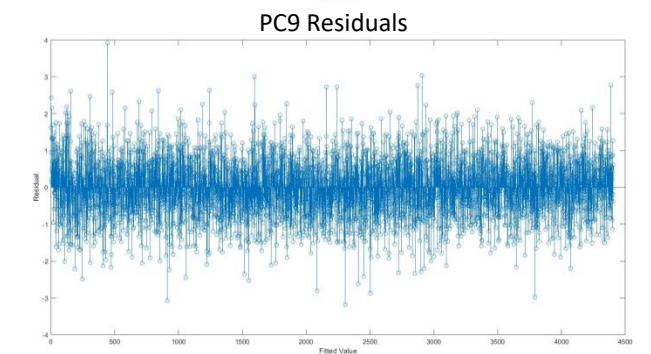
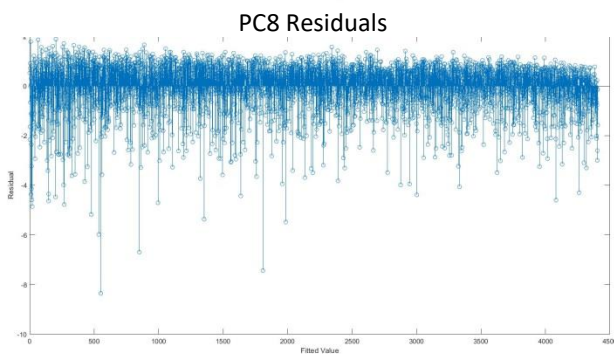
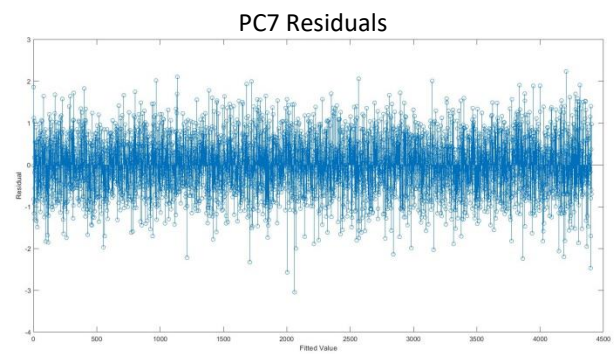
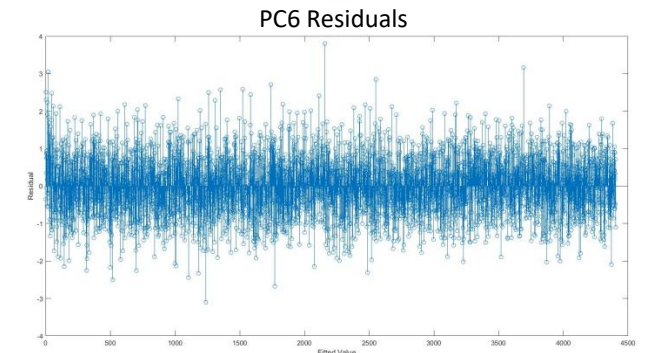
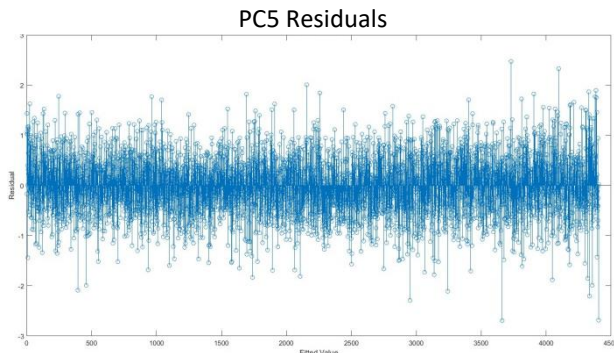
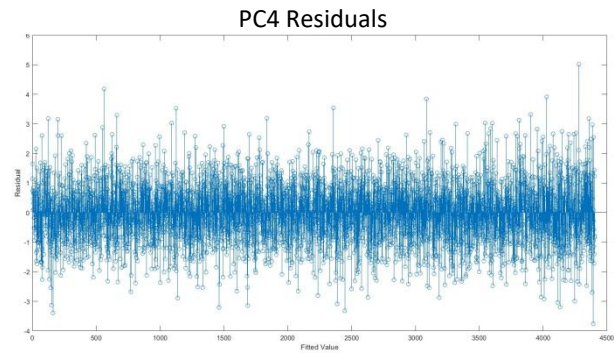
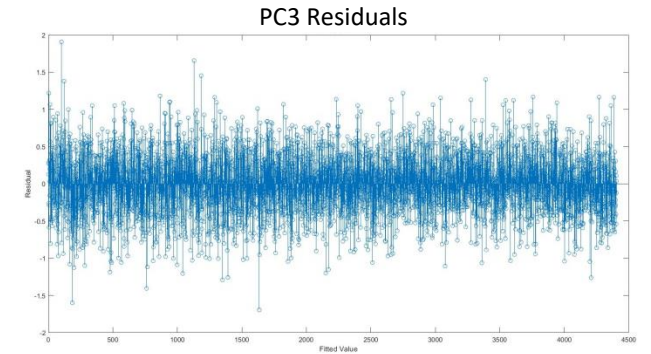
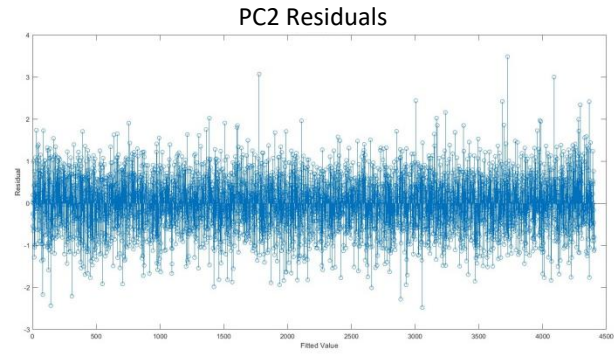
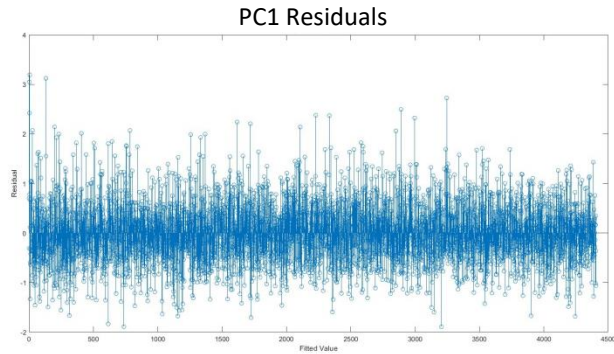
Waist - Buttock Height Left	-0.13(0.02)	0.1(0.01)	0.24(0.06)	-0.05(0.0)	0.09(0.01)	0.3(0.09)	0.24(0.06)	0.2(0.04)	0.04(0.0)
Waist - Buttock Height Right	-0.14(0.02)	0.11(0.01)	0.26(0.07)	-0.08(0.01)	0.1(0.01)	0.3(0.09)	0.25(0.06)	0.19(0.04)	0.03(0.0)
Waistband - Buttock Height Left	-0.34(0.11)	0.22(0.05)	0.34(0.12)	-0.03(0.0)	0.19(0.04)	0.05(0.0)	0.41(0.17)	0.1(0.01)	-0.18(0.03)
Waistband - Buttock Height Right	-0.34(0.11)	0.22(0.05)	0.34(0.12)	-0.04(0.0)	0.2(0.04)	0.05(0.0)	0.42(0.18)	0.09(0.01)	-0.18(0.03)
Torso Length	-0.03(0.0)	0.05(0.0)	0.2(0.04)	-0.05(0.0)	0.12(0.01)	0.3(0.09)	0.11(0.01)	0.22(0.05)	0.05(0.0)

A.4.6 Pearson correlation and effect size - size and shape female participants.

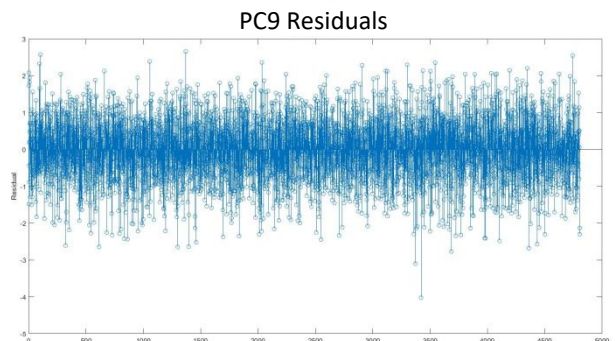
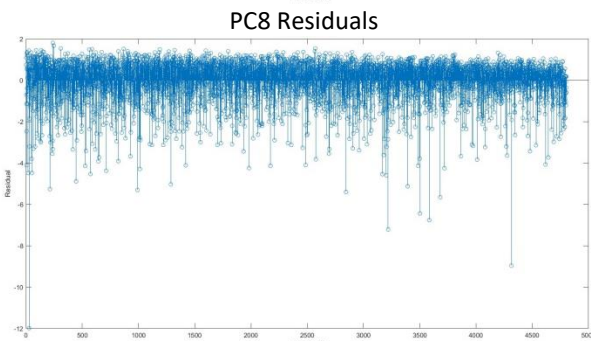
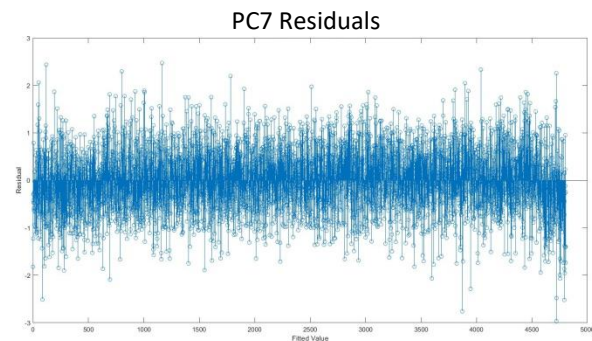
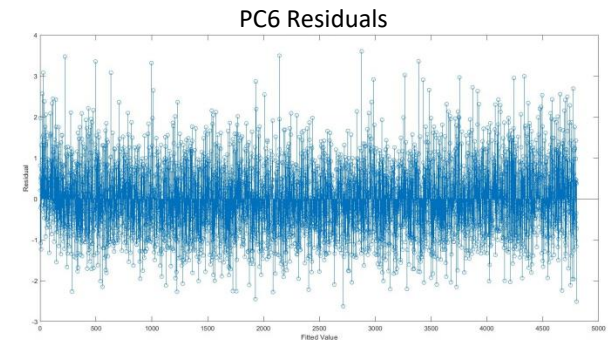
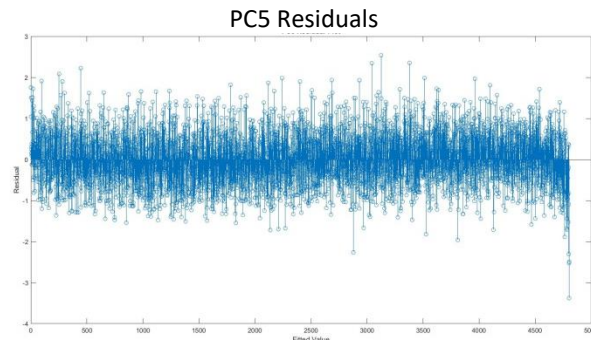
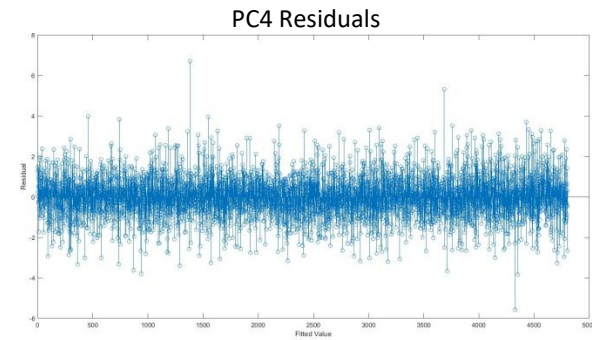
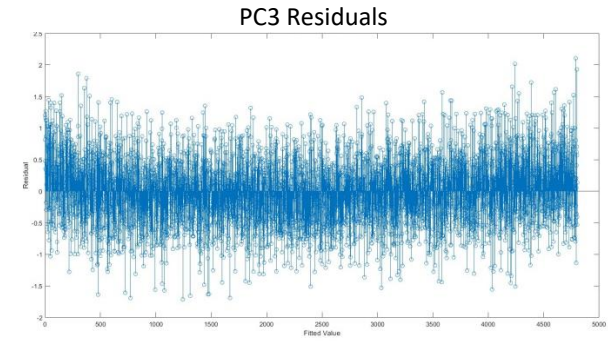
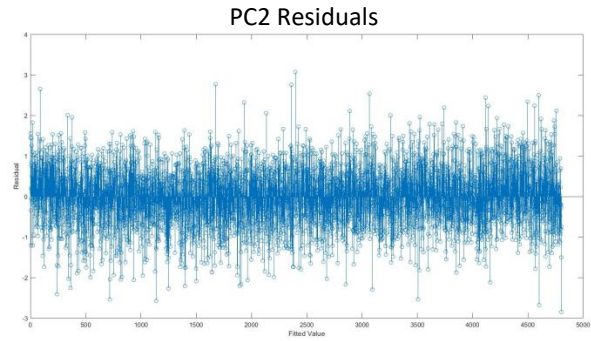
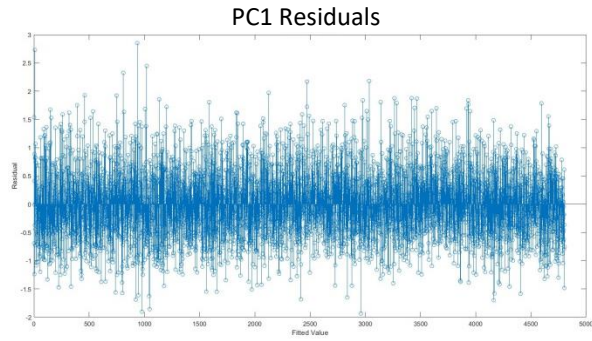
Size measures	Shape principal components								
	PC1	PC2	PC3	PC4	PC5	PC6	PC7	PC8	PC9
Age	0.27(0.07)	-0.18(0.03)	-0.31(0.1)	-0.02(0.0)	0.26(0.07)	-0.35(0.13)	-0.06(0.0)	0.01(0.0)	-0.15(0.02)
Weight	0.44(0.19)	-0.08(0.01)	-0.61(0.38)	-0.11(0.01)	0.22(0.05)	-0.15(0.02)	0.29(0.08)	0.07(0.01)	-0.13(0.02)
Waist Girth	0.56(0.32)	-0.24(0.06)	-0.65(0.43)	-0.12(0.01)	0.31(0.1)	-0.28(0.08)	0.11(0.01)	0.05(0.0)	-0.17(0.03)
Belly Circ.	0.51(0.26)	-0.21(0.04)	-0.68(0.47)	-0.12(0.01)	0.22(0.05)	-0.25(0.06)	0.13(0.02)	0.05(0.0)	-0.18(0.03)
Bust Chest Girth	0.57(0.32)	-0.27(0.07)	-0.56(0.31)	-0.12(0.02)	0.44(0.19)	-0.26(0.07)	0.17(0.03)	0.04(0.0)	-0.07(0.01)
Buttock Girth	0.39(0.15)	-0.04(0.0)	-0.65(0.43)	-0.11(0.01)	0.24(0.06)	-0.17(0.03)	0.34(0.11)	0.06(0.0)	-0.24(0.06)
High Hip Girth	0.49(0.24)	-0.19(0.03)	-0.7(0.49)	-0.12(0.01)	0.22(0.05)	-0.25(0.06)	0.14(0.02)	0.05(0.0)	-0.17(0.03)
High Waist Girth	0.59(0.34)	-0.25(0.06)	-0.63(0.4)	-0.11(0.01)	0.33(0.11)	-0.26(0.07)	0.17(0.03)	0.04(0.0)	-0.17(0.03)
Hip Girth	0.36(0.13)	-0.02(0.0)	-0.63(0.4)	-0.1(0.01)	0.22(0.05)	-0.15(0.02)	0.35(0.12)	0.05(0.0)	-0.24(0.06)
Middle Hip	0.46(0.22)	-0.15(0.02)	-0.72(0.52)	-0.11(0.01)	0.27(0.07)	-0.25(0.06)	0.19(0.04)	0.05(0.0)	-0.17(0.03)
Torso Width Waist	0.59(0.35)	-0.14(0.02)	-0.57(0.33)	-0.11(0.01)	0.2(0.04)	-0.2(0.04)	0.12(0.01)	0.07(0.01)	-0.08(0.01)
Under Bust Circ.	0.57(0.32)	-0.27(0.07)	-0.56(0.32)	-0.11(0.01)	0.35(0.12)	-0.23(0.05)	0.24(0.06)	0.0(0.0)	-0.13(0.02)
Waistband	0.56(0.31)	-0.18(0.03)	-0.66(0.44)	-0.12(0.01)	0.26(0.07)	-0.29(0.08)	0.13(0.02)	0.05(0.0)	-0.17(0.03)
Distance Neck - Hip	-0.33(0.11)	0.03(0.0)	0.1(0.01)	0.01(0.0)	-0.41(0.17)	0.16(0.03)	-0.11(0.01)	0.04(0.0)	0.12(0.01)
Side Upper Torso Length Left	-0.21(0.04)	-0.01(0.0)	0.09(0.01)	0.03(0.0)	-0.13(0.02)	0.12(0.01)	-0.14(0.02)	-0.01(0.0)	0.08(0.01)
Side Upper Torso Length Right	-0.24(0.06)	0.0(0.0)	0.12(0.01)	0.01(0.0)	-0.14(0.02)	0.15(0.02)	-0.16(0.02)	0.0(0.0)	0.09(0.01)
Cross Shoulder	0.49(0.24)	-0.18(0.03)	-0.42(0.17)	-0.1(0.01)	0.32(0.1)	-0.24(0.06)	0.14(0.02)	0.0(0.0)	-0.07(0.01)
Across Front Width	0.38(0.14)	-0.2(0.04)	-0.39(0.16)	-0.09(0.01)	0.3(0.09)	-0.23(0.05)	0.11(0.01)	-0.02(0.0)	-0.14(0.02)
Width Armpits	0.38(0.15)	-0.2(0.04)	-0.42(0.17)	-0.11(0.01)	0.29(0.08)	-0.18(0.03)	0.15(0.02)	0.0(0.0)	-0.1(0.01)

Across Back Width	0.43(0.19)	-0.11(0.01)	-0.3(0.09)	-0.09(0.01)	0.25(0.06)	-0.14(0.02)	0.13(0.02)	0.02(0.0)	0.0(0.0)
Neck - Waist Centre Back	0.17(0.03)	-0.12(0.01)	-0.31(0.1)	-0.05(0.0)	0.1(0.01)	-0.23(0.05)	-0.1(0.01)	0.01(0.0)	0.0(0.0)
Neck Left - Waist Back	0.17(0.03)	-0.15(0.02)	-0.34(0.12)	-0.04(0.0)	0.09(0.01)	-0.27(0.08)	-0.07(0.0)	0.0(0.0)	-0.06(0.0)
Neck Right - Waist Back	0.16(0.03)	-0.16(0.03)	-0.34(0.12)	-0.06(0.0)	0.09(0.01)	-0.28(0.08)	-0.08(0.01)	0.0(0.0)	-0.06(0.0)
Distance Across Back Width	-0.1(0.01)	-0.03(0.0)	-0.02(0.0)	0.02(0.0)	-0.05(0.0)	-0.11(0.01)	-0.16(0.03)	-0.04(0.0)	-0.04(0.0)
Waist - High Hip Back	-0.48(0.23)	0.1(0.01)	0.29(0.08)	0.06(0.0)	-0.56(0.31)	0.28(0.08)	0.04(0.0)	0.0(0.0)	0.12(0.02)
Waist - Buttock	-0.53(0.28)	0.06(0.0)	0.19(0.04)	0.05(0.0)	-0.52(0.27)	0.32(0.1)	0.12(0.01)	0.01(0.0)	0.15(0.02)
Waistband - Buttock	-0.32(0.1)	-0.1(0.01)	-0.17(0.03)	-0.03(0.0)	-0.22(0.05)	0.14(0.02)	-0.03(0.0)	0.02(0.0)	-0.04(0.0)
Crotch Length	0.33(0.11)	-0.08(0.01)	-0.65(0.42)	-0.08(0.01)	0.12(0.02)	-0.15(0.02)	0.49(0.24)	0.03(0.0)	-0.14(0.02)
Crotch Length Front	0.43(0.18)	-0.08(0.01)	-0.62(0.38)	-0.09(0.01)	0.14(0.02)	-0.17(0.03)	0.45(0.2)	-0.01(0.0)	-0.08(0.01)
Crotch Length Rear	0.18(0.03)	-0.06(0.0)	-0.6(0.36)	-0.07(0.01)	0.09(0.01)	-0.11(0.01)	0.48(0.23)	0.07(0.0)	-0.19(0.03)
Waist - Buttock Height Left	-0.47(0.22)	0.16(0.03)	0.34(0.12)	0.08(0.01)	-0.54(0.29)	0.26(0.07)	0.06(0.0)	0.0(0.0)	0.12(0.01)
Waist - Buttock Height Right	-0.47(0.22)	0.16(0.03)	0.35(0.12)	0.05(0.0)	-0.54(0.29)	0.27(0.07)	0.07(0.0)	0.0(0.0)	0.11(0.01)
Waistband - Buttock Height Left	-0.38(0.14)	0.13(0.02)	0.08(0.01)	0.02(0.0)	-0.26(0.07)	0.14(0.02)	-0.05(0.0)	-0.01(0.0)	0.0(0.0)
Waistband - Buttock Height Right	-0.38(0.14)	0.13(0.02)	0.08(0.01)	0.01(0.0)	-0.27(0.07)	0.15(0.02)	-0.04(0.0)	-0.01(0.0)	0.0(0.0)
Torso Length	-0.26(0.07)	0.1(0.01)	0.23(0.05)	0.0(0.0)	-0.25(0.06)	0.32(0.1)	-0.1(0.01)	0.07(0.0)	0.24(0.06)

A.4.7 Allometric Model - Residual vs Fitted Male Shape Variation Plots PC's 1-9.



A.4.8 Allometric Model - Residual vs Fitted Female Shape Variation Plots PC's 1-9.



Appendix 5

A.5.1 Pearson correlation coefficients and effect sizes male participants.

		WC	WHR	BMI
Existing indices	WHR	0.79(0.63)*		
	BMI	0.91(0.83)*	0.62(0.39)*	
Shape parameters	PC1	0.52(0.27)*	0.54(0.29)*	0.42(0.18)*
	PC2	-0.26(0.07)*	-0.39(0.15)*	-0.18(0.03)*
	PC3	-0.74(0.54)*	-0.65(0.43)*	-0.65(0.42)*
	PC4	0.02(0.00)	0.03(0.00)	0.00(0.00)
	PC5	-0.34(0.11)*	-0.35(0.12)*	-0.23(0.05)*
	PC6	-0.06(0.00)*	0.02(0.00)	-0.10(0.01)*
	PC7	-0.38(0.14)*	-0.53(0.28)*	-0.19(0.03)*
	PC8	-0.14(0.02)*	-0.12(0.01)*	-0.12(0.01)*
	PC9	0.01(0.00)	0.14(0.02)*	0.04(0.00)*

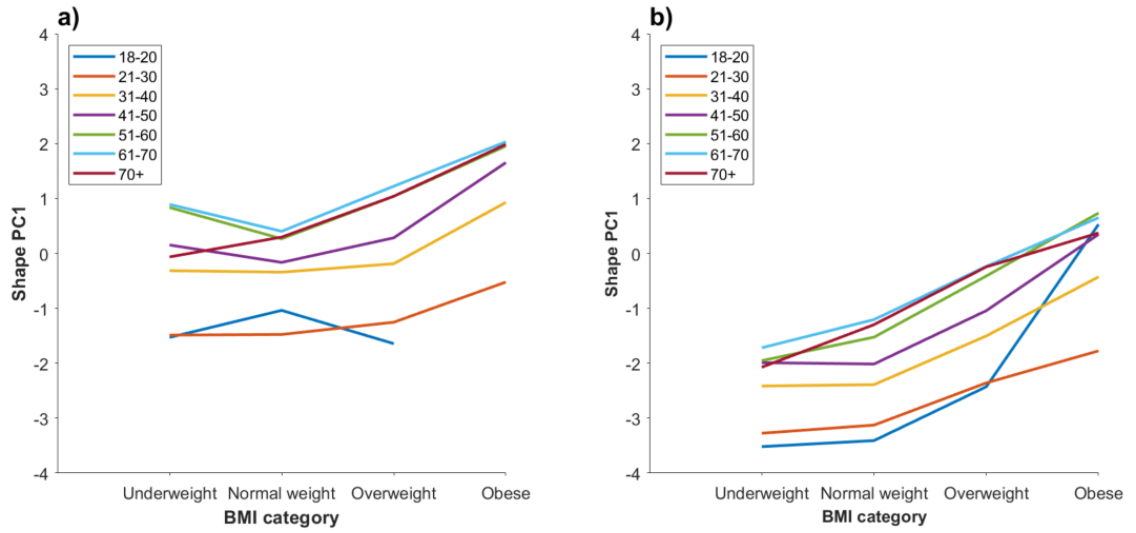
(*P < 0.05; BMI, Body-mass-index; WC, waist girth; WHR, waist-hip ratio)

A.5.2 Pearson correlation coefficients and effect sizes female participants.

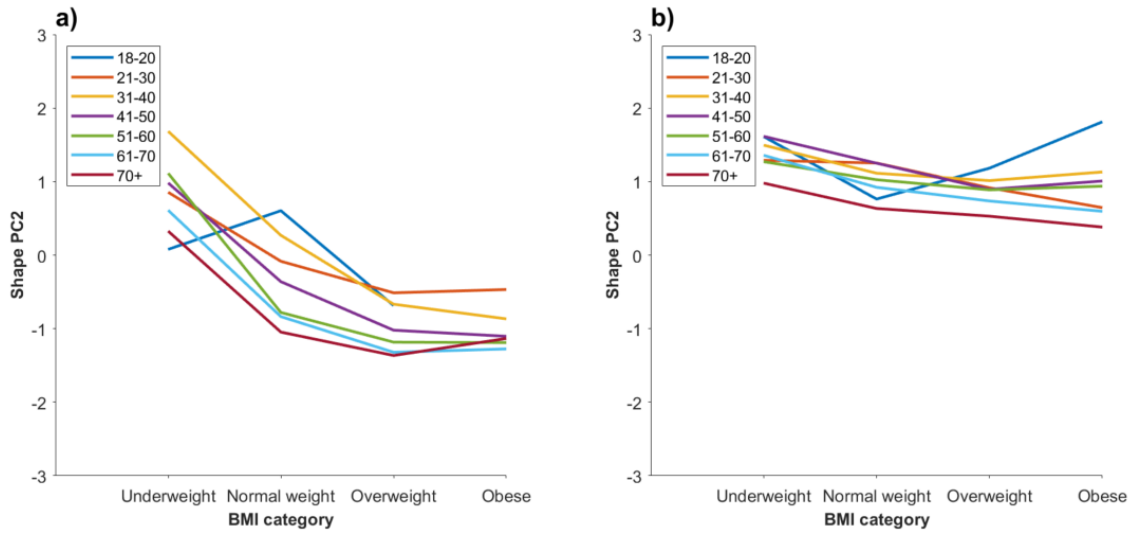
		WC	WHR	BMI
Existing indices	WHR	0.63(0.40)*		
	BMI	0.91(0.83)*	0.44(0.19)*	
Shape parameters	PC1	0.57(0.32)*	0.55(0.30)*	0.46(0.21)*
	PC2	-0.21(0.05)*	-0.34(0.11)*	-0.14(0.02)*
	PC3	-0.65(0.43)*	-0.34(0.12)*	-0.65(0.42)*
	PC4	-0.12(0.01)*	-0.07(0.00)*	-0.11(0.01)*
	PC5	0.29(0.08)*	0.21(0.04)*	0.26(0.07)*
	PC6	-0.25(0.06)*	-0.27(0.07)*	-0.17(0.03)*
	PC7	0.13(0.02)*	-0.15(0.02)*	0.32(0.10)*
	PC8	0.05(0.00)*	0.02(0.00)	0.05(0.00)*
	PC9	-0.2(0.04)*	0.01(0.00)	-0.16(0.02)*

(*P < 0.05; BMI, Body-mass-index; WC, waist girth; WHR, waist-hip ratio)

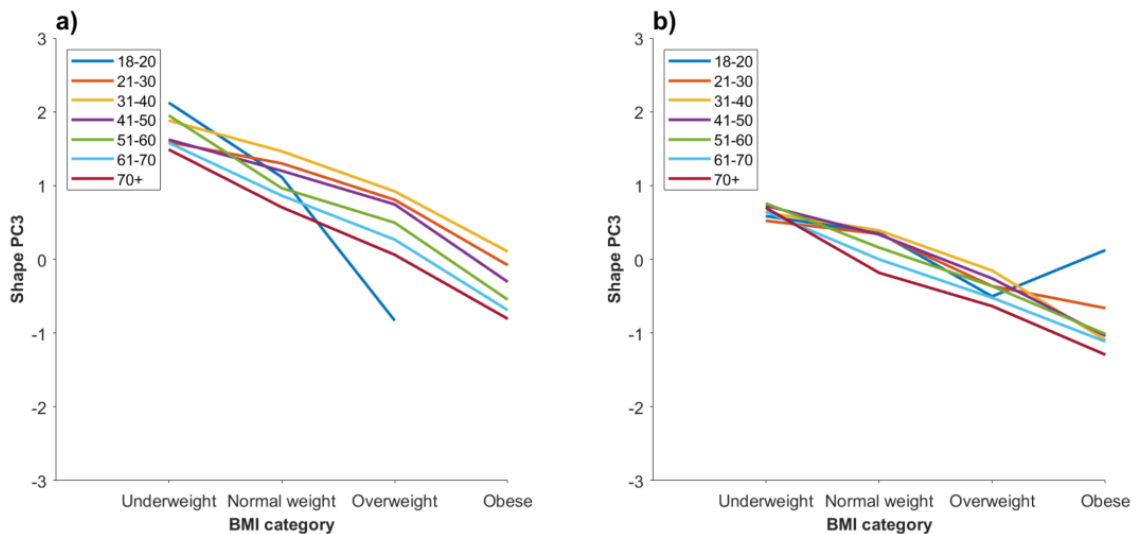
A.5.3 Shape PC1 by age and BMI category in a) males and b) females.



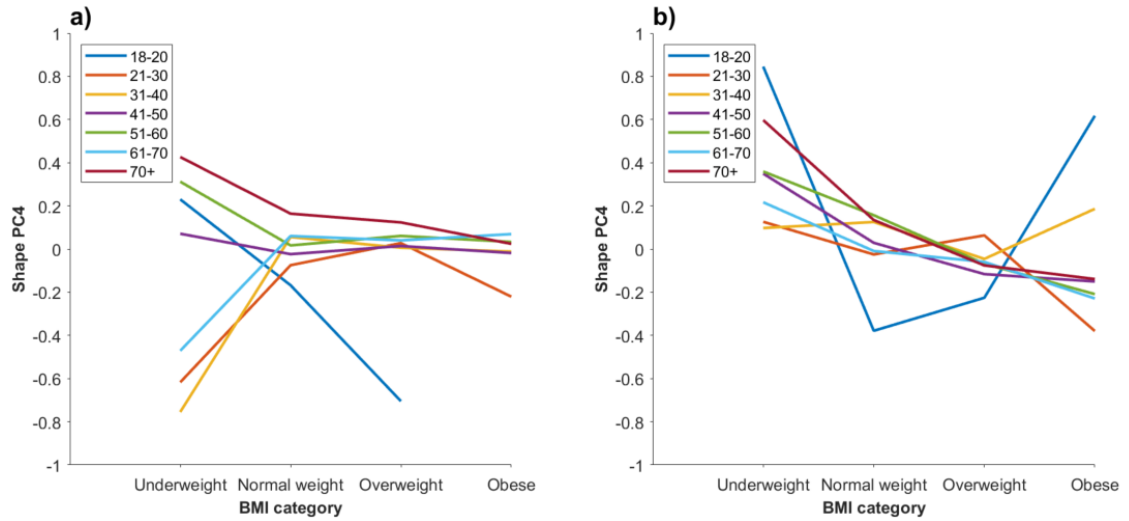
A.5.4 Shape PC2 by age and BMI category in a) males and b) females.



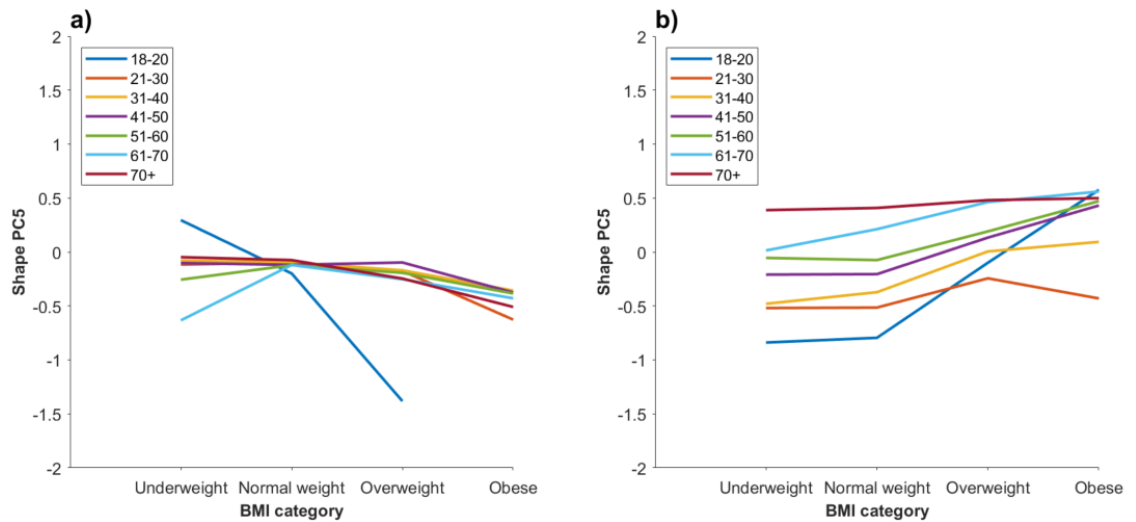
A.5.5 Shape PC3 by age and BMI category in a) males and b) females.



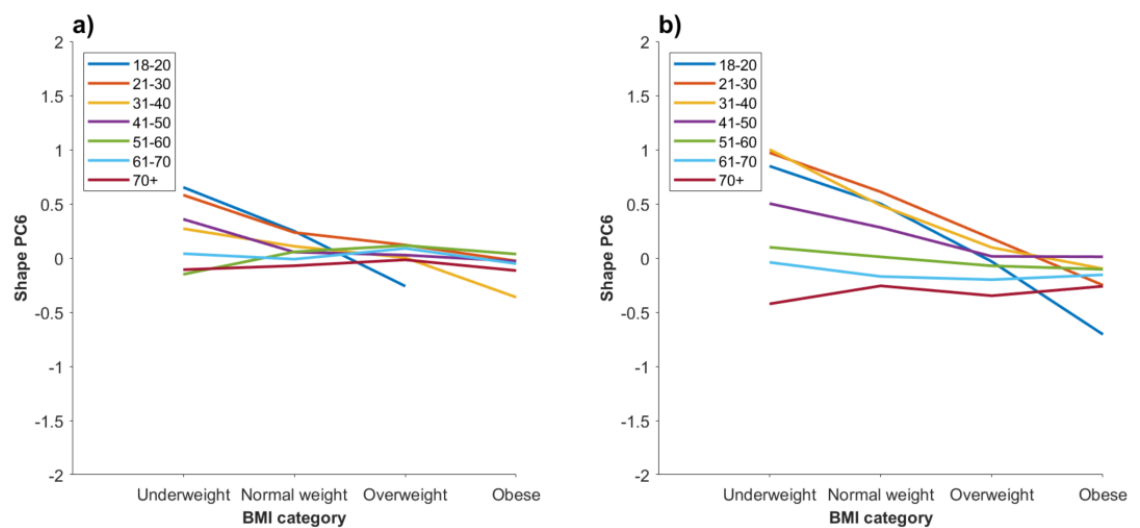
A.5.6 Shape PC4 by age and BMI category in a) males and b) females.



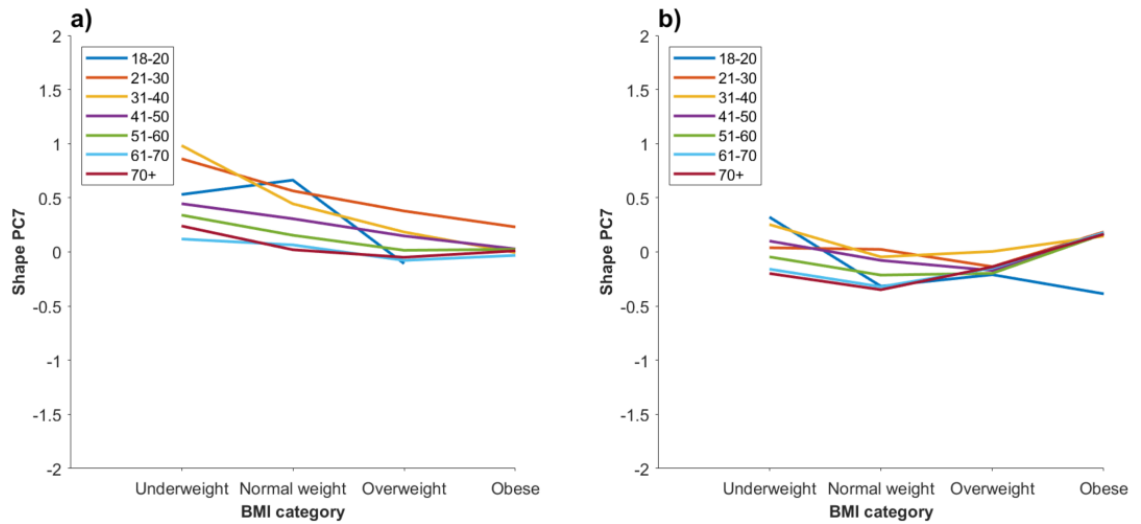
A.5.7 Shape PC5 by age and BMI category in a) males and b) females.



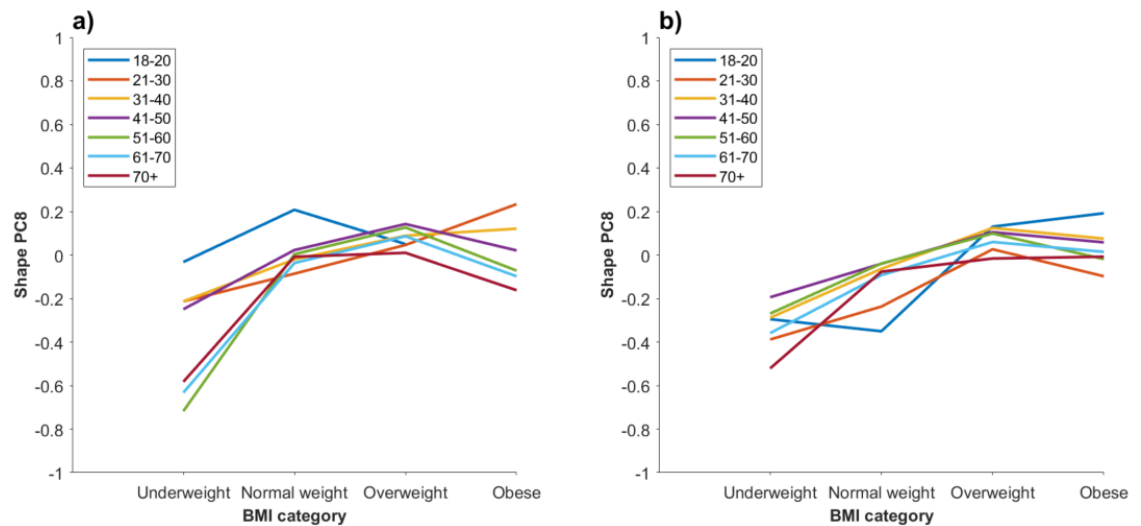
A.5.8 Shape PC6 by age and BMI category in a) males and b) females.



A.5.9 Shape PC7 by age and BMI category in a) males and b) females.



A.5.10 Shape PC8 by age and BMI category in a) males and b) females.



A.5.11 Shape PC9 by age and BMI category in a) males and b) females.

